

LATERAL LOAD DESIGN OF TALL BUILDINGS

EVALUATION AND COMPARISON OF FOUR TALL BUILDINGS IN MADRID, SPAIN



Study: Civil Engineering and Geosciences
Master: Building Engineering

Author: P.P. Hoogendoorn
Date: January 12th 2009

University: Delft University of Technology
Supervisors: Prof.Dipl.-Ing. J.N.J.A. Vamberský (Chairman)
Prof.ir. A.C.W.M. Vrouwenvelder
Prof.dr.ir. J.C. Walraven

Company: INTEMAC
Supervisor: Dr.Ing. R. Álvarez Cabal

Preface

Approximately one and a half years ago, I started a new, challenging chapter in my personal, academic and professional life. The present report reflects the undergone development in academic sense in the time period from June 2007 to January 2009.

This is the final report of my master thesis to obtain the Master of Science degree in Civil Engineering at Delft University of Technology. The study presented in this thesis has been entirely carried out at the head office of INTEMAC (Instituto Técnico de Materiales y Construcciones) in Madrid, Spain. From June 2007, I have dedicated my time at INTEMAC partially to internal projects and partially to this MSc thesis.

I would like to thank the following people for their contribution to this thesis.

First of all, I owe gratitude to the graduation committee at Delft University of Technology:

- The chairman of the graduation committee, Prof.Dipl.-Ing. J.N.J.A. Vamborský of the section Structural and Building Engineering, for his support during the complicated start-up period and his motivating technical advice.
- Prof.ir. A.C.W.M. Vrouwenvelder of the section Structural Mechanics and
- Prof.dr.ir. J.C. Walraven of the section Structural and Building Engineering, for their useful comments and criticism.

I would like to show my heartfelt appreciation to Dr.Ing. R. Álvarez Cabal, my daily supervisor at INTEMAC, for passing on to me his enthusiasm for structural engineering and for his readiness to discuss all kinds of tall building-related topics.

Last but not least, I would like to express my sincere thankfulness to my family, girlfriend and friends for their patience and support during the preceding one and a half years.

Peter Paul Hoogendoorn
Madrid, January 12th 2009.

Table of contents

| | |
|---|-----|
| Preface | i |
| Summary | v |
| List of figures | vii |
| List of tables | x |
| | |
| 1 Introduction | 1 |
| 1.1 Problem description | 1 |
| 1.2 Problem definition | 1 |
| 1.3 Objective | 2 |
| 1.4 Approach | 2 |
| | |
| 2 Tall buildings | 4 |
| 2.1 Historical overview | 4 |
| 2.1.1 Tall structures | 4 |
| 2.1.2 Tall buildings | 6 |
| 2.1.3 Trends | 10 |
| 2.2 General design considerations | 12 |
| 2.2.1 Development and management | 12 |
| 2.2.2 Architecture and urban development | 15 |
| 2.2.3 Building services and façade | 16 |
| 2.2.4 Structure | 20 |
| 2.2.5 Construction | 21 |
| 2.2.6 Fire engineering | 21 |
| 2.3 Structural design considerations | 23 |
| 2.3.1 Static loads | 23 |
| 2.3.2 Dynamic loads | 27 |
| 2.4 Lateral load resisting systems | 37 |
| 2.4.1 Braced-frame structure | 38 |
| 2.4.2 Rigid-frame structure | 39 |
| 2.4.3 Shear wall structure | 39 |
| 2.4.4 Coupled shear wall structure | 40 |
| 2.4.5 Shear wall - rigid frame structure | 41 |
| 2.4.6 Framed-tube structure | 42 |
| 2.4.7 Outrigger-braced structure | 44 |
| 2.4.8 Space frame structure | 46 |
| 2.4.9 Hybrid structure | 47 |
| | |
| 3 Wind loading | 48 |
| 3.1 Surface wind characteristics | 48 |
| 3.1.1 Variation with height and terrain roughness | 48 |
| 3.1.2 Turbulence | 52 |
| 3.1.3 Pressure | 56 |
| 3.1.4 Extreme wind probability | 58 |
| 3.2 Structural factor | 59 |

| | | |
|-------|--|-----|
| 3.2.1 | Size factor..... | 59 |
| 3.2.2 | Dynamic factor..... | 60 |
| 3.3 | Structural vibration | 63 |
| 3.3.1 | Vortex-shedding | 63 |
| 3.3.2 | Buffeting | 64 |
| 4 | General site and building description | 66 |
| 4.1 | Cuatro Torres Business Area | 66 |
| 4.2 | Torre Espacio..... | 67 |
| 4.3 | Torre de Cristal | 68 |
| 4.4 | Torre Sacyr Vallehermoso | 69 |
| 4.5 | Torre Caja Madrid | 71 |
| 5 | Structural analysis | 74 |
| 5.1 | General considerations | 74 |
| 5.1.1 | Typology and geometry | 74 |
| 5.1.2 | Mechanical properties | 75 |
| 5.1.3 | Support conditions | 80 |
| 5.1.4 | Wind action..... | 82 |
| 5.2 | Torre Espacio..... | 87 |
| 5.2.1 | Structure | 88 |
| 5.2.2 | Aerodynamic characteristics | 93 |
| 5.2.3 | Results | 96 |
| 5.3 | Torre de Cristal | 97 |
| 5.3.1 | Structure | 98 |
| 5.3.2 | Aerodynamic characteristics | 101 |
| 5.3.3 | Results | 104 |
| 5.4 | Torre Sacyr Vallehermoso | 105 |
| 5.4.1 | Structure | 106 |
| 5.4.2 | Aerodynamic characteristics | 111 |
| 5.4.3 | Results | 113 |
| 5.5 | Torre Caja Madrid | 114 |
| 5.5.1 | Structure | 114 |
| 5.5.2 | Aerodynamic characteristics | 119 |
| 5.5.3 | Results | 121 |
| 5.6 | Summary of results and discussion..... | 122 |
| 5.6.1 | Aerodynamic characteristics | 123 |
| 5.6.2 | Along-wind displacement..... | 125 |
| 5.6.3 | Along-wind acceleration | 125 |
| 6 | Comparison..... | 128 |
| 6.1 | Significant properties of the lateral load resisting system..... | 129 |
| 6.2 | Investment | 129 |
| 6.3 | Net operating income | 131 |
| 6.3.1 | Lateral displacement | 132 |
| 6.3.2 | Lateral acceleration | 133 |
| 6.3.3 | Floor area covered by the lateral load resisting system..... | 133 |
| 6.3.4 | Floor plan flexibility | 135 |

| | | |
|-------|---|-----|
| 6.3.5 | Net operating income | 136 |
| 6.4 | Net present value | 136 |
| 7 | Conclusions and recommendations | 138 |
| 7.1 | Conclusions | 138 |
| 7.1.1 | Conclusions associated with the four tall buildings | 138 |
| 7.1.2 | General conclusions | 139 |
| 7.2 | Recommendations | 140 |
| | List of references | 142 |

Summary

The design and operation of high-rise buildings is subjected to many specific problems. The design is characterised by a high complexity and strong interlinkage between design disciplines. Besides of course the technical feasibility, the financial feasibility of tall building projects is of the utmost importance.

Tall buildings are susceptible to dynamic horizontal loads such as wind and earthquakes. These horizontal forces bring about considerable stresses, displacements and vibrations due to the building's inherent tallness and flexibility. As far as wind action is concerned, displacement and vibration design considerations become critical with increasing height. Excessive displacements can cause damage to partitions, façade elements and interior finishes, whereas the human perception of building vibrations can induce concern regarding the structural safety and cause nausea to the occupants.

Recently, four tall buildings have been erected at the former sports complex of the local football club Real Madrid in Madrid, Spain. As far as their lateral load design is concerned, the principal load has been the wind action since the buildings are located in a low seismicity zone. The global dimensions and geotechnical conditions of the buildings are very similar, however the adopted lateral load resisting systems are different.

The first objective of this study is to evaluate the along-wind response in the serviceability limit state of these four tall buildings: Torre Espacio, Torre de Cristal, Torre Sacyr Vallehermoso and Torre Caja Madrid. Insight is gained into wind action and wind-induced structural response. Complete and detailed finite element models are developed of the structure of each high-rise building. In-depth structural analyses are carried out with regard to the serviceability limit state of the aforementioned tall buildings. Lateral displacements with a return period of 50 years are computed to evaluate the possibility of damage to non-structural elements. Furthermore, 5-year and 10-year horizontal accelerations are calculated at the top occupied floors to evaluate the human comfort.

Secondly, a comparison of the adopted lateral load resisting systems is carried out from the viewpoint of financial feasibility.

Historically, the technical and financial feasibility of tall building projects was governed by lateral load (structural) design considerations. Firstly as far as the technical feasibility is concerned, the advance in computational capacity has led to a vast offer of extremely powerful structural analysis tools with which any imaginable structure can be calculated. Therefore, the need for simplicity and a high level of repetition is highly diminished. Secondly, the financial feasibility of a tall building project is no longer governed by structural material efficiency considerations only. This is due to the increasing cost of building services and prefabricated façade elements, because of which the relative importance of structural material efficiency has become less.

In this thesis it is endeavoured to compare the adopted lateral load systems from the financial point of view of a real estate investor, i.e. to roughly estimate the influence of each lateral load resisting system on the net present value of the tall building. A set of criteria (properties of the lateral load resisting system) is drawn up that is believed to

most significantly influence the financial feasibility through construction and maintenance costs, and rental income, namely: building cost, wind-induced displacement and acceleration, amount of floor area covered by the structure and the flexibility of the floor plan. Assumptions are made with regard to the influence of the above criteria on the financial feasibility. Subsequently worst-case, best-estimate and best-case scenarios have been determined to determine the expected effect of each lateral load resisting system on the net present value of the building.

It is concluded that the lateral load design of Torre Sacyr Vallehermoso is the best alternative from a financial point of view. The financial feasibility of Torre Caja Madrid in comparison with the other buildings depends very much on the magnitude of the positive influence of the floor plan flexibility on the rental income. The lateral load resisting system of Torre Espacio uses little material throughout the building height, but the relative rental income and maintenance cost are negatively influenced by the other properties of the lateral load system. A less-than-mean performance is obtained by Torre de Cristal for all comparison criteria.

It is recommended that further research is carried out on the influence of the lateral load design on the financial feasibility through construction, operation and maintenance cost and rental income.

List of figures

| | |
|--|----|
| Figure 2.1-1: <i>Tower of Babel</i> by Pieter Bruegel 1563 [40]..... | 4 |
| Figure 2.1-2: Pyramid of Cheops [40]..... | 5 |
| Figure 2.1-3: San Gimignano [40]..... | 5 |
| Figure 2.1-4: Chartres cathedral [40]..... | 5 |
| Figure 2.1-5: Sears Tower in Chicago [9]..... | 6 |
| Figure 2.1-6: CN Tower in Toronto [40]..... | 6 |
| Figure 2.1-7: Equitable Life Insurance Building in New York [9]..... | 7 |
| Figure 2.1-8: Home Insurance Building in Chicago [9]..... | 7 |
| Figure 2.1-9: Empire State Building in New York [9]..... | 8 |
| Figure 2.1-10: John Hancock Center in Chicago [9]..... | 9 |
| Figure 2.1-11: Sears Tower in Chicago [9]..... | 9 |
| Figure 2.1-12: Bank of China in Hong Kong [9]..... | 10 |
| Figure 2.1-13: Jin Mao Tower in Shanghai [9]..... | 10 |
| Figure 2.1-14: Petronas Towers in Kuala Lumpur [9]..... | 10 |
| Figure 2.1-15: Two International Finance Centre in Hong Kong [9]..... | 10 |
| Figure 2.1-16: Taipei 101 in Taipei [9]..... | 10 |
| Figure 2.1-17: Burj Dubai rendering [2]..... | 10 |
| Figure 2.1-18: Burj Dubai under construction [40]..... | 10 |
| Figure 2.1-19: Mean height of hundred tallest buildings [8]..... | 11 |
| Figure 2.1-20: Hundred tallest buildings by region [8]..... | 11 |
| Figure 2.1-21: 100 tallest buildings by function [8]..... | 12 |
| Figure 2.2-1: Grouped-operation elevator system [9]..... | 18 |
| Figure 2.2-2: Sky-lobby elevator system [9]..... | 18 |
| Figure 2.2-3: Double-deck elevator [9]..... | 19 |
| Figure 2.2-4: Fire in Torre Windsor in Madrid [17]..... | 23 |
| Figure 2.3-1: Differential shortening in horizontal and vertical section..... | 24 |
| Figure 2.3-2: Spectral density of wind and earthquake action..... | 27 |
| Figure 2.3-3: Ground acceleration record at El Centro, California [35]..... | 29 |
| Figure 2.3-4: Spanish map of seismic activity [28]..... | 30 |
| Figure 2.3-5: Human perception levels and hindrance [33]..... | 33 |
| Figure 2.3-6: ISO 6897 5-year rms acceleration criteria [18]..... | 34 |
| Figure 2.3-7: AIJ 1-year peak acceleration criteria [34]..... | 35 |
| Figure 2.3-8: TMD in Taipei 101 [40]..... | 36 |
| Figure 2.4-1: Cantilever representation..... | 37 |
| Figure 2.4-2: Shear-dominated and bending-dominated displacement diagrams..... | 38 |
| Figure 2.4-3: Braced frame structure [33]..... | 39 |
| Figure 2.4-4: Rigid-frame structure [33]..... | 39 |
| Figure 2.4-5: Combined shear wall structure [33]..... | 41 |
| Figure 2.4-6: Coupled shear wall structure [33]..... | 41 |
| Figure 2.4-7: Wall-frame interaction [35]..... | 42 |
| Figure 2.4-8: Shear lag phenomenon in framed-tubes [35]..... | 43 |
| Figure 2.4-9: Braced-tube structure [33]..... | 44 |
| Figure 2.4-10: Outrigger-braced structure..... | 45 |
| Figure 2.4-11: Belt trusses in an outrigger-braced structure [33]..... | 45 |
| Figure 2.4-12: Optimum levels for top sway reduction..... | 46 |
| Figure 2.4-13: Optimum levels for base moment reduction..... | 46 |
| Figure 2.4-14: Bank of China in Hong Kong [9]..... | 47 |
| Figure 3.1-1: Boundary layer wind [24]..... | 49 |

| | |
|---|-----|
| Figure 3.1-2 Typical roughness lengths and surface drag coefficients [31]..... | 50 |
| Figure 3.1-3: Eurocode terrain categories [12] | 51 |
| Figure 3.1-4: Eurocode mean wind velocity profiles for $v_b = 26$ m/s..... | 52 |
| Figure 3.1-5: Relative turbulence intensity according to Eurocode 1 | 54 |
| Figure 3.2-1: Background response factor | 60 |
| Figure 3.2-2: Size factor | 60 |
| Figure 3.2-3: Spectral density function | 62 |
| Figure 3.2-4: Aerodynamic admittance function | 63 |
| Figure 3.3-1: Wake buffeting [24] | 64 |
| Figure 4.1-1: Scale model of CTBA [40] | 66 |
| Figure 4.1-2: CTBA, May 2007 | 66 |
| Figure 4.2-1: Torre Espacio | 67 |
| Figure 4.3-1: Torre de Cristal under construction | 68 |
| Figure 4.3-2: Artist impression of Torre de Cristal [16] | 68 |
| Figure 4.4-1: Torre Sacyr Vallehermoso under construction | 70 |
| Figure 4.4-2: Torre Sacyr Vallehermoso upon completion | 70 |
| Figure 4.4-3: Fish-scale outer façade | 70 |
| Figure 4.4-4: Outer façade detail | 70 |
| Figure 4.5-1: East elevation..... | 71 |
| Figure 4.5-2: South elevation..... | 72 |
| Figure 5.1-1: Element and joint representation of a structural core..... | 75 |
| Figure 5.1-2: Moment of inertia of a coupling beam [5] | 76 |
| Figure 5.1-3: Development of mean strength in time..... | 77 |
| Figure 5.1-4: Development of modulus of elasticity in time | 78 |
| Figure 5.1-5: Effective axial stiffness of composite columns | 79 |
| Figure 5.1-6: Basement layout..... | 80 |
| Figure 5.1-7: Basement connectivity Torre Espacio and Torre de Cristal | 81 |
| Figure 5.1-8: Basement connectivity Torre Sacyr Vallehermoso and Caja Madrid | 82 |
| Figure 5.1-9: Basic wind velocities in Spain according to CTE..... | 84 |
| Figure 5.1-10: 50-year peak and mean wind pressure profile | 84 |
| Figure 5.1-11: Size factor | 85 |
| Figure 5.1-12: Dynamic factor | 85 |
| Figure 5.1-13: External wind pressure coefficients [27]..... | 86 |
| Figure 5.2-1: Typical floor plan at basement, low-, mid- and high-rise level..... | 88 |
| Figure 5.2-2: Concrete transition block with strut-and-tie model | 90 |
| Figure 5.2-3: Outrigger structure | 91 |
| Figure 5.2-4: Detail of tendons | 91 |
| Figure 5.2-5: Transfer truss in plan..... | 92 |
| Figure 5.2-6: Transfer truss in elevation | 92 |
| Figure 5.2-7: Axes definition | 93 |
| Figure 5.2-8: Modal shape of natural vibration mode Y_1 | 94 |
| Figure 5.2-9: Equivalent static wind pressure | 95 |
| Figure 5.2-10: Force coefficient..... | 95 |
| Figure 5.2-11: Determination of force coefficient..... | 96 |
| Figure 5.3-1: Typical floor plan of basement, low-, mid- and high-rise section..... | 98 |
| Figure 5.3-2: Integrated floor beams | 100 |
| Figure 5.3-3: Column-beam connection | 100 |
| Figure 5.3-4: Mesnager joint [5]..... | 100 |
| Figure 5.3-5: Axes definition | 102 |
| Figure 5.3-6: Modal shape of natural vibration mode Y_1 | 103 |
| Figure 5.3-7: Equivalent static wind pressure profile | 104 |
| Figure 5.3-8: Force coefficient profile | 104 |

| | |
|---|-----|
| Figure 5.3-9: Determination of force coefficient..... | 104 |
| Figure 5.4-1: Construction of geometry | 106 |
| Figure 5.4-2: Typical floor plan of basement, low-, mid- and high-rise section..... | 107 |
| Figure 5.4-3: Column-girder and girder-beam joint..... | 108 |
| Figure 5.4-4: Outrigger structure | 109 |
| Figure 5.4-5: Transfer trusses in plan..... | 109 |
| Figure 5.4-6: Outer transfer truss | 110 |
| Figure 5.4-7: Axes definition | 111 |
| Figure 5.4-8: Modal displacement mode X_1 | 112 |
| Figure 5.4-9: Equivalent static wind pressure..... | 113 |
| Figure 5.4-10: Determination of force coefficient..... | 113 |
| Figure 5.5-1: Typical floor plan at basement, low-, mid- and high-rise section..... | 115 |
| Figure 5.5-2: Vertical section along x-axis [16]..... | 116 |
| Figure 5.5-3: Vertical section along y-axis [16]..... | 116 |
| Figure 5.5-4: Column detail to allow differential shortening [16]..... | 117 |
| Figure 5.5-5: Upper chord of transfer truss..... | 118 |
| Figure 5.5-6: Secondary transfer truss [16] | 118 |
| Figure 5.5-7: Primary transfer truss [16] | 118 |
| Figure 5.5-8: Axes definition | 119 |
| Figure 5.5-9: Modal displacement mode X_1 | 120 |
| Figure 5.5-10: Equivalent static wind pressure profile | 121 |
| Figure 5.5-11: Determination of force coefficient..... | 121 |
| Figure 5.6-1: Force coefficient along height | 124 |
| Figure 5.6-2: Equivalent static wind pressure | 124 |
| Figure 5.6-3: Wind load along height..... | 124 |
| Figure 5.6-4: 5-year rms acceleration..... | 126 |
| Figure 5.6-5: 10-year peak acceleration | 126 |
| Figure 5.6-6: Comparison with ISO 6897 | 127 |
| Figure 5.6-7: Comparison with BLWTL..... | 127 |
| Figure 6.4-1: Influence of discount rate on the net present value..... | 137 |

List of tables

| | |
|--|-----|
| Table 2.3-1: BLWTL 10-year acceleration criteria | 34 |
| Table 5.1-1: Ratio $E_{cm}(t)/E_{cm}$ for different ages and cement types | 78 |
| Table 5.1-2: Secant moduli of elasticity for different compressive strengths | 79 |
| Table 5.1-3: Translation of Spanish terms in figure 5.1-13 | 86 |
| Table 5.2-1: Gravity load per area | 93 |
| Table 5.2-2: Frequency of natural vibrations | 93 |
| Table 5.2-3: Along-wind building displacement | 97 |
| Table 5.2-4: Along-wind building acceleration | 97 |
| Table 5.3-1: Gravity load per area | 101 |
| Table 5.3-2: Frequency of natural vibrations | 102 |
| Table 5.3-3: Along-wind building displacement | 105 |
| Table 5.3-4: Along-wind building acceleration | 105 |
| Table 5.4-1: Gravity load per area | 111 |
| Table 5.4-2: Frequency of natural vibrations | 111 |
| Table 5.4-3: Along-wind building displacement | 114 |
| Table 5.4-4: Along-wind building acceleration | 114 |
| Table 5.5-1: Gravity load per area | 119 |
| Table 5.5-2: Frequency of natural vibrations | 119 |
| Table 5.5-3: Along-wind building displacement | 122 |
| Table 5.5-4: Along-wind building acceleration | 122 |
| Table 5.6-1: Aerodynamic building characteristics | 123 |
| Table 5.6-2: Along-wind displacement | 125 |
| Table 5.6-3: Along-wind acceleration | 126 |
| Table 6.2-1: Material employed in LLRS for lateral load design | 130 |
| Table 6.2-2: Comparison investment | 131 |
| Table 6.3-1: Lateral displacement ratio | 132 |
| Table 6.3-2: Comparison influence of lateral displacement on NOI | 132 |
| Table 6.3-3: Lateral acceleration | 133 |
| Table 6.3-4: Comparison influence of lateral acceleration on NOI | 133 |
| Table 6.3-5: Comparison LLRS-covered floor area | 134 |
| Table 6.3-6: Comparison influence of LLRS-covered floor area on NOI | 134 |
| Table 6.3-7: Comparison floor plan flexibility | 135 |
| Table 6.3-8: Comparison influence of flexibility on NOI | 135 |
| Table 6.3-9: Comparison of influence on NOI | 136 |
| Table 6.4-1: Comparison of influence on NPV | 136 |

1 Introduction

1.1 Problem description

From the first high-rise buildings constructed in the late 19th century until the modern-day skyscrapers, the structure has always played an important role in the overall design. Increasing height and slenderness brought about a change of the structural engineer's focus from static gravity loads to horizontal dynamic loads generated by wind and earthquakes.

These horizontal dynamic loads cause large stresses in structural members as well as lateral building motion. The former requires structural stability and sufficient strength, whereas the latter poses restrictions to the serviceability of the building. The building motion comprises lateral drift that may damage partitions, façade elements and interior finishes such as doors or elevators. In addition, the human perception of building motion can raise concern about the structural safety and cause nausea to the building occupants. For tall and flexible high-rise buildings, the limitation of wind-induced lateral building drift and motion perception becomes a key structural design criterion.

Traditionally the structural feasibility and material efficiency constituted governing considerations in the overall tall building design. The relative importance of the structural design in relation to other design disciplines was great because of the following reasons.

- The building cost of the structure covered a considerable part of the total building cost, making it very much worthwhile to optimise the structural material efficiency.
- Structural analyses were performed by hand with the help of calculating tools with very limited computational capacity. This called for simplicity and a high level of repetition in the structural design.

Because of this, the technical and financial feasibility was historically governed by material efficiency of the lateral load resisting system.

This has changed drastically in modern high-rise construction. The technical and financial feasibility is no longer governed by structural material efficiency considerations only, due to:

- Building service systems and prefabricated façade elements have become increasingly more complex and expensive, thus reducing the relative importance of material efficiency of the lateral load resisting system.
- The striking development of computational capacity has paved the way for extremely powerful structural analysis tools, highly reducing the need for structural simplicity and repetition.

1.2 Problem definition

Material efficiency considerations of the lateral load design of tall buildings do no longer constitute a sufficient basis upon which different lateral load resisting alternatives can be compared. Besides the structural material efficiency, the comparison of lateral load

designs has to include all factors that significantly affect the project's financial feasibility.

1.3 Objective

The objective of this master thesis is to evaluate and compare the lateral load design of four recently constructed tall buildings at the former sports complex of Real Madrid in Madrid, Spain.

Firstly, an extensive structural analysis is carried out with regard to the along-wind response in the serviceability limit state. Secondly a comparison is carried out between the lateral load resisting systems of the considered buildings. A set of comparison criteria is drawn up, including the structural response, to determine the attractiveness of each alternative from the financial viewpoint of a real estate investor.

1.4 Approach

First of all information is gathered about key aspects in tall building design. Besides all general design aspects, the focus lies on how certain building properties affect the financial feasibility of the project. (Chapter 2)

An in-depth study is performed to gain insight into the wind action, being the principal load this MSc thesis is focussed on. The interaction between the wind load and tall building structures is explored. (Chapter 3)

Information is obtained concerning the general site characteristics as well as the architectural properties of the four tall buildings. (Chapter 4)

An exhaustive description of the structure, and more specifically the lateral load design, of each building is presented. Complete finite element models are developed of each high-rise building. A thorough structural analysis is performed to determine the along-wind response in the serviceability limit state for the governing wind direction, in terms of the lateral building displacements and accelerations. (Chapter 5)

Properties of the lateral load resisting system are chosen that are believed to most significantly affect the building's financial feasibility. A model is set up to compare the influence of each lateral load system on the building's net value. The net value is considered to be the sum of the initial investment (construction cost) and the discounted sum of the net operating income. Assumptions are made to estimate the influence of each lateral load system property (comparison criterion) on the construction cost and operating income. Worst-case, best-estimate and best-case values are computed for the overall influence on the net present value to determine the most attractive lateral load design from an investor's financial point of view. (Chapter 6)

Building-specific conclusions are drawn concerning the along-wind structural response and the comparison of the financial feasibility of the lateral load design of the four high-rise buildings. General conclusions are presented with regard to all topics that are treated in this thesis. Finally, recommendations are made that are deduced from the foregoing conclusions. (Chapter 7)

2 Tall buildings

This chapter introduces the reader to tall buildings and the problems that arise during the design of those buildings. Section 2.1 starts with a broad and superficial description of tall structures and buildings and presents a timeline of high-rise buildings and high-rise trends. General and structural design considerations are dealt with in section 2.2 and 2.3 respectively, whereas section 2.4 discussed various lateral load resisting systems adopted in tall building structures.

2.1 Historical overview

2.1.1 Tall structures



“And they said to one another, “Come, let us make bricks, and burn them thoroughly.” And they had brick for stone, and bitumen for mortar. Then they said, “Come, let us build ourselves a city and a tower with its top in the heavens, and let us make a name for ourselves, lest we be dispersed over the face of the whole earth.””

Figure 2.1-1: *Tower of Babel* by Pieter Bruegel 1563 [40]

The cited paragraph from the book of Genesis (11:3-4) tells the storey of the Tower of Babel and the confusion of tongues. This example is not intended to serve as the first-known high-rise structure in history, but it serves moreover to illustrate the, apparent ever-existing drive of mankind to build towards the sky.

Throughout time and cultures, high-rise structures have always intrigued architects, builders and society itself. This has resulted in many examples of tall structures, built for different purposes and having different shapes. Below, a brief description is presented of some tall structures and their characteristics.

The great pyramid of Giza in Egypt, shown in figure 2.1-2, was built around 2570 BC. It is the oldest and tallest pyramid of a total of the three pyramids constructed at the Giza Necropolis. It serves as a tomb for the Egyptian pharaoh Cheops and reaches an astonishing height of approximately 140 m.



Figure 2.1-2: Pyramid of Cheops [40]

It is believed that ancient Egyptian obelisks symbolised their sun god. During the Roman Empire various Egyptian obelisks were transported to Rome to serve as a monument of won battles. The tallest obelisk is about 30 m tall and stands on the square in front of the Basilica of St. John Lateran in Rome.

The San Gimignano watching towers in Italy, depicted in figure 2.1-3, constitute an example of defence-purposes tall structures. Many of these structures have collapsed in time. The town has accomplished to conserve the medieval skyline consisting of fourteen watching towers built in between the 11th and 13th century. The tallest tower exceeds a height of 50 m.

Medieval cathedrals, such as the cathedral of Chartres in France in figure 2.1-4, became a symbol of a prosperous future after an era of cultural and socio-economical decline. The verticality in gothic cathedrals, even incorporated in towers and arches, was used to make the town feel humble towards God, to impress and let people focus on the heavenly. This vertical emphasis led to structures with heights up to approximately 160 m.



Figure 2.1-3: San Gimignano [40]



Figure 2.1-4: Chartres cathedral [40]



Figure 2.1-5: Sears Tower in Chicago [9]

More recent examples of tall structures are the telecommunication towers. The tallest one ever built is the CN tower in Toronto, Canada and is shown in figure 2.1-6. The structure was completed in 1976 and has a total height of approximately 550 m. Besides the restaurant and observation deck located at approximately two-thirds of the height, its function is purely technical.

Modern-day skyscrapers are habitable structures, usually comprising a great number of storeys. Its function can be to house residential, office, hotel and retail activities. Figure 2.1-5 presents an interesting high-rise building: the Sears Tower in Chicago which was completed in 1974.

It would be an unimaginably difficult task to list all types of tall structures. It has been seen in the above that tall structures have been build throughout time for all kinds of purposes.

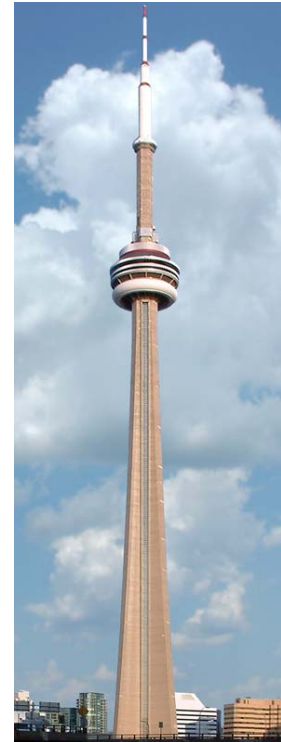


Figure 2.1-6: CN Tower in Toronto [40]

One implicit function, however, they all have in common; a statement of power.

2.1.2 Tall buildings

This thesis is focussed on tall buildings intending by such a vertically-arranged, enclosed and habitable space. Although the definition of a building can be intuitively well understood, this results less easy for the definition of tall. Some use rather arbitrary criteria in terms of height of number of storeys to define a tall building. It is believed that a more abstract, but meaningful, definition is better suited: whether or not the design or operation of the building is influenced by some aspect of *tallness*.

The Industrial Revolution during the 19th century led to, among other things, a fast development of transport systems such as trains, cars, and steam boats. It was partly due to these transport conditions and the prosperous economic future of Chicago and New York that the development of tall buildings in these cities took such a high pace.

During the era of the Industrial Revolution rapid improvements were made in construction materials: firstly wrought iron and subsequently steel was developed. Iron had a low resistance to tensile stresses that caused brittle failure of an iron structural member. This problem was solved by its steel counterpart.

Otis' invention of the safety elevator in 1852 paved the way for high-rise construction. The safety power elevator solved the fundamental problem of high-rise construction: the vertical transport.

The author believes that both the use of structural steel and the invention of the elevator constitute decisive aspects facilitating the kick-off of tall building construction.

The Equitable Life Insurance Building in New York, shown in figure 2.1-7, was the first building to incorporate an elevator. The office building had six storeys with a total height of roughly 38 m and was completed in 1870. For the first time, the upper storeys were as attractive to rent (or more) as the lower storeys. This was a major breakthrough for the financial feasibility of high-rise construction.

The first building to be supported entirely by a combined steel (rolled beam section) and cast-iron (columns) frame was the Home Insurance Building in Chicago. The designer, William LeBaron Jenney, had the ingenious idea to bear all gravity loads by a steel framework and let the masonry walls be suspended from the skeleton. This was very different from the tradition at that time being massive masonry walls bearing all loads. The building had a height of approximately 42 m and initially consisted of ten storeys (later two storeys were added). The building, shown in figure 2.1-8, was completed in 1885.

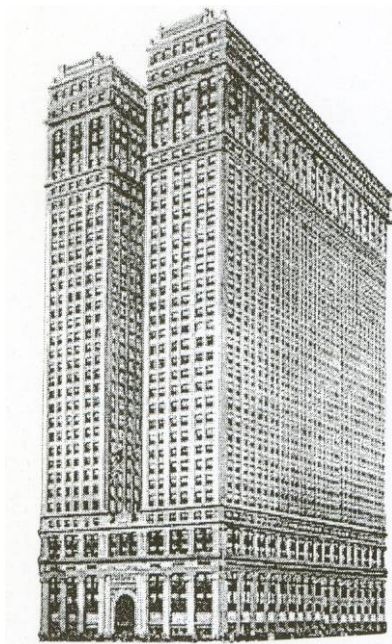


Figure 2.1-7: Equitable Life Insurance Building in New York [9]



Figure 2.1-8: Home Insurance Building in Chicago [9]

During the late 19th century and the beginning of the 20th century high-rise construction developed at a high pace, particularly in Chicago and New York. The New York Chrysler Building, completed in 1930, stands 319 m tall as an art deco monument of that era. In 1931 the Empire State Building was completed in New York. The architects of Shreve, Lamb & Harmon Associates designed this tall office building with a height of 381 m (not including antennae). An interesting detail is that the construction was completed in just over 18 months.



Figure 2.1-9: Empire State Building in New York [9]

The architects and engineers of Skidmore, Owings & Merrill (SOM) drastically changed the Chicago skyline in the seventies by designing two truly remarkable tall buildings: the John Hancock Center and the Sears Tower depicted in figure 2.1-10 and 2.1-11 respectively. The structural design of both high-rise buildings has been carried out by Fazlur Khan of the Chicago office of SOM. He has come up with several innovative structural solutions to the lateral stiffness problem of tall buildings. Examples are the bundled-tube structure employed in the Sears Tower and the braced-tube structure firstly adopted in the John Hancock Center.

The John Hancock Center consists of 100 storeys and reaches a height of 344 m (443 m including antennas). The building accommodates office, residential and retail use. The diagonal bracing stiffened the perimeter framed-tube, because of which the windows could be larger than in a normal framed-tube (subsection 2.4.5). This tapering steel building was completed in 1970.

The Sears Tower, designed by SOM, has a height of 442 m and was completed in 1974. The building is characterised by nine, architectonically, independent tubes all reaching different heights. The 110 above-ground stories house offices and retail space.



Figure 2.1-10: John Hancock Center in Chicago [9]



Figure 2.1-11: Sears Tower in Chicago [9]

The famous World Trade Center twin towers were completed in 1973 in New York. The architect was Yamasaki and the structural design was carried out by Leslie E. Robertson Associates (LERA). The twin towers had a respective height of 415 m and 417 m and were destroyed in 2001 by a terrorist attack.

During the nineties, Asia starts to take over the, historically, leading role of the United States. New tall buildings have been built in a short period of time in the Far East and Middle East. This development is still lasting (see subsection 2.1.3)

The Bank of China Tower is an exceptional high-rise building, designed by I.M. Pei & Partners (architect) and LERA (structural engineer), see figure 2.1-12. They have come up with a highly efficient three-dimensional, triangulated structure that dominates the architectural appearance. This office building is 367 m high, consists of 70 above-grade storeys and was completed in 1989 in Hong Kong.

The Jin Mao Tower in Shanghai was designed by SOM and completed in 1998. The 88-storey building is 421 m tall and houses office, hotel and retail. Figure 2.1-13 presents its tapering geometry, with the setbacks recalling traditional Chinese architecture.

Figure 2.1-14 depicts the Malaysian Petronas Towers in Kuala Lumpur. Upon completion in 1999, the tower stood 452 m tall. A skybridge connects the two towers at approximately mid-height. The architectural design was carried out by Cesar Pelli & Associates, whereas the structural engineering firm was Thornton-Tomasetti Engineers.



Figure 2.1-12: Bank of China in Hong Kong [9]



Figure 2.1-13: Jin Mao Tower in Shanghai [9]

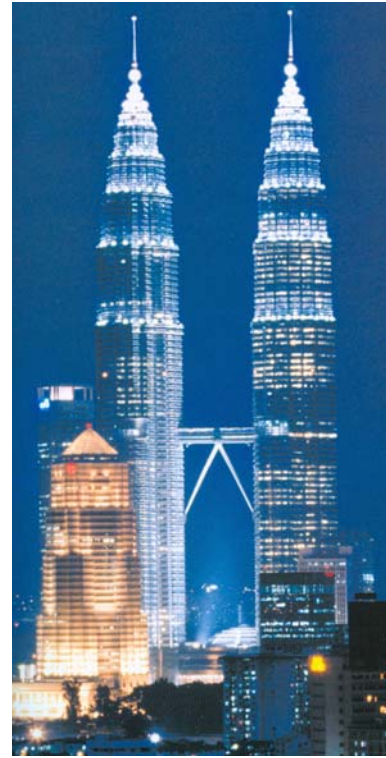


Figure 2.1-14: Petronas Towers in Kuala Lumpur [9]



Figure 2.1-15: Two International Finance Centre in Hong Kong [9]

The 420 m tall Two International Finance Centre in Hong Kong was designed by Cesar Pelli & Associates in collaboration with Ove Arup & Partners as far as the structural design is concerned (figure 2.1-15).

The tallest completed building in the world, at the moment of writing, is Taipei 101 in Taiwan (figure 2.1-16). The building was completed in 2004 and stands 508 m tall. This building was designed by C.Y. Lee & Partners and the structural design was carried out by Thornton-Tomasetti Engineers. The lateral load resisting system consists of a mega structure of corner columns. Another interesting feature is the auxiliary damping device at the top of the building to limit wind-induced motions, see subsection 2.3.2.



Figure 2.1-16: Taipei 101 in Taipei [9]

The next tallest building in the world will be the Burj Dubai Tower, currently under construction, in the United Arab Emirates. The design of this residential building was carried out by SOM and the lateral load system consists of a reinforced concrete so-called buttressed core, as in a tripod-like stance. The spiralling setbacks have been adopted to reduce across-wind building motion. The reader is referred to reference [20] for an interesting paper concerning the wind engineering-design interaction during the design of this building. The exact height has not yet been officially revealed, however SOM engineers have stated that the final height will exceed 800 m. Figure 2.1-17 and 2.1-18 show a rendering of the building and the elevation of the building under construction respectively.



Figure 2.1-17: Burj Dubai rendering [2]



Figure 2.1-18: Burj Dubai under construction [40]

2.1.3 Trends

From the first tall buildings built in the United States during the late 19th century and early 20th century, an accelerating increase of tall buildings can be seen in our modern cities.

The three following figures 2.1-19, 2.1-20 and 2.1-21 are taken from reference [8] and illustrate the trends of the hundred tallest buildings in the world in time regarding height, region and function.

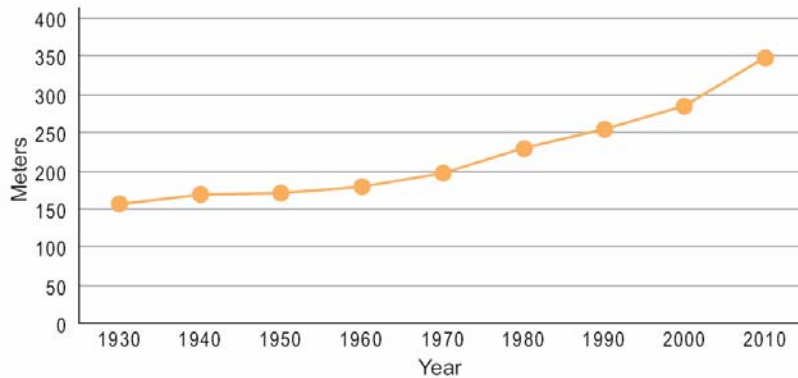


Figure 2.1-19: Mean height of hundred tallest buildings [8]

Figure 2.1-19 shows the mean height of the hundred tallest buildings. Note that the height modestly increases until the Second World War, after which a clear acceleration takes place. We find ourselves at the moment in a period of truly spectacular growth in building height. This is expressed by the 800+ m Burj Dubai Tower and the 1000+ m Nakheel Tower, both currently under construction in Dubai in the United Arab Emirates [37].

Figure 2.1-20 provides a graph of the geographical region of the hundred tallest buildings.

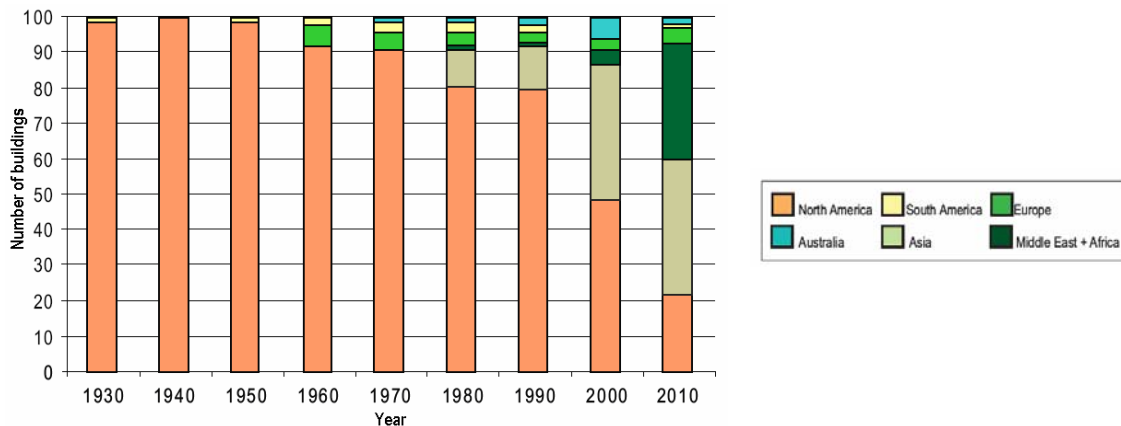


Figure 2.1-20: Hundred tallest buildings by region [8]

The above figure illustrates the shift of the centre of gravity in high-rise construction. North America, traditionally the leading region, is becoming increasingly less important regarding the region of tallest buildings. By 2010, the vast majority of skyscrapers will be located in Asia and the Middle East. Note the rather modest position of Europe when it comes down to high-rise buildings.

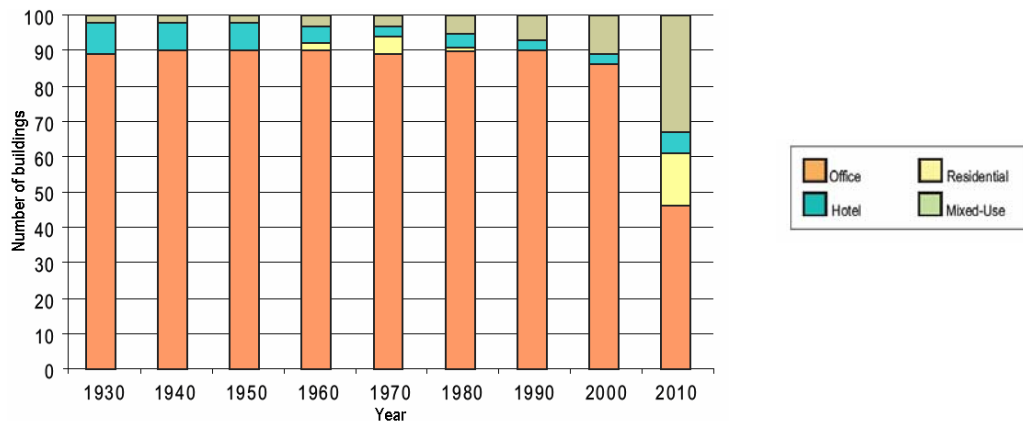


Figure 2.1-21: 100 tallest buildings by function [8]

The trend in time of the function of the tallest buildings is provided in figure 2.1-21. Whereas the main function of tall buildings up to 2000 was to provide office space, the trend towards mixed-use buildings is booming in the last decade.

As far as construction material is concerned, high-rise building structures were predominantly constructed in steel. In the last few decades a tendency towards reinforced concrete or composite structural systems can be observed.

2.2 General design considerations

In the introduction of this chapter it was stated that various aspects of tallness, not typically encountered in low-rise building design, should be addressed during the design of a high-rise building. This section attempts to give an overview of the most significant aspects in tall building design.

High-rise buildings are highly complex buildings. They are designed to accommodate a large number of people, reaching up to the number of inhabitants of medium-size towns, and to provide a safe and comfortable environment. It is impossible, and not within the scope of this thesis, to present a complete and detailed description of all aspects related to tall buildings.

2.2.1 Development and management

First of all, any tall building project constitutes an enormous financial investment. As holds for every investment, investors are interested in obtaining the highest possible yield. Financial feasibility and efficiency are of utmost importance as a consequence of the great capital costs incurred on the purchase or construction of a high-rise building. Many tall building design criteria are derived from financial efficiency considerations. It is not only construction, operation and maintenance costs, but also the financial appraisal of the building's quality in terms of rent or selling price, in time that determines the financial feasibility.

Both the management of quality, time and finance, as well as development of high-rise buildings is treated in this paragraph. The tall building project is hereafter divided in three phases: the design, construction and operation phase.

Design phase

The design is generally carried out by multidisciplinary design teams, due to the high complexity tasks and interlinkage between (traditionally) individual disciplines. Relatively little money is invested notwithstanding the fact that the decisions taken in this phase can have a decisive influence on the final financial feasibility.

Great care has to be taken to design a financially feasible building meeting, of course, all safety requirements. To accomplish the latter, design criteria are drawn up as to measure beforehand different relations between construction costs and revenues, as for example the lettable-to-gross floor area ratio. These design criteria are treated in the paragraph describing the operation phase during which practically all revenues are generated.

Construction phase

The contrary, with regard to investment and influence on financial feasibility, holds for the construction phase. A great amount of money is invested while generally no, or relatively little, income is generated for the developer. In addition, hardly any influence can be exerted at this stage on the financial feasibility. Earnings are generated with tenant occupancy or when building space is being sold.

Reducing the erection period of the project, on one hand, leads to the fact that income is generated sooner. On the other hand, interest paid on the granted credit to cover the construction costs, are cut. Different measures can be taken in order to reduce construction time:

- Making designs that allow an easy and fast erection with preferably high-repetition connections.
- Prefabrication of elements in the largest possible size.
- Just-in-time delivery of construction elements and material.
- Reducing demand of crane capacity.

Operation phase

The operation phase covers by far the largest part of the lifetime of a tall building. The generated cash flow, consisting mainly of revenues through rent and maintenance and operation costs, discounted in time is of utmost importance for the financial feasibility of a tall building project. Important criteria influencing revenues and costs in this phase can be roughly divided in geometrical ratios, maintenance, adaptability and the consumption of resources.

Revenues generated by rent due to tenant occupancy or by the price paid by new owners depend on the lettable floor area. The lettable floor area is the useful floor area

that can be rented by tenants, not including for example the area encompassing building services installations and shafts, structural elements, etc. Furthermore, building codes can prescribe certain minimum labour conditions such as a maximum distance in office buildings between the employee's desk and daylight entrance. Such a prescription exists in the Dutch building code. This has a great influence on the financially efficient building dimensions and therefore, through the structural challenges arising from very slender high-rise designs, on the height of tall buildings in the Netherlands. It is noted that the Spanish building codes do not contain such a prescription for office buildings.

A first financial-feasibility ratio is the lettable-to-gross floor area ratio, being the relation between the rent-generating area and the total constructed area. Secondly, the façade-to-floor area ratio should be mentioned. This ratio relates the relatively high costs of prefabricated and complex facade elements to a measure for the revenue-generating floor area. Façade elements are subjected to high demands with regard to thermal and acoustic insulation, protection from sun, rain and wind, etc because of which they constitute an important part of the total construction costs. Both geometrical ratios are useful tools as to assess beforehand the financial feasibility of the building.

Tall buildings are rather susceptible to maintenance problems, because of their height, complexity and high demands of building services. Often innovative and expensive technology is used in high-rise buildings that has not been tested as thoroughly as traditional building services systems. Therefore designers should thoroughly think through the detailing of the building and the employed technologies to reduce maintenance costs. Durability of materials and construction elements has to be taken into account from the beginning of the design process.

The development of high-rise building projects can only be financially feasible when they are designed to last a long period of time with due consideration of changing demands in the future. Office space is usually rented by different tenants during the lifetime of a tall building. Future changing tenants, as well as existing tenants, are likely to have different desires concerning office layout having effect on partitioning and building services systems and layout. This requires an adaptability in order to be attractive for different tenants and demand changes. The floor plan has to provide a certain flexibility to ensure the building's adaptability. The latter can be accomplished by use of:

- Modular dimensions in the building's structure and finishing.
- Light-weight movable partitions.
- Using suspended ceilings and/or raised floors.
- Reducing the amount and size of vertical load bearing elements.

Building service systems such as heating and cooling, elevators and ICT applications consume a great amount of energy. As a consequence of the concentration of advanced building services systems, tall buildings consume far more energy than traditional buildings. The energy consumption should be reduced as much as possible. This is needed firstly, for simple financial reasons and secondly, because of the global need for sustainability. A large part of the energy demand is covered by -depending on the local climate conditions- heating or cooling which illustrates the great importance of thermal insulation characteristics of curtain wall facades. Ingenious systems have been designed to reduce energy consumption, for example by using the outgoing office ventilation to reduce heat transfer between a double-skin façade and the interior or by

recycling or renewable energy. Solar energy can be used to partly cover the building's energy consumption by means of photo-voltaic façade elements. Recently, buildings have been designed (Bahrain World Trade Center for instance, see reference [32]) with wind turbines attached to the building in order to take advantage of high steady winds at great heights and the local flow acceleration caused by the building.

2.2.2 Architecture and urban development

Raison d'être

As has been stated before, the Industrial Revolution and the invention of the safe power elevator constituted the necessary conditions for the construction of modern skyscrapers. However, the *raison d'être* of tall buildings is harder to univocally define.

Some state that high-rise construction is the solution to urban density, while others point out the highly stimulating effect of tall buildings on urban density. The latter is predominantly caused by rising land prices in dense urban areas, because of which it becomes financially interesting to create vertically stacked buildings (in case the land price is only depending on land area and not, as occurs in some countries, on total constructed floor area).

Tall buildings consume far more energy than traditional buildings, particularly because of its intrinsic verticality and the relatively poor heat-insulation performance of curtain walls. Nevertheless, some people suggest that a conceptually vertical city with high-rise buildings is far more energy efficient than the traditional horizontal urban development. The concentration of human activity would highly reduce the need for horizontal transport and, as a consequence, transportation means and infrastructure.

Geographical limitations can play an important role in large-scale tall building development. For example the Manhattan-district in New York is bound by the Hudson River and Chicago by Lake Michigan.

Looking at the development of high-rise construction around the world, in relation to the local geographical and urban development conditions, it can be tentatively stated that the only *real* reason is the need for a simple statement of power. It concerns a corporate symbol of financial power for the typical North American skyscrapers. Individual tall building structures can even become a cultural power symbol as was the case for the World Trade Center twin towers in New York. Economic power is expressed by the modern high-rise buildings in the Middle East and Far East.

Social and environmental effects

A few isolated tall buildings within a mainly horizontal city can radiate an aura of superiority and therefore emphasize social and financial differences. Inhabitants can feel repelled by tall buildings due to this overlooking effect, whereas to others it can represent the start of a financially prosperous period.

It seems there is no clean-cut answer to the question whether high-rise construction is good or bad, nice or ugly. This may well be the reason that the appearance and social effects of tall buildings sometimes become a society-broad discussion and not only a topic that architects and urban planners discuss about.

Tall buildings can cause strong and uncomfortable winds on street level and therefore pose a problem to pedestrians.

A tall building constitutes a sudden and drastic intrusion in the urban and social landscape, of which the social and environmental desirability has to be considered with great caution.

Design

Designing a well functioning tall building is a very complex task. The building's primary characteristic is the vertical division of building space making vertical transport of people and services a governing design criterion. High-density buildings require sound transportation solutions inside and outside the building, without which the building will most likely become a failure.

Building floors have large openings to allow for vertical transport shafts. The amount of space that is required by the shafts is very dependent of the use, or different uses, of the building. Office buildings require high-capacity transport of people on fixed moments on the day while heating and cooling services, of course depending on the number of tenants, can be controlled centrally. Residential buildings generally require individually controllable units as far as building services are concerned and elevator demand will be more flattened out throughout the day. In mixed-use buildings different functions will require independent elevators and building services possibly increasing the area covered by service shafts and ducts. It is important to limit this vertical and horizontal area in design, because it reduces the profitable lettable building area.

It is desirable that architects and urban planners incorporate specialist information from a multidisciplinary design team from an early stage of the tall building design or urban planning.

2.2.3 Building services and façade

A building has to provide a safe and comfortable environment. Building services comprise everything between such an environment and a mere shelter, and they typically include:

- Vertical and horizontal transport.
- Heating, ventilation and air-conditioning (HVAC).
- Natural and artificial lightning.
- Energy and water supply (as well as waste water subtraction).
- Communication networks.
- Fire detection and protection.
- Security and alarm systems.

The building's façade firstly constitutes a barrier between the internal and external environment, as to protect the internal environment from rain, wind, and extreme temperatures. Curtain wall facades, usually adopted as cladding in modern tall buildings, in time have become more complex elements. Often they play an important role in one or more of the above listed building services. Because of this, the façade is treated in this subsection together with building service systems.

Vertical and horizontal transport

Vertical and horizontal transport of people and building services (cables and ducts) is of utmost importance in tall building design.

The vertical transport of people and services require openings in floors and the shafts they require are generally centrally grouped. These groups of transport and services shafts are often enveloped by a structural core, as to provide for structural stiffness and strength. The required openings in floors pose a danger for the financial viability of high-rise construction because they limit the rentable floor area. Therefore, the area occupied by vertical shafts should be limited as much as possible though satisfying the vertical transport capacity requirements.

Especially safe and fast vertical transport of people by means of elevators is of vital importance to the well-functioning of a tall building. The average waiting time of high-rise users is determined by the type, number and arrangement of elevator cars. The car size, velocity and (braking) acceleration can be increased shortening the average waiting time. Note that the velocity and acceleration are to a certain extent bounded by physical limits; high car velocities produce annoying ear popping-effects, whereas an excessive acceleration can cause nausea. In addition, it is believed that the elevator arrangement determines to a greater extent the time- and space-efficiency of elevator systems. Below some elevator arrangements are discussed.

Group operation

In this elevator arrangement a separate shaft is still needed for each elevator. The difference with a normal, basic arrangement is that each elevator or elevator group only serves a certain range of floors. For example in a 60-storey building one group serves from the entrance level to storey 20, another group from level 20 to 40 and so on. Each elevator group has to overlap at least one floor with the succeeding one to allow transfers. The advantage of this system is that the number of shafts, and therefore area of floor openings, decreases with height. A group-operation elevator system is illustrated in figure 2.2-1.

Sky-lobby

This elevator arrangement is based on large and fast shuttle or express elevators serving a small number of central change-over floors called sky-lobbies. Each sky-lobby serves a unit of local individual or group-operated elevators, in turn serving all floors in between sky-lobbies. In this way the vertical transport consists of a number of identical, vertically stacked, elevator units. This system highly diminishes the mean

passenger waiting time, because of which it requires far less elevator shafts than grouped-operation elevator systems. The above was first incorporated in the vertical transportation system of the World Trade Center Towers in New York, shown in figure 2.2-2. The superimposing of local elevators on the same vertical axis of the sky-lobby concept offers unlimited possibilities in terms of building height.

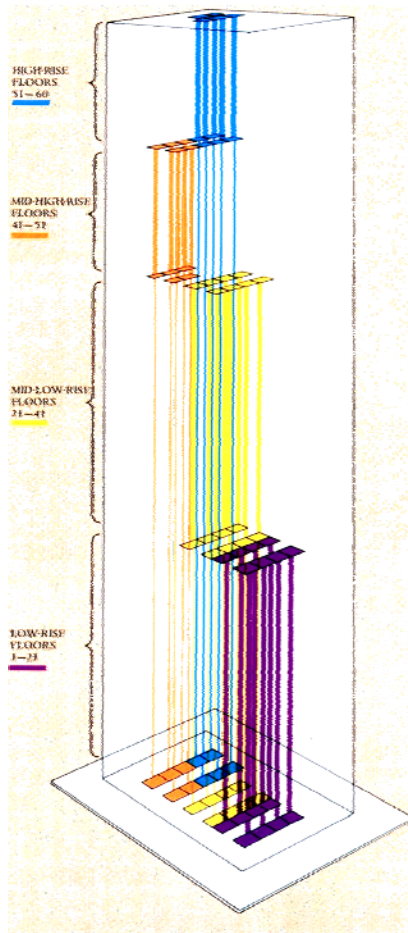


Figure 2.2-1: Grouped-operation elevator system [9]

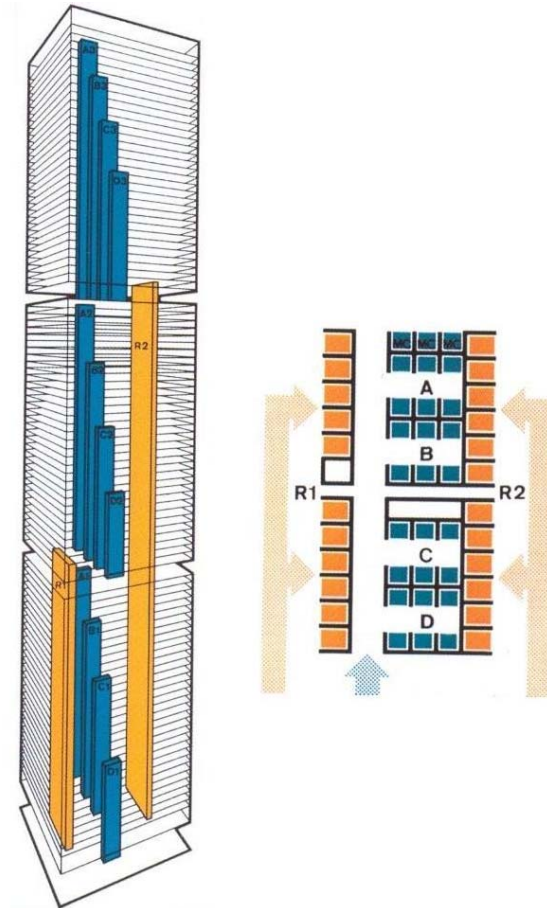


Figure 2.2-2: Sky-lobby elevator system [9]

Double-deck elevators

Using double-deck elevators is another means of saving lettable floor area by reducing the number of elevator trips, and thus reducing the amount of needed elevator shafts. The system, as depicted in figure 2.2-3, consists of a double-deck car serving simultaneously odd and even floors. Taipei 101 combines the sky-lobby arrangement with double-deck elevator cars.

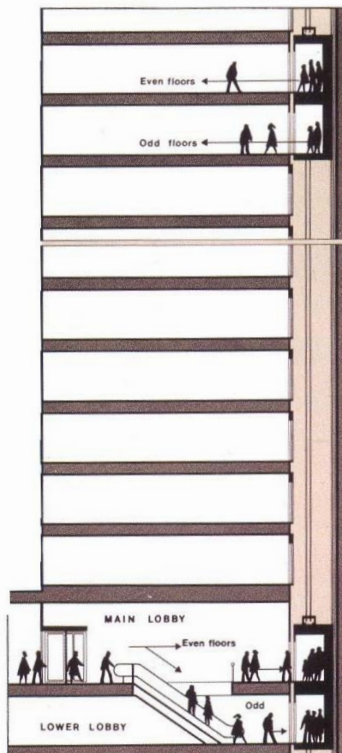


Figure 2.2-3: Double-deck elevator [9]

Building services

All building services need their own (vertical and horizontal) cables and ducts to provide access to each part of the building. Especially communication systems, in modern ICT-controlled times, require vast and complex cabling and ducting.

To allow future changes in the horizontal distribution of building services, often false or technical floors (raised) and ceilings (suspended) are used in tall buildings.

Because of safety and cost considerations, it is not desirable to use high-pressure water ducts and high-voltage electricity cables in high-rise buildings. Therefore, vertically arranged distribution centres are located throughout the building height. These distribution centres are called mechanical or building services levels and typically occupy the entire floor and are one or two storeys high. Mechanical levels are not subjected to typical tenant space demands making them extremely useful to accommodate structural systems such as outriggers or belt structures (subsection 2.4.6).

Façade

The façade constitutes the principal enclosure of a building. Its primary goal is the protection of the internal environment from undesired external influences like wind, water, and extreme temperatures.

The separation of the structural skeleton and the façade has led to the widely-used curtain wall systems in high-rise construction. Due to the relatively low thermal insulation of glass, glass curtain walls play a very important role in the building's energy consumption with regard to heating and/or cooling (depending on the climatologic conditions).

Modern high-rise façade elements are storey-high prefabricated elements that are hoisted on site and inserted between two structural floors. This prefabrication has led to improved quality control, on-site safety and construction economy.

The tall building facade and their fixings to the structure have to meet more stringent requirements than traditional building façade:

- Thermal insulation of glass curtain walls is of key importance to reduce the large energy demand of tall buildings.
- High local wind velocities impose important water and air tightness demands, and induce high suction forces.

- Dimensional tolerances are considerable due to the building's inherent flexibility.
- Replacement or repair of non-fulfilling façade elements is expensive due to the limited access at great heights.
- The structural fixing to the structure deserves special consideration because of the danger of falling façade elements.

2.2.4 Structure

Gravitational loads and their effect on vertical load resisting systems, that is horizontal members, have been quite thoroughly studied and are currently well understood. Nevertheless, the high vertical forces in tall buildings do bring along some specific design problems such as the P-delta effect, differential shortening between vertical elements and temperature effects. These topics are treated more in-depth in section 2.3. The high-rise industry has been a driving force, because of the elevated vertical forces and the general architectural desire of transparency, behind the development of high resistant concrete and steel.

Gravity load constitutes the governing design load in fundamental load combinations for normal non-slender buildings, i.e. with a small aspect ratio (height divided by in-plan dimension). In general, if normal building structures are designed to resist the gravity loads with due eccentricities, it is not a problem to provide sufficient lateral stiffness. The building's *tallness* affects the structural design in the sense that the governing design load becomes a horizontal load: the wind action or earthquake-induced inertial forces. The nature of these horizontal actions is highly dynamic, whereas gravity loads can be treated as static as far as the global structure is concerned (i.e. live loads on flexible floor structures, for instance, should be considered as dynamic loads).

Wind is an important design parameter for every tall building, while the seismic risk depends especially on local geological conditions. Wind can pose a special danger to high-rise building in hurricane-prone regions.

The wind flow exerts a pressure or suction on the building surface that is proportional to the square root of the wind velocity. At the stagnation point on the leeward face of the structure, where the wind flow is completely blocked, the imposed wind pressure equals the dynamic wind pressure at that height:

$$q_w = \frac{1}{2} \cdot \rho \cdot v^2 \quad (2.1.1)$$

where q_w wind pressure [Pa]
 ρ air density [kg/m³]
 v wind velocity [m/s]

The wind velocity variation with height is described by a logarithmic law, as explained in chapter 3.

Let us consider a cantilever subjected to a steady state wind pressure being constant along the height. It is known from fundamental mechanics that the shear in the structure is proportional to $q_w \cdot h$ and the bending moment to $q_w \cdot h^2$ being the first

term the wind-exerted pressure and the right-hand side term the cantilever height. Gravitational forces are roughly proportional to h . The above shows the increasing importance with height of the wind action compared to the gravity load. The top deflection of a flexural, i.e. with infinite shear stiffness, cantilever depends on $q_w \cdot h^4$. This simply illustrates that with increasing height, serviceability limit state considerations become more important than ultimate limit state design considerations. The main structural design challenge for tall buildings is to meet the lateral stiffness and strength requirements.

The serviceability limit states encompass, as far as the wind action is concerned, limitations for lateral building displacements and human motion perception. Especially the latter has received growing attention from the 70's and still much research is needed, since consensus does not seem to exist in the international community concerning human motion perception criteria. More detailed information is provided in subsection 2.3.2.

2.2.5 Construction

The verticality of high-rise buildings makes the vertical transport crucial during the operation and construction phase. During erection, the vertical transport of building material and personnel is of great importance. Construction sites are often located in very dense urban area, limiting the available work space and storage area. Planning all the different construction works on limited construction sites is a very complex task.

On a small tall building site, crane capacity is usually low while the demand is very high. It is important to consider this when designing the structural and erection system. Building elements are preferably made and assembled in a factory for better quality control and to limit on-site handling. Just-in-time delivery is desirable to let transportation vehicles occupy the construction site for the smallest period of time. The construction crew, and all rebars and formwork, has to be ready when the concrete delivery takes place. Concrete pumps and ducts are increasingly subjected to great internal pressures with increasing building heights.

More stringent safety requirements are to be met than for traditional construction. Working at great heights strongly increases risks for both people working inside the building as people below on the construction site. Falling elements pose an extreme hazard for workers involved in tall building construction.

2.2.6 Fire engineering

Fire constitutes an extraordinary risk, in terms of human life and property loss, during both construction and operation phase of all buildings. However in tall buildings it poses an even greater hazard because of the following reasons:

- A great amount of combustible materials is present in typical tall buildings, like furniture, carpeting, paper and kilometres of communication, electrical and air-conditioning wiring running vertically and horizontally through the building. Furthermore, these burning materials fill the environment with toxic gasses.

- Typical high-rise skeleton structures instead of traditional massive walls facilitate the horizontal spread of fire, smoke and toxic gasses.
- Atriums, chimney-type stairwells and elevator shafts, not duly sealed ducts, etc. allow smoke and toxic gasses to travel to higher floors.
- After a certain time the breaking of glass curtain walls causes the fire to travel upwards from floor to floor.
- Due to the vertical arrangement of high-rise buildings, it is likely for people to find themselves trapped between the roof and the seat of the fire.
- The time between the start and extinction of a fire, as well as the evacuation time, is higher mainly because of the fact that fire fighters and occupants have to climb / descend a great number of flights of stairs.

To prevent the spread of fire, smoke and toxic gasses, a good fire compartmentation is critical. Furthermore, staircases and shafts may be pressurised to prevent smoke from entering.

Fire- and smoke-free floors have to be incorporated in the design, for trapped people to find a safe temporary shelter until the entire building can be evacuated. These fire-safe zones are especially important for people with reduced mobility (elderly and handicapped).

Several measures can be taken to decrease the time between the start of a fire and the fire extinction and evacuation:

- Smoke and heat detectors, preferably connected to a central alarm system indicating the location of the fire.
- Heat-activated automatic sprinkler systems.
- Manual fire extinguishers available at each floor and education of occupants regarding fire safety.
- Pressurised staircases facilitate the evacuation of the building as well as the ascending of fire fighters.
- Well-marked fire exits and escape routes.
- Decreasing the in-plan distances to fire exits.

With regard to sprinkler systems, the U.S. National Fire Protection Association states in reference [30] that the death rate is 57% lower for properties with a sprinkler system included in comparison to buildings not including such a system. In addition, the property loss for most building functions is lowered by one-third to two-thirds.

To ensure a complete building evacuation, the building structures must not collapse for a certain period of time (laid down in national building codes). This period of time normally depends on the building height, building function as well as the nature and amount of combustible materials inside the building.

Because of the above discussed fire safety-aggravating aspects, high-rise structures generally have to meet a period of fire-resistance of 120 min or more. Steel loses an important part of its resistance and modulus of elasticity for normal fire temperatures. Therefore, all steel structures have to be protected from extreme heat by, for instance, a fire resistant coating or encasement. A cheap and often applied solution is a concrete encasement for steel columns and a sprayed layer of mortar for beams and metal sheet floors. For reinforced concrete elements it is important that the extreme heat of the fire cannot reach the mild steel rebars. Regarding concrete members, the application of a greater concrete rebar cover and/or increasing the amount of reinforcement suffices to meet the fire-resistance requirements.



Figure 2.2-4: Fire in Torre Windsor in Madrid [17]

Figure 2.2-4 shows the fire raging in Torre Windsor in Madrid. This fire occurred on February 12th of 2005 and led to the partial collapse of the building, completely ruining the rest of the building. Luckily no people were inside the building at the moment of the fire, so there were no casualties reported.

2.3 Structural design considerations

The structural design of tall buildings is characterised by other problems than traditional building design, as pointed out in 2.2.4. This section deals with the main structural challenges, along the distinction between static or dynamic actions.

2.3.1 Static loads

Static loads mainly consist of gravity loads, being composed of:

- Dead loads; time-independent own weight of all structural and non-structural elements.
- Live loads: time-dependent loads derived from occupancy (people, machines, furniture, etc.).

Note that live loads are classified as static loads in the above enumeration, although it is actually a dynamic load due to its time-dependent nature. However, it usually does not cause significant acceleration of the structure or structural elements.

Differential shortening

In a typical tall building, the elevator and building services shafts are centrally grouped for floor efficiency reasons. In many cases these shafts are enclosed by a reinforced or steel structural core. A horizontal floor structure spans between the structural core and the perimeter columns.

The forces acting on the core are small in relation to its tributary area, due to the fact that the inner-core floors are typically perforated by vertical shafts. The columns bear half the span of the floor structure and façade elements. The preceding is illustrated on the left-hand side of figure 2-3.1.

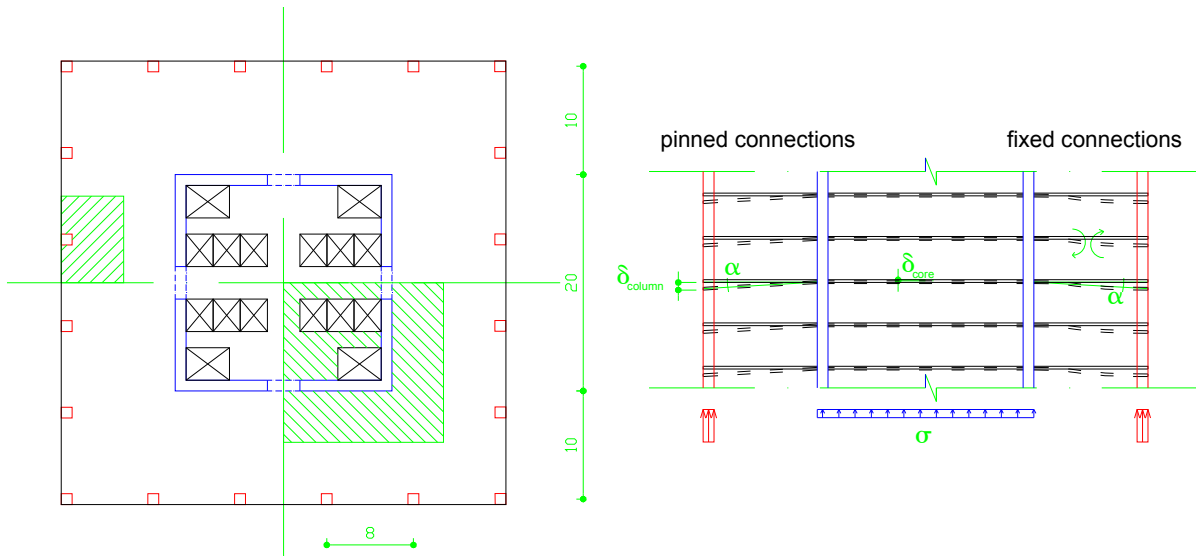


Figure 2.3-1: Differential shortening in horizontal and vertical section

Transparency of the floor plan is often desired by tenants and architects. For that reason columns are designed to have small cross-sectional dimensions. The core structure is, on one hand, not limited by architectural requirements as far as its in-plan dimensions are concerned. On the other hand, the core—being the main lateral load resisting element—often requires a greater moment of inertia and area. The above results in higher stresses in columns compared to the core in the quasi-permanent gravity load combination.

This difference in stress level and therefore, according to Hooke's law $\sigma = \varepsilon \cdot E$ and assuming an equal modulus of elasticity E , the elastic strain causing differential shortening between core and columns.

Because of the aforementioned reasons, as far as the perimeter columns are concerned, a tendency exists towards the application of materials with increasing strength characteristics. For both steel and concrete reinforced columns, this means a worsening of the differential shortening-induced problems. It is true that an increase of the concrete compressive strength comes along with an increasing modulus of elasticity, as is shown in subsection 5.1.2. The area reduction of the columns is approximately proportional to the increase in strength, whereas the modulus of elasticity is proportional to the cubic root of the compressive strength, because of which a net negative effect results.

Differential shortening between perimeter columns and core can lead to a noticeable floor inclination, as can be seen in figure 2-2.1. If this effect is not duly considered, important serviceability and structural problems can occur. Firstly, serviceability criteria

require the floors to be levelled as to create no problems in interior finishes. These problems can include for instance doors that cannot be properly closed, cracks in partitioning walls, etc. Secondly, structural problems can arise when the floor structure has a great flexural stiffness and is fixed to the core. It causes the perimeter columns to be suspended from the core through the floor structure. The calculation of the horizontal structure has to account for the additional bending moment.

Elastic shortening of columns and core can be easily calculated by means of the elastic strain in the above presented expression of Hooke. The manufacturing of steel elements has very small dimensional tolerances and the deformation of steel columns is limited to the elastic deformation. Because of this, the expected shortening of steel columns can be easily compensated by simply producing the columns with a height that is some millimetres greater than after the building occupancy. The casting of concrete columns has dimensional tolerances being too large to compensate shortenings in the order of millimetres. More significant is the time-dependent behaviour of concrete which induces plastic deformations due to creep and shrinkage. Concrete column shortening due to creep and shrinkage are harder to recuperate completely because of their time-dependent nature.

P-delta effect

Whereas columns with a small aspect ratio fail by crushing or yielding of the material, a slender column fails by bending due to the P-delta effect. Pure buckling instability, i.e.

failure according to Euler's expression for the critical buckling load $F_c = \frac{2\pi \cdot EI}{l^2}$, is not

likely to occur. In building structures it is usually the P-delta effect due to eccentricities that governs the failure of slender columns. The calculation of P-delta effects is an iterative process in which a horizontal displacement, caused by an initial misalignment or horizontal load, causes an increasing eccentricity of the gravity load. The eccentricity of the gravity loads is equilibrated by an internal moment increasing the horizontal displacement and again the eccentricity of the gravity load (delta and P), etc. This process continues until the compression member is in equilibrium or collapses.

All compression members should be designed with due account for P-delta effects. The global tall building structure can also be considered as a compression member with initial eccentricities. The P-delta effect causes second order moments and displacements that can affect the dimensions of structural members.

A P-delta analysis should consider the rotational flexibility of the foundation and, in the case of ultimate limit state calculations, the mechanical properties of elements in the deformed stage. This means for concrete members that concrete cracking has to be considered by the moment of inertia corresponding to the cracked section in the equilibrium stage, i.e. at the end of the iterative P-delta calculation. Note that torsional P-delta effects can be considerable for buildings with small rotational stiffness.

Creep, shrinkage and temperature effects

As has been pointed out above, creep and shrinkage are time-dependent deformations associated with concrete elements.

Shrinkage is a time-dependent decrease in concrete volume compared with the original placement volume of concrete. The total shrinkage is composed of plastic and drying shrinkage, with the former occurring in the plastic concrete phase directly after it has been cast. The latter results from moisture exchange between the concrete element and the environment after initial hardening.

Creep depends for a given concrete mixture mainly on the loading history and applied stress. An important characteristic is that concrete elements at an early age present far greater creep deformations than when older concrete is loaded.

In the structural design of normal buildings, creep, shrinkage and temperature effects are usually only considered in horizontal sense. Strains in vertical elements in tall buildings can, however, lead to significant shortenings or elongations. Shrinkage and creep-induced shortening of tall concrete columns can be in the order of several centimetres. Both effects should be considered in tall building designs, especially in relation to the fixings of building services to the structure. The possibility of differential vertical movements should be provided for as far as the fixings of vertical building services to the structure are concerned. A case is known where horizontal sanitation ducts, cast within a massive concrete slab and fixed to the vertical duct, broke out of the concrete floor slab simply pushing off the concrete topping, due to time-dependent shortening of concrete supports.

Temperature differences cause strains in elements, proportional to the coefficient of thermal expansion α times the temperature difference. For elements with large dimensions, temperature effects can become governing. For instance thick foundation slabs may have to be poured in several layers in order to limit the concrete temperatures and thus the restrained movements. Extra attention has to be paid to temperature effects when the structure is located outside the building. A large temperature difference between exterior structural elements and the interior structural elements can occur. It is not only air temperature differences causing this problem, but also heating by solar radiation plays an important role.

2.3.2 Dynamic loads

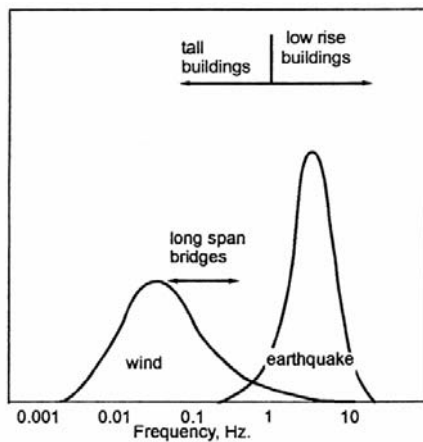


Figure 2.3-2: Spectral density of wind and earthquake action

A dynamic load is a load of which the magnitude, direction, or position varies with time. Dynamic actions of interest to tall building structures are wind and seismic action.

The exciting dynamic force can be thought of as a superposition of short-term and long-term waves with different amplitudes. Figure 2-3.2 shows the spectral density functions of the wind action and earthquake-induced inertial forces. The peaks correspond to the part of the spectra containing the highest energy, i.e. most frequently occurring frequencies of the respective action.

The wind load spectral density function shows a peak at low frequencies, whereas the earthquake spectral density has its peak at far higher frequencies.

The latter is an important observation since the natural frequencies of tall buildings are relatively close to the low-frequency wind load range while low-rise buildings have natural frequencies that are generally close to the peak of the earthquake frequency range.

The natural frequency of a structure is the frequency of its free or natural vibration, i.e. the steady-state undamped vibration after an initial excitation. For a simple mass-spring system the frequency yields

$$f = \frac{1}{2\pi} \sqrt{\frac{k}{m}} \quad (2.3.1)$$

where f is the natural frequency in Hz and k and m are the stiffness and mass respectively. With expression (2.3.1) it can easily be understood that low-rise buildings generally have high natural frequencies, while tall flexible buildings are characterised by low natural frequencies. Resonance occurs when the frequency of excitation is close to a system's natural frequency.

Therefore low-rise buildings are more susceptible to earthquake-induced loads than to wind loads. The wind pressure acts on the stiff building as if it were a static load; the building has a great inertia impeding any resonance interaction with the low-frequency wind gusts.

Although tall buildings are more flexible and therefore further away from the peak in the spectral density function of earthquakes, they are susceptible to the low-frequency range of seismic action. Wind action poses a special hazard for all tall buildings, since their fundamental frequencies move towards the wind-spectrum peak with higher flexibility.

The tendency in high-rise design is towards buildings with greater heights, built with higher strength materials. The initial tall buildings constructed in the late 19th and early 20th century contained very stiff masonry partitions and façades representing a large part of the total building stiffness and damping. Because of this, the susceptibility of tall buildings to wind action has become of increasing importance.

Wind action

The wind action is the principal load that the case study, incorporated in this thesis, is focussed on. Because of this, chapter 3 is specifically dedicated to wind and wind-induced building response and the reader is referred to this chapter for an in-depth description of wind action.

The wind action is generally treated as a quasi-static load in structural engineering. A quasi-static approach of the wind load consists of applying static loads in static model which are multiplied by factors accounting for the dynamic behaviour of both action and response.

For low-rise buildings, a full static approach using peak dynamic wind pressures yields conservative results, because of their high natural frequencies. Tall building design should always account for an assessment of the dynamic susceptibility to wind gusts, because resonance between wind gusts and the structure's free vibrations can considerably amplify the building response.

Wind pressure increases with building height and decreases with the roughness of the building's surrounding. Large, nearby located structures can accelerate the local air flow hence increasing the wind-exerted pressures on the building surface. Local wind pressures do not present any resonance with façade elements. Nevertheless, the determination of reliable local wind pressure and suction is very important for the structural calculation of façade elements, such as glazing, and fixings. Wind suction is especially high near building discontinuities such as corners and roofs.

A classic example of wind-induced problems is the John Hancock Tower in Boston [40]; glass façade panes detached of the building and crashed on the sidewalk and nauseating sways have been reported for rather moderate wind velocities, causing to enormous financial damage.

Wind-induced lateral building displacements and vibrations, as well as proposed limits, are treated hereafter.

Seismic action

The earth's superficial crust located above the molten mantle is composed of more or less a dozen of large plates and several smaller ones. These plates are continuously moving and their motion creates volcanoes, mountains and earthquakes.

When tectonic plates are moving one over another, strains and stresses are built up within the rock of which the plates are made of. At some point, stresses become too high causing either the rock to break or slippage due to the fact that the built-up stresses exceed the friction between the plates. In both cases, the accumulated strain

energy is suddenly released and propagates in all directions in a series of shock waves. The earth's motions caused by these shock waves can last a couple of seconds to even minutes for large earthquakes. Seismographs measure earthquake intensity in terms of accelerations in the horizontal and vertical directions. Figure 2.3-3 provides a ground acceleration record of El Centro, California.

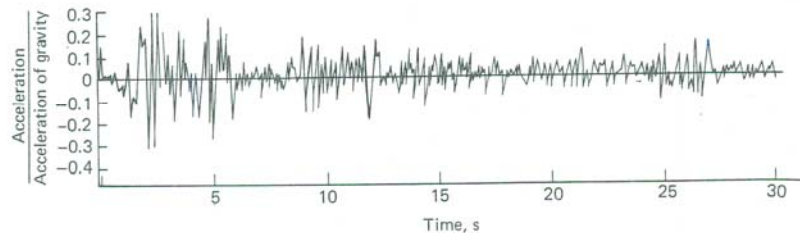


Figure 2.3-3: Ground acceleration record at El Centro, California [35]

The earth's acceleration causes inertial forces in structures. These inertial forces act in both horizontal and vertical direction. The earthquake-induced vertical forces are usually not considered, since usually the structure will have enough redundancy to resist these forces. However horizontal inertial forces do have a great impact on buildings.

Buildings cannot be economically designed to withstand major earthquakes without damage. Therefore, earthquake-resistant design is based on resisting minor earthquakes without damage. While moderate earthquakes should not produce any structural damage, non-structural damage is accepted. In case of very strong ground shaking non-structural and structural damage is accepted but collapse should be prevented.

Building deformation dissipates energy of the induced ground accelerations. Furthermore, tall buildings are characterised by low-frequency natural vibrations that are quite far away from the spectral peak of earthquake-induced ground accelerations. Thus, in general a tall flexible building would experience much less inertial forces than stiff, low-rise buildings. Nevertheless, earthquake ground motion is highly irregular and composed of low- and high-frequency components. The low-frequency components of ground acceleration can pose a danger for tall buildings, when they act for a prolonged time and they are close to the building's natural frequency.

In general, the intensity of ground motion decreases with the distance to the earthquake's epicentre. The reduction of ground motion occurs at a lower rate for low-frequency components than it does for high-frequency components. This means that tall buildings are susceptible to the long-term components of ground motion from a larger distance than low-rise buildings are for short-term components.

The resulting response, i.e. the corresponding horizontal inertia forces, of earthquakes on tall buildings depends on ground acceleration, local soil characteristics and the building characteristics in terms of mass, stiffness and damping.

Figure 2.3-4 shows the seismic map of Spain, providing the basic ground accelerations. Note that a basic ground acceleration of less than 0,04 g is attributed to

Madrid. According to Eurocode 8 [14] such a zone is classified as having a very low seismicity for which earthquake-induced actions will not have to be considered.



Figure 2.3-4: Spanish map of seismic activity [28]

Lateral building displacements

As far as the ultimate limit state is concerned, building displacements due to horizontal loads must be limited to prevent collapse due to P-delta effects. In the serviceability limit state, the lateral displacements are to be limited to prevent damage to or malfunctioning of non-structural components such as cladding on the building façade, partitions and interior finishes (doors, elevators, etc.). These problems in non-structural elements are caused by inter-storey drift.

No universally adopted criterion exists with regard to the lateral displacement limit in the serviceability limit state. Nevertheless, values of the inter-storey drift of up to $H/400$ are normally considered as acceptable. In order to avoid an exhaustive calculation of all storey displacements, usually a global drift criterion is adopted with a limit of $H/500$, where H refers to the building height. Note that the overall drift criterion can be more or less conservative depending on the displacement diagram, i.e. whether the displacement diagram is shear or bending-dominated. The aforementioned global and inter-storey drift criteria have been adopted in the structural analyses presented in chapter 5.

Human comfort criteria

First of all, it is noted that no consensus has been reached yet among structural engineers concerning rational comfort criteria to limit human motion perception.

The perception of oscillatory motion in resonating tall building structures can cause serious comfort issues to their occupants, such as concern about the quality and integrity of the structure, anxiety, fear, nausea and sickness. Human motion perception thresholds vary strongly from person to person depending mainly on:

- Frequency of oscillation.
- Physiological factors: body orientation, posture and movement.
- Psychological factors: expectancy of movement, comments by other occupants as well as audio and visual cues.

The frequency dependence of motion perception thresholds is not universally accepted. Reference [21] claims complete frequency independence. In the following, a brief summary is presented of the research on human motion perception.

Research

Traditionally, research has been focussed on experiencing body forces as a result of the induced accelerations. This is in contrast to the frequency dependence reported in many studies suggesting that human motion perception is influenced by the rate of change of the acceleration (so-called jerk).

Proposed human motion perception thresholds have, historically, been based on the reactions of people subjected to so-called moving room experiments. The moving room experiment consists of an acoustically and visually insulated motion simulator, excited by a uni-axial sinusoidal motion. Important early studies of this type were carried out by Chen and Robertson [6] and Irwin [19]. In both studies, a frequency dependence of perception thresholds was found: the human perception thresholds in terms of acceleration increases with decreasing frequency.

However, the above reported moving room experiments do not correspond to the real situation of tall buildings vibrating under natural wind excitation because of the following:

- The resonance of tall buildings with along-wind turbulence results in a narrow-band random motion instead of a sinusoidal motion. The peak factor, being the relation between the peak and root-mean-square (rms) value of the acceleration, is not the same for a sinusoidal and random motion. Hereafter, in the discussion of rms or peak accelerations the importance of this difference is demonstrated.
- The real tall building motion is a spatial combination of two translational and a rotational movement instead of a uni-axial one. First of all, in-plan rotation obviously intensifies the resulting horizontal acceleration in the neighbourhood of the building corners. In addition, a more important effect is that humans are especially sensitive to motion when they notice a rotation of the horizon (visual cue).

- Psychological factors are not accounted for; people do usually not expect the motion and the adverse effect of comments by other occupants is not considered.
- Audio and visual cues are not taken into account; the noise of the wind, cracking of the structure and the aforementioned effect of a rotating horizon.

Especially the psychological factors are very subjective. Hansen et al. [15] were the first to investigate subjective reactions to real tall building motion. After two wind storms in 1971, they performed a survey among occupants of two buildings and asked them with what recurrence they would accept such building movements. Furthermore, they asked to several prominent building owners and one competent engineer: *“What percentage of the top one-third of the building can object to the sway motion every year without seriously affecting your renting program?”* From these results they considered that 2% was a reasonable limit. This in combination with the measured and calculated top-floor accelerations of the two considered buildings led to the proposal to limit the 6-year rms accelerations to 0,005 g.

Two other researchers combined the work of Hansen et al. with already established perception threshold criteria to propose new comfort criteria [3]. Irwin, on one hand, simply calibrated his motion perception thresholds, maintaining the frequency dependence, through the mentioned comfort criterion. A slight adjustment was made to use a 5-year interval instead of the 6-year interval adopted by Hansen et al. This proposal was later converted into the ISO 6897 guidelines [18]. On the other hand, Davenport proposed a 2- and 10-percentile comfort criteria curve relating acceleration to recurrence interval, without frequency dependence. These curves were drawn to agree with Hansen’s criteria and the 2% and 10% motion thresholds proposed by Chen and Robertson. Davenport’s comfort curves finally developed into the criteria adopted by the Boundary Layer Wind Tunnel Laboratory (BLWTL) of the University of Western Ontario.

Vibration perception tests have been conducted by Tamura et al. [34] for a wide range of frequencies from low-rise to high-rise buildings. The effect of random elliptical building motion has also been considered in the performed experiments. After a probabilistic analysis of the results, human motion perception thresholds are presented for different percentiles of the population objecting to the motion for the frequency range 0,125 Hz - 6,0 Hz. Important findings of this study are that there existed no significant difference in thresholds between sinusoidal and random motion, and that the frequency dependency of motion perception thresholds is weaker for random for random motion than for sinusoidal motion. This work carried out by Tamura et al. served as a basis for the Guidelines for the Evaluation of Habitability to Building Vibration of the Architectural Institute of Japan (AIJ).

Peak or root-mean-square acceleration

The majority of research results have been presented in terms of the rms acceleration. Nevertheless, no consensus exists in the international community concerning peak or rms accelerations.

On one hand, motion-induced discomfort can be the result of a sustained phenomenon, best described by an averaged effect over a period of time. The rms value constitutes a representation of this time-averaged effect, i.e. the intensity of acceleration. It is argued

by Irwin [19] that: "During the peaks of wind storms, accelerations much in excess of the suggested average magnitudes will occur for short periods but these higher levels, briefly experienced, are not considered to have any great contribution to the memory of the storm.... Short periods of higher acceleration which occur during the worst 10 minutes of the storm occurrence are accounted for in the r.m.s. value of the vibration of the structure of a storm peak."

On the other hand, researchers claim that people are affected most by the largest peak of vibration and tend to forget less-than-peak vibrations.

Guidelines

Reference [33] provides upper bounds for peak acceleration for different perception and hindrance levels, as a function of the period of vibration (figure 2.3-5). The letters A, B, C and D correspond to the perception threshold, desk work and psychological limit, ambulatory limit and building motion limit respectively. The numbers correspond to the different perception levels defined in the table on the right-hand side.

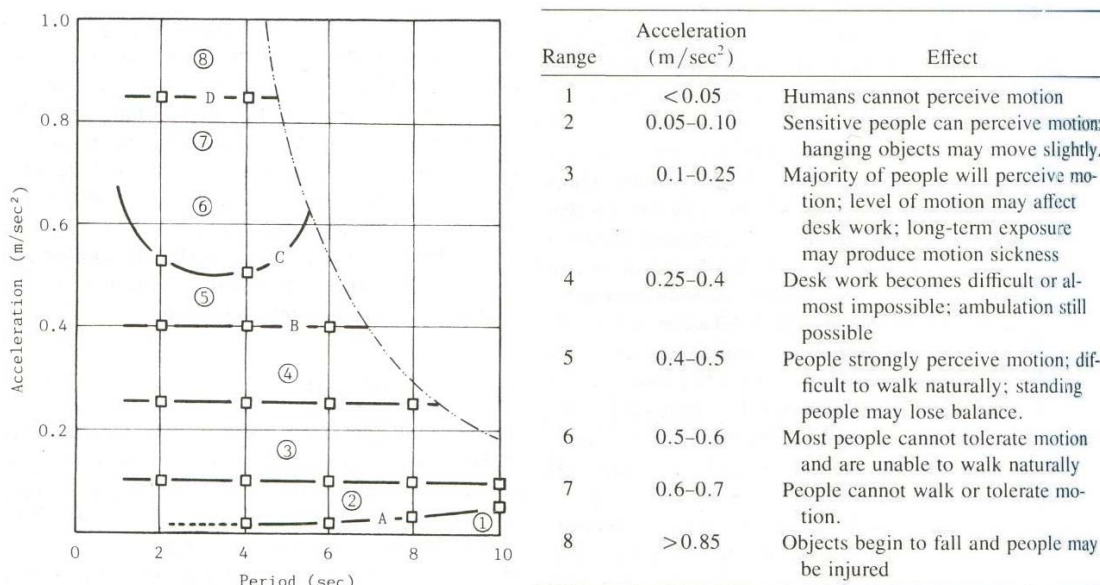


Figure 2.3-5: Human perception levels and hindrance [33]

The figure above shows human perception and tolerance thresholds. To evaluate the comfort for a tall building occupant it is necessary to relate perception and tolerance to recurrence intervals, i.e. what acceleration levels are accepted for a certain recurrence interval.

Various guidelines are available to the structural engineer to evaluate the comfort of tall building occupants. Herein, three guidelines are treated: the ISO 6987 (figure 2.3-6), BLWTL and AIJ guidelines.

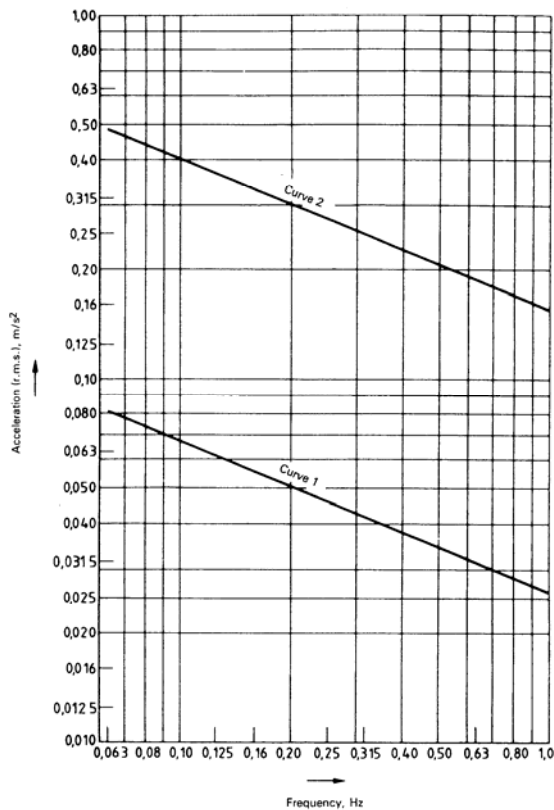


Figure 2.3-6: ISO 6897 5-year rms acceleration criteria [18]

ISO 6987 [18] proposes maximum values of the root-mean-square acceleration with a return period of 5 years at the top occupied floor, during the 10 severest minutes of a wind storm, as a function of the building's fundamental frequency of vibration. The denominated Curve 1 constitutes the proposed limits for general-purpose buildings, whereas curve 2 holds for offshore structures. No distinction is made to account for different occupancy rates in buildings.

The BLWTL criteria for office and residential buildings are shown in table 2.3-1 taken from reference [21]. Afterwards, the criterion for hotels has been added. Maximum values of the 10-year peak horizontal accelerations are provided for the top occupied floor. Note that distinction is made for building occupancy and that the proposed limits are independent of the frequency of oscillation. The BLWTL criteria are widely used in North American structural engineering practise.

| | range [$g \cdot 10^{-3}$] |
|-----------|-----------------------------|
| office | 20 - 25 |
| hotel | 15 - 20 |
| residence | 10 - 15 |

Table 2.3-1: BLWTL 10-year acceleration criteria

The AIJ-2004 proposed peak acceleration limits with a recurrence rate of 1 year are provided in figure 2.3-7, as a function of the building's occupancy. Note that the peak accelerations are presented in cm/s^2 and that daily comfort is evaluated rather than more extreme events with a return period of 5, 10 or more years. The terms H-10 till H-90 represent the probability of perception of the given comfort criteria curve.

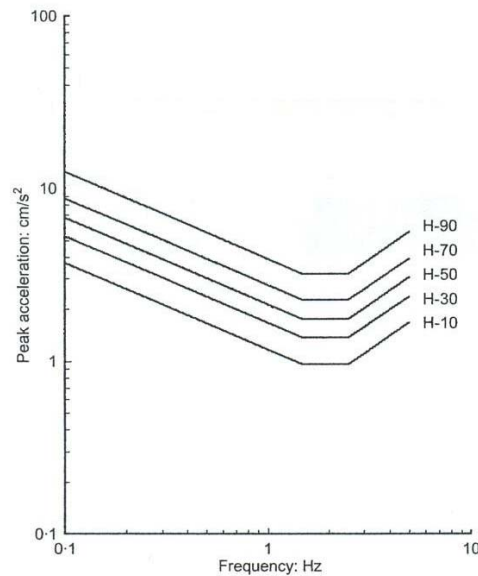


Figure 2.3-7: AIJ 1-year peak acceleration criteria [34]

To evaluate the occupant's comfort of the tall buildings analysed in this thesis, the ISO 6897 and BLWTL criteria are adopted.

Auxiliary damping devices

Auxiliary damping devices are mainly used to mitigate wind-induced building motion, although seismic applications of damping devices are also known.

For a given geometry, tall building motion is primarily depending on the mass and stiffness distribution and the total effective damping. If an evaluation of tall building occupants comfort yields negative results, the engineer can act to change one of the three mentioned aspects. The stiffness could be increased to make the building less susceptible to wind buffeting. This is however a very costly operation and, furthermore, increases the natural frequency due to which (according to some human motion perception studies) the motion perception threshold decreases. Acting on the mass of the building would result in extra structure and foundation costs and, in addition for earthquake-prone regions, would increase the seismic inertial forces. That leaves only the effective damping as an instrument to mitigate excessive building motion.

Four major sources of damping exist: structural, aerodynamic, soil and auxiliary damping. Structural damping consists of inherent material damping of steel and concrete. Aerodynamic damping may contribute in along-wind direction, but can be negative (adverse) as far as cross-wind vibrations is concerned. Damping to soil-foundation interaction is generally not accounted for in tall building design. The latter three components of the effective damping all have a modest contribution and their estimation is far from accurate. This leads to a high level of uncertainty in the estimation of normal building damping. Auxiliary damping devices may be integrated in the structural design, in cases where the inherent damping is not sufficient, to provide for more damping being more predictable and possibly adaptable.

A global distinction for auxiliary damping devices is made between passive, with indirect and direct energy dissipation, and active damping devices. Active damping devices need a power source because of which it is questionable whether they can be considered in ultimate limit state calculations.

Examples of passive dampers with indirect energy dissipation are tuned mass dampers (TMDs) and tuned liquid dampers (TLDs). A TMD typically consists of an inertial mass located on rubber bearings at the top of the building and connected to the structure by means of a spring and damping mechanism. Inertial forces are transmitted to the building structure to reduce its motion. An early application of a TMD is found in the 244 m high John Hancock Tower in Boston. Another application of a TMD is shown in figure 2.3-8, at the top of Taipei 101 in Taiwan.



Figure 2.3-8: TMD in Taipei 101 [40]

Viscoelastic dampers (VEDs) were first used in the World Trade Center Towers in New York, and are an example of passive damping devices with direct energy dissipation. A VED consists generally of a viscoelastic material placed between steel plates adopted. A VED can be used for instance in a diagonal steel bracing. The wind-induced elongation or shortening of the brace leads to an energy-dissipating shear deformation in the viscoelastic material as well as a restoring force out of phase with the displacement. Other direct energy dissipation applications of passive dampers are viscous damping devices (VDD) and friction systems.

Active mass dampers (AMD) are an application of active auxiliary damping devices and are quite similar to tuned mass dampers as explained above. On one hand, they require a far smaller damper mass due to higher levels of efficiency. Yet, on the other hand, operation and maintenance costs are higher. In addition, because they are computer controlled, questions arise about their reliability in ultimate limit states. A

computer analyses the building oscillation and then actuates on the mass to counteract the induced motion more efficiently.

The reader is referred to reference [23] for a more extensive description of auxiliary damping devices.

2.4 Lateral load resisting systems

This section is focussed on lateral load resisting systems (LLRSs) in tall building structures. Firstly, a simplified cantilever analogy is presented to gain insight in the structural behaviour of tall buildings excited by horizontal loads. The different lateral load resisting systems, with their corresponding advantages and disadvantages, are discussed in the following subsections 2.4.1 till 2.3.9.

The first function of a lateral load resisting system is to ensure the building's global stability. Besides stability, a LLRS has to provide sufficient lateral and rotational stiffness, as to prevent collapse due to the P-delta effect of applied gravity loads and to prevent excessive building motion due to horizontal loads.

For a good understanding of the underlying principles of LLRSs it can be useful to take a closer look at the mechanical basics. A building subjected to wind loading can be represented as a cantilevered column subjected to a horizontal load, as illustrated in figure 2.4-1. The equivalent cantilevered column has the bending and shear stiffness corresponding to the mechanical properties of the actual building.

It is useful to examine two extreme types of theoretical deformation. The foundation stiffness has not been considered, because it is independent of the mechanical properties of the cantilevered column.

The left-hand side diagram in figure 2.4-2 illustrates a shear-dominated displacement, having infinite bending stiffness. A bending-dominated displacement diagram is presented on the right-hand side, i.e. the cantilevered column has infinite shear stiffness.

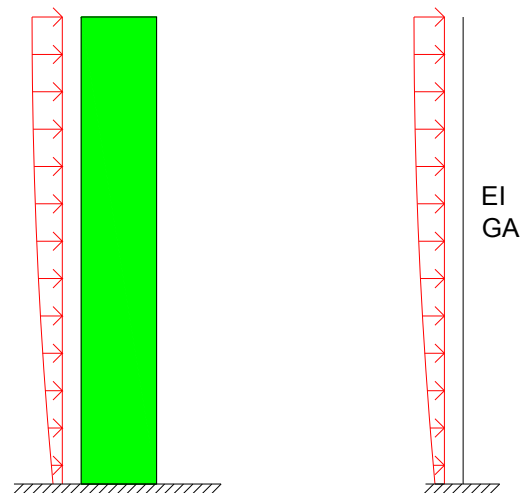


Figure 2.4-1: Cantilever representation

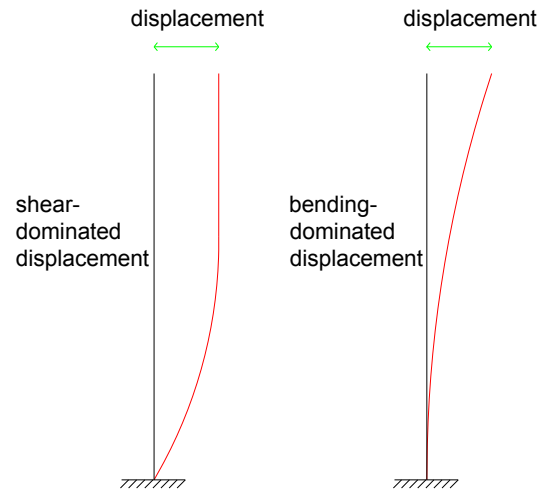


Figure 2.4-2: Shear-dominated and bending-dominated displacement diagrams

In case of real tall buildings, the lateral displacements are never solely described by one of the above sketched theoretical displacement diagrams. Usually, to a greater or smaller extent a mix of these different displacements is found in tall building sway.

Hereafter a description of the principal LLRSs, nowadays used in tall building structures, is presented. Although, some are more suited for either steel or concrete construction, no distinction is made in materials. Deliberately no material efficiency ranges are provided that are usually encountered in high-rise building text books. The author believes that structural material efficiency considerations do not constitute anymore the governing design criterion for this type of structures (at least not as substantially as in the past). On one hand, modern architectural and building service requirements often overrule structural considerations. An astonishing increase in computational capacity, on the other hand, has made it less necessary to reduce structural complexity and discontinuities. Please note that the latter does not mean that structural engineers do not still need a sound understanding of mechanical behaviour. In the following the mechanical behaviour of the LLRSs are treated with their corresponding (dis)advantages.

The author does not pretend to give a complete description of all systems available to structural engineers. In the past, a great variety of systems has been developed; often combining two or more LLRSs. Structural engineers will always be challenged to come up with new, stiffer and/or more functional structural systems.

2.4.1 Braced-frame structure

A cantilever truss beam laterally stabilises the building frame, being the truss composed of columns (truss chords), floors and diagonals (truss web). In analogy to the truss beam for large spans, bracings constitute an efficient means of transmitting horizontal wind loads to the foundation, i.e. by axial forces instead of bending moments.

The bending stiffness of the truss is proportional to the axial stiffness EA of the chords times the square distance between the columns. The shear stiffness is relatively small

because of the little material employed in the truss' web, and is determined by the axial stiffness of the horizontal and diagonal web members.

Different types of bracings can be adopted in the design, as shown in figure 2.4-3. The best solution from a lateral stiffness point of view would be the double diagonal bracing. Diagonal braces, however, impedes the possibility to have a corridor or door opening in the considered bay. A solution to this functional problem could be the application of K- or knee bracings. From a stiffness point of view this is not a very efficient solution.

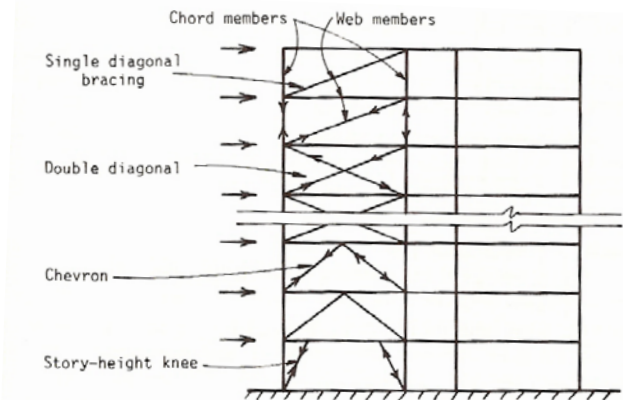


Figure 2.4-3: Braced frame structure [33]

2.4.2 Rigid-frame structure

In contrast to braced-frame structures, a rigid-frame structure transmits the horizontal loads to the foundation by predominantly bending moments in the columns and beams, and axial forces in the columns near the building perimeter. The connections between columns and beams are moment-resistant, i.e. fixed. The abovementioned beam can also consist of a plate or slab.

The displacement diagram of rigid-frame structures is shear-dominated. The lateral stiffness is obtained from the combined bending stiffness of columns and beams (and for steel structures the panel zone of the joint).

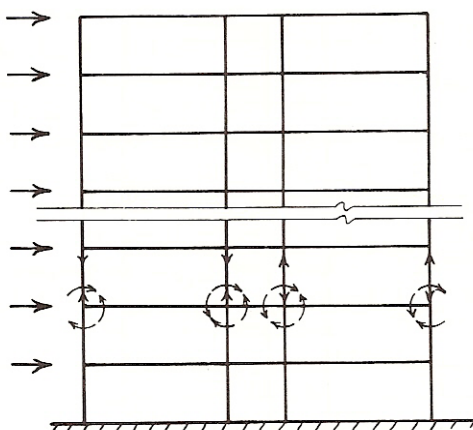


Figure 2.4-4: Rigid-frame structure [33]

The material efficiency of this LLRS is rather low due to the high bending moments in the structural members. Furthermore, all structural members have to be designed independently of one another to bear the specific wind-induced bending moments. This makes this system less appropriate to be assembled of prefabricated elements than, for instance, a braced-frame structure. However, the wide and open rectangular spaces are a great advantage of this system.

2.4.3 Shear wall structure

In shear wall structures, the shear walls provide the entire lateral stiffness and strength. Because of their very high in-plan stiffness and strength, shear wall structures are

much stiffer than rigid-frame structures. Shear wall structures can encompass one or more planar elements or, as is illustrated in figure 2.4-5, an in-plan assembly of interconnected shear walls around elevators, stairs and building service shafts.

Normal, closed, shear wall structures are characterised by bending-dominated displacement due to horizontal loads. The shear stiffness of these elements can be considered infinitely large in relation to the flexural stiffness. Whereas rigid-frame structures allow complete freedom in planning open internal spaces, closed shear walls pose a restriction for the functional planning. This characteristic, in combination with good thermal and acoustic insulation as well as fire resistance, makes it an especially well-suited solution for residential and hotel buildings.

Punched shear walls, i.e. shear walls allowing corridor or door openings, are frequently used in the assembly of vertical structural cores enveloping the elevator and services shafts. The displacement of punched shear walls is still bending-dominated, even though the shear stiffness cannot be considered infinitely stiff. The stiffness reduction, due to shear flexibility, has to be taken into account in the structural analysis and depends on the pattern and size of the openings.

For parallel shear walls, interconnected by a pinned floor structure, every shear wall simply bears the part of the total horizontal load according to the relative in-plan stiffness. When shear walls are efficiently located in the building plan, the gravity loads can compensate the tensile stresses due to wind loading. Then, the shear walls can be designed to have only the minimum reinforcement.

2.4.4 Coupled shear wall structure

Coupled shear wall structures are composed by one or more shear walls (more or less in the same plane) interconnected by a flat plate, slab or coupling beam (see figure 2.4-6). The connection between the beam and shear walls is moment-resisting, because of which the coupling beam acts like a “shear connector”.

The shear connection creates a composite behaviour of the shear walls instead of being two or more independent flexural cantilevers, highly increasing the horizontal stiffness. The composite behaviour introduces a simultaneous compression and tension in the opposite shear walls. The composite behaviour and therefore the lateral stiffness is enhanced by a stiffer coupling beam or floor.

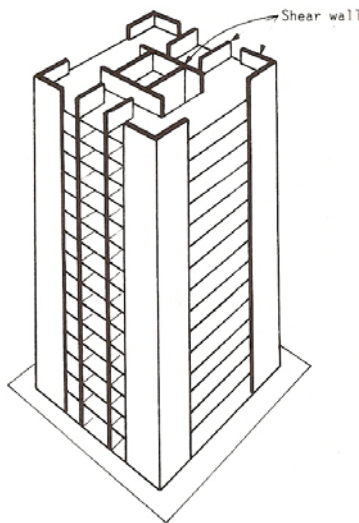


Figure 2.4-5: Combined shear wall structure [33]

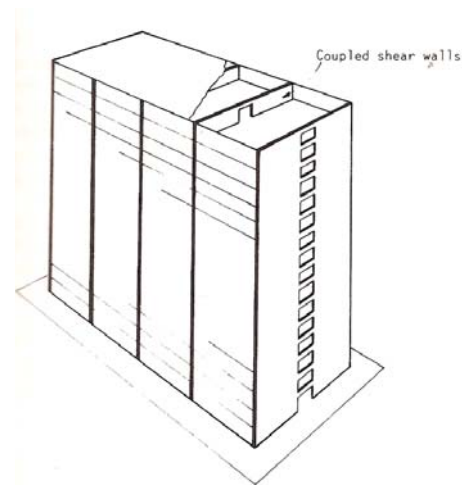


Figure 2.4-6: Coupled shear wall structure [33]

2.4.5 Shear wall - rigid frame structure

This LLRS combines both the shear wall and the rigid frame system in one structure. The two systems are interconnected by floors or beams.

The shear wall-rigid frame concept is based on the combination of the pure bending and shear displacement diagram. It can be seen in figure 2.4-2 that the shear-dominated diagram has the largest rotation (increase of displacement) in the lower part of the structure while the rotation of the bending-dominated diagram is greatest in the top part of the structure. When an interconnection is used with high axial stiffness, the shear mode is resisted by the flexural mode in the lower part and the flexural mode is resisted to move laterally by the shear mode for the upper part of the building. This interaction between displacement diagrams generates interaction forces in the horizontal members, as is illustrated in figure 2.4-7.

The advantage of this system is that shear walls can be used around service shafts and a rigid frame can be adopted for the outer part of the floor plan leaving rectangular, open spaces where needed. The structural behaviour is rather complex and therefore needs due consideration in the structural design. Horizontal beams or floor structures have to bear the interaction forces and the tensile forces need to be duly anchored in the structure.

The sketched interesting theoretical collaboration between the two systems does not always occur to the expected extent. On one hand, service shaft-enclosing punches shear walls tend to display a considerable shear deformation. When moment frames, on the other hand, are designed to have closely spaced columns and deep spandrel beams, the lateral stiffness is composed of a considerable flexural stiffness. These two aspects undermine the effectiveness of the conceptual interaction.

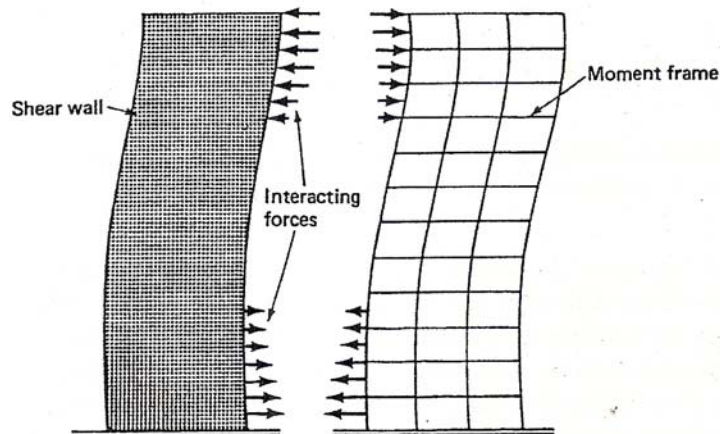


Figure 2.4-7: Wall-frame interaction [35]

2.4.6 Framed-tube structure

The framed-tube lateral system is a stiff moment-frame, generally composed of closely-spaced columns and deep spandrel beams, wrapped around the building perimeter. The horizontal load resisting material is located as far as possible from the structure's centroid, thus resulting in great lateral stiffness and smaller wind-induced stresses in the perimeter columns.

The mechanical behaviour is comparable to a cantilevered rectangular or square hollow section; acting the along-wind faces as the tube's web and the across-wind faces as the flanges. Both shear and bending deformation takes place in this kind of structures. Framed-tubes with closely-spaced columns and deep connecting beams will tend to have a more bending-dominated displacement diagram.

A phenomenon needs special consideration in the structural design of framed-tube buildings; the so-called shear lag. Due to the shear deformation of the frame, the shear stresses in the centre of the flanges and web tend to lag behind the higher corner shear stresses. As a consequence, the mid-flange and mid-web columns are less stressed than the corner columns and the mid-face columns are, therefore, not fully contributing to resist the wind-induced bending moment. The foregoing is illustrated in figure 2.4-8, where the upper right side figure shows the shear stress distribution and the lower figure the axial stress distribution.

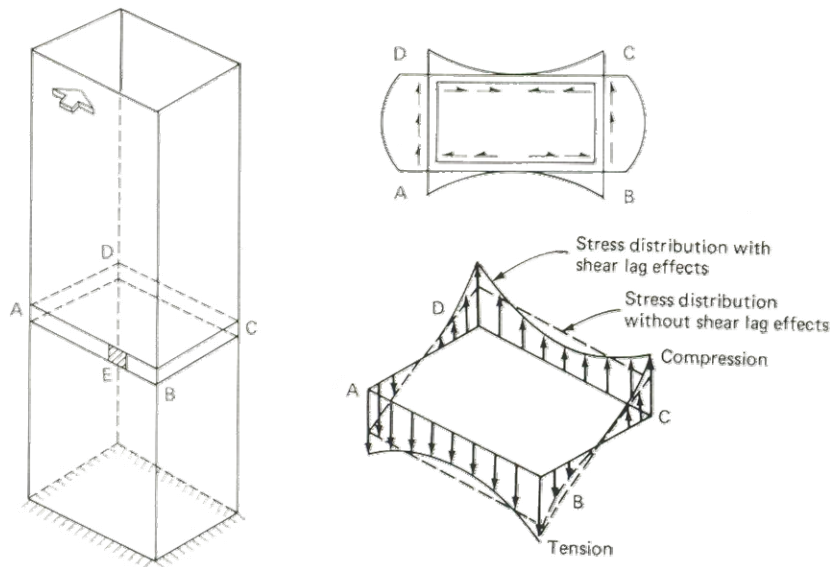


Figure 2.4-8: Shear lag phenomenon in framed-tubes [35]

Because of the repetition of framed-tube structures, they are especially well-suited for prefabrication. Due to high static indeterminacy, framed-tube structures are highly redundant structures and they are sensitive to differential settlements.

Tube-in-tube structure

The tube-in-tube structure is composed of a perimeter moment-frame and an internal core enveloping the building services shafts. When the internal core has a bending-dominated displacement, some shear-bending interaction may occur as explained in subsection 2.4.5. Due to the far greater lever arm of the perimeter tube, however, the contribution of the internal tube to the lateral stiffness is generally small.

Bundled-tube structure

The aforementioned shear lag phenomenon in tube structures can be greatly reduced by simply adding internal webs, as to flatten-out the shear stress distribution in the flange columns. In this way the flange columns are more evenly stressed and equally contributing to the lateral resistance resulting in greater material efficiency and lateral stiffness.

This concept was first used by the firm Skidmore, Owings and Merrill (SOM) in the Sears Tower in Chicago, see figure 2.1-5 and 2.1-11.



Figure 2.4-9: Braced-tube structure [33]

Braced-tube structure

Diagonal bracing of a framed-tube structure highly reduces the bending moments in the frame members. Therefore it diminishes the shear deformation of the structure. Bracing is another way of eliminating the shear lag and increasing the material efficiency.

Because shear lag in braced-tubes is not as important as in normally framed-tubes, the column spacing can be greater and the spandrel beams smaller resulting in larger window openings.

A well-known application of a braced-tube in a tall building structure is the John Hancock Building in Chicago designed by SOM, as sketched in figure 2.4-9.

2.4.7 Outrigger-braced structure

Outriggers are structural members with a large bending stiffness connecting the primary LLRS with generally perimeter columns, in this way locally increasing the lever arm. The connection between the lateral system, usually a shear wall or core assembly, and the outrigger has to be moment resistant. In this way the principal lateral system's rotation is used to activate perimeter columns. The simultaneous shortening and elongation of opposite columns induces a counteracting bending moment in the core diminishing the internal bending moments and highly increasing the lateral stiffness. The latter is illustrated in figure 2.4-10.

More columns can be activated than the ones in the same plane as the lateral system, by adopting belt trusses. Belt trusses run along the building's envelope and connect other perimeter columns to the outrigger structure, as is shown in figure 2.4-11. In order to be effective, both outrigger and belt truss have to be designed for great bending stiffness.

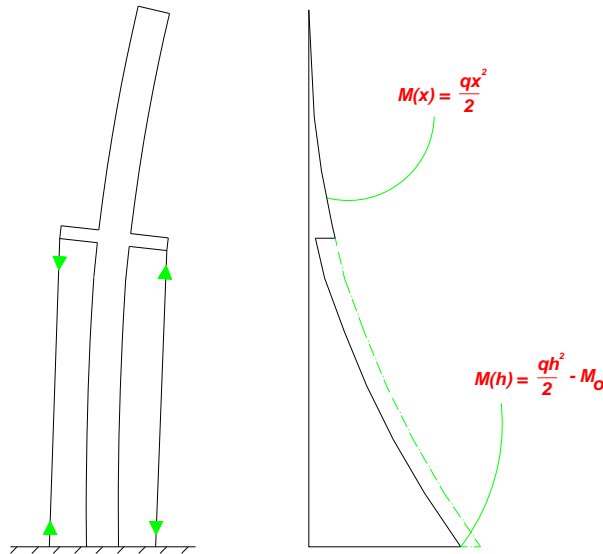


Figure 2.4-10: Outrigger-braced structure

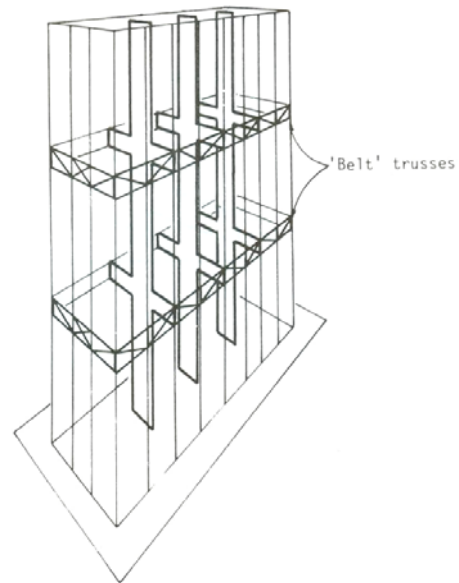


Figure 2.4-11: Belt trusses in an outrigger-braced structure [33]

Due to its large bending stiffness, the outrigger has as a side effect that the axial forces in the connected columns tend to be transmitted to the core. The gravity loads on the floors just below the outrigger are almost entirely borne by the column, but the live loads are likely to be hung up from the core by means of the outrigger. An important part of the gravity and live loads borne by the column sections above the outrigger is, in the same way, transmitted to the core. This side effect reduces differential shortening problems, especially in concrete tall buildings, as explained in subsection 2.3.1. Another important feature of outriggers is that they give redundancy to the building structure. When a column, for whatever reason, stops to bear vertical loads the loads can be borne by the rest of the structure due to the outrigger's stiffness.

Note that the outrigger's efficiency is proportionally to the bending-dominated part of the LLRS displacement diagram, i.e. an outrigger bracing a theoretical shear cantilever is highly inefficient. The exact reduction of building sway and bending moment depends on the latter, the height location of the outrigger, and on the relation between the core and outrigger bending stiffness and the axial stiffness of the connected columns.

A parametric study of optimum locations of single-outrigger structures is provided in appendix I. Optimum outrigger levels are presented for base moment and top building sway reduction, as a function of the stiffness relation between core, columns and outrigger. Furthermore, the reduction of the lateral sway and base bending moment are graphically presented for different stiffness relations.

In this subsection, only the optimum locations of a single-outrigger structure for sway and base moment are presented in figure 2.4-12 and 2.4-13 respectively.

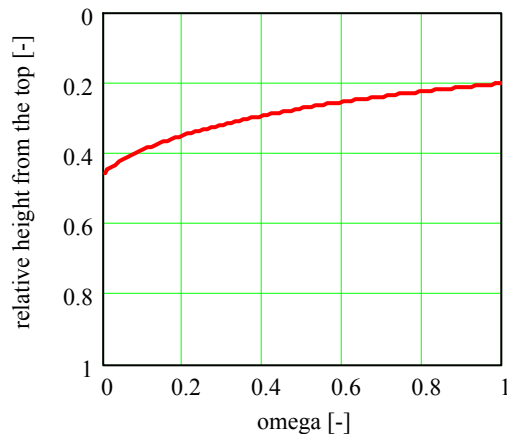


Figure 2.4-12: Optimum levels for top sway reduction

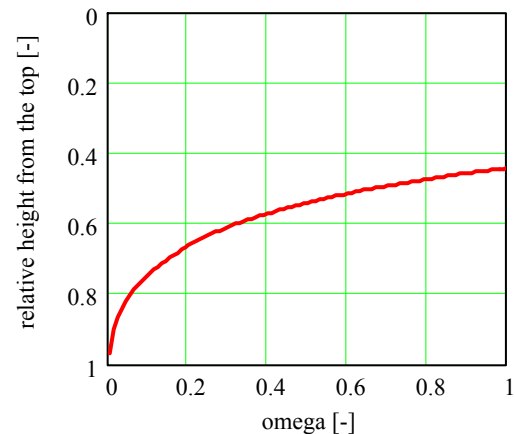


Figure 2.4-13: Optimum levels for base moment reduction

In the above figures, omega represents the relation between the column's axial stiffness and the bending stiffness of the outrigger. High values of omega reflect a relative small bending stiffness of the outrigger and vice versa.

Note that, as far as lateral displacement reduction is concerned, the optimum levels are not found at the top of the building as one might expect. For an infinitely stiff outrigger optimum lies at 0,46 H from the top. Optimum sway-reduction levels of single-outriggers for practical values of omega are approximately between 0,3 H and 0,4 H from the top. This corresponds to approximately an optimum at about two-thirds of the building height.

As far as the base moment is concerned, it is shown in figure 2.4-13 that the largest reduction is obtained for small relative heights up to more or less mid-height with increasing value of omega. This observation can be useful when stiffness requirements are already met by the lateral system and the structural engineer wishes to reduce the base acting moment. Note that obtaining the smallest base moment does not mean that the bending moment along the building height does not exceed the former value. This is especially true for the lower left-hand side of figure 2.4-13, that is for very large relative outrigger bending stiffness and small relative heights.

The reader is referred to [33] for the results of multiple-outrigger parametric studies.

2.4.8 Space frame structure

Space frame structures are a very efficient means of resisting lateral loads. The primary lateral structural system consists of a three-dimensional triangulated frame in which the members resist both gravity and horizontal loads. This LLRS was incorporated in the design of the Bank of China in Hong Kong by the engineering firm LERA, as shown in figure 2.1-12 and 2.4-14. This design has proved to be very cost efficient and in general the LLRS has a potential for reaching greater heights.

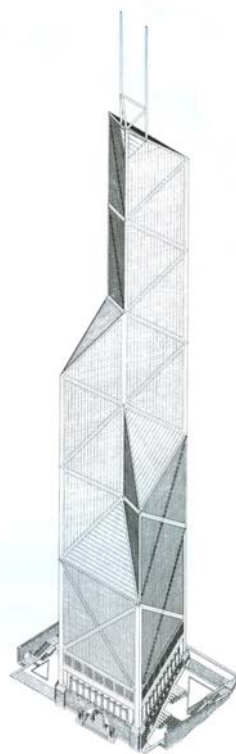


Figure 2.4-14: Bank of China in Hong Kong [9]

2.4.9 Hybrid structure

Some of the above discussed lateral load resisting systems (LLRSs) have typical advantages for a particular building-use (like shear walls for residential buildings) and disadvantages for another building function. Adopting one structural system is the most efficient solution for a single-use tall building. In addition, the ease of calculation is a big advantage of employing one (combined) lateral system along the building height.

However, during the last decades a trend is noticed towards mixed-use tall buildings. Furthermore, computational capacity has increased at a very high pace. Extremely powerful structural analysis programs are available nowadays for the structural engineer on a normal personal computer. The architectural freedom to house different functions in one tall building is structurally responded to by means of hybrid structures, i.e. the vertically stacked functions are followed by sub-optimal vertically stacked lateral systems.

Seemingly, any structural shape can be realised if the designing engineer is equipped with a sound understanding of structural behaviour.

3 Wind loading

The principal horizontal load this thesis is focussed on, the wind action, is dealt with in this chapter. An introduction is presented to wind loading and wind-induced building response. It is endeavoured to combine both wind engineering and the building code prescriptions. The recommendations of Eurocode 1 [12] are discussed and on occasion compared with the consulted literature on wind engineering.

Practically all building codes consider the wind action as a quasi-static load. To allow a static structural calculation, factors are introduced accounting for the spatial and temporal averaging of wind gustiness and the dynamic amplification of the building response.

Eurocode 1 defines the wind load acting on any structure or element by

$$F_w(z) = c_s c_d \cdot c_f \cdot q_p(z) \cdot A_{ref} \quad (3.1)$$

where F_w wind force [N]
 c_s, c_d structural factor [-]
 c_f force coefficient [-]
 q_p peak wind pressure [Pa]
 A_{ref} reference area [m²]

Section 3.1 treats the surface wind characteristics, while the structural factor is dealt with in section 3.2. Wind-induced structural vibrations are discussed in section 3.3.

3.1 Surface wind characteristics

Wind is defined as the motion of air with respect to the earth's surface. The motion is caused by pressure differences in air layers of the same altitude. These different air pressures are caused by variable solar heating of the atmosphere. Since buildings are located at the surface of the earth we are especially interested in the surface wind characteristics.

3.1.1 Variation with height and terrain roughness

The surface wind varies strongly with height. It is approximately zero at the surface, and it increases with height in a layer δ ; ranging approximately from 100 m for low wind velocities over smooth surfaces to 4 km for extreme winds over rough surfaces. This layer is called the atmospheric boundary layer, and is schematically sketched in figure 3.1.1. Above this boundary layer the wind flows approximately with a constant gradient wind velocity along the pressure isobars.

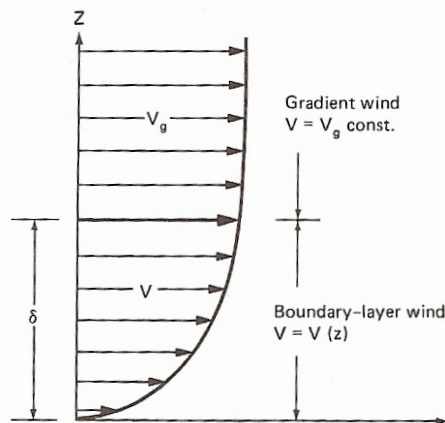


Figure 3.1-1: Boundary layer wind [24]

In the atmospheric boundary layer, the wind cannot freely flow due to obstacles that cause friction and, hence, decelerate the air flow. The Coriolis force causes the wind to change direction with height. This spiralling movement of the wind vector is called the Ekman spiral. Within the heights of normal tall buildings, i.e. up to a few hundreds of metres, this effect on the wind direction is negligible for structural engineering purposes [31].

Mean wind velocity variation with height and terrain roughness

The boundary layer wind profile is described by a logarithmic expression (3.1.1). Some building codes use a power law because it allows for easy mathematical manipulations. Eurocode 1 adopts a simplified logarithmic formula. The variation of the mean wind velocity with height, for moderate and strong winds, over horizontal terrain with homogeneous roughness is described according to the Joint Committee on Structural Safety [22] by

$$v_m(z) = \frac{1}{k} \cdot v_*(z_0) \cdot \left[\ln\left(\frac{z}{z_0}\right) + 5,75 \frac{z}{\delta} - 1,87 \left(\frac{z}{\delta}\right)^2 - 1,33 \left(\frac{z}{\delta}\right)^3 + 0,25 \left(\frac{z}{\delta}\right)^4 \right] \quad (3.1.1)$$

- where $v_m(z)$ mean wind velocity at height z [m/s]
 k von Karman constant, approximately equal to 0,4 [-]
 $v_*(z_0) = \sqrt{\tau_0 / \rho}$ friction or shear velocity at height z_0 [m/s]
 z height above ground [m]
 z_0 roughness length as a measure for the eddy size at the ground [m]
 δ boundary layer depth [m]

Up to 200 m or 0,1 δ , only the first logarithmic term has to be taken into account in order to obtain accurate results [22]. The Eurocode prescriptions for the variation of mean wind velocities with height are based on the simplified logarithmic expression presented in (3.1.2). It is, therefore, that the Eurocode limits its use to the calculation of wind loads for buildings with heights not greater than 200 m.

$$v_m(z) = \frac{1}{k} \cdot v_*(z_0) \cdot \ln\left(\frac{z}{z_0}\right) \quad (3.1.2)$$

The reader is referred to appendix II.1 for a comparison between the mean wind velocities calculated by formulae (3.1.1) and (3.1.2). It is shown in this appendix that, for the terrain roughness and basic wind velocity associated to the location under consideration, the error of using (3.1.2) for prismatic buildings up to a height of 250 m is 5% for the wind velocity and 6% and 8% for the base shear and overturning moment respectively. These errors are approximately equal to the error for an urban area (terrain category IV) up to 200 m, i.e. the maximum error implicitly accepted by Eurocode 1.

The shear stress of the wind at the surface is defined

$$\tau_0 = \kappa \cdot \rho \cdot v_{ref}^2 \quad (3.1.3)$$

where κ the surface drag coefficient [-]
 ρ air density [kg/m³]
 v_{ref} wind velocity at reference height, usually taken at 10 m [m/s]

The parameters z_0 and κ are empirically determined and are related as follows

$$\kappa = \left[\frac{k}{\ln(z_{ref} / z_{0,ref})} \right]^2 \quad (3.1.4)$$

Values of the roughness length and the surface drag coefficient for various types of terrain and for $z = 10$ m are given in figure 3.1-2. The reader should be aware of the fact that the values for built-up terrain shown in this figure are associated with the American meaning of suburbs and large cities.

| Type of Surface | z_0 (cm) | $10^3 \kappa$ |
|--|---------------|---------------|
| Sand ^a | 0.01–0.1 | 1.2–1.9 |
| Snow surface | 0.1–0.6 | 1.9–2.9 |
| Mown grass (~0.01 m) | 0.1–1 | 1.9–3.4 |
| Low grass, steppe | 1–4 | 3.4–5.2 |
| Fallow field | 2–3 | 4.1–4.7 |
| High grass | 4–10 | 5.2–7.6 |
| Palmetto | 10–30 | 7.6–13.0 |
| Pine forest (mean height of trees: 15 m; one tree per 10 m ² ; $z_d \approx 12$ m [2–40]) | 90–100 | 28.0–30.0 |
| Sparsely built-up suburbs ^b | 20–40 | 10.5–15.4 |
| Densely built-up suburbs, towns ^b | 80–120 | 25.1–35.6 |
| Centers of large cities ^b | 200–300 | 61.8–110.4 |

^aReference [2-38].

^bValues of z_0 to be used in conjunction with the assumption $z_d = 0$ [2-42].

Figure 3.1-2 Typical roughness lengths and surface drag coefficients [31]

The Eurocode proposes five different terrain categories with the corresponding roughness length and minimum height of validity, shown in figure 3.1-3.

| Terrain category | | z_0 m | z_{min} m |
|--|--|------------|----------------|
| 0 | Sea or coastal area exposed to the open sea | 0,003 | 1 |
| I | Lakes or flat and horizontal area with negligible vegetation and without obstacles | 0,01 | 1 |
| II | Area with low vegetation such as grass and isolated obstacles (trees, buildings) with separations of at least 20 obstacle heights | 0,05 | 2 |
| III | Area with regular cover of vegetation or buildings or with isolated obstacles with separations of maximum 20 obstacle heights (such as villages, suburban terrain, permanent forest) | 0,3 | 5 |
| IV | Area in which at least 15 % of the surface is covered with buildings and their average height exceeds 15 m | 1,0 | 10 |
| NOTE: The terrain categories are illustrated in A.1. | | | |

Figure 3.1-3: Eurocode terrain categories [12]

The formula adopted by the Eurocode for the calculation of the mean wind velocity profile is given by (3.1.5)

$$v_m(z) = c_r(z) \cdot c_o(z) \cdot v_b \quad (3.1.5)$$

where

- $c_r(z)$ roughness factor at height z [-]
- $c_o(z)$ orography factor at height z [-]
- v_b basic wind velocity [m/s]

Appendix II.2 shows that formula (3.1.5) is the simplified logarithmic formula (3.1.2) fitted to terrain category II.

Topographic elements, such as hills, valleys, mountains etc. change the air flow. The orography factor takes into account that these elements can locally increase wind velocities. The Eurocode states that orography effects may be neglected when the slope of the upwind terrain is less than 3° .

The basic wind velocity v_b is the 10-minute average wind velocity measured at 10 m above ground in open terrain (terrain category II), with an annual probability of exceedance of 0,02, i.e. having a 50-year return period. Different building codes use different basic wind velocities, for example the fastest mile winds and hourly mean winds. Figure 3.1-4 shows the Eurocode mean wind velocity profiles, with varying terrain roughness, calculated according to (3.1.3) and with $v_b = 26$ m/s.

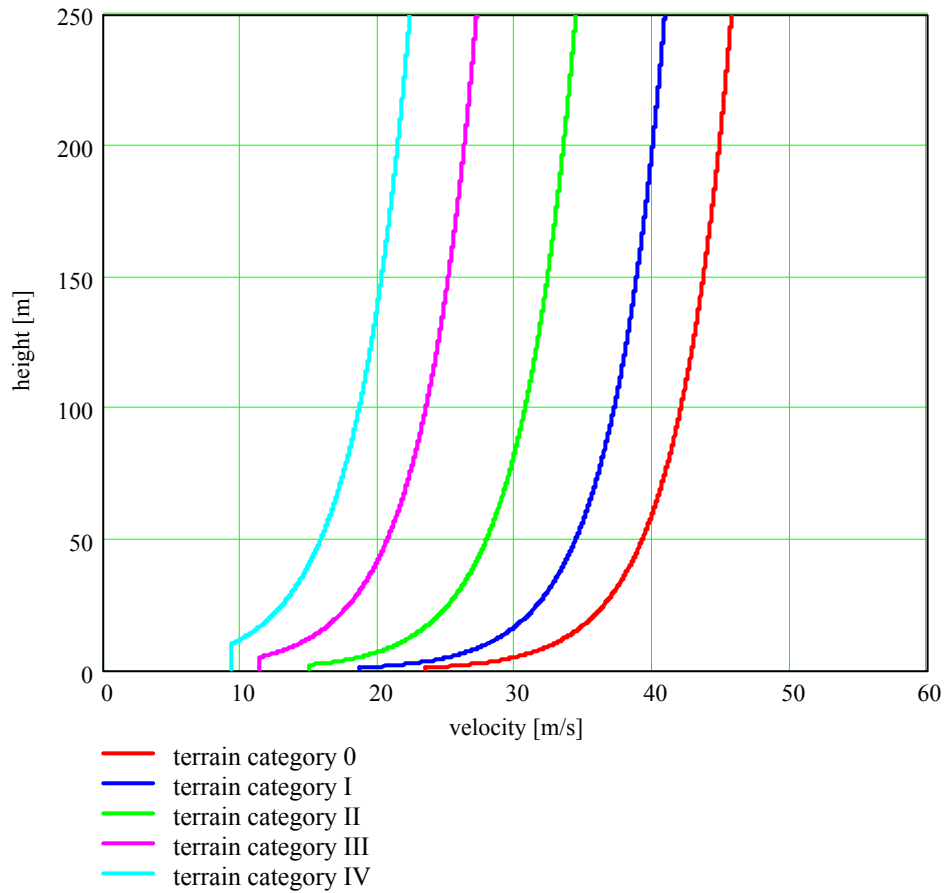


Figure 3.1-4: Eurocode mean wind velocity profiles for $v_b = 26$ m/s

However, structures are susceptible to peak wind gusts with duration of a few seconds instead of 10-minute mean wind velocities. To calculate this peak wind velocities, the wind turbulence has to be considered which is dealt hereafter.

3.1.2 Turbulence

The wind flow is, especially near the earth's surface, highly turbulent in three dimensions. Let the instantaneous longitudinal wind velocity be the sum of a mean and a fluctuating wind velocity

$$v(z, t) = \bar{v}(z) + \tilde{v}(z, t) \quad (3.1.6)$$

A measure of the intensity of horizontal turbulence is the root-mean-square value of the fluctuating part of the wind velocity. Then the fluctuating component of the wind velocity has a standard deviation equal to

$$\sigma_v(z) = \sqrt{\frac{1}{n} \cdot \sum_{i=1}^n \tilde{v}(z, t)^2} \quad (3.1.7)$$

Reference [22] gives the following expression for the longitudinal turbulence intensity

$$\sigma_v(z) = \beta \cdot \left(1 - \frac{z}{\delta}\right) \cdot v_* \quad (3.1.8)$$

with β varying between 2,0 and 3,1 for centres of large cities and open sea/smooth flat country respectively. Values of β in between 2,0 and 2,55 are recommended by [31], while assuming $z/\delta \approx 0$, for roughness lengths ranging from 0,005 m to 2,5 m respectively.

The relative turbulence intensity is defined as the standard deviation of the fluctuating part of the wind velocity divided by the mean wind velocity

$$I_v(z) = \frac{\sigma_v(z)}{v_m(z)} \quad (3.1.9)$$

Substituting (3.1.8) and (3.1.2) in (3.1.9) and subsequently taking the mean value of β and for small heights in relation to the boundary layer depth, one obtains the expression of the relative turbulence intensity adopted by Eurocode 1

$$I_v(z) = \frac{\beta \cdot \left(1 - \frac{z}{\delta}\right) \cdot v_m(z) \cdot k}{v_m(z) \cdot \ln\left(\frac{z}{z_0}\right)} \approx \frac{1}{\ln\left(\frac{z}{z_0}\right)} \quad (3.1.10)$$

Figure 3.1-5 shows the relative turbulence intensity with height for all five terrain categories defined in the Eurocode.

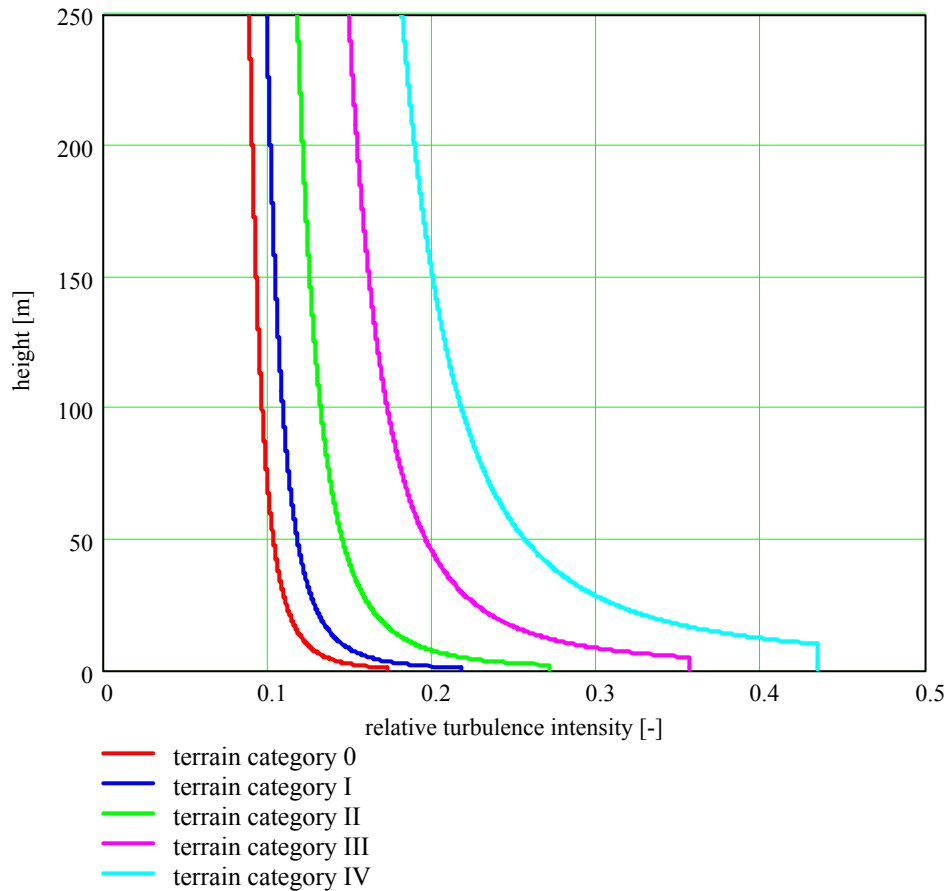


Figure 3.1-5: Relative turbulence intensity according to Eurocode 1

It is shown in appendix II.3 that expression (3.1.10) yields considerably lower values of the longitudinal wind turbulence in comparison to [22]. The difference is greater for smoother surfaces and greater heights. Eurocode 1 results in slightly greater values of the relative turbulence intensity than those following from the listed values of β recommended in [31].

Integral scales of turbulence

Turbulent velocity fluctuations in the air flow passing a point can be considered to be caused by a superposition of rotating “eddies”, transported by the wind with the mean velocity. These rotating eddies are three-dimensional turbulent vortices of varying size.

Integral scales of turbulence represent a measure of the average size of turbulent eddies in the air flow. A total of nine integral scales exist; three (dimensions of the eddy) for every component of the velocity fluctuation being longitudinal, transverse and vertical.

The average longitudinal (u) eddy size associated with longitudinal velocity fluctuations (x) is defined by

$$L_u^x = \frac{1}{\overline{\tilde{v}^2}} \int_0^\infty \tilde{v}(x, t) \cdot \tilde{v}(x + \xi, t) \cdot d\xi \quad (3.1.11)$$

where $\overline{\tilde{v}^2}$ mean-square value of the longitudinal velocity fluctuation
 $\tilde{v}(x)$ longitudinal velocity fluctuation at x
 ξ shift in distance from x

If it is assumed that the velocity fluctuations travel with the mean velocity \bar{v} then $\tilde{v}(x, \tau + t)$ can be written as $\tilde{v}(x - \xi / \bar{v}, \tau)$ where t is time and τ the time shift. With this result (3.1.11) can be rewritten to

$$L_u^x = \frac{\bar{v}}{\overline{\tilde{v}^2}} \int_0^\infty \tilde{v}(x, t) \cdot \tilde{v}(x, t + \tau) \cdot d\tau \quad (3.1.12)$$

The latter observation is important because the average longitudinal eddy size (associated with longitudinal turbulence) can now be measured at a fixed point.

Reference [31] provides two approximated expressions to calculate the average eddy size of the transverse and vertical component of longitudinal turbulence in (3.1.13) and (3.1.14) respectively.

$$L_u^y \approx 0,2 \cdot L_u^x \quad (3.1.13)$$

$$L_u^z \approx 6 \cdot z^{0,5} \quad (3.1.14)$$

When the two above integral length scales are small in comparison to the building's dimensions normal to the wind flow, it indicates that the effect of longitudinal turbulence on the overall wind loading is small. It will, however, have an important influence on local wind loads. The contrary, integral turbulence length scales that are large in relation to the building dimensions, means that the turbulent eddy envelopes the entire building surface and then the global effect of turbulence will be significant.

The total turbulence intensity may be thought of as the summation of the eddy turbulence intensities over a frequency interval dn . If instead of turbulence intensity (root-mean-square value) the mean-square value of turbulence is taken, the integral can be written as

$$v_t^2 = \overline{\tilde{v}^2} = \int_0^\infty S(n) \cdot dn \quad (3.1.15)$$

where v_t^2 squared intensity generated by all eddies
 $S(n)$ power spectrum

The power spectrum $S(n)$ is also referred to as the spectral density function of longitudinal turbulence. The spectral density function of longitudinal turbulence can be

empirically determined by means of a spectrometer. Numerous proposals for the spectral density function of wind turbulence exist of which Eurocode 1 adopted the Solari spectrum [25]. Reference [31] presents several spectra that can be used for structural design purposes.

The spectral density plays an important role in wind engineering, because it shows the energy contained in longitudinal wind turbulence for different frequency ranges. Resonance of the structure with the wind turbulence is assessed with spectral density function.

3.1.3 Pressure

Pressure is the force exerted on the surface per unit area. For hollow structures, like buildings, there exists an externally and internally acting pressure. Depending on the wind direction and the porosity distribution of the building envelope, they can act in the same or opposite direction.

The reference pressure in wind engineering is taken as the ambient pressure being the atmospheric pressure for true scale buildings. A pressure above atmospheric is called positive and below atmospheric is denominated negative or suction.

There is a stagnation point on the windward side of buildings where the wind is completely blocked and where the above-atmospheric pressure can be written as, according to Bernoulli's theorem for incompressible fluids

$$p = p_{abs} - p_a = \frac{1}{2} \cdot \rho \cdot v^2 \quad (3.1.16)$$

where p pressure [Pa]
 p_{abs} absolute pressure [Pa]
 p_a ambient pressure [Pa]
 ρ air density [kg/m³]
 v upstream wind velocity [m/s]

The right-hand term of equation (3.1.16) denotes the dynamic pressure or stagnation pressure and represents the maximum steady-state pressure that can be exerted on a structure by wind.

To simply determine the pressure distribution on structure surfaces a dimensionless pressure coefficient is used such that

$$c_p = \frac{p}{\frac{1}{2} \cdot \rho \cdot v^2} \quad (3.1.17)$$

Note that the dynamic pressure is always associated to a certain height z . For low-rise buildings the roof height is usually taken as the reference height, whereas the local height is usually adopted for tall buildings.

Various types of pressure coefficients exist, depending on the location and measurement time. Local mean pressure coefficients are those based on a time-averaged value of p and v , whereas the area mean pressure coefficient is obtained after integration of the latter over a certain area. The area mean pressure coefficients are normally adopted for the determination of the global wind load, although often simply referred to as *pressure coefficients*. For the calculation of facade elements and their fixing, the peak fluctuating pressure and the root-mean-square (rms) pressure fluctuations are of great importance, with their corresponding pressure coefficients. Note that the two latter are calculated with the time-averaged wind velocity.

It is at this point interesting to note that Eurocode 1 prescribes mean area pressure coefficients of +0,8 and -0,7 for the windward and leeward wall respectively of rectangular buildings. When these coefficients are used to calculate the global wind force, the lack of full correlation between windward pressure and leeward suction has to be accounted for. This is done by multiplying the wind force by 0,85 for non-slender buildings ($h/d \leq 1$) and by 1 for slender buildings ($h/d \geq 5$). Linear interpolation may be applied for intermediate aspect ratios. This implicates a total external pressure coefficient of 1,5 for rectangular tall buildings, meaning an increase of 25% of the global wind load if compared to the former Spanish code NBE-AE88 and the Dutch NEN 6702 (both adopting +0,8 and -0,4). For small aspect ratios the total pressure coefficient yields 1,3, supposing an increase of 8% but corresponding to other international wind codes.

The reason for the abovementioned increase of wind load for tall buildings in the Eurocode is not well understood. It seems, however, reasonable to adopt a higher correlation between pressure and suction for tall buildings due to the increasing eddy size of longitudinal turbulence with height (see appendix III.1.2). It is well known that large discrepancies exist between pressure coefficients obtained from smooth flow and turbulent boundary layer flow wind studies. Former building codes have been based predominantly on smooth flow wind tunnel studies, since boundary layer wind tunnels were not available at a large scale.

Peak wind pressure

The wind pressure, as the wind velocity, can be thought of as being composed of a mean and fluctuating part. The peak wind pressure, i.e. the dynamic pressure exerted by the peak wind velocity, is then given by

$$q_p(z) = \frac{1}{2} \cdot \rho \cdot [\bar{v}(z) + \tilde{v}(z)]^2 \quad (3.1.18)$$

after rearranging

$$q_p(z) = \frac{1}{2} \cdot \rho \cdot \bar{v}(z)^2 \cdot \left[1 + 2 \cdot \frac{\tilde{v}(z)}{\bar{v}(z)} + \frac{\tilde{v}(z)^2}{\bar{v}(z)^2} \right] \quad (3.1.19)$$

The right-hand side term can be neglected and when we recall the general definition of the relative turbulence intensity (3.1.9), expression (3.1.18) can be rewritten as

$$q_p(z) = \frac{1}{2} \rho \cdot \bar{v}(z)^2 \cdot [1 + 2 \cdot k_p \cdot I_v(z)] \quad (3.1.20)$$

where k_p peak factor of the velocity fluctuations
 I_v relative turbulence intensity

The peak factor of a signal is the ratio between the peak value and the root-mean-square value. The peak factor of longitudinal turbulence is then $\hat{v} / \sqrt{\bar{v}^2} = \hat{v} / \sigma$. Different wave signals have different peak factors, for instance the peak factor of a square wave signal yields 1 and for a harmonic signal $\sqrt{2}$.

The Eurocode adopts a peak factor of 3,5 for the longitudinal wind turbulence, which results in the expression for the peak wind pressure

$$q_p(z) = \frac{1}{2} \rho \cdot \bar{v}(z)^2 \cdot [1 + 7 \cdot I_v(z)] \quad (3.1.21)$$

3.1.4 Extreme wind probability

The wind velocities used for ultimate limit state calculations of tall building structures usually have a mean recurrence interval of 50 years. A sufficiently large data set of measured annual extremes of the mean wind velocity is analysed to obtain the extreme wind probability distribution. It is generally assumed that the extreme value distribution type I (Gumbel distribution) yields best estimated annual extreme wind velocities. Reference [22] provides the distribution function shown hereafter.

$$F_{\max, \bar{v}}(x) = e\{-e[-\alpha_1(x - u_1)]\} \quad (3.1.22)$$

where α_1 and u_1 are parameters depending on the distribution and calculated by

$$\alpha_1 = 1,282 / \sigma_1 \quad (3.1.23)$$

and

$$u_1 = m_1 - 0,577 / \alpha_1 \quad (3.1.24)$$

where m_1 and σ_1 are the mean and standard deviation respectively of the dataset. The above is valid for thunderstorm wind velocities only, not for hurricanes.

It is stated in reference [31] that at most stations in the United States of America a better fit, resulting in lower wind velocities, is obtained by the reverse Weibull distribution. The Gumbel distribution yields a slightly conservative extreme values for 50-year recurrence periods, but the difference can be very significant for return periods associated with the nominal wind speed (after multiplication by the load factor).

The basic wind velocity in the Eurocode has a mean recurrence interval of 50 years. It is reminded that this is not the maximum wind velocity during a 50 year design lifetime of a structure. There should not be confusion between the return period (inverse of

annual exceedance probability) and the design lifetime of a structure. The general expression for the probability of exceedance of a reference speed with return period R in T years is

$$P(v \geq v_b) = 1 - P(v \leq v_b) = 1 - \left(1 - \frac{1}{R}\right)^T \quad (3.1.25)$$

Thus, the probability that the basic wind velocity is exceeded in a 50 year design lifetime, typical design life time of building structures, is 64%. This demonstrates the need for a load factor in ultimate limit states. For reversible serviceability limit state calculations, such as lateral building deflections and accelerations, a higher probability of failure is accepted and hence the used load factor is 1,0.

It is noted that building deflection is a reversible serviceability limit state as far as the structure is concerned, but can result in an irreversible ultimate limit state for non-structural elements as façade elements and partitions. This clearly shows that adequate load factors have to be applied to building deflections, when they are used to determine dimensional tolerances for non-structural elements.

The direction-dependence of extreme natural wind velocities is significant. This effect is, conservatively, not being considered by the Eurocode.

3.2 Structural factor

The peak wind pressure and pressure coefficients, as used in expression (3.1), have been dealt with in the foregoing. The quasi-static approach of wind loading in the Eurocode requires the use of an additional factor to account for the dynamic effects in a static calculation. The Eurocode denominates the total dynamic effect as the structural factor.

The structural factor is defined as the product of the size factor and the dynamic factor. The size factor c_s takes the improbability into account of the simultaneous presence of wind gusts over the building surface. The dynamic factor c_d takes into account the amplification of the structural response due to the resonance of the building structure with the longitudinal turbulence.

The reader is referred to appendix III.1.2 for a detailed description of the general determination of the structural factor. Both dynamic and size factor account for global dynamic effects and are calculated at a reference height z_s equal to 0,6 H for prismatic buildings.

3.2.1 Size factor

The size factor represents the ratio of the spatial average of the peak wind pressure over the building area and the peak wind pressure assuming full correlation.

$$c_s = \frac{1 + 7 \cdot I_v(z_s) \cdot \sqrt{B^2}}{1 + 7 \cdot I_v(z_s)} \quad (3.2.1)$$

where I_v relative turbulence intensity [-]
 B background response factor [-]

The background response factor accounts for the lack of full correlation between the pressures fluctuations on the building surface and is calculated by

$$B = \sqrt{\frac{1}{1 + 0,9 \cdot \left[\frac{b+h}{L_i(z_s)} \right]^{0,63}}} \quad (3.2.2)$$

where L_i is the integral length scale of longitudinal turbulence, b the building width and h the building height in m.

Figure 3.2-1 and 3.2-2 depict the background response factor and size factor respectively, as a function of $(b+h)/L$.

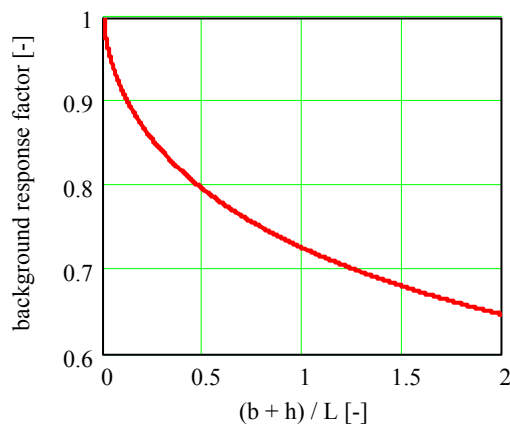


Figure 3.2-1: Background response factor

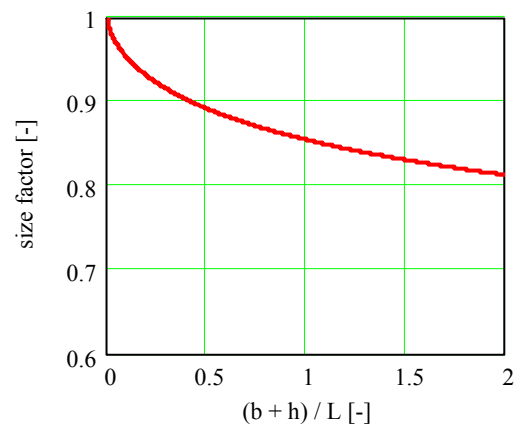


Figure 3.2-2: Size factor

3.2.2 Dynamic factor

The dynamic factor accounts for the resonance of the structure with the turbulent wind gusts and is calculated by

$$c_d = \frac{1 + 2 \cdot k_p \cdot I_v(z_s) \cdot \sqrt{B^2 + R^2}}{1 + 7 \cdot I_v(z_s) \cdot \sqrt{B^2}} \quad (3.2.3)$$

where I_v relative turbulence intensity [-]
 k_p peak factor of the structural response [-]
 B background response factor [-]
 R resonant response factor [-]

Firstly, note that the dynamic factor accounts for an interaction of the structural response with the wind turbulence. Because of this, the peak factor is not associated with the wind turbulence itself, but with the turbulence-induced structural response.

The expression for the resonant response factor is given by

$$R = \sqrt{\frac{\pi^2}{2 \cdot \delta} \cdot S_L(z_s, n) \cdot R_h(\eta_h) \cdot R_b(\eta_b)} \quad (3.2.4)$$

where δ logarithmic damping decrement [-]
 S_L power spectral density function [-]
 R_h aerodynamic admittance with respect to height [-]
 R_b aerodynamic admittance with respect to breadth [-]

Damping

Eurocode 1 adopts the logarithmic damping decrement as a measure of the rate of damping. The logarithmic damping decrement is defined by

$$\delta = \frac{2\pi \cdot \zeta}{\sqrt{1 - \zeta^2}} \quad (3.2.5)$$

where ζ is the ratio of the system's damping and critical damping. Because of the small damping values associated with wind-induced building response, the denominator can be approximated by 1 and expression (3.2.5) reduces to

$$\delta = 2\pi \cdot \zeta \quad (3.2.6)$$

Three sources of damping are accounted for: structural, aerodynamic and active damping. Structural damping is inherent to friction in the materials concrete and/or steel. In fact, (initially) non-structural elements such as stiff partitions and facade elements can also contribute to the total damping, i.e. traditional buildings with heavy masonry partitions and perimeter walls are known to have more damping than modern skeleton structures. However Eurocode 1 conservatively considers only the damping due to the structural elements, recommending values of the logarithmic decrement of damping of

- 0,10 for reinforced concrete buildings
- 0,05 for steel buildings, and
- 0,08 for composite buildings

Note that the classification of the material is especially associated with the lateral load resisting system and not as much with the gravity system. Keep in mind that Eurocode 1 only recommends damping values associated with ultimate limit state calculations. These values cannot be used to evaluate human comfort because smaller wind loads lead to smaller motions and therefore damping.

The aerodynamic damping is associated with changes in relative velocity of the air with respect to the building due to the building's vibration. Its determination is uncertain, and it is therefore prudent to neglect it in structural vibration calculations. Aerodynamic damping has been considered in the analyses performed on the four tall buildings this thesis is concerned with.

Active damping is represented by any auxiliary damping device. The reader is referred to subsection 2.3.2 for more information about damping devices.

Spectral density

The power spectral density function adopted by Eurocode 1 is the following expression of Solari

$$S_L(z_s, n) = \frac{n \cdot S_v(z_s, n)}{\sigma_v^2} = \frac{6,8 f_L(z_s, n)}{(1 + 10,2 f_L(z_s, n))^{5/3}} \quad (3.2.5)$$

with f_L being a dimensionless frequency, $n \cdot L(z_s) / v_m(z_s)$ where n is the fundamental building frequency in Hz.

Numerous proposals for the spectral density of along-wind turbulence have been published and considerable differences exist among different building codes.

An example plot of the spectral density function of longitudinal turbulence, as a function of frequency, can be seen in figure 3.2-3. The peak of the spectral density function is located at a frequency of the order of 0,01 Hz.

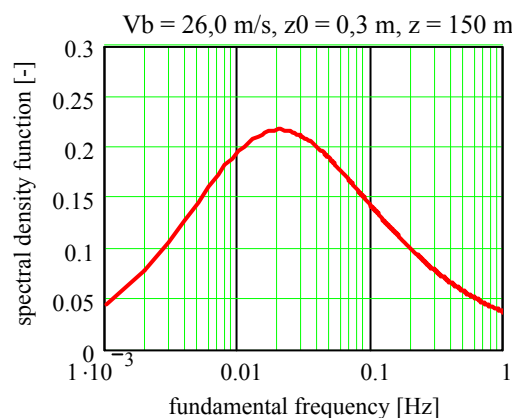


Figure 3.2-3: Spectral density function

Aerodynamic admittance

The aerodynamic admittance represents a modifying adjustment of the ideal case of turbulence with full spatial correlation enveloping the building. It is a function of building dimensions, fundamental frequency and the wind turbulence characteristics.

Figure 3.2-4 shows the aerodynamic admittance as a function of the frequency for a typical tall building.

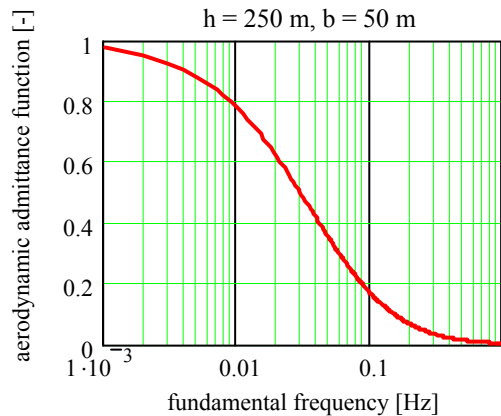


Figure 3.2-4: Aerodynamic admittance function

3.3 Structural vibration

Flexible structures, such as tall buildings and long-span bridges, are susceptible to wind-induced vibrations. These vibrations are determined by the building properties and wind characteristics. On one hand, the most important building factors are geometry, mass, stiffness and damping. The wind velocity and turbulence characteristics are of great importance on the other hand.

The trend towards higher buildings designed with high-strength materials increases the flexibility and decreases the mass and the structural damping. This guarantees the future importance of stability and vibration considerations.

There exist two groups of wind-induced vibrations; those caused by aerodynamic instabilities and those by aeroelastic instabilities. Aerodynamic instabilities are associated to air flow fluctuations around structures, whereas aeroelastic instabilities entail the interaction between the air flow and the structural motion.

The reader is referred to appendix II.5 for a description of different types of wind-induced structural vibrations. Herein, only the wind-induced vibrations are discussed that typically concern tall buildings: vortex-shedding and buffeting.

3.3.1 Vortex-shedding

Vortex-shedding occurs when vortices are shed alternatively from opposite sides of the building, creating in that way fluctuating loads perpendicular to the wind direction. Dangerous resonance may occur when the frequency of vortex-shedding is the same as the building's natural vibration. The frequency of vortex-shedding depends on the Strouhal number which, in turn, depends on the building's cross section. The Strouhal number is calculated as follows

$$St = \frac{n \cdot D}{v} \quad (3.3.1)$$

where St Strouhal number [-]
 n full cycle frequency of vortex shedding [Hz]
 D characteristic body dimension normal to the flow [m]
 v relative velocity [m/s]

When the building breadth is taken as the characteristic dimension normal to the air flow, a critical wind velocity can be defined at which the vortex-shedding frequency is equal to a natural building frequency n_i such that

$$v_{crit,i} = \frac{n_i \cdot B}{St} \quad (3.3.2)$$

Eurocode 1 states that the effect of vortex-shedding does not need to be investigated if $v_{crit} > 1,25 v_m$, with the mean wind velocity at the location where vortex-shedding occurs.

All buildings are subjected to vortex-shedding; however it is most likely to become a governing load for circular prismatic buildings. The probability of occurrence of a regular pattern of vortex-shedding is diminished by wind turbulence. Measures against vortex-shedding can be based on changing the separation points of the wind flow on the building surface. For rectangular or square buildings, this usually means chamfering the corners whereas circular buildings are enhanced by increasing the envelope's roughness or porosity.

3.3.2 Buffeting

We have seen that vortex-shedding induced vibrations are greater in a uniform air flow. Buffeting, on the contrary, is stronger in a turbulent air flow. Buffeting is the unsteady loading of a structure caused by upstream wind velocity fluctuations.

Two types of buffeting exist: buffeting induced by wind turbulence and by turbulence caused by upstream buildings or objects. The latter is called wake buffeting or interference and is especially important for tall buildings that are located nearby, see figure 3.3-1.

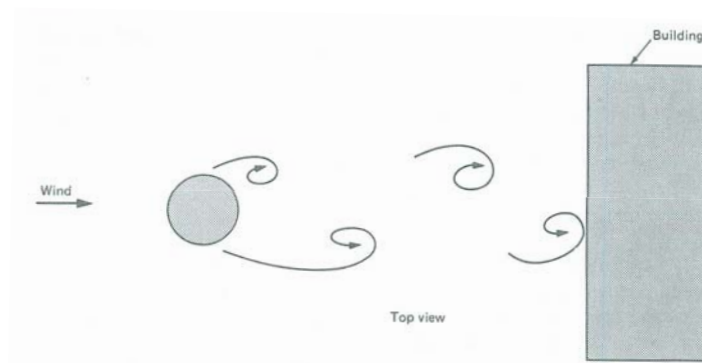


Figure 3.3-1: Wake buffeting [24]

Interference should be assessed in wind tunnel studies by modelling the direct environment of the building.

Eurocode 1 addresses normal wind buffeting in its appendix. The along-wind accelerations, of which the results are presented in chapter 5, are calculated according to those provisions.

The Eurocode expression for the root-mean-square value of the along-wind accelerations due to wind turbulence is as follows

$$\sigma_a(z) = \frac{c_f \cdot \rho \cdot b \cdot I_v(z_s) \cdot v_m(z_s)^2}{m_1} \cdot R \cdot K \cdot \Phi_1(z) \quad (3.3.3)$$

| | |
|-------------|---------------------------------------|
| where c_f | force coefficient [-] |
| ρ | air density [kg/m^3] |
| b | building breadth [m] |
| I_v | relative turbulence intensity [-] |
| v_m | mean wind velocity [m/s] |
| z_s | reference height of 0,6 H [m] |
| m_1 | fundamental modal mass [kg] |
| R | resonant response factor [-] |
| K | non-dimensional coefficient [-] |
| Φ_1 | fundamental along-wind mode shape [-] |

The calculation of along-wind accelerations is presented in appendix III for each building structure analysed in this thesis.

It is noted that the use of appendix B of Eurocode 1 may lead to confusion. At some point, an expression is given to calculate the equivalent mass it is suggested in this appendix that the equivalent modal mass is calculated. Furthermore, a calculation method of the modal mass is lacking. It is believed that this should be corrected as to prevent confusion to designers.

4 General site and building description

4.1 Cuatro Torres Business Area

The Cuatro Torres Business Area, in the following referred to as CTBA, is a recent urban development project facing the Paseo de la Castellana in Madrid, Spain. The project encompasses the construction of four tall buildings, a large convention centre, and an underground car park and ring road. Figure 4.1-1 shows a scale model of the CTBA while figure 4.1-2 shows the buildings under construction. The tall building are called, from north to south (right to left in figure 4.1-2), Torre Espacio, Torre de Cristal, Torre Sacyr Vallehermoso and Torre Caja Madrid.

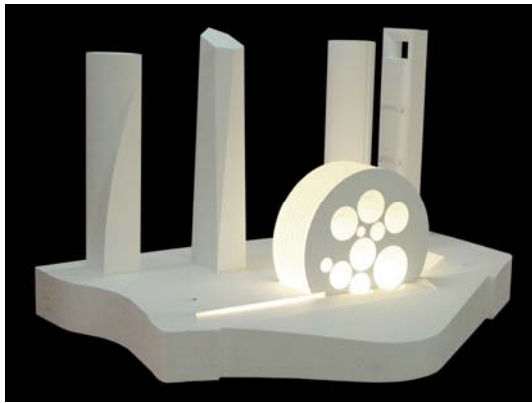


Figure 4.1-1: Scale model of CTBA [40]



Figure 4.1-2: CTBA, May 2007

The CTBA is often referred to as “Antigua Ciudad Deportiva” being the former sports complex of the local football club Real Madrid. The development of this 30,000 m² large area was made possible by an agreement between the city council, the regional government and Real Madrid. The latter moved its sports facilities to a location outside the city. In turn, the municipality changed the site’s urban development plan to enable the construction aforementioned buildings. Real Madrid, the municipality and the regional government became the owners of the building plots.

The four tall building plots were sold to interested developers, after which architects were invited to subscribe to an international design competition individually organised by each developer. The winning architects completed their designs and the construction started in 2004. Torre Espacio, Torre de Cristal and Torre Sacyr Vallehermoso were inaugurated in 2008, whilst the inauguration of Torre Caja Madrid is expected in 2009. These buildings are Spain’s four tallest buildings with heights ranging from approximately 220 m to 250 m.

Three tall buildings are exclusively designed to house offices whereas one building is designed to provide for hotel and office space. Each building plot covers an area of 75 m x 100 m and facilitates a five- or six-level car park.

4.2 Torre Espacio

Architecture

This office building, designed by Pei, Cobb, Freed & Partners in collaboration with Reid Fenwick Asociados, is characterised by its unusual geometry based on a the cosine function. At ground level the square floor plan has approximate dimensions of 43 m x 43 m and towards the top it progressively converts into a quasi-elliptic plan composed of two arcs of a circle (figure 4.2-1). The above ground height of the building is approximately 219 m, whereas the basement reaches -18 m.

The building was commissioned by Inmobiliaria Espacio (Grupo Villar Mir) and reached its final height in March of 2007. Each storey is divided into two fire compartments.

The building has three commercial-use storeys, forty-three office levels, two sky-lobbies, two storeys for the corporative management and three mechanical floors.

The building's envelope consists of storey-high double-skin façade elements with a modular width of 1,20 m. The façade is composed of a double-glazed curtain wall, a cavity with computer-controlled sunshades and an interior glazed panel. The return air from the office climate system is used to ventilate the façade's cavity and thus save on energy consumption. A cold ceiling has been adopted in this building; cooled water runs through ducts within the lowered ceiling.



Figure 4.2-1: Torre Espacio

Smoke detectors are used in the building in combination with heat detectors in the basement. An automatic sprinkler system is used to prevent fire propagation, besides other fire safety measures such as alarm buttons and fire extinguishers.

Structure

The structural design has been carried out by the local engineering firm MC2. The structure of Torre Espacio is extensively dealt with in section 5.2.

The supporting structure is composed of three reinforced concrete cores with reinforced or composite perimeter columns. The composite columns, with rolled steel sections, are mainly used to reduce the column dimensions at entrance level. The floor

structure consists of a reinforced concrete flat plate structure. An in-situ concrete floor system has been adopted to claim as few as possible the scarce crane capacity and to allow a traditional construction technique.

4.3 Torre de Cristal

Architecture

The Torre de Cristal, describing the diamond-like shape of the building, is also known as the Torre Mutua Madrileña after the insurance company that developed this office building. Cesar Pelli & Associates, in collaboration with Ortiz & Leon Arquitectos, designed this diamond-like office building. The building has a rectangular floor plan of approximately 50 m x 30 m at ground level. The corners are progressively “cut” towards the top exposing large triangles at the building’s corners, as can be seen in figure 4.3-1. The reflecting glass envelope accentuates the building’s shape.



Figure 4.3-1: Torre de Cristal under construction



Figure 4.3-2: Artist impression of Torre de Cristal [16]

This building, with a total height of approximately 250 m, is composed of forty-six office storeys, five mechanical levels, a retail-use entrance lobby and a 40 m high winter garden at the top of the building. This winter garden will be lit at night, which will give the building a kind of lighthouse appearance (figure 4.3-2).

The building's envelope consists of prefabricated modular elements with dimensions of 2,4 m x 4,2 m. A double-skin curtain wall with an intermediate air cavity of 20 cm constitutes the building's façade. The air cavity is ventilated with return-air from every floor to transfer local excessive cold or heat to the internal mechanical ventilation system. The façade element fixing is done by mobile cranes from the inside onto a steel rail that is cast in the edges of the concrete floor. The climate system is located above a suspended ceiling with a height of 60 cm. A 40 cm high technical floor is used to house the cables and ducts for telecommunication, data and electricity.

Each floor is divided into two fire compartments and the maximum in-plan evacuation distance is 25 m. The structure and partition walls have a 180 min. fire resistance. Every floor is equipped with an automatic sprinkler system and all escape routes are pressurised to prevent smoke from entering. Furthermore, every 10 storeys the building has a shelter area with a capacity of up to 150 people.

Structure

A composite structural system has been adopted by the Madrid-based engineering firm OTEP to bear the vertical and horizontal loads. A large central reinforced concrete core with composite perimeter columns supports the building. The horizontal floor structure generally comprises an integrated floor beam system supporting hollow-core concrete slabs.

The reader is referred to section 5.3 for a more in-depth discussion of the structure of Torre de Cristal.

4.4 Torre Sacyr Vallehermoso

Architecture

Torre Sacyr Vallehermoso is the only building design by an all-Spanish design team, being the architect Rubio & Álvarez-Sala and the structural engineering firm MC2. The building has a height of approximately 232 m and the lower two-thirds are occupied by a hotel whilst the upper third is designed to house offices. The prismatic geometry of the floor plan is quasi-circular (see section figure 4.4-1 and 4.4-2) and was based on aerodynamic, façade-to-floor area ratio and optical slenderness considerations.

The construction started in 2004, commissioned by Testa Inmuebles en Renta (Grupo Sacyr Vallehermoso), and was completed in 2008.



Figure 4.4-1: Torre Sacyr Vallehermoso under construction



Figure 4.4-2: Torre Sacyr Vallehermoso upon completion

The building's envelope comprises two separated façade panels; one interior double-glazed façade as the primary building enclosure and a second single-glass façade element with a distance of approximately 1 m between each other. As is shown in figure 4.4-3 and 4.4-4, the outer façade panels are placed in fish-scale pattern and result in an open and permeable layer. The air can freely circulate in between the mentioned façade layers ventilating this space when heated by solar radiation. From the structural point of view, it is suggested that the roughness and permeability reduces the across-wind vibrations induced by vortex-shedding.



Figure 4.4-3: Fish-scale outer façade

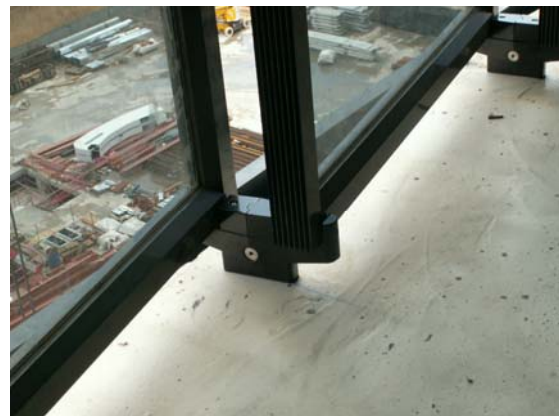


Figure 4.4-4: Outer façade detail

Following directly from the building's geometry, each floor is divided into three fire compartments. The extension of the floor slabs outside the internal façade impedes fire jump-over between floors. Three pressurised evacuation stairwells (limiting the maximum evacuation distance to 20 min) in the building's corners and small fire-free shelter areas every two floors are provided. All structural steel elements are coated with a fire resistant mortar.

Structure

The vertical structure consists of a central reinforced concrete core with two rings of mainly composite columns. The use of composite columns was chosen because of the fast erection time of the steel frame and the independency during construction between the concrete and steel structure. A composite metal deck floor with composite beams constitutes the horizontal structure outside of the core.

The structure, designed by the local engineering firm MC2, is discussed thoroughly in section 5.4.

4.5 Torre Caja Madrid



Figure 4.5-1: East elevation

Architecture

The initial developer of the Torre Caja Madrid (formerly known as Torre Repsol), oil and gas company Repsol, commissioned the design in January 2002. The construction of Foster & Partners design started in 2004 and the inauguration of the building is expected in 2009.

The building is divided into three segments consisting of two mechanical levels and eleven (twelve in the middle segment) office storeys. Two more mechanical levels are located in the arch-like crown of the building (see figure 4.5-1) and an auditorium suspended from the structure above the entrance lobby. Each block of office storeys, measuring approximately 43 m x 32 m, is supported by large trusses in the mechanical levels. These trusses span in between the building's lateral cores.

Figure 4.5-1 and 4.5-2 provide two side-elevations of the building.

A glazed and open appearance is obtained in north-south direction towards the city centre and the Guadarrama Mountains. The lateral cores in the east-west direction give the building a rather solid and closed appearance. This orientation blocks the entrance of direct sunlight during normal office hours.



Figure 4.5-2: South elevation

A total number of twelve columns run through every office block; only four of them are internal columns. The flexibility of the floor plan, together with the highly transparent floor plan, is the greatest advantage of Torre Caja Madrid.

The office-storey façade elements are double-skin elements with motorised blinds in between the inner and outer glass panel.

The tower has a 180 min fire rating and the stairwells, shelter areas and lobbies are pressurized to prevent smoke and toxic gasses from entering. An automatic fire detection system is linked to a sprinkler system.

Structure

The structural design of Torre Caja Madrid has been carried out by Halvorson and Partners.

The mega structure consists of two lateral reinforced concrete cores with three steel trusses framing into the cores, and a steel pin-connected structure at the top of the building (arch). The secondary structure consists of twelve steel or composite columns and a composite steel deck floor slab with composite beams.

Each steel truss, located in the mechanical levels, architecturally highlighted by a set-back in the façade supports one office block. The building provides structural

robustness and redundancy by means of these trusses; each truss is designed to resist the gravity load from an additional office block in the event that one truss cannot fulfil its load bearing function.

5 Structural analysis

The wind-induced along-wind response, in terms of lateral displacement and acceleration, of the aforementioned tall buildings is being analysed in this chapter. The material properties, loads and load combinations are applied according to the relevant Eurocodes. Nonlinear elastic calculations, i.e. accounting for the P-delta effect (see subsection 2.3.1), are carried out with the finite element structural analysis program SAP2000 to obtain the building's natural vibration characteristics as well as the along-wind building displacements. Along-wind building accelerations are calculated according to appendix B.4 of Eurocode 1 [11].

Firstly some general considerations applying to the structural analysis of all four buildings are presented in section 5.1. The subsequent sections 5.2, 5.3, 5.4 and 5.5 are dedicated to the structural analyses of Torre Espacio, Torre de Cristal, Torre Sacyr Vallehermoso and Torre Caja Madrid respectively. The obtained results are summarised and discussed in section 5.6.

5.1 General considerations

This section firstly treats the typology and geometry of the building structures and their representation in the finite element model. Mechanical properties are considered in subsection 5.1.2 and the vertical and horizontal support conditions are dealt with in subsection 5.1.3. This section concludes with a discussion of the wind action acting on the four tall buildings in subsection 5.1.4.

5.1.1 Typology and geometry

Beams and columns, i.e. predominantly one-dimensional elements, are represented by *frame* elements in the computer model. *Thin-walled shell* elements are used where a two-dimensional representation of the element is desired, for instance for punched shear walls and floor slabs. In some cases fictitious elements are used to allow a simple application of loads, e.g. the application of uniformly distributed loads on a steel floor structure. Element properties of fictitious elements are adjusted in order to correspond to the real structural behaviour.

The six degrees of freedom of each joint are either free or completely fixed, i.e. no spring stiffness is assigned to structural joints.

The structural elements are represented by their centre line of gravity. The element with the greater cross-sectional dimension is governing as far as the location of the joint is concerned, meaning that the member having a smaller dimension is being elongated into the element having a greater dimension as illustrated in figure 5.1-1. This leads to a slight overestimation of the total area but results in a more exact computation of the global bending stiffness, being the latter proportional to the area of the elements times the squared distance from the structure's centroid.

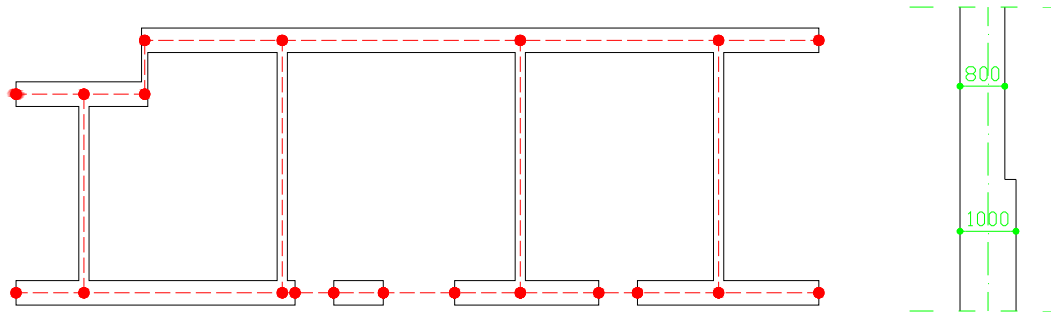


Figure 5.1-1: Element and joint representation of a structural core

The use of climbing or gliding formwork generally requires that one face of the wall is kept in-line throughout the building height. At locations where the wall thickness is changed, this leads in practice to an eccentricity as shown in figure 5.1-1. This is not covered by the finite element models for reasons of simplicity. Furthermore, wall openings with an area less than approximately 2,5 m² are omitted from the computer model.

5.1.2 Mechanical properties

Mechanical properties such as axial stiffness EA and bending stiffness EI are determined by cross-sectional dimensions and the modulus of elasticity E . Their calculation may seem in fact straightforward from the initial geometry and material properties of the considered element. This does not always hold however, especially not for concrete structures. The following paragraphs address the computation of the mechanical properties of the structural elements.

Moment of inertia

It is well known that cracking occurs in concrete elements subjected to a bending moment. These cracks appear wherever tensile stresses exceed the scarce tensile resistance of concrete. Furthermore, the addition of reinforcement results in a heterogeneous section and hence structural behaviour. The last two aspects have an important influence on the element's moment of inertia.

In figure 5.1-2, taken from reference [5], a coupling beam is shown and three ways are presented to calculate the moment of inertia I . Case A shows the computed moment of inertia of the cracked concrete section while taking into account the rebars. Case B represents the moment of inertia of the gross concrete section considered uncracked and without considering the reinforcement. Case C is the moment of inertia considering an uncracked concrete section with reinforcement steel.

Although the influence of the reinforcement could be easily accounted for in structural analyses, this results more difficult for concrete cracking especially in complex structures. The occurrence of cracks in concrete elements depends on the development of the real stress history.

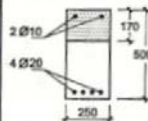

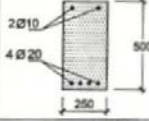
| CASE | CONSIDERED SECTION | VALUE OF I (mm ⁴) |
|------|---|-------------------------------|
| A |  | 153300 · 10 ⁴ |
| B |  | 260400 · 10 ⁴ |
| C |  | 322300 · 10 ⁴ |

Figure 5.1-2: Moment of inertia of a coupling beam [5]

It is observed that case B is quite close to the average of the two extreme situations A and C, corresponding to a fully cracked and uncracked situation respectively. This thesis is focussed on the structural behaviour in the serviceability limit state, because of which the applied bending stresses are relatively small. Therefore the moment of inertia is in general computed by disregarding the effects of concrete cracking and reinforcement; simply considering the gross concrete area. For singular structural elements, such as outrigger structures and foundation slabs, the calculation method is decided upon case by case.

For reinforced concrete shear walls it is checked that no tensile stresses, exceeding the mixture's mean tensile strength, occur due to the wind-induced overturning moment.

Modulus of elasticity

The governing material property within the scope of this thesis is the modulus of elasticity or Young's modulus. The determination of this material property is treated in what follows for concrete, steel and composite members.

Concrete members

The variation in time of the secant modulus of elasticity of different concrete qualities can be estimated according to Eurocode 2 [13] by

$$E_{cm}(t) = \left(\frac{f_{cm}(t)}{f_{cm}} \right)^{0,3} E_{cm} \quad (5.1.1)$$

where $E_{cm}(t)$ modulus of elasticity at t [MPa]
 t time [days]
 $f_{cm}(t)$ mean compressive strength at t [MPa]
 f_{cm} mean compressive strength at 28 days [MPa]
 E_{cm} modulus of elasticity at 28 days [MPa]

The development of the mean compressive strength depends predominantly on the cement type used in the concrete mixture, the temperature during concrete hardening and the relative air humidity. For a mean temperature of 20° and relative air humidity equal to, or greater than, 95% the development of the mean compressive strength is given by

$$\left(\frac{f_{cm}(t)}{f_{cm}} \right) = \beta_{cc}(t) = e^s \left[1 - \left(\frac{28}{t} \right)^{1/2} \right] \quad (5.1.2)$$

where s is a coefficient that depends on the cement type:

- 0,20 for cement of strength classes CEM 42,5 R, CEM 52,5 N and CEM52,5 R
- 0,25 for cement of strength classes CEM 32,5 R and CEM 42,5 N
- 0,38 for cement of strength class CEM 32,5 N

When the mean temperature is not equal to 20° C the age of the concrete has to be substituted by a corrected age t_T given by [5]

$$t_T = \sum_{i=1}^{i=n} \Delta t_i e^{-\left[\frac{4.000}{273+T(\Delta t_i)} - 13,65 \right]} \quad (5.1.3)$$

Where T is the temperature in degrees Celsius and Δt the time period associated with temperature T .

Figure 5.1-3 shows the development of the mean compressive strength for a C25/30 concrete quality over a period of 60 days assuming a mean temperature of 20°, relative humidity of 95% and a cement strength class CEM 32,5 R.

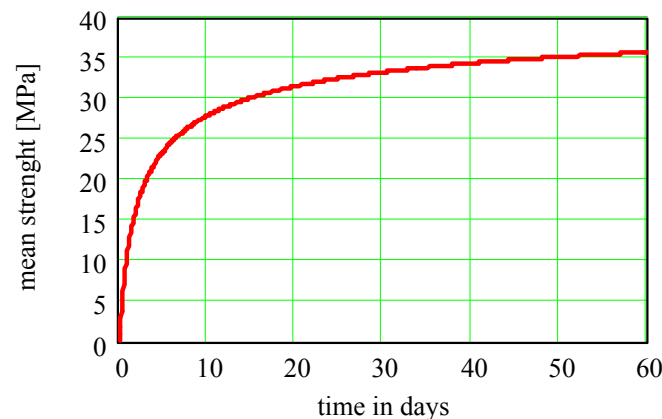


Figure 5.1-3: Development of mean strength in time

The modulus of elasticity of concrete largely depends on its composition and thus the aggregate. The mean modulus of elasticity at 28 days for concrete with quartzite aggregate and for $\sigma_c < 0,4 f_{cm}$ is estimated by

$$E_{cm} = 22.000 \cdot \left(\frac{f_{cm}}{10} \right)^{0,3} \quad (5.1.4)$$

with

$$f_{cm} = f_{ck} + 8MPa \quad (5.1.5)$$

where f_{ck} is the 28 days characteristic cylinder compressive strength in MPa.

For limestone and sandstone aggregates the obtained value in expression (5.1.4) should be reduced by 10% and 30% respectively, while the value should be increased by 20% for basalt aggregates.

The development of the mean modulus of elasticity for a concrete strength C25/30 with the aforementioned characteristics over a period of 60 days is shown in figure 5.1-4.

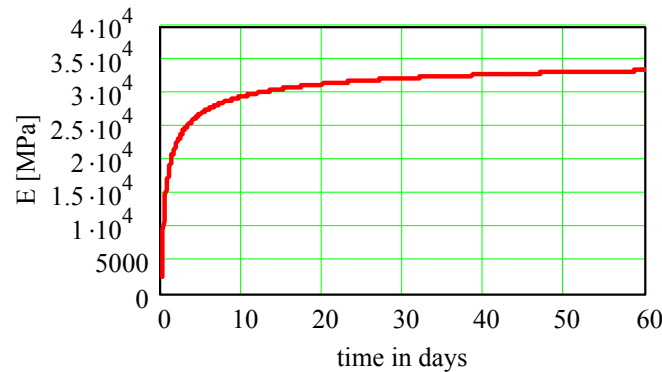


Figure 5.1-4: Development of modulus of elasticity in time

Table 5.1-1 presents the ratio $E_{cm}(t)/E_{cm}$ as a function of different ages and cement types for the given mean temperature and relative humidity.

| time in days | 7 | 28 | 90 | 365 |
|--------------|------|------|------|------|
| s = 0,20 | 0,91 | 1,00 | 1,05 | 1,08 |
| s = 0,25 | 0,88 | 1,00 | 1,06 | 1,10 |
| s = 0,38 | 0,83 | 1,00 | 1,09 | 1,15 |

Table 5.1-1: Ratio $E_{cm}(t)/E_{cm}$ for different ages and cement types

The modulus of elasticity adopted in this thesis is the 28 days value of the mean modulus of elasticity calculated according to expression (5.1.4). Note that employing the 28 days value is rather conservative considering the typical construction time of tall buildings.

Wind action is a short term load for which time differential effects can be safely neglected. No adjustments of the modulus of elasticity are made to account for creep or shrinkage effects.

Table 5.1-2 shows the 28 days value of the secant modulus of elasticity for different characteristic cylinder compressive strengths, as used in the structural analysis.

| | | | | | | | | | | |
|----------------|------|------|------|------|------|------|------|------|------|------|
| f_{ck} [MPa] | 25 | 30 | 35 | 40 | 45 | 50 | 55 | 60 | 65 | 70 |
| E_{cm} [GPa] | 31,2 | 32,8 | 34,1 | 35,2 | 36,3 | 37,3 | 38,2 | 39,1 | 39,9 | 40,7 |

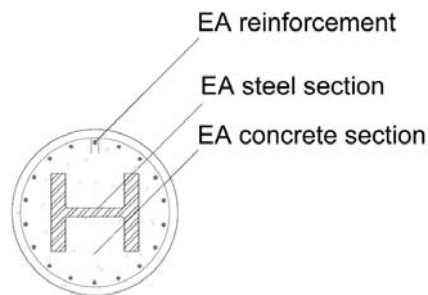
Table 5.1-2: Secant moduli of elasticity for different compressive strengths

Steel members

A range of different steel qualities is used in the analysed building structures. For all types of steel the same modulus of elasticity is considered being $E = 210$ GPa.

Composite members

In the strict sense of the word practically all concrete elements used in the building industry are composite members due to the addition of reinforcement. In this thesis however, no normally reinforced concrete members are meant when referring to composite members. In general members are denominated composite when they consist of other than the traditional concrete-rebar interaction.



$$\Sigma(EA_i) = EA_{\text{column}}$$

Figure 5.1-5: Effective axial stiffness of composite columns

For heavily reinforced concrete and composite columns predominantly subjected to axial loading, the effective axial stiffness is considerably larger than the axial stiffness of the gross concrete section. Whenever this effect for a given member yields an increase of more than 5%, it is taken into account in the structural analysis. Full collaboration by means of friction and adherence between steel and concrete is assumed for serviceability limit state considerations (figure 5.1-5).

This increase is taken into account in the structural analysis by multiplying the gross member area by a factor k , as shown in expression (5.1.6), relating the effective axial stiffness to the axial stiffness of the gross concrete section.

$$k \cdot A_{c,gr} = \frac{\sum_{i=1}^{i=n} EA_i}{E_c} \quad (5.1.6)$$

It is shown in appendix III.1.3 and III.2.3 that values of k of over 60% are obtained for heavily reinforced and composite concrete columns.

5.1.3 Support conditions

The building structures are vertically and horizontally supported by the foundation and possibly by the basement. The soil-structure interaction is accounted for in the structural analyses. The vertical support conditions are represented by the entire foundation supported by linear vertical springs with the corresponding spring constant. The perimeter slurry walls with the diaphragm action of the basement floors are included, with the corresponding elastic support, to provide a realistic representation of the horizontal support conditions.

Vertical support

As far as the vertical support conditions are concerned, three of the four buildings have a shallow foundation by means of a large footing with a height of in between 4 m and 5 m. The local soil conditions are exceptionally good; the soil underneath the building structures (mainly compact fine sand) has a very high resistance and stiffness characteristics. The soil-structure interaction is represented by a series of vertical springs underneath the foundation slab with a spring constant based on an estimated modulus of subgrade reaction $K = 25.000 \text{ kN/m}^3$. The latter value is taken from a geotechnical report used in the structural design of one of the building structures.

The foundation of Torre de Cristal consists of a deep slurry wall foundation with a height of 20 m beneath basement level -6. The structure is considered to be vertically restrained at the wall's toe level. The foundation stiffness is hence governed by the axial stiffness of the slurry wall.

Horizontal support

Figure 5.1-6 sketches the vertical perimeter basement structure with the building projection. Two buildings with their corresponding basement share one excavation and therefore a perimeter slurry wall. At level -2 a ring road is constructed around the plots to connect all parking basements with the aboveground road system.

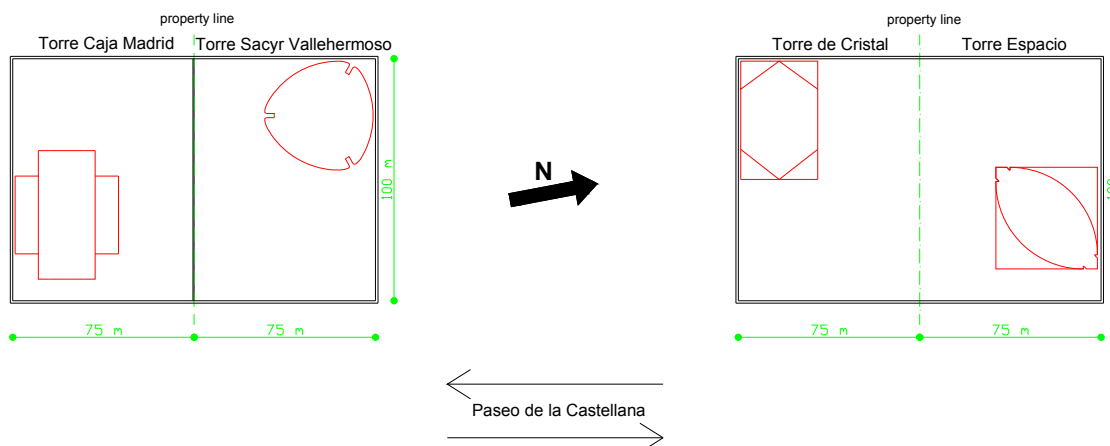


Figure 5.1-6: Basement layout

The basement structure clearly entails a horizontal support to the building structure. This support is given by the high in-plane stiffness of the slurry walls and the soil support perpendicular to those walls. The latter, however, cannot be guaranteed throughout the lifetime of a tall building. It is possible, since no influence can be exerted outside the building plot, that new underground road systems reduce the lateral support represented by the soil. Therefore, only the in-plane stiffness of the slurry wall is accounted for in the finite element model. The perimeter walls are included in the model with an elastic support represented by vertical springs.

The connectivity of the building structure with the basement structure determines whether or not the building is horizontally supported. Figure 5.1-7 and 5.1-8 show the connectivity of the buildings with the basement in horizontal plane. When no specification is given, it concerns structural joints with at least a shear connection. In either way, the basement floors of each building are not connected to the basement floors of the adjacent building.

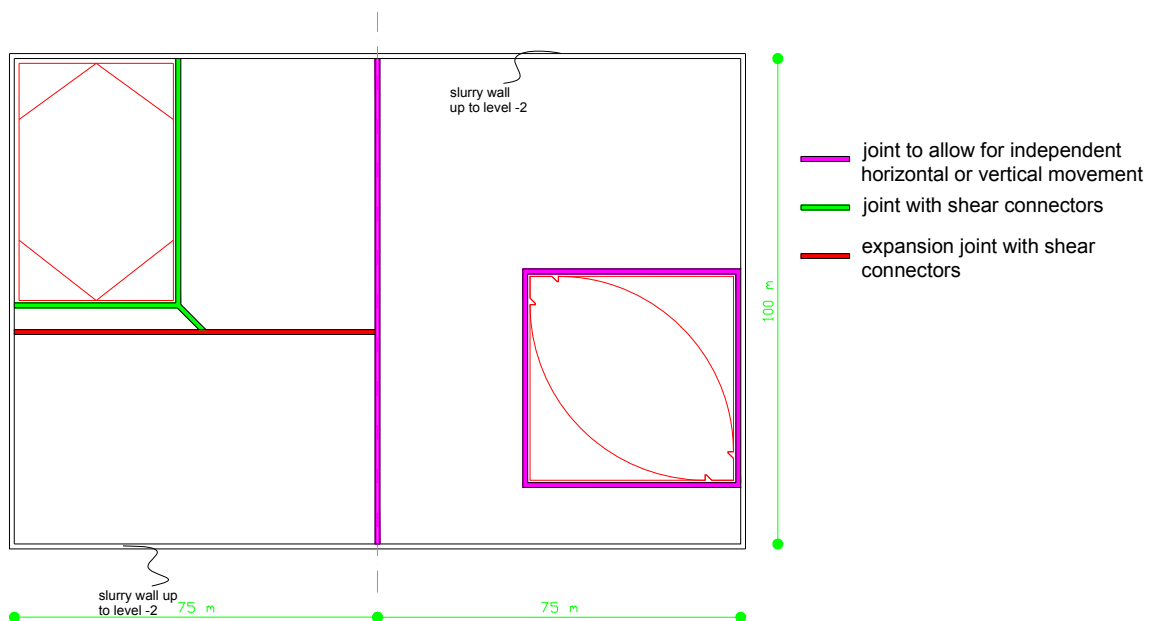


Figure 5.1-7: Basement connectivity Torre Espacio and Torre de Cristal

Torre Espacio, being the right-hand side building in figure 5.1-7, is not connected to the basement structure by any means. The basement and the building are two completely independent structures.

Torre de Cristal, however, is directly connected to the upper longitudinal and transverse slurry wall. Through the diaphragm action of the basement floors in the horizontal direction in figure 5.1-7, the structure is also supported by the lower longitudinal slurry wall. Thus Torre de Cristal is elastically supported in horizontal sense by the perimeter slurry walls from level -2 down.

Torre Sacyr Vallehermoso is horizontally supported from level -2 due to the in-plane stiffness of the slurry walls, by means of the diaphragm action of the basement floors as can be seen in figure 5.1-8.

The slurry walls around Torre Caja Madrid have been elongated to grade and another wall has been built next to the property line from the foundation to grade level. This structure experiences a flexible horizontal support from ground level down to the foundation level.

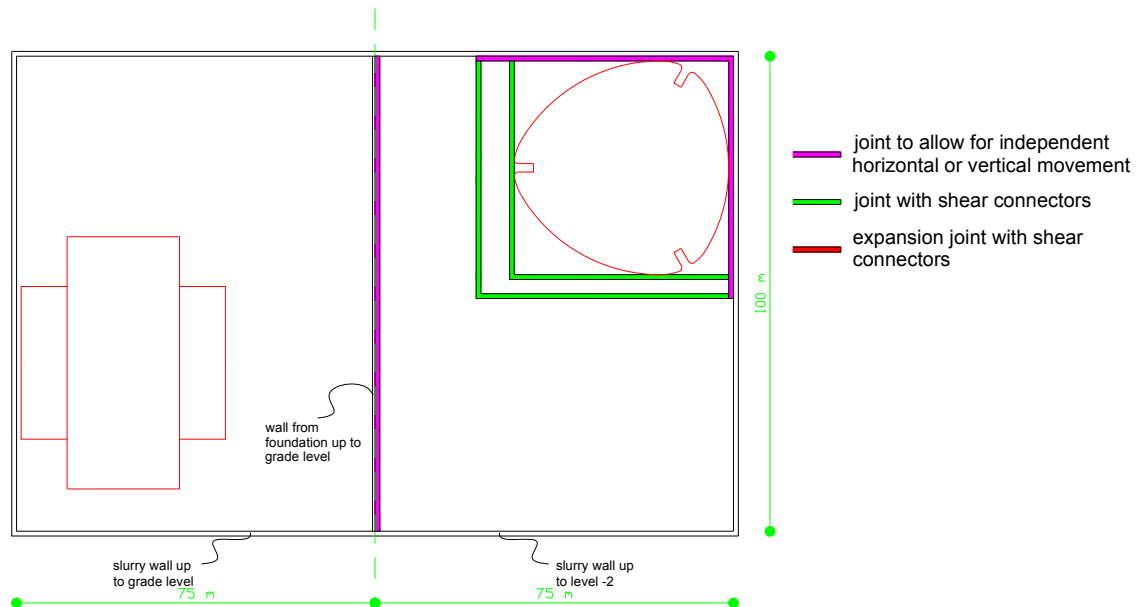


Figure 5.1-8: Basement connectivity Torre Sacyr Vallehermoso and Caja Madrid

5.1.4 Wind action

It has been stated in the preceding chapters that the wind load is a dynamic load. In building codes the wind action is usually treated as a quasi-static load, i.e. introducing factors accounting for the dynamic characteristics of the load and structural response, to enable a static structural analysis.

The structure's susceptibility to the wind action depends, among other aspects, on the lowest natural (fundamental) vibration of the structure in the considered wind direction.

Natural vibrations

Eurocode 1 proposes expression (5.1.7) to obtain, a fairly rough, estimation of the fundamental frequency for buildings with a height greater than 50 m.

$$n = \frac{46}{h} \quad (5.1.7)$$

where h building height [m]
 n fundamental frequency [Hz]

Within the scope of this thesis, it is considered that expression (5.1.7) is far too general, because the fundamental building frequency has a great influence on the susceptibility to wind action. Modal analyses are carried out with the finite element models in SAP2000 to obtain a more reliable estimation of the natural building frequencies and mode shapes.

The modal analyses for serviceability limit states are based on a quasi-permanent gravity load combination, as defined in Eurocode 0 [10]

$$\sum_{j \geq 1} G_{k,j} + \sum_{i \geq 1} \psi_{2,i} \cdot Q_{k,i} \quad (5.1.8)$$

where the value of ψ_2 is recommended 0,3 for both office and residential areas.

Wind load

The calculation of the 50-year static equivalent wind load as well as the estimation of the 5-year and 10-year lateral building accelerations has been carried out according to Eurocode 1 [12]. The use of the cited Eurocode is limited to buildings with a height of up to 200 m. It is shown in appendix II.1 that for the given building heights and terrain roughness, the error in the results of Eurocode's simplified logarithmic formula is approximately equal to the range of error implicitly accepted by Eurocode 1.

Eurocode 1 adopts expression (5.1.9) for the calculation of the wind-induced force on any structure or element

$$F_w(z) = c_s c_d \cdot c_f \cdot q_p(z) \cdot A_{ref} \quad (5.1.9)$$

where c_s, c_d structural factor [-]
 c_f force coefficient [-]
 $q_p(z)$ peak wind pressure at height z [Pa]
 A_{ref} reference area [m²]

The basic wind velocity, being the 10-minute average measured at a height of 10 m in open terrain (category II) with a return period of 50 years, for Madrid is 26,0 m/s and taken from figure 5.1-9 from the current Spanish building code Código Técnico de la Edificación (CTE).

The terrain is considered as terrain category III with a corresponding roughness length of 0,3 m. Appendix III.1.1 presents the calculation of the roughness factor, relative turbulence intensity as well as the peak and mean wind velocity and wind pressure as a function of the height. The resulting 50-year wind velocity profile is sketched in figure 5.1-10.

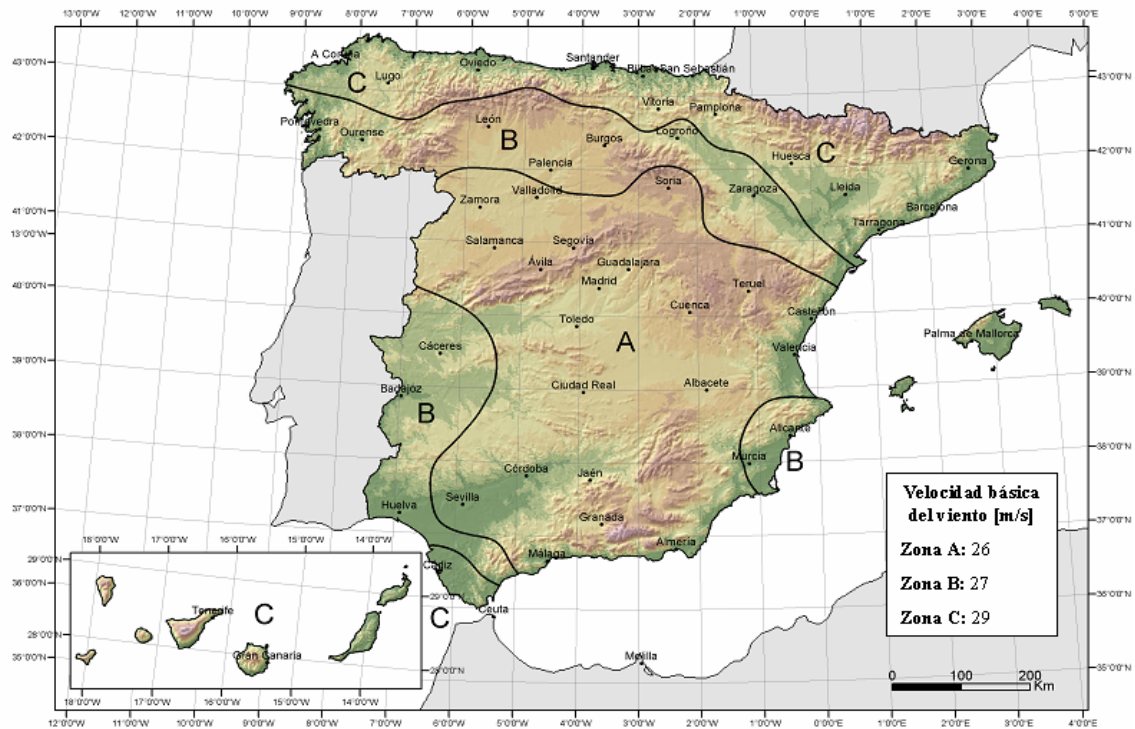


Figure 5.1-9: Basic wind velocities in Spain according to CTE

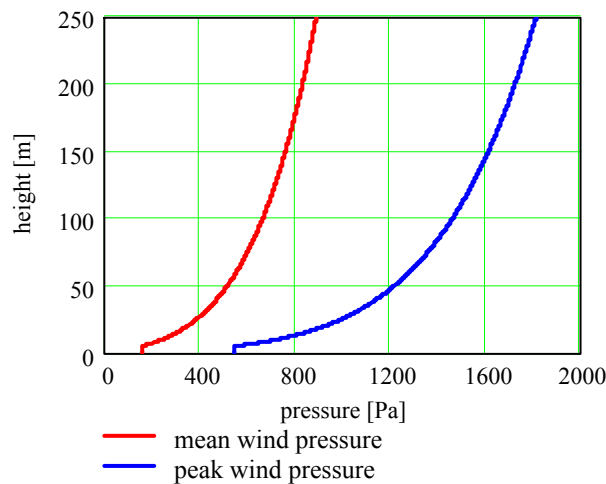


Figure 5.1-10: 50-year peak and mean wind pressure profile

The structural factor is composed of the size and dynamic factor. The former accounts for the correlation of peak wind pressures over the building surface, while the latter represents the dynamic amplification due to the resonance of the structure with the wind gusts. Both factors are calculated for all four buildings with the most significant differences found in the dynamic factor.

In appendix III.1.2 the calculation method for both factors is explained by means of graphs based on example variables.

Figure 5.1-11 provides a plot of the size factor as a function of the sum of the building width and height divided by the integral length scale of longitudinal turbulence. The y-axis represents the spatial average of the peak wind force in relation to the peak wind force assuming full spatial correlation between wind gusts. The dynamic factor as a function of the fundamental building frequency, is plotted in figure 5.1-12 for the given example variables in appendix III.1.2. In this case the y-axis presents the dynamic wind-induced forces, as a result of the resonance of the structure with the wind gusts, in relation to the surface-averaged peak wind force.

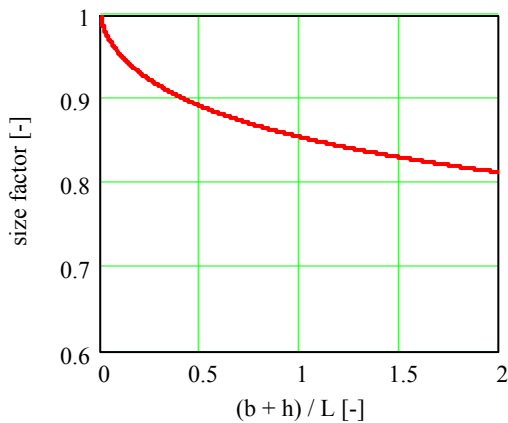


Figure 5.1-11: Size factor

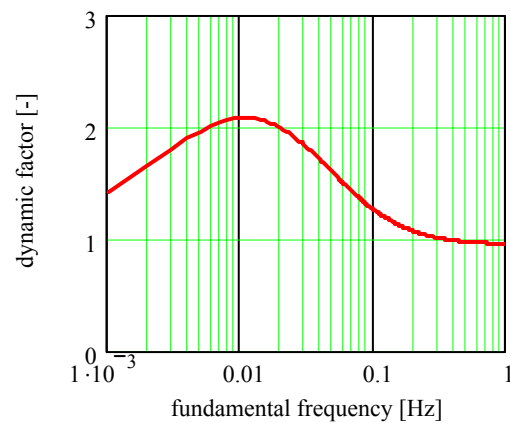


Figure 5.1-12: Dynamic factor

As far as the force coefficient c_f is concerned, the Eurocode only prescribes values for regular building geometries. The determination of the force coefficients is usually done by means of wind tunnel testing which is, obviously, not within the scope of this thesis. Instead, the external wind pressure coefficients shown in figure 5.1-13, recommended by the former Spanish building code NBE AE88 [27], are used.

Finally the wind force is applied to the finite element models of the buildings at every storey on a fictitious perimeter beam. The applied wind force is the product of the global structural factor, 50-year peak wind pressure, external wind pressure coefficient and the storey height. The latter procedure is followed to obtain the 50-year lateral building displacements.

The 5 and 10-year building accelerations are calculated according to appendix B of Eurocode 1. Different return periods are related to different wind velocities by the following formula

$$\frac{v_T}{v_{50}} = \left[\frac{1 - 0,2 \cdot \ln\left(-\ln\left(1 - \frac{1}{T}\right)\right)}{1 - 0,2 \cdot \ln\left(-\ln\left(1 - \frac{1}{50}\right)\right)} \right]^{0,5} \quad (5.1.10)$$

with T being the return period and both coefficients 0,2 and 0,5 as recommended by the Eurocode.

accelerations of the four tall buildings analysed in this thesis, because of the small distance between them.

Vortex-shedding occurs when vortices are shed alternatively from opposite sides of the building, creating in that way fluctuating loads perpendicular to the wind direction. Dangerous resonance may occur when the frequency of vortex-shedding is the same as the building's natural vibration. The frequency of vortex-shedding depends on the Strouhal number which, in turn, depends on the building's cross section. The Strouhal number is calculated as follows

$$St = \frac{n \cdot D}{v} \quad (5.1.10)$$

where St Strouhal number [-]
 n full cycle frequency of vortex shedding [Hz]
 D characteristic body dimension normal to the flow [m]
 v relative velocity [m/s]

When the building breadth is taken as the characteristic dimension normal to the air flow, a critical wind velocity can be defined at which the vortex-shedding frequency is equal to a natural building frequency n_i such that

$$v_{crit,i} = \frac{n_i \cdot B}{St} \quad (5.1.11)$$

Eurocode 1 states that the effect of vortex-shedding does not need to be investigated if $v_{crit} > 1,25 v_m$, with the mean wind velocity at the location where vortex-shedding occurs.

With the given mean wind velocity profile in figure 5.1-10, vortex-shedding is not likely to result in a governing load case as far as Torre Espacio, Torre de Cristal and Torre Caja Madrid are concerned. This is, firstly, due to the relative low Strouhal numbers associated with the building geometries. Secondly, it concerns non-prismatic buildings (with changing in-plan geometry) because of which no uniform vortex-shedding can occur along the building height. The geometry of Torre Sacyr Vallehermoso, however, would make a vortex-shedding analysis necessary due to the high Strouhal number for circular sections (appendix II.5). However, it is believed that the building envelope's porosity and relative roughness creates a turbulent layer around the building due to which no uniform vortex-shedding pattern can be established along the building height.

5.2 Torre Espacio

The structural analyses of the building structure of Torre Espacio are presented in this section. The structure and its representation in the finite element model are treated in subsection 5.2.1. Subsection 5.2.2 and 5.2.3 discuss the aerodynamic building characteristics and the results in terms of lateral displacement and acceleration.

5.2.1 Structure

The square floor plan at base level has approximate dimensions of 42 m x 42 m. The floor plan changes progressively towards the top in a quasi-elliptical shape composed of two arcs of a circle with a radius of 35,6 m. The building has the greatest cross sectional dimension along the x-axis, as can be seen in figure 5.2-1, being approximately 59 m. The total building height above grade is approximately 223 m, while the substructure consists of a six-level basement with a total depth of 18 m.

The vertical structure consists of three reinforced concrete cores with composite or reinforced concrete columns. One central, relatively large, box-shaped core runs along the total height of the building and two lateral C-shaped cores reach up to approximately one-third and two-third of the building height.

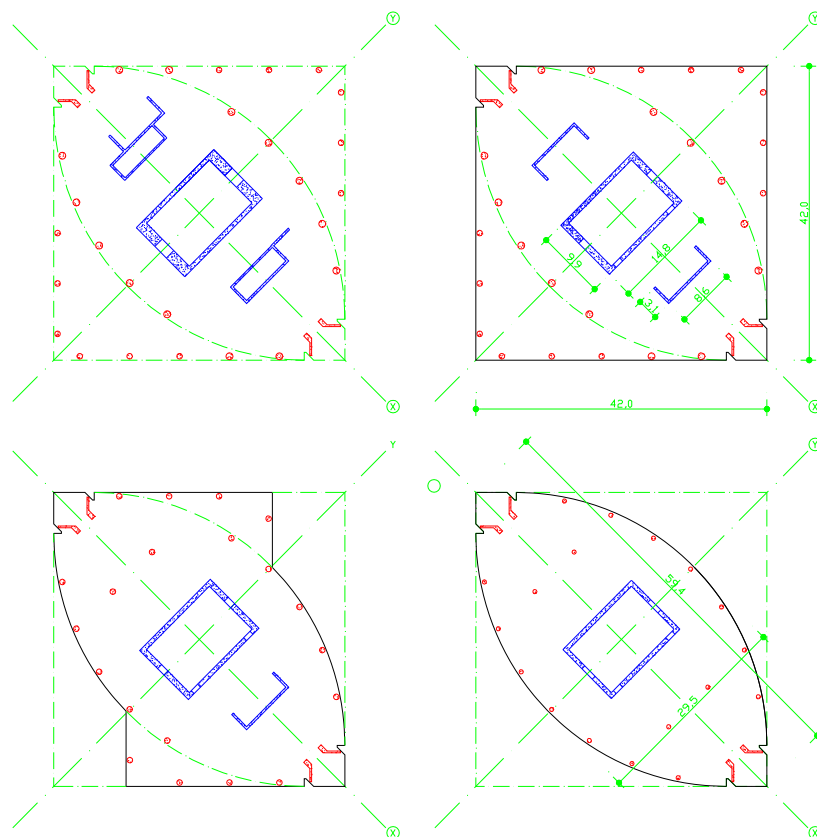


Figure 5.2-1: Typical floor plan at basement, low-, mid- and high-rise level

A two-way reinforced concrete flat plate constitutes the floor system in the entire building. Two great discontinuities exist in the building structure: an outrigger structure at approximately two-third of the building height and a transfer structure at the first mechanical level (see figure 5.2-3 and 5.2-5 respectively). A shallow slab-on-grade foundation has been employed to transmit the loads to the underlying soil.

Core structure

The central core has a box shape with approximate in plan dimensions of 10 m x 15 m. The wall thickness of the longitudinal shear walls is 600 mm throughout the entire height, while the transverse walls have a varying thickness of 1500 mm, 1000 mm, 800 mm, and 400 mm. From the foundation up to the first storey a C70/85 concrete quality has been used, being the concrete quality C40/50 up to storey 8. From that storey up to the top, with exception of the outrigger levels, a C30/37 concrete quality has been used. The two outrigger level floors are poured with C70/85 due to the high local stresses.

The two lateral cores of approximately 3 m x 9 m have an open C-shape. The left-hand side core goes up to storey 14 and the one on the right-hand side up to mechanical level 2 "M2". All shear walls have a constant thickness of 300 mm. Both lateral cores are poured with the same concrete quality variation as the main central core.

The effective axial stiffness of the shear walls, especially of those near the base level, is considerably higher than the axial stiffness corresponding to the gross concrete area as a result of relatively high level of reinforcement. It can be seen in appendix III.2.3 that the maximum increase of axial stiffness is around 7%. Adjustments have been made in the computer model for elements with an effective axial stiffness more than 5% greater than the axial stiffness of the gross concrete section. This resulted in adjusting the cross section of the shear walls with a thickness of 800 mm and 1200 mm.

Columns

The inner columns, forming the two arcs of a circle in figure 5.2-1, run along the entire building height. The outer columns form the square shape at base level, being the ones on the upper and lower part in figure 5.2-1 straight and the left- and right-hand side columns curved as to provide for the progressively changing floor geometry. The outer curved columns are finally converted into an inner column and their transition, being complicated by the eccentricity between both columns, is solved by one-storey high massive concrete transition blocks (figure 5.2-2 and 5.2-3).

Where the two lateral C-shaped cores stop, at level 14 and M2, concrete reinforced columns are used to bear the floor loads up to the top of the building.

Column diameters range from 1200 mm, 1000 mm, 900 mm, 800 mm and 600 mm. The concrete qualities that have been applied are C70/85 up to the first storey, C40/50 up to storey 30 and C30/37 until the building top.

In the lower part of the building composite columns with reduced cross-sectional dimensions are employed for aesthetical requirements. Rolled steel sections, either HEM-300 or HEM-500, are placed in the centre of the concrete area in combination with welded steel plates 2 x 390 x 30 mm or 2 x 390 x 50 mm.



Figure 5.2-2: Concrete transition block with strut-and-tie model

The floor structure has a high bending stiffness because of which the columns participate in resisting the lateral forces. This, in combination with the high axial stiffness of the columns, leads to a relatively large part of the overturning moment that is borne by the columns. Therefore, the effective axial stiffness has been computed for all columns. It is shown in appendix III.2.3 that an increase of gross axial stiffness of up to 56 % is obtained for composite columns at entrance level.

Floors

A uniformly thick reinforced concrete plate is adopted throughout the entire building, as previously pointed out. The typical floor height is 280 mm and in some cases with complex geometry or high gravity loading a height of 350 mm is used. The two post-tensioned concrete floors that are connected to the outrigger structure have a height of 380 mm. The upper floor 29 is post-tensioned to (partly) compensate the tensile forces that are induced by the stiff outrigger under gravity loads, while the post-tensioning of the lower floor is carried out to compensate the horizontal component of tension in the transition block at the same level.

The used concrete quality is C40/50 for the floors up to storey 28, C70/85 for the two floors M2 and 29 connected to the outrigger, and C30/37 for the floors up to the top of the building. From the first floor up this coincides with the concrete quality variation of the columns.

The columns in the lower part of the building are cast with C70/85 concrete. The intersection with the floors, having a characteristic strength of 40 MPa, is carried out with circular rebars that confine the concrete joint or by casting the concrete intersection with 70 MPa concrete.

Outrigger

At approximately two-third of the building height, a mechanical floor accommodates an outrigger structure. The outrigger's main goal is to reduce the building sway due to wind load, while at the same time it reduces the bending moment in the core. The location of the outrigger is, from a structural point of view, the optimum (see appendix I). A secondary effect, caused by its large flexural stiffness, is that it transfers a great part of the column loads above the outrigger to the core considerably reducing the effects of differential shortening of vertical load bearing elements (see section 2.2).

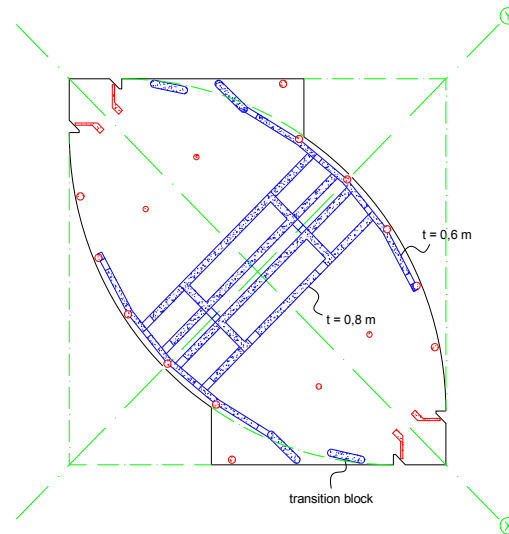


Figure 5.2-3: Outrigger structure

It can be seen in figure 5.2-3 that the outrigger provides extra stiffness predominantly in the Y-direction. Four one-storey high shear walls are protruding from the core and connected in the façade to a one-storey high belt structure. The belt structure is a 600 mm thick post-tensioned concrete wall that connects five inner columns to the core by means of four 800 mm thick post-tensioned concrete walls.

The four outrigger walls are connected to the upper and lower floor as to create a series of I sections. Under gravity load the upper part of the outrigger structure will bear great tensile forces. The upper floor and the upper part of the 4 protruding outrigger walls are, therefore, post-tensioned in order to increase the outrigger's stiffness and strength properties, see figure 5.2-4.

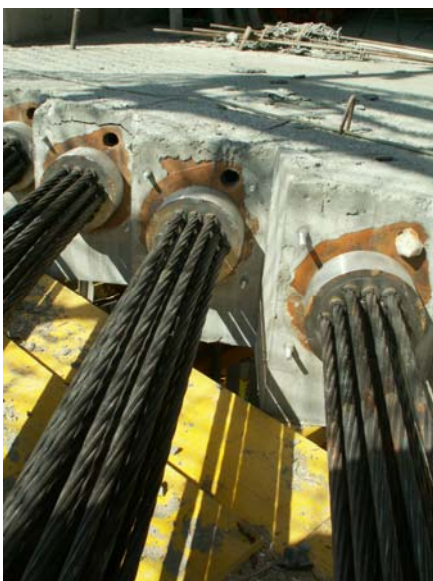


Figure 5.2-4: Detail of tendons

The entire outrigger system, composed of floors and walls, is poured with a C70/85 concrete quality. In the structural analysis neither concrete cracking nor reinforcement is considered as far as the effective moment of inertia is concerned. The latter is considered to be an acceptable approximation of the structural behaviour because of the application of post-tensioning at locations where tensile stresses are to be expected and the relatively low stresses in the serviceability limit state.

Transfer truss

At base level an open entrance is created by transferring the loads from three outer columns to the corner columns on two sides of the building.

The transfer structure consists of a two-storey high steel truss as shown in figure 5.2-5 and 5.2-6, located at a mechanical level. The steel trusses have been post-tensioned to counteract vertical deformations. The post-tensioning has been carried out in various phases according to the measured deformations.

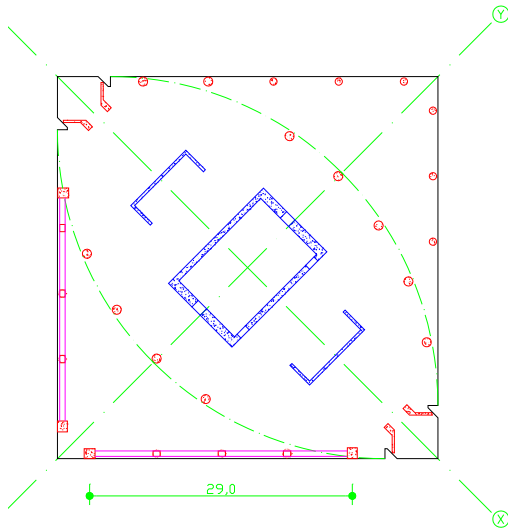


Figure 5.2-5: Transfer truss in plan



Figure 5.2-6: Transfer truss in elevation

Basement

The parking basement and the building are two completely independent structures. A non-structural joint exists between all basement floors inside and outside the building's projection.

A slurry wall is located directly on the north side of the building. Compressive foam has been used in the joint between the building floors and the slurry wall to allow differential vertical deformation. This joint could provide for some horizontal support in one direction. However, no horizontal support of the slurry wall and soil is taken into account because the future existence of the soil (presently providing the horizontal support) cannot be guaranteed.

Foundation

The foundation system adopted for the Torre Espacio is a 4 m thick reinforced concrete mat footing with approximate dimensions of 53 m x 43 m, being slightly larger than the building plan. The foundation mat has been post-tensioned in order to limit the height of the element. It has been constructed in two parts; two slabs with a thickness of 2 m each.

The concrete mat footing has a characteristic strength of 30 MPa. The full moment of inertia is used in the structural analysis, i.e. considering neither concrete cracking nor reinforcement. The soil-structure interaction is represented by a series of vertical

springs with a spring constant based on a modulus of subgrade reaction $K = 25.000 \text{ kN/m}^3$.

5.2.2 Aerodynamic characteristics

This subsection discusses the aerodynamic characteristics of Torre Espacio as well as the resulting 50-year equivalent static wind load acting upon it.

Natural vibration modes and modal mass

The natural vibration modes are determined by the stiffness and mass distribution of the building. A modal analysis has been carried out in order to obtain the building's natural vibration modes.

The acting mass is derived from the quasi permanent gravity load combination as defined in subsection 5.1.1. Table 5.2-1 shows the values of the dead and live load acting on a typical building floor.

| | outside core | inside core | stairs |
|------------------------|--------------|-------------|--------|
| G [kN/m ²] | 7,8 | 8,5 / 10,6 | 3,3 |
| Q [kN/m ²] | 4,0 | 4,0 | 4,0 |

Table 5.2-1: Gravity load per area

The massive concrete floor system obviously leads to a high value of the dead load.

Table 5.2-2 presents the first three natural vibration frequencies with the axes as shown in figure 5.2.7. Geometric nonlinearity has been incorporated in the modal analysis, i.e. the P-delta effect is accounted for; the structural "softening" due to gravity loads and the influence of the foundation's rotational flexibility. The P-delta effect increases the moments and displacements with 13 %, 11 % and 21 % for the X-, Y- and rotational direction respectively.

| | frequency [Hz] | period [s] |
|----------------|----------------|------------|
| X ₁ | 0,125 | 7,98 |
| Y ₁ | 0,135 | 7,39 |
| T ₁ | 0,322 | 3,11 |

Table 5.2-2: Frequency of natural vibrations

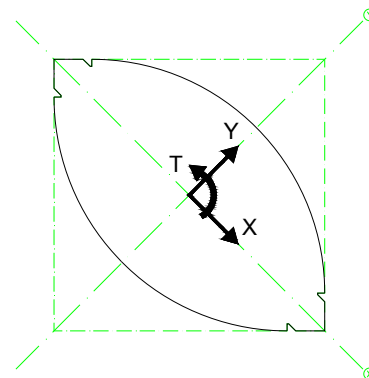


Figure 5.2-7: Axes definition

As can be seen in table 5.2-2, Torre Espacio is a quite flexible building with the two fundamental translational modes having a period in between 7,4 and 8 seconds. The great bending stiffness of the flat plate floor structure results in a rather large

contribution of the columns to the lateral stiffness. This contribution is further enhanced by the application of the outrigger and belt structure. A thorough analysis revealed that the contribution of the cores and columns to the lateral stiffness in the y-direction is approximately 35% - 65% (40% due to the floors and 25% due to the outrigger and belt structure). In the x-direction the stiffness distribution resulted 30% - 70% for the cores and columns respectively. Note that this is a highly unusual stiffness distribution between core and columns.

The modal shape of natural vibration mode Y_1 , corresponding to the governing wind direction, is presented in figure 5.2-8.

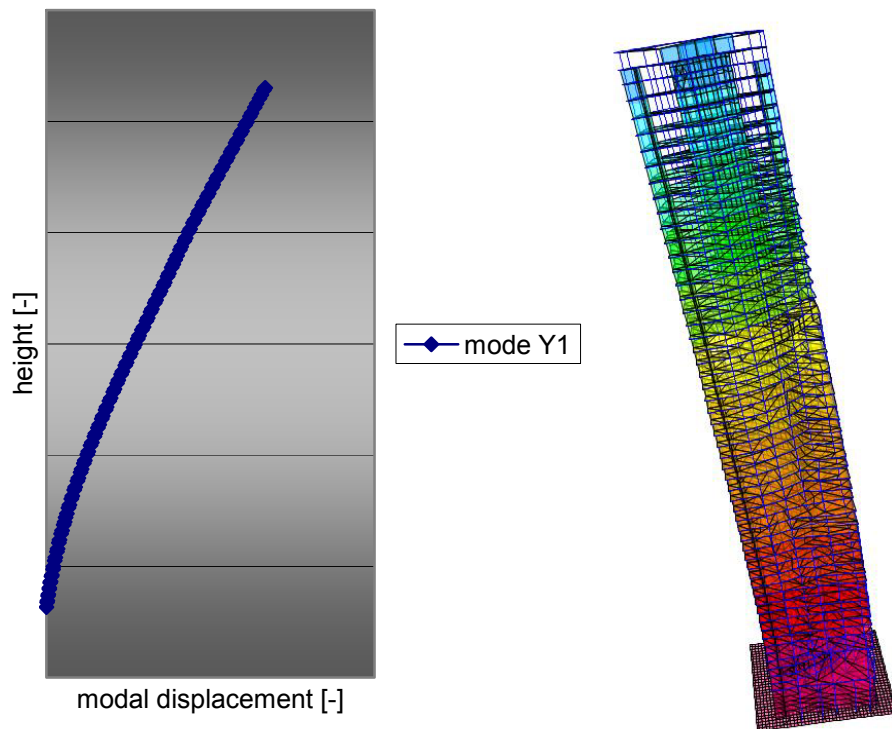


Figure 5.2-8: Modal shape of natural vibration mode Y_1

The modal mass per unit length of the fundamental vibration in y-direction can now be calculated by

$$m_{m,Y1} = \frac{\int_0^h u_{Y1}(z) \cdot m(z) dz}{h} \approx 0,42 \cdot 307,5 \cdot 10^3 \frac{kg}{m} \quad (5.2.1)$$

The last term is the equivalent mass as defined by the Eurocode, being the average value of the building mass per unit length over the upper one-third. Note that 42 % of the building mass is being excited in the considered vibration mode.

Wind load

The effects of wind loading are calculated for the governing y-direction of the building. Appendix III.2.1 presents the calculation of the structural factor and the equivalent static wind load. The size factor yields 0,84 while a dynamic amplification factor is obtained of 1,15.

The dynamic amplification depends on building geometry, fundamental frequency and damping. The logarithmic decrement of the total damping is 0,12 which corresponds to 1,9 % of critical damping.

Figure 5.2-9 plots the equivalent static wind pressure diagram as applied in the structural analysis. The obtained values for the wind pressure range from 1,23 kPa to 1,70 kPa for the base and top part respectively. The force coefficient profile is provided in the right-hand side diagram.

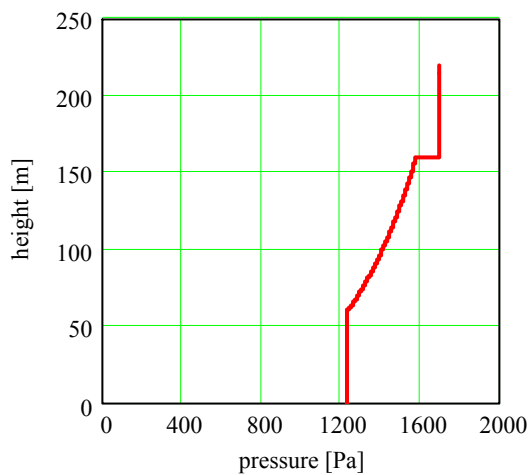


Figure 5.2-9: Equivalent static wind pressure

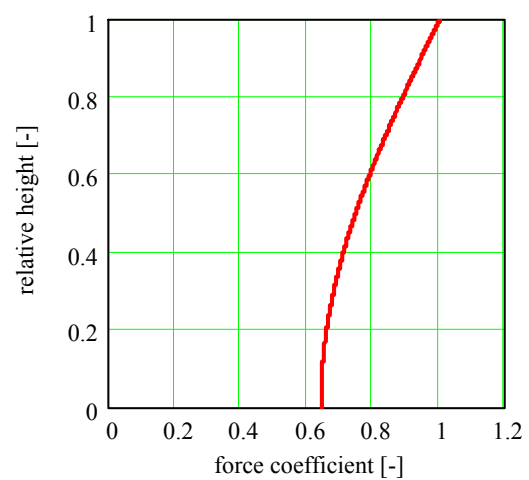


Figure 5.2-10: Force coefficient

The determination of the corresponding force coefficients along the building height is illustrated in figure 5.2-11.

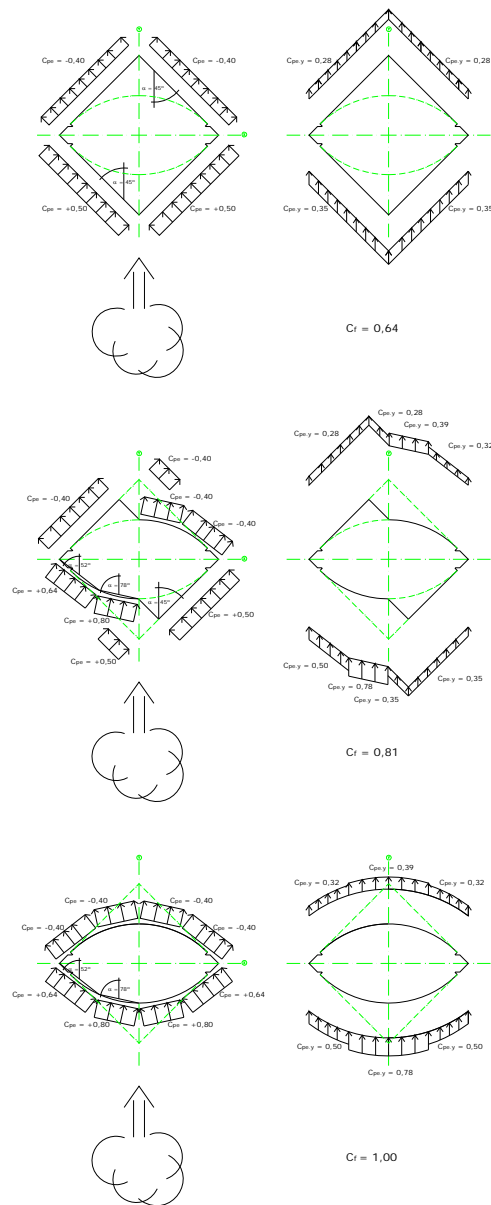


Figure 5.2-11: Determination of force coefficient

5.2.3 Results

In this subsection the results obtained from the performed structural analyses are summarised. The 50-year lateral building displacements are shown as well as the 5-year and 10-year accelerations.

Along-wind displacement

The along-wind displacement in y-direction due to a 50-year wind storm has been measured at the base level and at the top of the building. The building drift values are shown in table 5.2-3. Below grade no façade elements or partitions exist that could be damaged by excessive building drift, because of which the global displacement limitation has been applied to above-grade height.

| direction | height [m] | u_y [m] | height/ u_y [-] |
|-----------|------------|-----------|-------------------|
| Y | 0,00 | 0,001 | 488 |
| | 219,15 | 0,450 | |

Table 5.2-3: Along-wind building displacement

The 50-year wind-induced building drift exceeds the usually adopted criterion of H/500. A more thorough analysis of the lateral displacement, however, reveals that the maximum inter-storey height-to-drift ratio is about 420 for the upper part of the building. The latter value does meet the criterion for inter-storey drift of H/400.

Along-wind acceleration

The horizontal accelerations due to resonance with the turbulent wind are calculated in appendix III.2.2. A total damping has been adopted of 1% of critical. Table 5.2-4 shows the 5 and 10-year horizontal acceleration for the top occupied floor at 203,7 m in terms of the 10-minute root-mean-square acceleration and the peak acceleration.

| direction | T_{ret} [year] | height [m] | damping [-] | σ_a [m/s^2] | a_{peak} [m/s^2] |
|-----------|------------------|------------|-------------|------------------------|------------------------|
| Y | 5 | 203,70 | 1,00% | 0,063 | 0,200 |
| | 10 | 203,70 | 1,00% | 0,074 | 0,235 |

Table 5.2-4: Along-wind building acceleration

The ISO 6897 criterion proposes a limit for the 5-year rms acceleration of $0,059 m/s^2$ for the given fundamental frequency. Note that Torre Espacio does not satisfy this limit. The 10-year peak building acceleration does comply with the BLWTL criterion for office buildings, being $0,245 m/s^2$.

5.3 Torre de Cristal

The structural analysis of Torre de Cristal is presented in this section. Subsection 5.3.1 deals with the structure in general and discusses more in-depth the structural elements and their representation in the computer model. The aerodynamic building characteristics are treated in subsection 5.3.2 while subsection 5.3.3 lists the obtained results in terms of along-wind building displacement and acceleration.

5.3.1 Structure

The in-plan geometry of Torre de Cristal at ground level is rectangular with approximate dimensions of 32 m x 48 m. The geometry changes towards the top into an irregular hexagon (six-sided polygon), as illustrated in figure 5.3-1. The building height above grade is approximately 249 m, measured at the top of the steel roof structure, whereas the substructure consists of a six-level basement with a total depth of 19 m.

The vertical structure is composed of a large reinforced concrete core and 18 composite perimeter columns. A composite metal deck is used within the core to solve the floor system. Outside the core a precast concrete hollow-core slab is employed. The building roof is constituted by a complex, approximately 40 m high, steel structure. The loads from the building are transmitted to the soil by means of a deep slurry wall foundation.

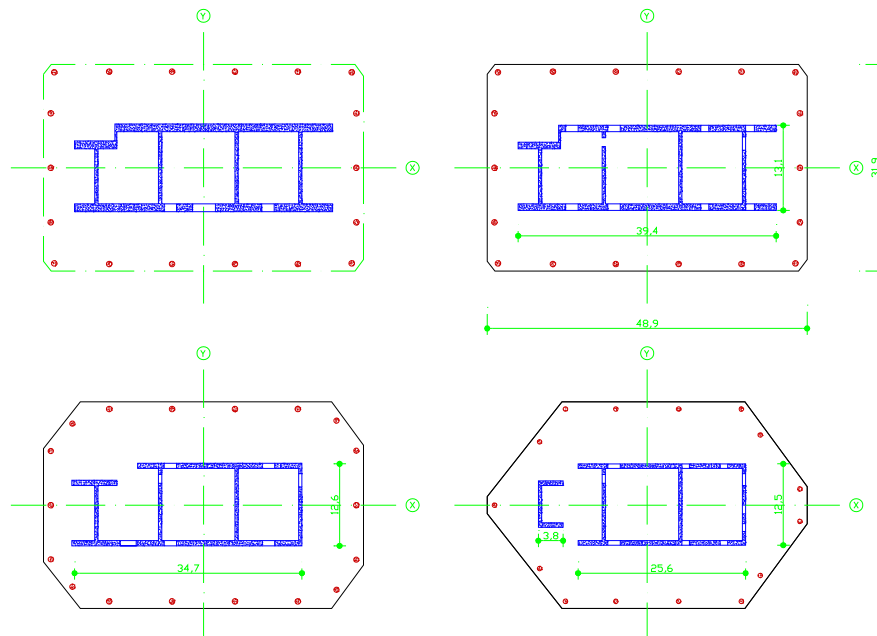


Figure 5.3-1: Typical floor plan of basement, low-, mid- and high-rise section

Core structure

The core is composed of two longitudinal and four transverse concrete reinforced walls and covers an approximate area of 39 m x 13 m at grade. The core geometry changes slightly throughout the height as can be seen in figure 5.3-1.

The transverse walls have constant thickness throughout their height of 500 mm. The thickness of both longitudinal walls changes from 1200 mm at basement level to 700 mm in the upper part of the building.

The concrete quality employed for all shear walls is C45/55. The amount of vertical reinforcement is relatively low being the basic reinforcement for all shear walls $\varnothing 25/300$ mm. As can be seen in the Appendix III.3.3, this leads to a maximum increase of less

than 5% of the effective axial stiffness, because of which its effect is not considered in the structural analysis.

Columns

The composite concrete columns employed in the building structure are circular with a diameter varying between 950 mm and 700 mm with ascending height. The column-to-column distance is typically 9,6 m. The embedded rolled steel sections range from HD400x990 in the basement level to HD360x134 for the upper part of the building.

All columns, just like the core shear walls, are cast with a C45/55 concrete quality. Due to the heavy embedded rolled steel sections the effective axial stiffness is considerably greater than the axial stiffness derived from the gross concrete section. For the basement columns a mean increase of the effective axial stiffness of over 65% is computed in appendix III.3.3.

Floors

Different floor systems have been applied within the building; below grade, and inside and outside the core above ground level.

The basement floor is typically a 300 mm thick reinforced concrete plate with a characteristic strength of 30 MPa. Locally a floor height of 350, 400 or 500 mm is adopted.

Above grade, inside the core, a composite metal deck floor is employed with a C30/37 concrete topping and a total height of 270 mm.

The floor system outside the core is composed of a precast concrete hollow-core slab spanning in between integrated floor beams. The precast concrete hollow-core planks have a height of 220 mm at office floors and 300 mm at mechanical levels with a typical in-situ concrete topping of 50 mm. The integrated floor beams consist of a half HEB360 section which is welded to a wider 500 mm x 20 mm steel plate that supports the prefabricated floor planks. The girders span in between the central core and the building's envelope with a centre-to-centre distance between girders of 4,8 m. A perimeter beam IPE500 spans between the columns and supports every other girder as shown in figure 5.3-2. Another function of the aforementioned perimeter beam is to provide for structural integrity and "tie" the columns together, i.e. equilibrating the horizontal components of the inclined corner columns. Moment resisting connections are assumed for both the column-beam joints (figure 5.3-3) and the core-beam joint.



Figure 5.3-2: Integrated floor beams



Figure 5.3-3: Column-beam connection

Basement

Torre de Cristal shares the basement perimeter slurry walls, from basement level -2, with the plot of Torre Espacio as explained and sketched in section 5.1.3. The connection of the tower basement floors with the slurry walls is carried out with a simple shear connection, while the connection with the basement floors outside the building projection is carried out by two lines of Mesnager joints (figure 5.1-7 and 5.3-4). Because of the foregoing no bending moments are generated in the adjacent structure due to the wind action.

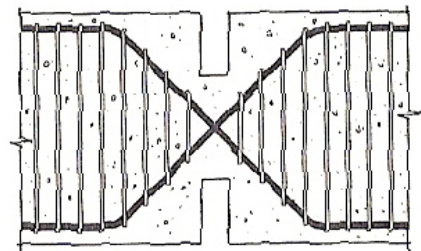


Figure 5.3-4: Mesnager joint [5]

A longitudinal expansion joint with shear connectors has been constructed in the east direction (see figure 5.1-7)

The building experiences a flexible horizontal support of the three perimeter slurry walls. The wind-induced shear is partially transferred to the perimeter walls by the diaphragm action of the basement floors.

Foundation

The superstructure columns and shear walls are connected to a 1,5 m thick C45/55 concrete pile cap with approximate in-plan dimensions of 51 m x 35 m at basement level -6. Slurry walls, with a height of 20 m, bear the superstructure and foundation slab to transmit the loads to the underlying soil.

The foundation walls are supported rigidly at a depth of 20 m below the pile cap, i.e. the vertical foundation stiffness depends only on the elastic axial stiffness of the foundation walls. It is considered that the conservative assumption of disregarding the skin friction of the pile shaft is compensated by the slight overestimation of the support stiffness.

5.3.2 Aerodynamic characteristics

This subsection treats the aerodynamic characteristics of Torre de Cristal and the 50-year equivalent static wind load acting on the building.

Natural vibration modes

The natural vibration modes are determined by the stiffness and mass distribution of the building. A modal analysis in SAP2000 has been carried out in order to obtain the building's natural vibration modes.

The building mass distribution is derived from the quasi-permanent gravity load combination as defined in subsection 5.1.3. Table 5.3-1 shows the values of the dead and live load acting on a typical building floor.

| | outside core | inside core | stairs |
|------------------------|--------------|-------------|--------|
| G [kN/m ²] | 5,0 | 7,0 | 5,5 |
| Q [kN/m ²] | 4,5 | 7,0 | 5,5 |

Table 5.3-1: Gravity load per area

The frequencies of the first four natural vibrations are listed in table 5.3-2, according to the axes definition shown in figure 5.3-5. The P-delta effect is accounted for in the modal analysis and is approximately 7% and 2% for the fundamental translational vibration Y_1 and X_1 respectively, being the P-delta effect negligible for the rotational mode.

| | frequency [Hz] | period [s] |
|-------|----------------|------------|
| Y_1 | 0,156 | 6,43 |
| X_1 | 0,296 | 3,38 |
| Y_2 | 0,769 | 1,30 |
| T_1 | 0,818 | 1,22 |

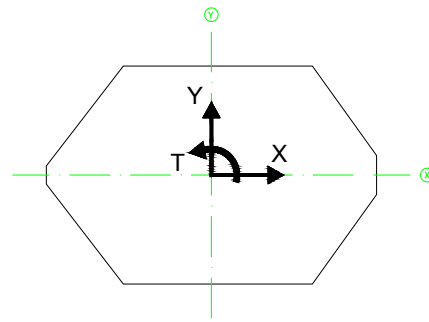


Table 5.3-2: Frequency of natural vibrations

Figure 5.3-5: Axes definition

The central core of the building provides by far the greatest part of the building's lateral stiffness. The contribution of the columns, activated by the rigidly connected girders, is approximately 5% and 10% in the x-direction and y-direction respectively.

Two observations are made regarding the natural vibrations of Torre de Cristal: the stiffness in the y-direction is approximately 3,6 times smaller than in the x-direction and the frequency of mode Y_2 is very close to the rotational mode T_1 .

Because of the great stiffness of natural modes Y_2 and T_1 (the vibration frequency is far away from the peak in the spectral density function of the wind turbulence, see appendix III.1.2), a possible coupling of both vibration modes is not likely to generate forces and displacements of any importance.

It is, however, striking that the building has a lateral stiffness in the y-direction being 3,6 times smaller than in the x-direction, while the building experiences a far greater wind excitation in the flexible y-direction. This dissimilarity in stiffness distribution and wind excitation, and therefore inefficient material use, is a direct consequence of the architectural design of the service core. Nevertheless, it is the author's opinion that this could have been easily (at least partially) solved by using one or more outrigger structures in the y-direction. Furthermore, these outriggers would not have great architectural implications when located at mechanical levels.

The modal shape in the governing y-direction of the building is presented in figure 5.3-6.

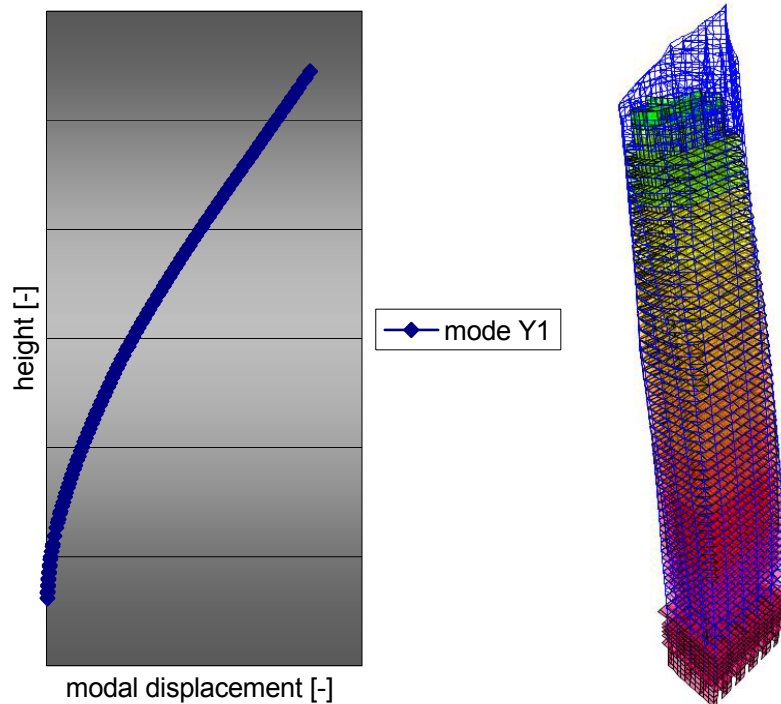


Figure 5.3-6: Modal shape of natural vibration mode Y_1

The modal mass per unit of length associated with the fundamental vibration mode Y_1 is now calculated by integrating the modal displacement times the mass distribution over the height, such that

$$m_{m,Y1} = \frac{\int_0^h u_{Y1}(z) \cdot m(z) dz}{h} \approx 0,39 \cdot 313,9 \cdot 10^3 \frac{kg}{m} \quad (5.3.1)$$

i.e. 39% of the building mass is excited in the first mode of vibration. The right-hand side term in (5.3.1) is the equivalent mass as defined by the Eurocode, being the average building mass per unit length of the upper one-third of the building.

Wind load

50-year along-wind building displacements are calculated in the governing y-direction. The size factor and dynamic factor of Torre de Cristal are calculated in appendix III.3.1 and yield 0,84 and 1,10 respectively. The logarithmic decrement of damping for wind action with an annual recurrence rate of 0,02, is 0,12 corresponding approximately to 1,9% of critical damping.

The resulting equivalent static wind pressure profile is presented in figure 5.3-7 with values ranging from 1,13 kPa to 1,69 kPa. Right-hand side figure 5.3-8 depicts the variation of the force coefficient with height. Note that the changing in-plan geometry towards an irregular hexagon results in a more aerodynamic shape with increasing

height. The determination of the force coefficient at every storey is illustrated in figure 5.3-9.

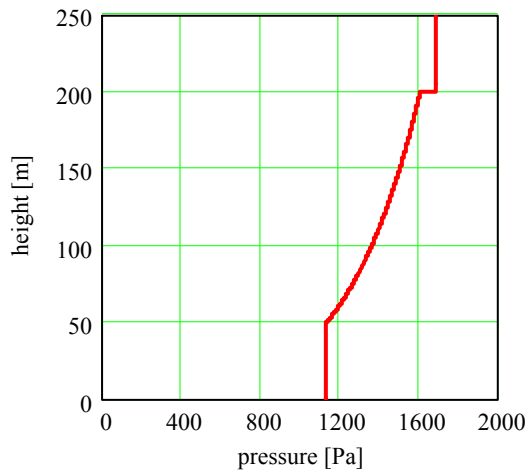


Figure 5.3-7: Equivalent static wind pressure profile

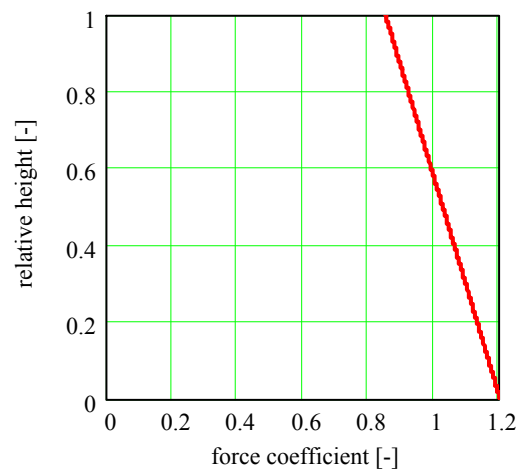


Figure 5.3-8: Force coefficient profile

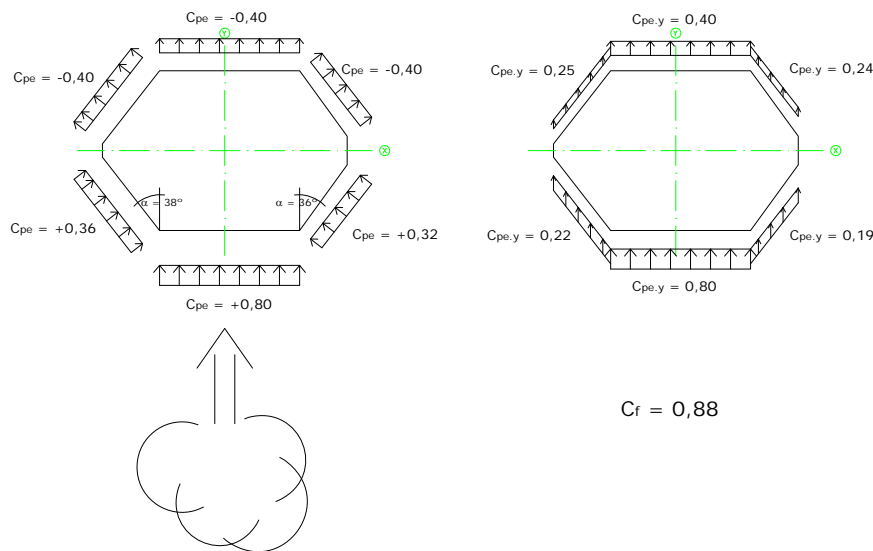


Figure 5.3-9: Determination of force coefficient

5.3.3 Results

This subsection summarises the obtained results from the performed structural analyses as far as Torre de Cristal is concerned. First of all, the 50-year lateral building displacement is presented and, secondly, the 5 and 10-year horizontal building acceleration.

Along-wind building displacement

The lateral displacement in the Y-direction due to a 50-year wind storm has been measured in the finite element model at ground level and at the storey located at 210 m. This interval is chosen to compute the global drift ratio, because below grade and above 210 m no storey-high façade elements or partition walls exist that could be damaged by excessive building drift.

| direction | height [m] | u_y [m] | height/ u_y [-] |
|-----------|------------|-----------|-------------------|
| Y | 0,00 | 0,004 | 666 |
| | 210,00 | 0,320 | |

Table 5.3-3: Along-wind building displacement

The value of the global displacement reported in table 5.3-3 is smaller than the usually adapted criterion of $H/500$.

Along-wind building acceleration

The 10-minutes root-mean-square acceleration for a 5-year wind storm and the 10-year peak acceleration at the top occupied floor are calculated in appendix III.3.2. It is noted that the effective height of the building is taken as the height of the structure's centroid, i.e. not up to the highest point of the steel roof structure at 250 m. Table 5.3-4 summarises the obtained results. The damping associated to these return periods of the wind action is assumed to be 1% of critical.

| direction | T_{ret} [year] | height [m] | damping [-] | σ_a [m/s ²] | a_{peak} [m/s ²] |
|-----------|------------------|------------|-------------|--------------------------------|--------------------------------|
| Y | 5 | 210,00 | 1,00% | 0,069 | 0,223 |
| | 10 | 210,00 | 1,00% | 0,082 | 0,263 |

Table 5.3-4: Along-wind building acceleration

The 10-year peak building acceleration as shown in table 5.3-4 is slightly greater than the upper limit proposed by BLWTL for office buildings being $25 \times 10^{-3} g$. The ISO 6897 criterion proposes a limit for the 5-year rms-acceleration of $0,052 \text{ m/s}^2$ for the given fundamental frequency, which is approximately 25% smaller than the value reported in table 5.3-4.

5.4 Torre Sacyr Vallehermoso

This section treats the along-wind structural response in the serviceability limit state of Torre Sacyr Vallehermoso.

Subsection 5.4.1 firstly discusses the building structure in general, after which the focus lies on the specific structural elements and their representation in the analysis. The aerodynamic building characteristics and equivalent static wind load are dealt with in subsection 5.4.2. Finally, this section is concluded by a summary of the obtained results in terms of lateral building displacements and accelerations.

5.4.1 Structure

The cross-sectional geometry remains the same throughout the entire building height. It is defined by two types of arc of a circle, as can be seen in figure 5.4-1. The three large arcs of a circle have a radius of approximately 34,8 m and the three smaller ones have a radius of 11,6 m. This leads to a greatest cross-sectional dimension of around 46 m. The maximum building height is 231,8 m. A six-level parking basement is located below ground level with a total depth of approximately 21 m.

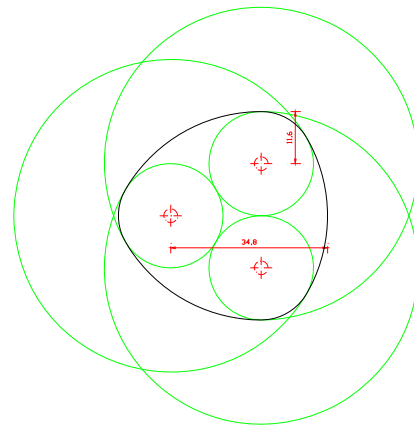


Figure 5.4-1: Construction of geometry

The vertical structure is principally composed of a complex central reinforced concrete core and two rings of reinforced concrete or composite columns, as depicted in figure 5.4-2. A composite metal deck with composite beams constitutes the floor system. A two-storey high transfer truss is located in the lower part of the building to locally increase the column centre-to-centre distance. One of the upper floors is used to accommodate an outrigger structure. The transmission of the loads from the tower to the underlying soil is carried out by a shallow slab-on-grade foundation.

Core structure

The complex reinforced concrete core structure consists of three interconnected square-shaped cores housing the elevator and installation shafts. The square cores are connected by means of a 1400 mm high coupling beam on the small parallel core sides and by a 340 mm high flat plate in the core-enclosed triangle shown in figure 5.4-2. The shear wall cross-sectional dimensions are greater towards the outside of the core in order to create greater inertia. Shear wall thickness ranges in between 300 mm and 1550 mm.

Two different concrete qualities have been used for the construction of the core, being C30/37 for the upper part from level 34 and C45/55 for the lower part of the building. Relatively high percentages of reinforcement are utilised which leads for some shear walls to a maximum increase of the effective axial stiffness of 11 % (as calculated in appendix III.4.3).

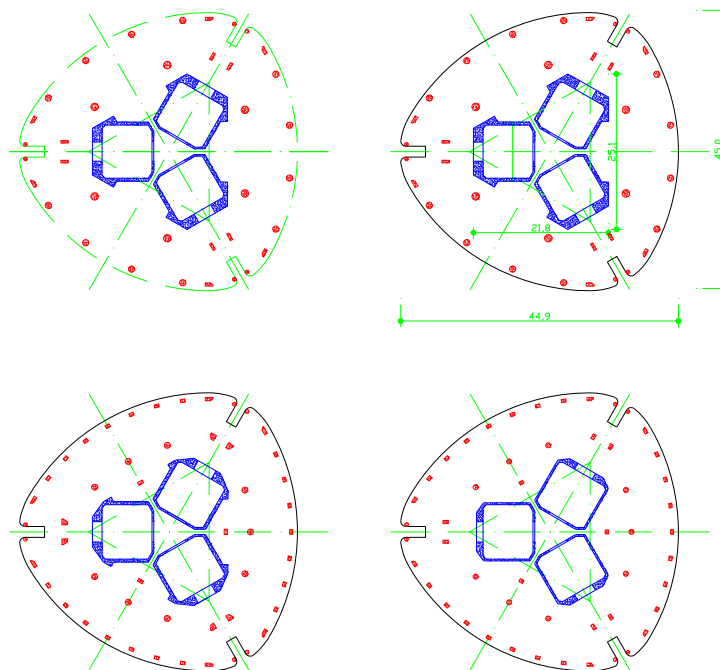


Figure 5.4-2: Typical floor plan of basement, low-, mid- and high-rise section

Columns

As has been stated in the introduction, two concentric column rings exist in between the core and the building envelope. The employed columns are composite, in general all columns comprised between level 4 and 52, or reinforced concrete columns. The superstructure columns have considerable dimensions of up to a diameter of 1200 mm for circular columns, and 1450 mm x 600 mm for rectangular columns.

The columns are cast with a concrete quality of C70/85 up to level 27, C45/55 from level 28 to 42, and C30/37 up to the top of the building. The composite columns are composed of an imbedded steel section, varying from HEM160 to HEM450, with or without extra steel plates welded to the section's web. The only columns that collaborate to resist the lateral loads are those connected by the outrigger, as illustrates hereafter, because the girders are considered not to transmit any bending moments. Therefore, the effective axial stiffness has been calculated only for the six interior columns parallel to the axes defined in 5.4-2. It is shown in appendix III.4.3 that a maximum increase of more than 40% is obtained for these columns.

Floors

Different solutions have been adopted for the basement and inner and outer core floor structures.

Below grade, the uniform floor plates are typically 350 mm high and cast with C30/37.

Inside the core a two-way reinforced concrete floor plate has been adopted with a thickness of 340 mm and a concrete quality of C30/37.

A composite metal deck floor with composite beams has been employed outside of the core. The floor consisting of a 60 mm steel sheet with a C30/37 concrete topping has a height of 180 mm, excluding the composite beams. Girders span in between the columns in a circumferential direction into which the secondary beams are framed. The secondary beams span in radial direction with a centre-to-centre distance of approximately 2,1 m and are stiffly connected to the composite metal deck floor by means of welded studs. Thus the metal deck spans perpendicular to the secondary beams as is shown in figure 5.4-3.



Figure 5.4-3: Column-girder and girder-beam joint

The girder-beam joint as well as the column-girder and core-girder joints are simply bolted connections in the web of the steel section, i.e. allowing for free rotation. Fictitious shell elements are used in the computer model representing the whole floor structure to provide for a simple application of uniformly distributed gravity loads and masses. The fictitious element has a negligible bending stiffness and a membrane stiffness that corresponds to the 120 mm concrete topping.

Outrigger

A 5 m high outrigger structure is located between level 54 and level 55+1. Two 800 mm thick shear walls protrude from each of the square-shaped cores to connect two inner columns, see figure 5.4-4.

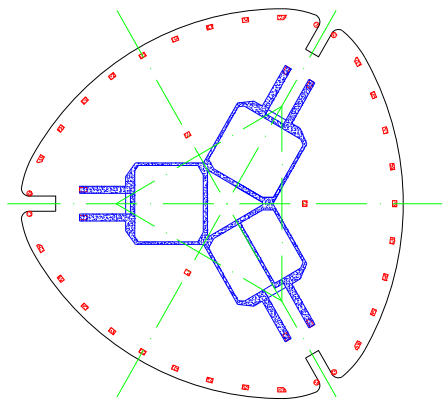


Figure 5.4-4: Outrigger structure

The outrigger activates a total of six columns, having a free span of approximately 5,5 m. The protruding shear walls are connected at level 54 and level 55+1 with a concrete 340 mm thick floor. The outrigger reduces the wind-induced building displacements, but not very effectively due to its location in the upper part of the building. The reader is referred to appendix I for a parametric study on the optimum location of single-outrigger structures. An additional effect of the outrigger's high bending stiffness is that the six columns are practically hung up from the outrigger. Almost the entire variable load-induced axial force of several lower storeys is transferred from the columns to the core.

The concrete quality of the outrigger walls as well as of the upper and lower floor is C30/37. For both the protruding shear walls and the connected floors the gross concrete section is considered as far as the membrane and bending stiffness is concerned, i.e. neither concrete cracking nor the increase in stiffness due to reinforcement has been accounted for.

Transfer truss

A two-storey high composite truss has been built between level 4 and 6 to double the centre-to-centre distance between inner and outer ring columns, see figure 5.4-5.

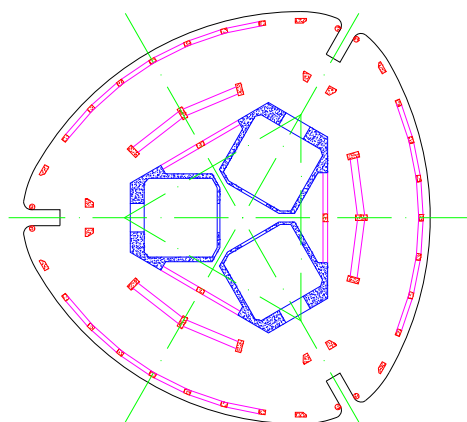


Figure 5.4-5: Transfer trusses in plan



Figure 5.4-6: Outer transfer truss

Basement

The connectivity between the building and the surrounding basement structure is illustrated in figure 5.1-8. The below-grade building floors are connected to the basement floors outside of the building projection by means of two shear connected joints. The connection between the building floors and the perimeter slurry wall is a Styrofoam joint. The foregoing allows differential settlements between the building and basement structure. The basement floors outside the building projection are connected to the perimeter walls through a shear connection. The latter, in combination with the shear connectors between building and basement floors, provides a flexible horizontal support due to the high in-plane stiffness of the perimeter walls.

Foundation

A shallow foundation system has been adopted to transmit the loads to the underlying soil. A 4 m thick post-tensioned foundation slab with a concrete quality of C30/37 constitutes the slab-on-grade foundation. The gross concrete section is considered as far as the moment of inertia is concerned. It is supposed that the effect of the passive reinforcement and post-tensioning, which reduces the serviceability limit state tensile stresses, more or less compensates the effect of concrete cracking.

5.4.2 Aerodynamic characteristics

The aerodynamic building characteristics and the equivalent static wind load are dealt with in this subsection.

Natural vibration modes

Table 5.4-1 lists the gravity load values per area as used in the quasi-permanent load combination defined in section 7.1. The masses used in the modal analysis are computed by dividing the values in table 5.4-1 by the gravitational acceleration.

| | outside core | inside core | stairs |
|------------------------|--------------|-------------|--------|
| G [kN/m ²] | 5,0 | 9,9 | 6,5 |
| Q [kN/m ²] | 5,5 / 9,5 | 5,5 | 4,5 |

Table 5.4-1: Gravity load per area

Table 5.4-2 shows the results of the modal analysis in terms of the frequencies of the first three natural modes. The definition of the motion directions is according to figure 5.4-7. The structural softening due to the quasi-permanent axial force, also known as the P-delta effect, is 9% and 1% for the two translational and rotational vibration modes respectively.

| | frequency [Hz] | period [s] |
|----------------|----------------|------------|
| X ₁ | 0,131 | 7,65 |
| Y ₁ | 0,135 | 7,39 |
| T ₁ | 0,402 | 2,49 |

Table 5.4-2: Frequency of natural vibrations

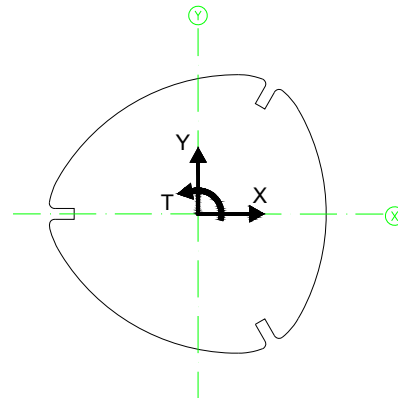


Figure 5.4-7: Axes definition

The first two translational modes are similar due to the practically circular stiffness distribution of the core. The outrigger structure has a modest influence on the lateral building stiffness; the contribution of the outrigger and the outrigger-activated inner columns constitutes approximately 15% of the total lateral stiffness. This modest contribution is because of the not fully effective location of the outrigger in height (see appendix I.2) and the in-plan distribution.

Figure 5.4-8 depicts the modal shape of the governing fundamental mode shape in x-direction.

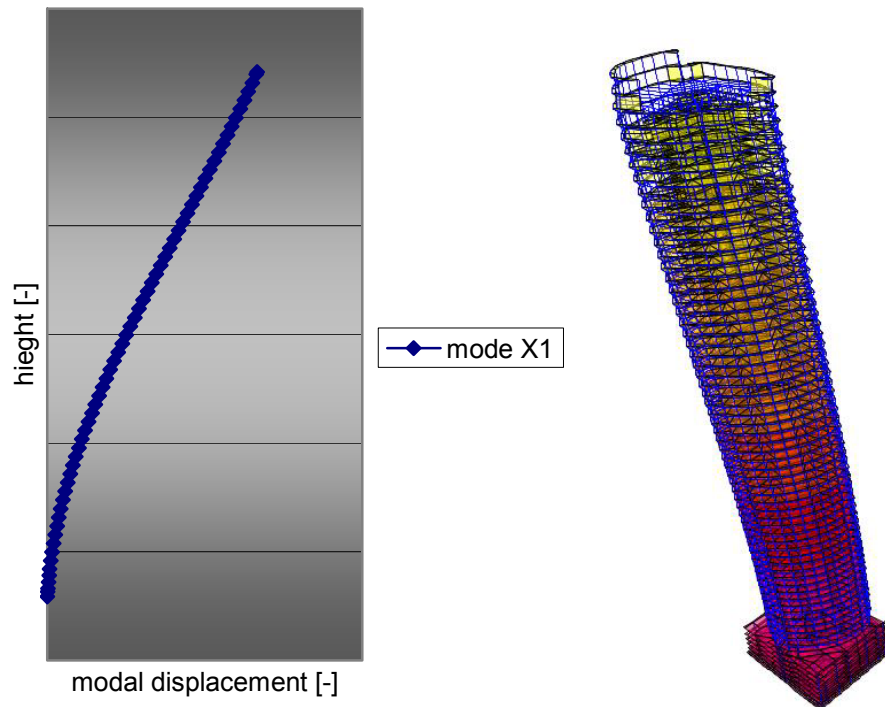


Figure 5.4-8: Modal displacement mode X_1

The modal mass per unit of length associated to the fundamental vibration mode X_1 is calculated by integrating the modal displacement times the mass distribution over the height, such that

$$m_{m.X1} = \frac{\int_0^h u_{X1}(z) \cdot m(z) dz}{h} \approx 0,41 \cdot 439,6 \cdot 10^3 \frac{kg}{m} \quad (5.4.1)$$

Note that the equivalent mass per unit length, the right-hand side term as defined in Eurocode 1, is relatively high. In the fundamental vibration motion 41% of the building mass is excited.

Wind load

The wind-induced building response is calculated in negative x-direction because the building has the smallest stiffness in this direction in combination with the greatest wind excitation. Appendix III.4.2 provides the calculation of the 50-year equivalent wind load and thus of the structural factor. The structural factor is composed of the size and dynamic factor yielding 0,85 and 1,17 respectively. Note the great dynamic amplification due to the high fundamental period of the structure in the governing wind direction.

The logarithmic decrement of damping, having a great influence on the aforementioned dynamic amplification factor, is taken as 0,11 being approximately equal to 1,8% of critical damping.

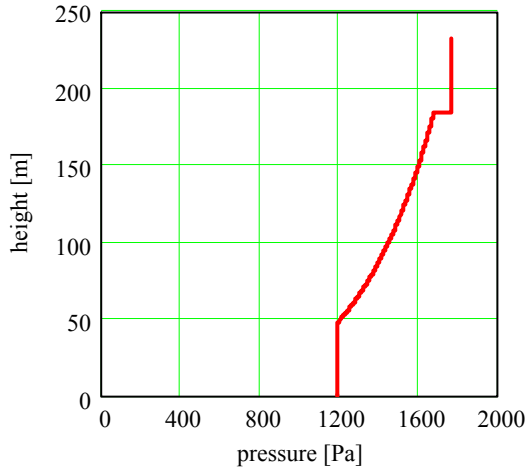


Figure 5.4-9: Equivalent static wind pressure

The equivalent static wind pressure profile, as applied to the building in the structural model, is plotted in figure 5.4-9. The equivalent static wind pressure ranges from 1,19 kPa at the base to 1,77 kPa at the top.

The force coefficient equals 0,71 and is constant throughout the height. The determination of the force coefficient, based on the local pressure coefficients in figure 5.1-13 as a function of the angle of attack of the wind, is illustrated in figure 5.4-10. The fish scale-like rough building façade (see section 4.4) slightly increases the along-wind drag compared with a smooth surface.

As far as the across-wind excitation is concerned, it is believed that the roughness and porosity of the building's envelope reduces the resulting across-wind stresses, displacements and vibrations.

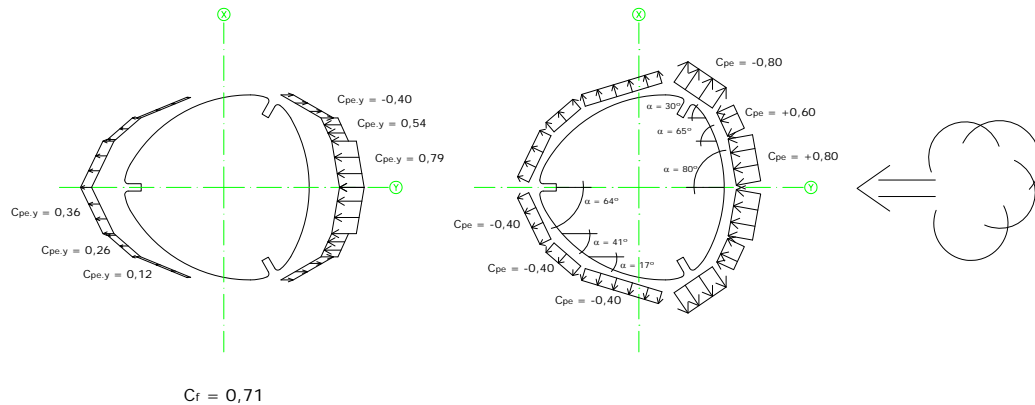


Figure 5.4-10: Determination of force coefficient

5.4.3 Results

The results obtained from the structural analyses are presented in this subsection; in terms of the 50-year along-wind building displacement and the 5 and 10-year accelerations.

Along-wind building displacements

The 50-year wind-induced displacement in the X-direction is measured at grade and at the top of the building.

| direction | height [m] | u_x [m] | height/ u_x [-] |
|-----------|------------|-----------|-------------------|
| X | 0,00 | 0,006 | 931 |
| | 231,80 | 0,255 | |

Table 5.4-3: Along-wind building displacement

The value of the global displacement reported in table 5.4-3 is smaller than the global criterion of $H/500$.

Along-wind building acceleration

In appendix III.4.2, the 5-year rms acceleration and the 10-year peak acceleration at the top occupied floor are calculated. The obtained results are summarised in table 5.4-4. A damping value of 1% of critical is adopted in the calculation of wind-induced building response for these return periods.

| direction | T_{ret} [year] | height [m] | damping [-] | σ_a [m/s^2] | a_{peak} [m/s^2] |
|-----------|------------------|------------|-------------|------------------------|------------------------|
| Y | 5 | 195,80 | 1,00% | 0,037 | 0,116 |
| | 10 | 195,80 | 1,00% | 0,043 | 0,136 |

Table 5.4-4: Along-wind building acceleration

The upper limit of the 5-year rms building acceleration is according to ISO 6897 for the computed fundamental period $0,060 m/s^2$. The estimated building accelerations at the top occupied floor are far below the upper limits proposed by the criteria adopted in this thesis.

5.5 Torre Caja Madrid

The structure of Torre Caja Madrid, in relation to its representation in the finite element model, is treated in subsection 5.5.1. Subsection 5.5.2 presents the aerodynamic characteristics of the building and the equivalent static wind loading acting on it. This section concludes with the results in terms of the horizontal building displacement and acceleration.

5.5.1 Structure

The office building Torre Caja Madrid has a total height of 250 m above grade and the five-storey parking basement has a height of approximately 18 m. The in-plan dimensions of a typical office floor are 53 m x 43 m. The geometry of the building is characterised by three office blocks supported by two lateral cores and an opening on top. Figure 5.5-1 shows a typical floor plan of a basement, low-, mid- and high-rise section.

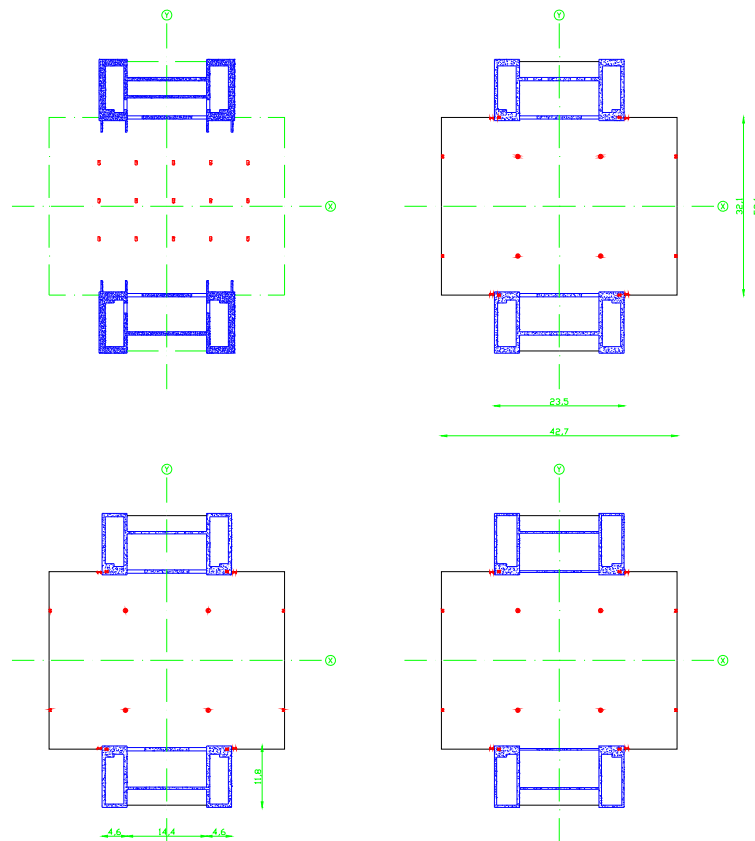


Figure 5.5-1: Typical floor plan at basement, low-, mid- and high-rise section

The primary structure is composed of two lateral reinforced concrete cores, three two-storey high steel trusses framing into them and a steel structure connected to the cores by means of a pinned connection at the top of the building. Figure 5.5-2 and 5.5-3 show a vertical section in x and y-direction respectively to clarify the above.



Figure 5.5-2: Vertical section along x-axis [16]



Figure 5.5-3: Vertical section along y-axis [16]

The secondary structure is composed of eight composite columns and two embedded rolled steel sections in the core as far as the vertical structure is concerned. A composite steel deck slab with composite beams constitutes the floor system. The loads of the building are transmitted to the soil by a shallow slab-on-grade foundation.

Core structure

The two concrete reinforced cores have approximate in-plan dimensions of 12 m x 24. The shear walls composing the cores have a maximum thickness of 2 m corresponding to the location where the transfer trusses frame into the cores, as explained hereafter.

As far as the concrete quality is concerned, C55/67 has been used up to storey 2 at approximately 39 m above grade, C50/60 up to storey 13 and C40/50 in the upper part of the core. The part of the cores comprised between storey 23 and 25 is cast in C50/60. This level corresponds to the two mechanical storeys wherein transfer truss 3 is located and the upper and lower storey. Appendix III.5.3 shows the calculation of the effective axial stiffness of all shear wall sections. The maximum increase, in relation to the gross concrete section, that has been obtained is 4% for the 2 m thick shear walls on the 'inside' of the core structures and generally between 1% and 2% for the other shear walls. Because of this, the modest effect of steel addition on the axial stiffness is not accounted for in the model.

Columns

The secondary vertical structure consists of a total of sixteen columns: four interior steel columns with concrete encasement, four steel façade columns, four steel columns next to the lateral cores and four embedded steel columns in the thick shear walls. The interior columns and the façade columns are rolled HD section, whereas a HEM600 profile constitutes the columns running alongside the core. The embedded columns are built-up wide flange profiles.

The two latter columns are located next to each other as can be seen in figure 5.5-4. The cantilevered beam depicted in the figure spans in x-direction from the core to the façade. Differential vertical movement between the concrete and steel structure can be expected due to creep and shrinkage of the concrete cores. This differential movement is provided by the joint shown in figure 5.5-4 at mid height of the HEM600 column.

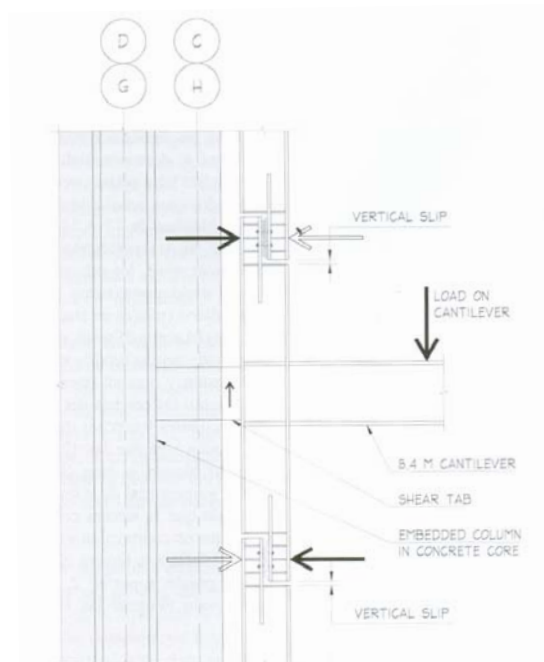


Figure 5.5-4: Column detail to allow differential shortening [16]

Floors

The horizontal structure in between the concrete cores typically consists of a 76 mm steel deck composite floor with a total height, including the lightweight C30/37 concrete topping, varying between 150 mm and 200mm. Floor beams and the steel deck slabs behave compositely in structural sense by means of studs welded on the top flange of the beams.

Inside the core a two-way reinforced concrete slab with a height of 400 mm is adopted, while a post-tensioned 1900 mm high slab is used at the storeys where the transfer trusses are connected to the cores. The inner core slabs are cast with a C30/37 concrete quality, except for the post-tensioned slabs that are poured with C55/65.

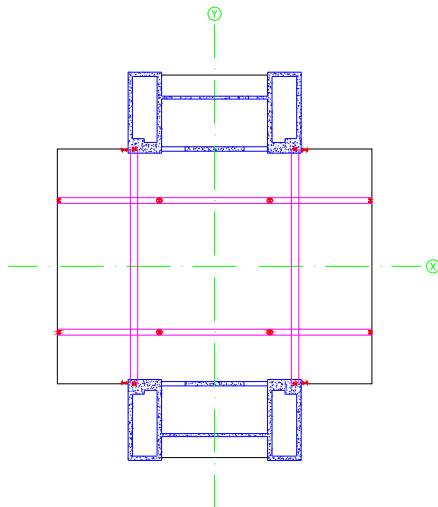


Figure 5.5-5: Upper chord of transfer truss

Transfer trusses

The office blocks, shown in figure 5.5-3 and 5.5-4, are supported by three two-storey high steel transfer trusses located at building services storeys. Figure 5.5-5 shows the upper chord of the transfer trusses. The secondary transfer trusses, shown in figure 5.5-6, span in x-direction and support the interior columns as well as the façade columns. The primary transfer trusses in figure 5.5-7, in turn, support the secondary trusses and transmit the loads of each office block to the two lateral cores.

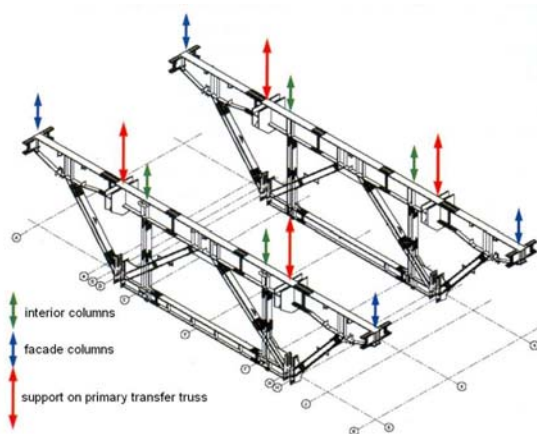


Figure 5.5-6: Secondary transfer truss [16]

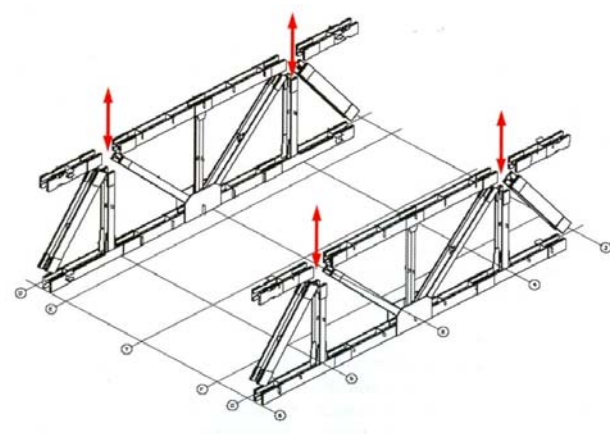


Figure 5.5-7: Primary transfer truss [16]

Basement

The substructure consists of a five-storey parking basement. The building's basement floors are rigidly connected to both the basement floors outside the building projection as the perimeter walls.

The slurry walls up to basement level -2 are elongated up to ground level, as shown in figure 5.1-8. An extra wall has been built on the property line which highly reduces the eccentricity of the horizontal support of the U-shaped perimeter slurry wall. Thus, the building experiences a flexible horizontal support from grade down to the foundation as far as wind loading is concerned.

Foundation

The loads are transmitted to the underlying soil by a shallow foundation; a 5,0 m high reinforced C45/55 concrete foundation slab. The soil-structure interaction is accounted for by a series of vertical springs below the foundation mat with a spring stiffness corresponding to a modulus of subgrade reaction $K = 25.000 \text{ kN/m}^3$.

5.5.2 Aerodynamic characteristics

The aerodynamic characteristics and the equivalent static wind load acting are dealt with in this subsection.

Natural vibration modes

A modal analysis has been carried out with SAP 2000 to obtain, through the stiffness and mass distribution of the building, the natural vibration modes.

The masses are derived from the quasi-permanent gravity load combination as defined in subsection 5.1.3. Table 5.5-1 shows the values of the gravity load per area on a typical building floor.

| | outside core | inside core | stairs |
|------------------------|--------------|-------------|--------|
| G [kN/m ²] | 3,7 / 4,6 | 12,6 | 7,6 |
| Q [kN/m ²] | 3,0 | 5,0 | 5,0 |

Table 5.5-1: Gravity load per area

Note that table 5.5-1 only shows the gravity load acting on a typical building floor and does not reflect the self-weight of the vertical structure. The latter is important in this case due to the great amount of concrete used in the lateral cores.

Table 5.5-2 lists the frequencies and periods of the thirist free natural vibrations in accordance with the coordinate system shown in figure 5.5-8. The P-delta effect is small being 4%, 5% and 1% for the fundamental translational vibrations X_1 and Y_1 and the rotational mode respectively.

| | frequency [Hz] | period [s] |
|-------|----------------|------------|
| X_1 | 0,185 | 5,41 |
| Y_1 | 0,187 | 5,35 |
| T_1 | 0,487 | 2,05 |

Table 5.5-2: Frequency of natural vibrations

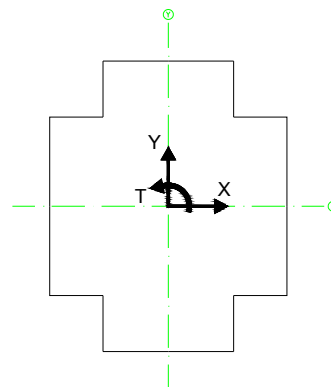


Figure 5.5-8: Axes definition

Note that the frequencies of natural vibration are quite high, especially considering the very high own weight of the building structure. The enormous own weight has, therefore, to be compensated by a great moment of inertia in both translational directions.

The structural behaviour in x-direction is bending-dominated and composed of the two cantilevered concrete cores. In y-direction a more complicated behaviour is observed due to the rigidly connected transfer trusses; about 60% of the stiffness in y-direction is due to the frame action.

The governing wind direction is the x-direction because the lateral stiffness is slightly smaller and the wind-exposed area is greater in that direction. Figure 5.5-9 shows the fundamental mode shape in that direction.

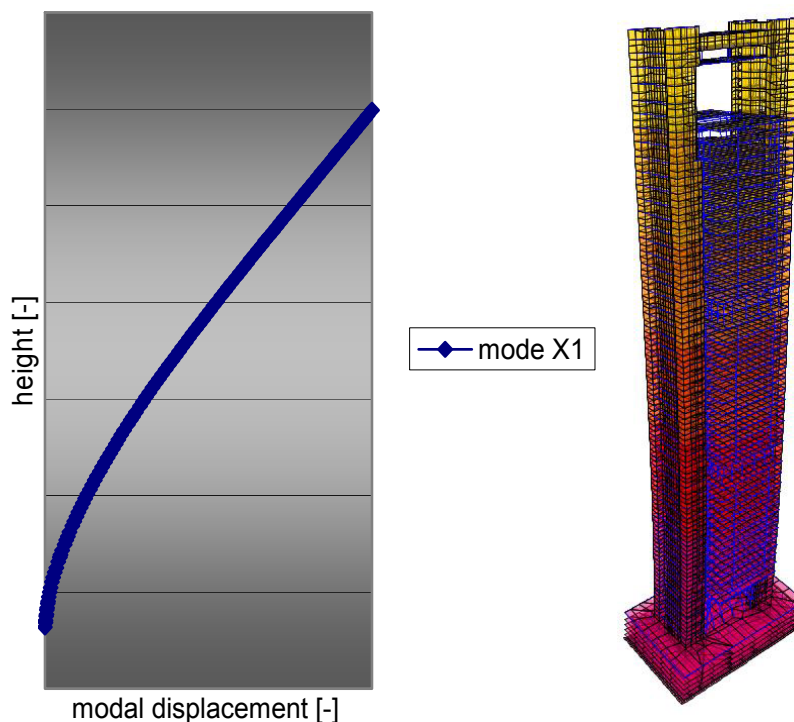


Figure 5.5-9: Modal displacement mode X₁

By integrating the product of the modal displacements and the mass distribution over the height, one obtains the modal mass associated to the corresponding natural vibration mode. The modal mass per unit length is then determined as follows

$$m_{m.X1} = \frac{\int_0^h u_{X1}(z) \cdot m(z) dz}{h} \approx 0,41 \cdot 398,2 \cdot 10^3 \frac{kg}{m} \quad (5.5.1)$$

The right-hand side term is the equivalent mass per unit length as defined in Eurocode 1 being the building mass averaged over the upper one-third. Note that 41% of the building mass is excited in the considered fundamental mode.

Wind load

Appendix III.5.1 provides the calculation of the 50-year equivalent static wind load acting on Torre Caja Madrid. The size factor, accounting for the lack of full correlation between the wind pressure peaks over the wind-exposed area, yields 0,84. The value of the dynamic factor, taking into account the resonance between the wind gusts and the building structure, equals 1,07. The logarithmic decrement of damping for wind action with an annual recurrence rate of 0,02 is 0,12 corresponding approximately to 1,9% of critical damping.

Figure 5.5-10 provides the resulting equivalent static wind pressure profile with values ranging from 1,11 kPa to 1,63 kPa. The force coefficient equals 1,20 (figure 5.5-11) and does not vary along the building height.

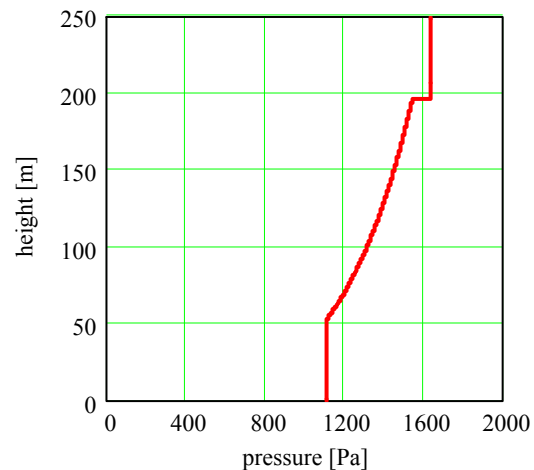


Figure 5.5-10: Equivalent static wind pressure profile

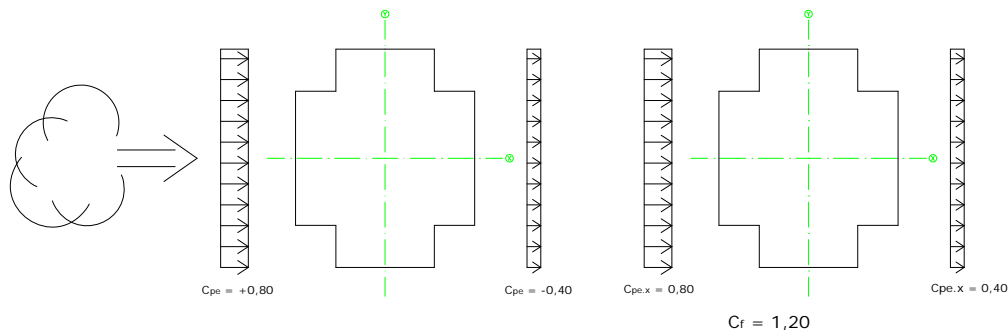


Figure 5.5-11: Determination of force coefficient

5.5.3 Results

The results obtained from the structural analyses are presented in this subsection. The results are shown in terms of the 50-year lateral building displacement and the 5 and 10-year accelerations.

Along-wind building displacement

Table 5.5-3 provides the 50-year along-wind displacements at grade and at an approximate height of 220 m. The latter level corresponds to the level above which the opening in the building envelope is located and hence neither partitions nor storey-high façade elements exist.

| direction | height [m] | u_y [m] | height / u_y [-] |
|-----------|------------|-----------|--------------------|
| Y | 0,00 | 0,003 | 1.164 |
| | 219,67 | 0,192 | |

Table 5.5-3: Along-wind building displacement

The global building displacement is rather small and complies with the criterion of $H/500$.

Along-wind building acceleration

Appendix III.5.2 provides the calculation of the 5-year rms acceleration and the 10-year peak acceleration at the top occupied floor. It is noted that an effective building width is used in the determination by the turbulent wind-induced along-wind force, as to account for the hole in the upper part of the building. The obtained results are summarised in table 5.5-4. The damping associated to these return periods of the wind action is assumed to be 1% of critical.

| direction | T_{ret} [year] | height [m] | damping [-] | σ_a [m/s^2] | a_{peak} [m/s^2] |
|-----------|------------------|------------|-------------|------------------------|------------------------|
| Y | 5 | 215,15 | 1,00% | 0,049 | 0,160 |
| | 10 | 215,15 | 1,00% | 0,058 | 0,189 |

Table 5.5-4: Along-wind building acceleration

The ISO 6897 criterion for general-use buildings recommends an upper limit of the 5-year rms accelerations for the considered fundamental frequency of $0,052 m/s^2$. The BLWTL criterion for office buildings is $0,245 m/s^2$. Note that the estimated along-wind accelerations of Torre Caja Madrid comply with both criteria.

5.6 Summary of results and discussion

In this section the results obtained from the structural analyses of all four tall buildings are presented and discussed. In subsection 5.6.1 the aerodynamic building characteristics are dealt with. Subsection 5.6.2 and 5.6.3 treat the along-wind building displacements and accelerations respectively. The results are provided only for the governing wind direction.

It is reminded that interference effects, although very likely to increase the along-wind response of the buildings under consideration, are not accounted for neither in the along-wind displacements nor in the accelerations. As far as the lateral accelerations are concerned, the Eurocode's recommendations are intended for buildings with a linearly varying or constant mass distribution. This condition is not met by Torre de Cristal (40 m high light roof structure) and Torre Caja Madrid (hole in upper part). In

addition, the wind-induced horizontal accelerations are highly dependent of the total damping. However, the damping in the structure cannot be accurately estimated until the structure is completed (errors in its estimation are often very considerable). The above should be kept in mind when evaluating the results presented in this section.

5.6.1 Aerodynamic characteristics

Table 5.6-1 contains the aerodynamic building characteristics of each building structure. The first two columns list the modal mass per unit length and the period of vibration of the governing fundamental mode. The third column shows the logarithmic decrement of total damping associated with a 50-year extreme wind, whereas the two right-hand side columns present the resulting size and dynamic factor.

| | m_1 [kg/m] | period [s] | δ_{total} [-] | C_s [-] | C_d [-] |
|--------------------------|--------------------|------------|----------------------|-----------|-----------|
| Torre Espacio | $155,6 \cdot 10^3$ | 7,39 | 0,12 | 0,84 | 1,14 |
| Torre de Cristal | $122,4 \cdot 10^3$ | 6,43 | 0,12 | 0,84 | 1,10 |
| Torre Sacyr Vallehermoso | $180,2 \cdot 10^3$ | 7,65 | 0,11 | 0,85 | 1,17 |
| Torre Caja Madrid | $163,3 \cdot 10^3$ | 5,41 | 0,12 | 0,84 | 1,06 |

Table 5.6-1: Aerodynamic building characteristics

The modal mass of both Torre de Cristal and Torre Espacio are relatively small. As far as Torre de Cristal is concerned, this is mainly because of the 40 m high, light roof structure that is to house a small garden. The geometry of Torre Espacio reduces the floor plan dimensions and therefore the mass in the upper part of the building. In spite of the great mass of the structure of Torre Caja Madrid, its fundamental modal mass is relatively modest because of the opening in the upper part of the building.

Torre Espacio and Torre Sacyr Vallehermoso have the highest fundamental period in the governing wind direction, whilst Torre Caja Madrid has the lowest period. This, in relation to the modal mass, means that the moment of inertia of Torre Espacio is rather small whilst the contrary holds for Torre Caja Madrid.

The total damping is composed of structural and aerodynamic damping. More or less the same values are found for all buildings because their lateral load resisting systems are all reinforced concrete structures. Note that the governing wind direction for Torre Caja Madrid is the x-direction in which the lateral load resisting system is composed of two cantilevered cores only, without the interaction of the steel transfer trusses.

The size factor represents the improbability that peak wind gusts act simultaneously on the entire building surface. The obtained values are practically the same for all buildings which is quite logical considering that the global building dimensions are similar.

The resonance of the structure with wind gusts is accounted for by the dynamic factor. For given wind characteristics, the dynamic amplification depends on the fundamental period of vibration, damping and the dimensions of the wind-exposed area. The latter two are very similar for each building. Therefore the dynamic amplification varies with the period of fundamental vibration. Note that a dynamic amplification of up to 17% is obtained for Torre Sacyr Vallehermoso.

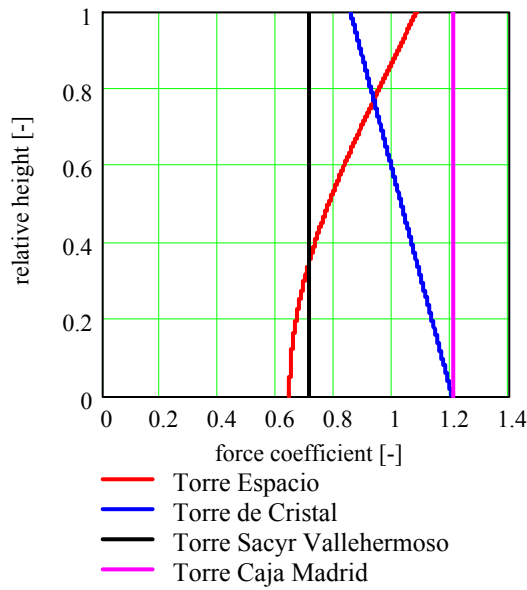


Figure 5.6-1 depicts the force coefficient profile along the. The geometry of Torre de Cristal changes towards the top into a more aerodynamic shape, whereas Torre Espacio becomes less aerodynamic with increasing height.

In figure 5.6-2 the equivalent static wind pressure profiles (50-year peak pressure times the structural factor) are shown. The resulting wind load per unit length is provided in 5.6-3. This diagram represents the product of the structural factor, the force coefficient, the peak wind pressure profile and the building width according to expression (5.1.9).

Figure 5.6-1: Force coefficient along height

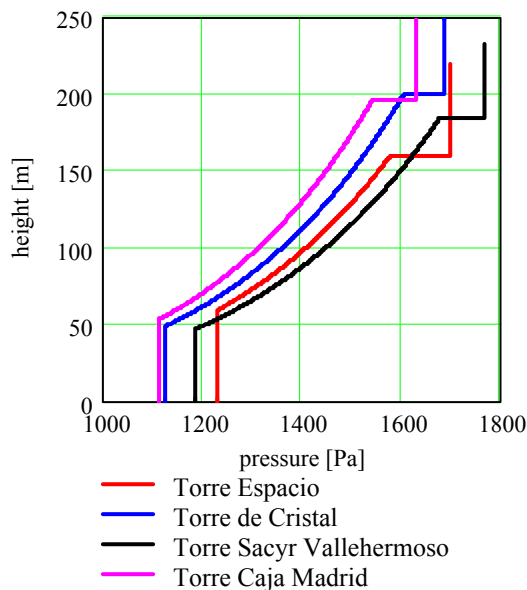


Figure 5.6-2: Equivalent static wind pressure

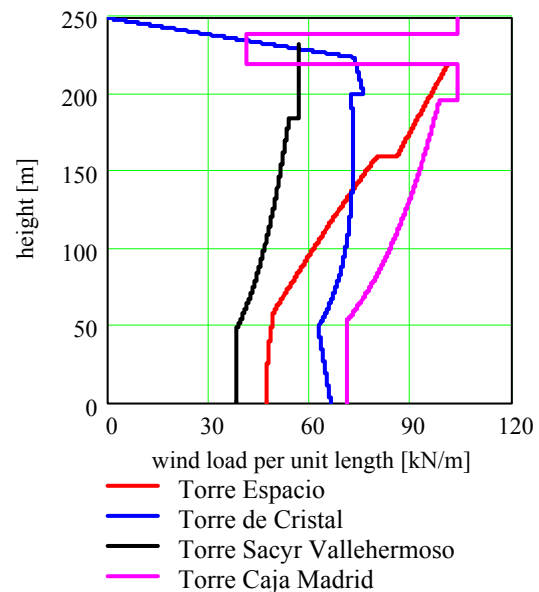


Figure 5.6-3: Wind load along height

Figure 5.6-3 clearly demonstrates the aerodynamic design of Torre Sacyr Vallehermoso, despite experiencing the highest dynamic amplification. The building has a relatively small width and force coefficient due to the almost circular floor plan. Torre Caja Madrid experiences the greatest wind excitation of all due to its non-aerodynamic design in spite of being subjected to the lowest dynamic amplification. The great changes in the wind load diagrams of Torre de Cristal and Torre Caja Madrid in the upper part are attributed to local changes in geometry.

5.6.2 Along-wind displacement

The resulting 50-year along-wind building displacements are presented in table 5.6-2.

| | z [m] | u [m] | ratio z/u [-] |
|--------------------------|--------|-------|---------------|
| Torre Espacio | 219,15 | 0,449 | 488 |
| Torre de Cristal | 210,10 | 0,315 | 666 |
| Torre Sacyr Vallehermoso | 231,80 | 0,249 | 931 |
| Torre Caja Madrid | 219,67 | 0,189 | 1.164 |

Table 5.6-2: Along-wind displacement

The left-hand side column presents the height at which the lateral building drift is measured in the finite element models. The second column shows the net displacement; the displacement between grade and the height shown in the first column. Finally on the right-hand side, the building's drift ratio is presented.

All buildings, except Torre Espacio, comply with the adopted criterion for global lateral displacement of $H/500$. As has been pointed out in subsection 2.3.2, it is actually the inter-storey drift that is important when evaluating the risk for damage in partitions, façade elements and interior finishes (doors, elevators, etc.). A more exhaustive analysis can be carried out with regard to the lateral displacements, limiting the inter-storey displacements to $H/400$ (H being the inter-storey height). Such an additional analysis has been performed for Torre Espacio. It is noted that the maximum inter-storey drifts are approximately $H/420$ for the upper part of the building, which is considered acceptable.

Torre Sacyr Vallehermoso and Torre Caja Madrid experience the smallest along-wind displacements (drift ratios). In the latter case this is predominantly due to the large moment of inertia of the lateral cores, whereas Torre Sacyr Vallehermoso takes advantage of its highly aerodynamic design.

5.6.3 Along-wind acceleration

Figure 5.6-4 presents the 10-minute root-mean-square values of the 5-year along-wind building acceleration along the height, whereas figure 5.6-5 provides the 10-year peak acceleration diagrams.

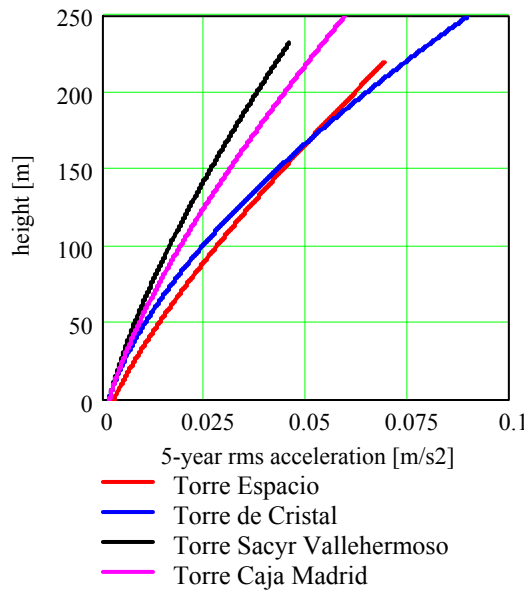


Figure 5.6-4: 5-year rms acceleration

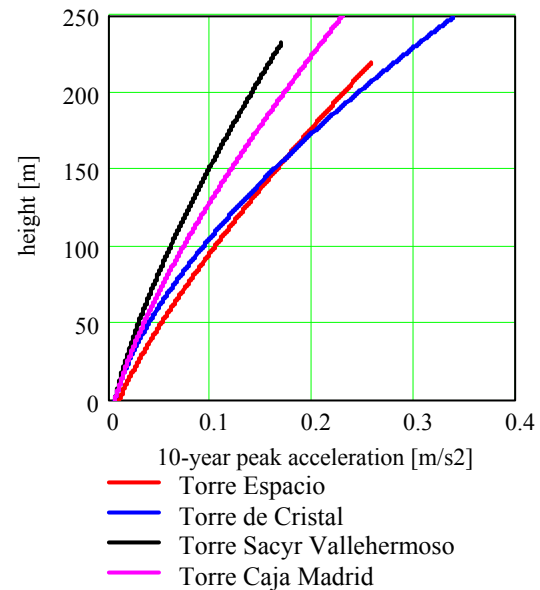


Figure 5.6-5: 10-year peak acceleration

The estimated along-wind accelerations with a return period of 5 and 10 year are shown in table 5.6-3 for the top occupied floor.

| | m_1 [kg/m] | δ_{total} [-] | z [m] | $\sigma_{5\text{ year}}$ [m/s ²] | $a_{10\text{ year}}$ [m/s ²] |
|--------------------------|--------------------|----------------------|---------|--|--|
| Torre Espacio | $155,6 \cdot 10^3$ | 0,06 | 203,60 | 0,063 | 0,235 |
| Torre de Cristal | $122,4 \cdot 10^3$ | 0,06 | 210,00 | 0,069 | 0,263 |
| Torre Sacyr Vallehermoso | $180,2 \cdot 10^3$ | 0,06 | 195,80 | 0,037 | 0,136 |
| Torre Caja Madrid | $163,3 \cdot 10^3$ | 0,06 | 215,15 | 0,049 | 0,189 |

Table 5.6-3: Along-wind acceleration

The structural damping associated with wind-induced building motion with a return period of 5 or 10 years is smaller than for a 50-year extreme wind. The total logarithmic decrement of damping is taken 0,06 for all four buildings, corresponding to 1% of critical damping.

Figure 5.6-6 and 5.6-7 provide a graphical comparison of the above accelerations at the top occupied floor, in relation to the criteria of ISO 6897 and BLWTl.

It is noted that the red line in figure 5.6-6 does not represent the exact ISO 6897 criterion. An approximation of that curve is drawn, according to $e^{(-3,65-0,41\ln)}$, which agrees well with the ISO 6897 curve 1.

Furthermore, it is noted that ISO 6897 is more conservative for office buildings while the BLWTl criteria are more conservative for residential buildings.

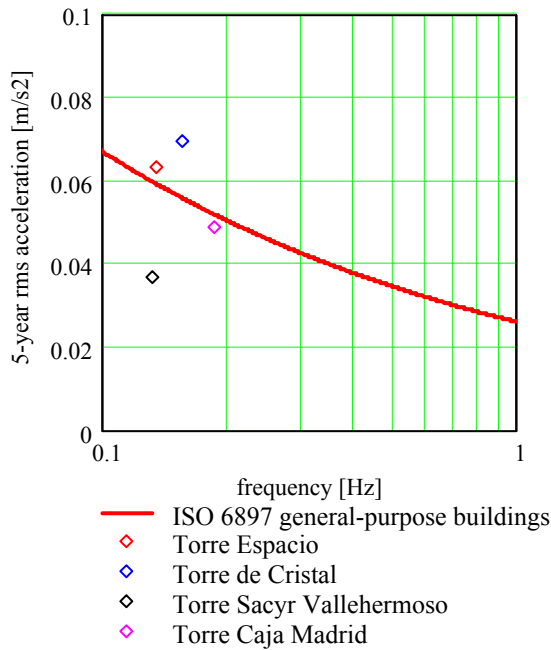


Figure 5.6-6: Comparison with ISO 6897

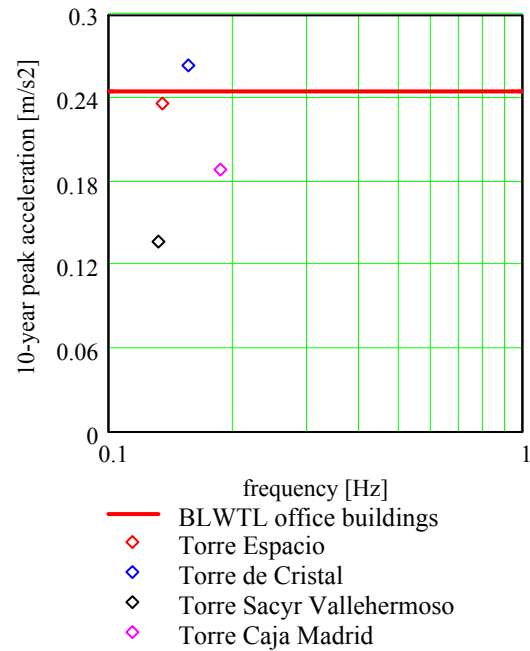


Figure 5.6-7: Comparison with BLWTL

Figure 5.6-6 and 5.6-7 provide a clear comparison of the obtained accelerations in relation to the adopted human comfort criteria. For Torre de Cristal values of 5-year and 10-year acceleration are obtained that are higher than the proposed criteria. Torre Espacio does not comply with the ISO 6897 criterion but the 10-year peak accelerations are within the BLWTL criterion.

Again, a sound structural performance is shown by Torre Caja Madrid and Torre Sacyr Vallehermoso. The BLWTL criterion for the lower two-third of Torre Sacyr Vallehermoso, to be used for hotel purposes, is $20 \cdot 10^{-3} \text{ g}$. It can be seen in figure 5.6-5 that acceleration at the top occupied office-storey results more critical than the top hotel accelerations.

6 Comparison

In decision-making problems, different alternatives can be compared in various ways, depending on the adopted stakeholder's perspective. In this thesis the lateral load resisting systems (LLRSs) of the four tall buildings in Madrid are compared from the point of view of a real estate investor letting the property. When an investor has to choose between various lateral load resisting alternatives, he will rationally prefer that investment alternative that represents the highest expected net present value (NPV).

The NPV is the sum of the discounted¹ cash flow. A typical cash flow diagram for a (tall) building project is characterised by a large initial investment (negative cash flow) and a net positive cash flow throughout the building's economic lifetime. The initial investment consists of design and construction cost, of which the construction cost represents by far the largest part. The operating cash flow is generally composed of rental income and operation and maintenance costs, and is often referred to as net operating income (NOI).

In this chapter, a comparison is presented of the influence of each lateral load resisting system (LLRS) on the NPV of the entire building project, being the sum of the discounted investment and the net operating income (NOI). It was found that insufficient information is available to exactly determine the influence of the principal LLRS characteristic on the NPV; for example the influence of strong building vibrations on rental income, or the damage caused to non-structural elements by excessive lateral displacements. Mainly due to this uncertainty it was believed not to be feasible to carry out a complete NPV calculation.

A simplified comparison is carried out that incorporates a best-estimate influence of each significant LLRS property on the net present value (NPV). The uncertainty associated with this estimation is reflected by adopting a (large) variation on the best-estimate influence. In this way, worst-case and best-case estimations of the effect on the NPV are obtained.

First of all, section 6.1 explores in which way a LLRS affects the net present value (NPV is the sum of the investment and the discounted net operating income NOI) of a tall building project. Subsequently, a set of the most significant LLRS properties is drawn up for the comparison of the buildings that this thesis is concerned with. The influence of these characteristics of the LLRS on the investment and NOI is estimated in section 6.2 and 6.3 respectively. Finally, section 6.4 combines both results from section 6.2 and 6.3 and presents the comparison of the expected total influence on the NPV for a worst-case, best-estimate and best-case scenario.

For each LLRS property the average value among the four buildings is computed. The investment and net operating income resulting from these mean values is set at -100% and 100% respectively. It is assumed that the investment takes place at time

¹ Discounting cash flows means adjusting future cash flows for the time value of money consisting of opportunity cost, inflation and risk. An future cash flow is discounted to the present value as follows

$$PV = \frac{CF_t}{(1+r)^t} \text{ with } CF \text{ being the cash flow, } t \text{ the time in years and } r \text{ the discount rate.}$$

$t=0$ and, therefore, the investment does not have to be discounted. As far as the net operating income (NOI) is concerned, it is assumed that the discount rate is equal to the inflation and that rental income and maintenance cost increase with the inflation. Therefore, the variations in the NOI can be directly translated to a variation in the NPV, i.e. a 10% higher rental income throughout the building's economic lifetime results in a 10% higher NOI and, therefore, in a 10% higher NPV.

It is noted that the comparison presented in this chapter is only valid for the considered four tall buildings. It is not intended to suggest a general method of comparison for LLRSs, because other kinds of lateral load systems may affect the NPV in other ways.

6.1 Significant properties of the lateral load resisting system

The initial investment of a tall building project is primarily determined by the construction cost associated with the LLRS. The LLRS influences the project's net operating income (NOI) principally through maintenance cost and rental income.

Construction cost can be influenced by LLRSs through the following aspects.

- Material, labour and machinery costs incurred during the erection of the LLRS, obviously, increase the total construction cost.
- LLRSs can impose the structural floor height, when the dimensions of horizontal members are governed by lateral load design (for instance in tube structures). An increment of floor height results in more (expensive) façade area and thus increasing the construction cost.

Excessive lateral building displacements can cause damage to cladding, partitions and interior finishes such as doors, elevators etc. Repairing these damaged elements increases the maintenance cost.

Rental income can be affected by a LLRS by means of the following aspects.

- Excessive vibrations adversely affect the occupant comfort. A bad reputation of the building as well as loss of labour productivity, due to this discomfort, can lead to a decrease of rental income.
- Lettable floor area (and therefore rental income) is reduced by the floor area that is covered by vertical members of the LLRS.
- The flexibility of the floor plan can be influenced by the size and position of the LLRS. If the building cannot meet changing tenant needs, this will result in a reduction of the rental income.
- The transparency is often an important selling point of a tall building. In some LLRSs, such as tube structures, the columns are closely spaced in the building envelope thus reducing the window openings. This could lead to a lower financial appraisal of the building tenants.

6.2 Investment

The investment in a (tall) building project is principally determined by the construction cost. The construction cost is made up of machinery, labour and material costs.

When comparing the construction cost associated with the LLRSs of the four tall buildings in Madrid, machinery and labour cost can be disregarded; the principal lateral load resisting element in the governing wind direction is in all cases a reinforced concrete core. Therefore, the erection technique will be the same for each building which means that machinery and labour costs can be thought of as being proportional to the employed material.

So, as far as the investment is concerned, the LLRSs are compared in terms of the material costs incurred during their erection. The material costs are assumed to be proportional to the mean concrete area used for lateral load design over four typical building sections: basement, low-, mid- and high-rise.

The LLRSs are not designed only to resist lateral loads but they should also resist the fundamental gravity load combination. A lateral load system can be efficiently located (from a material point of view) in the building plan to bear a large part of the gravity load as well. In this way, less extra material is needed to meet the stiffness requirements imposed by serviceability limit state considerations.

The lateral load design (LLD)-part is determined by calculating the gravity load design (GLD)-part according to $A_{GLD} = 1 - A_{LLD}$. In order to calculate the GLD-part, the mean design stresses under the fundamental gravity load combinations are calculated at basement level and divided by the concrete design compressive strength. The LLD-part of the concrete area is then calculated by expression (6.2.1).

$$A_{LLRS.LLD} = A_{LLRS} \cdot \left(1 - \frac{\sigma_{d,GLD}}{f'_{c,d}} \right) \quad (6.2.1)$$

The calculation of the mean LLRS concrete area and the LLD-factor of each building structure is presented in appendix IV.

The results are presented in table 6.2-1.

| | $A_{LLRS} [m^2]$ | LLD-factor [-] | $A_{LLRS.LLD} [m^2]$ | mean $[m^2]$ |
|--------------------------|------------------|----------------|----------------------|--------------|
| Torre Espacio | 37,2 | 65% | 24,1 | 42,4 |
| Torre de Cristal | 77,4 | 63% | 48,7 | |
| Torre Sacyr Vallehermoso | 50,3 | 52% | 26,2 | |
| Torre Caja Madrid | 110,6 | 64% | 70,5 | |

Table 6.2-1: Material employed in LLRS for lateral load design

The first column presents the average concrete area used in the principal lateral load resisting elements (structural cores). The second and third column shows the LLD-factor at basement level and the average LLD-concrete area respectively.

Important differences exist among the four tall buildings. For the construction of Torre Espacio and Torre Sacyr Vallehermoso a relative small amount of concrete is used for the LLD. Torre de Cristal employs a considerable amount of concrete which is due to the questionable lateral load design, as stated in 5.3.2. Observe the very large amount of concrete employed in Torre Caja Madrid.

These variations in material cost of the LLRS have to be translated to the total construction cost. Let us assume that the structure accounts for 20% to 30% of the

total cost of a tall building. Reference [35] states that for buildings above 50 stories the cost of a reasonable wind bracing system may constitute one-third of the structural cost and thus between 7% and 10% of the total cost.

The mean LLD-concrete area of the LLRS over all buildings (shown in the right-hand side column of table 6.2-1) is set at 8,5% of the total building cost (average of the range given in reference [35]). Then the relative total construction cost, and therefore the tall building investment, can be calculated as shown in expression (6.2.1). A minus sign is used because it concerns a negative cash flow.

$$-\left(\frac{A_{LLRS.LLD_i}}{A_{LLRS.LLD_{mean}}} 8,5\% + 81,5\%\right) \quad (6.2.1)$$

The above formula results in the following values of total building cost as listed in table 6.2-2.

| | investment |
|--------------------------|------------|
| Torre Espacio | -96,3% |
| Torre de Cristal | -101,3% |
| Torre Sacyr Vallehermoso | -96,8% |
| Torre Caja Madrid | -105,6% |

Table 6.2-2: Comparison investment

6.3 Net operating income

The net operating income is composed of maintenance and operation cost and rental income. It is believed that LLRSs principally influence the maintenance cost and rental income (see section 6.1). In this section the LLRS properties are dealt with that are thought to most significantly influence the net operating income (NOI) and therefore the net present value (NPV) of the tall building project.

Very little information is available about to what extent LLRS properties affect the NOI. As a consequence, the relative importance of each of these aspects in relation to the other NOI-influencing aspects cannot be determined. In this study it is attempted to estimate the influence of these characteristics on the NOI. A best-estimate influence is assumed as well as a variation range resulting, finally, in a worst-case, best-estimate and best-case NOI. Furthermore, a linear relation is assumed between the LLRS-property deviation from the mean and the NOI deviations from the mean.

The following four properties of the LLRS are considered to be most significant.

- Lateral displacement.
- Lateral acceleration.
- Floor area covered by the LLRS.
- Floor plan flexibility.

6.3.1 Lateral displacement

The along-wind height-to-drift ratio due to the 50-year peak wind velocity has been calculated in chapter 5. The lateral displacement should be limited to ensure the well-functioning and appearance of non-structural elements. Excessive building drift can cause damage to façade elements, partitions and interior finishes.

The building drift ratios for each building are presented in table 6.3-1. The reader is referred to section 5.6 for an extensive comparison and interpretation of the lateral drift results.

| | lateral displacement ratio [-] | mean [-] |
|--------------------------|--------------------------------|----------|
| Torre Espacio | 488 | 812 |
| Torre de Cristal | 666 | |
| Torre Sacyr Vallehermoso | 931 | |
| Torre Caja Madrid | 1.164 | |

Table 6.3-1: Lateral displacement ratio

From a reference (tall building) project it is deduced that the non-structural members that may be damaged by excessive building drift – façade elements, partitions, elevators and doors – cover approximately 40% of the total building cost. It is estimated that reducing the mean drift ratio in table 6.3-1 by 10% would require repairing these non-structural elements with a cost of 3% of their construction cost. This means that a building with a drift ratio 10% lower than the mean value will incur 1,2% less maintenance cost during its lifetime. A variation of +/- 0,5% is considered to account for the uncertainties in the estimation.

The influence (compared to the average over all four buildings) of the building drift on the NOI is calculated for each building by

$$100\% + \left(\frac{DriftRatio_i}{DriftRatio_{mean}} - 1 \right) \cdot 12\% \pm 5\% \quad (6.3.1)$$

The results of expression (6.3.1) are provided in table 6.3-2.

| | lateral displacement | +/- var |
|--------------------------|----------------------|---------|
| Torre Espacio | 95,2% | 2,0% |
| Torre de Cristal | 97,8% | 0,9% |
| Torre Sacyr Vallehermoso | 101,8% | 0,7% |
| Torre Caja Madrid | 105,2% | 2,2% |

Table 6.3-2: Comparison influence of lateral displacement on NOI

Torre Sacyr Vallehermoso and Torre Caja Madrid show a rather good performance. In case of Torre Caja Madrid this is mainly caused by the great moment of inertia offered by the two lateral cores. Torre Sacyr Vallehermoso takes advantage of its aerodynamic design in combination with the outrigger-braced core structure. Torre Espacio and Torre de Cristal perform considerably worse than average.

6.3.2 Lateral acceleration

The 10-year along-wind peak accelerations at the top occupied floor are calculated in chapter 5. The lateral accelerations should be limited as to not create any occupant comfort problems.

Table 6.3-2 shows the calculated peak accelerations at the top occupied floor for each building, as well as the average value.

| | lateral acceleration [m/s ²] | mean [m/s ²] |
|--------------------------|--|--------------------------|
| Torre Espacio | 0,235 | 0,206 |
| Torre de Cristal | 0,263 | |
| Torre Sacyr Vallehermoso | 0,136 | |
| Torre Caja Madrid | 0,189 | |

Table 6.3-3: Lateral acceleration

A high level of motion perception adversely affects the human comfort, which can give the building a bad reputation and cause a loss of labour productivity. This will lead to a reduction of the tenant's financial appraisal of the building, resulting in a loss of rental income.

It is estimated that a 10% increase of lateral acceleration results in a 1% decrease of rental income and, therefore, net operating income (NOI). To account for the uncertainty of this estimation a 0,5% variation is adopted. Expression 6.3.2 shows how the calculated 10-year peak accelerations are assumed to influence the rental income.

$$100\% - \left(\frac{Acceleration_i}{Acceleration_{mean}} - 1 \right) \cdot 10\% \pm 5\% \quad (6.3.2)$$

Table 6.3-4 lists the results of the foregoing formula.

| | lateral acceleration | +/- var |
|--------------------------|----------------------|---------|
| Torre Espacio | 98,6% | 0,7% |
| Torre de Cristal | 97,2% | 1,4% |
| Torre Sacyr Vallehermoso | 103,4% | 1,7% |
| Torre Caja Madrid | 100,8% | 0,4% |

Table 6.3-4: Comparison influence of lateral acceleration on NOI

As discussed in section 5.6, a rather good score is obtained by Torre Sacyr Vallehermoso while Torre de Cristal shows a relatively poor performance. The peak acceleration of Torre Sacyr Vallehermoso is rather small because of its aerodynamic shape and large modal mass. By contrast, Torre de Cristal has the lowest fundamental modal mass.

6.3.3 Floor area covered by the lateral load resisting system

The floor area covered by LLRS structural members cannot be let and, therefore, will not generate any rental income. To measure the reduction of the total lettable floor area, the following calculation is performed.

$$\frac{A_{LLRS,LLD_i}}{GFA_{mean}} = \frac{A_{LLRS_i} \cdot \left(1 - \frac{\sigma_{d,GLD_i}}{f'_{c,d_i}}\right)}{GFA_{mean}} \quad (6.3.3)$$

where $A_{LLRS,LLD}$ LLD-concrete area of the LLRS [m²]
 A_{LLRS} gross concrete area of the LLRS [m²]
 GFA gross floor area [m²]

$$\left(1 - \frac{\sigma_{d,GLD}}{f'_{c,d}}\right) \text{ LLD-factor}$$

The calculation of the mean gross floor area of a typical low-, mid- and high-rise section of the buildings is presented in appendix IV. The mean gross floor area over all four buildings is taken as the reference value, being equal to 1566,9 m².

Table 6.3-5 shows the LLD-concrete area of the LLRSs in relation to the gross floor area.

| | A_{LLRS} [m ²] | LLD-factor [-] | $A_{LLRS,LLD}$ [m ²] | $A_{LLRS,LLD} / GFA$ [-] | mean [-] |
|--------------------------|------------------------------|----------------|----------------------------------|--------------------------|----------|
| Torre Espacio | 31,5 | 65% | 20,5 | 1,3% | 2,4% |
| Torre de Cristal | 67,6 | 63% | 42,6 | 2,7% | |
| Torre Sacyr Vallehermoso | 47,5 | 52% | 24,7 | 1,6% | |
| Torre Caja Madrid | 97,1 | 64% | 61,9 | 4,0% | |

Table 6.3-5: Comparison LLRS-covered floor area

The area covered by structural elements of the LLRS does not generate any rental income. The influence of each LLRS on the NOI is then computed as shown in formula (6.3.3).

$$100\% - \left(\frac{A_{LLRS,LLD_i}}{GFA_{mean}} - \frac{A_{LLRS,LLD_{mean}}}{GFA_{mean}} \right) \quad (6.3.3)$$

The results are listed in table 6.3-6

| | LLRS-covered floor area |
|--------------------------|-------------------------|
| Torre Espacio | 101,1% |
| Torre de Cristal | 99,7% |
| Torre Sacyr Vallehermoso | 100,8% |
| Torre Caja Madrid | 98,4% |

Table 6.3-6: Comparison influence of LLRS-covered floor area on NOI

As is to be expected, the buildings with a better-than-average performance are the same as in the construction cost comparison. However, the influence on the net present value is different (in this case relatively modest).

6.3.4 Floor plan flexibility

The flexibility of a floor plan is determined by its ability to fulfil changing tenant demands. As far as office buildings are concerned, the flexibility can be expressed as the ability to accommodate different office layouts. The ease with which various layouts can be implemented in a certain floor plan is directly dependent on the area in between obstructing elements (in this case the principal lateral load resisting elements). It is proposed that the flexibility of this area is determined by its smallest dimension. For example, a rectangular floor plan enclosed by a tube structure provides far more flexibility than the same area wrapped around an internal core structure.

For central core structures, the dimension that determines the floor plan's flexibility is taken as the lease span, being the free distance between the core and the façade.

The reader is referred to Appendix IV for a calculation of the mean effective lease span of the considered tall buildings. The results are presented in table 6.3-7.

| | $L_{m.eq}$ [m] | mean [m] |
|--------------------------|----------------|----------|
| Torre Espacio | 12,7 | 16,2 |
| Torre de Cristal | 9,5 | |
| Torre Sacyr Vallehermoso | 11,0 | |
| Torre Caja Madrid | 31,5 | |

Table 6.3-7: Comparison floor plan flexibility

It is estimated that increasing the flexibility by 10% will lead to an increase of rental income of 0,8%, with a variation of 0,5% to account for the large uncertainty in this estimation.

$$100\% + \left(\frac{L_{m.eq_i}}{L_{m.eq_{mean}}} - 1 \right) \cdot 8\% \pm 5\% \quad (6.3.4)$$

The estimated influence of each LLRS on the floor plan flexibility, and therefore the rental income, is reflected in table 6.3-8.

| | flexibility | +/- var |
|--------------------------|-------------|---------|
| Torre Espacio | 98,3% | 1,1% |
| Torre de Cristal | 96,7% | 2,1% |
| Torre Sacyr Vallehermoso | 97,5% | 1,6% |
| Torre Caja Madrid | 107,6% | 4,7% |

Table 6.3-8: Comparison influence of flexibility on NOI

An enormous difference is noted between Torre Caja Madrid and the other three tall buildings. The two exterior cores of Torre Caja Madrid have a clear advantage over the other central-core structures with regard to the floor plan's flexibility. It is, however, difficult to estimate the influence of this flexibility on the future rental income.

6.3.5 Net operating income

The influence of the LLRS on the net operating income (NOI) is composed of the four influences mentioned above. The best-estimate and variation values from table 6.3-2, 6.3-4, 6.3-6 and 6.3-8 are added to obtain the total weighted influence.

Table 6.3-9 provides the expected influence of each LLRS on the NOI.

| | displacement | acceleration | LLRS-covered floor area | flexibility | NOI | +/- var. |
|--------------------------|--------------|--------------|-------------------------|-------------|--------|----------|
| Torre Espacio | 95,2% | 98,6% | 101,1% | 98,3% | 93,1% | 3,8% |
| Torre de Cristal | 97,8% | 97,2% | 99,7% | 96,7% | 91,4% | 4,4% |
| Torre Sacyr Vallehermoso | 101,8% | 103,4% | 100,8% | 97,5% | 103,4% | 4,0% |
| Torre Caja Madrid | 105,2% | 100,8% | 98,4% | 107,6% | 112,0% | 7,4% |

Table 6.3-9: Comparison of influence on NOI

It is expected that Torre Caja Madrid generates the highest NOI of all four buildings, being mainly due to a good displacement and an outstanding flexibility performance. However, also note that this estimation is subjected to the highest uncertainty. The expected NOI of Torre Sacyr Vallehermoso is better than average due to its sound performance as far as lateral displacement and acceleration is concerned. Both Torre Espacio and Torre de Cristal are expected to generate a lower-than-mean NOI.

6.4 Net present value

As stated earlier, the net present value is obtained by adding the (negative) investment and the sum of the discounted net operating income throughout the economic lifetime of the building.

Table 6.4-1 shows the net present value (NPV) for the LLRSs of each building for a worst-case, best-estimate and best-case scenario. Again, a 100% score for the best-estimate scenario corresponds to the overall performance averaged over the four buildings.

| | worst case | best estimate | best case |
|--------------------------|------------|---------------|-----------|
| Torre Espacio | 93,0% | 96,8% | 100,6% |
| Torre de Cristal | 85,8% | 90,1% | 94,5% |
| Torre Sacyr Vallehermoso | 102,6% | 106,6% | 110,6% |
| Torre Caja Madrid | 99,9% | 106,4% | 113,8% |

Table 6.4-1: Comparison of influence on NPV

The maximum influence of the displacement, acceleration and flexibility characteristic yields the worst-case results for Torre Espacio and Torre de Cristal and the best-case score for Torre Caja Madrid and vice versa. Torre Sacyr Vallehermoso obtains the best-case NPV for minimum influence of the floor plan's flexibility and maximum influence of the building displacement and acceleration. The worst case is obtained for the maximum influence of the flexibility and minimum influence of displacement and acceleration.

The best-estimate influence of the LLRS on the NPV is the same for Torre Sacyr Vallehermoso and Torre Caja Madrid. In the case of Torre Sacyr Vallehermoso, this is due to the relatively small amount of concrete employed for the LLD and the sound structural performance. As far as Torre Caja Madrid is concerned, it is because of the enormous flexibility provided by the floor plan and the relatively small along-wind displacement. Due to this, the estimate for Torre Caja Madrid is subjected to a much larger uncertainty. However, note the relatively high uncertainty of the computed best-estimate value. The lateral load design of Torre Espacio and Torre de Cristal is considered to represent a worse-than-average NPV. Especially the latter obtains a relatively bad performance for all comparison criteria: construction cost, displacement, acceleration, lettable floor area and flexibility.

Discount rate

For reasons of simplicity of calculation the discount rate has been taken equal to the inflation. Because of this, the influence on future cash flow was proportional to the influence on the net present value.

However, the time value of money should consist of inflation, opportunity cost and risk. The opportunity cost is represented by the interest that could have been earned on the invested money. Future earnings are always subjected to the possibility that less or more will be received or that the inflation has been incorrectly estimated. This causes that an investor will always prefer to earn (or save) money today than in the future, thus reducing the present value of future positive cash flow. The foregoing is illustrated in figure 6.4-1, where the left graph represents the situation in which the discount rate equals the inflation and the right-hand side graph shows the normal situation in which the discount rate is higher than the inflation. The abbreviations DCF and NPV stand for discounted cash flow and net present value respectively.

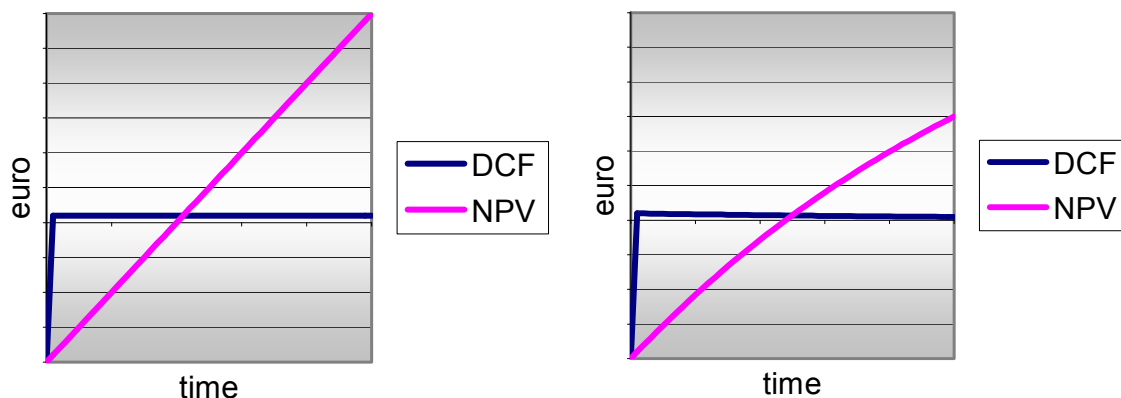


Figure 6.4-1: Influence of discount rate on the net present value

Because of opportunity cost, saving on construction cost becomes relatively more important than increasing the future net operating income. Therefore, Torre Sacyr Vallehermoso and Torre Espacio are actually more interesting, from a financial feasibility point of view, than suggested in table 6.4-1.

7 Conclusions and recommendations

This chapter presents the conclusions that are drawn from this study in section 7.1. The recommendations, following from these conclusions, are provided in section 7.2.

7.1 Conclusions

Firstly in subsection 7.1.1, conclusions are drawn with regard to the analysed four tall buildings in Madrid.

Subsection 7.1.2 presents some general conclusions that were drawn throughout this thesis.

7.1.1 Conclusions associated with the four tall buildings

According to the recommendations laid down in Eurocode 1, structural analyses in the serviceability limit state have been performed with complete finite element models of each building. The structural analyses resulted in values for the 50-year along-wind displacements, and 5 and 10-year along-wind accelerations at the top occupied floor. These results are summarised and discussed in section 5.6.

The following conclusions are drawn.

1. With regard to the along-wind response in the serviceability limit

- All buildings comply with the global drift limit of $H/500$ or the inter-storey drift limit of $H/400$.
- The 10-year and 5-year accelerations on the top occupied floor of Torre Sacyr Vallehermoso and Torre Caja Madrid are within the limits proposed by ISO 6897 and the Boundary Layer Wind Tunnel Laboratory of the University of Western Ontario. Torre Espacio satisfies the latter criterion, but the 5-year acceleration slightly exceeds the former limit. The occupants of Torre de Cristal are calculated to be subjected to accelerations that are slightly higher than the cited criteria.

Subsequently, a comparison (presented in chapter 6) has been carried out between the adopted lateral load resisting systems of each building. The comparison is performed from the financial point of view of a real estate investor. A set of properties of the lateral load system has been chosen that is believed to most significantly influence the financial feasibility of the considered tall buildings (lateral displacement and acceleration, floor area covered by structural members and floor plan flexibility). A comparison model has been established in which the construction cost, and the future rental income and maintenance cost (together the operating income) are related to the net present value of the tall building investment. Assumptions have been made with regard to the influence of each lateral load system property on the net present value.

The conclusions of this comparison are provided hereafter.

2. Concerning the comparison of the lateral load designs

Torre Espacio

- The relatively small amount of concrete employed in the lateral load resisting system of Torre Espacio leads to a considerable saving on the total construction cost. However, the net present value is negatively influenced by relatively high values of the lateral displacement and acceleration.

Torre de Cristal

- The lateral load design of Torre de Cristal yields higher construction cost in comparison to the other buildings. Furthermore, the expected operating income will be less than average, because of a relatively poor performance for all comparison criteria.

Torre Sacyr Vallehermoso

- Investment savings result from the lateral load design of Torre Sacyr Vallehermoso due to the small amount of employed material. In addition, its sound structural performance influences positively the relative net operating income.

Torre Caja Madrid

- The lateral cores of Torre Caja Madrid employ a large amount of concrete and this, as a consequence, results in higher-than-mean construction cost. The operating income, however, will be relatively high because of the building's sound structural performance and the great flexibility of the floor plan.

Comparison

- The lateral load design of Torre Sacyr Vallehermoso represents the best alternative from a financial point of view. This is mainly because of its aerodynamic shape and efficient lateral load resisting system.
- The lateral load resisting system of Torre de Cristal constitutes the least interesting alternative of the four analysed building; principally due to the questionable design of the lateral load system.

7.1.2 General conclusions

The following general conclusions were drawn throughout the performed study.

3. Regarding the method of comparison

- The use of this method is limited to the herein analysed building structures.
- Insufficient information is available about the effect of lateral load resisting systems on the financial feasibility to take rational design decisions based on accurate quantitative considerations.

4. Concerning the Eurocode 1 recommendations

- Confusion is caused in appendix B and F of Eurocode 1, because of an ambiguous description of the calculation of the along-wind fundamental

equivalent mass. Furthermore, these appendices lack a calculation method for the fundamental modal mass.

- Approximate values of the logarithmic decrement of structural damping in the fundamental mode are proposed in appendix F, but are not explicitly related to a (ultimate or serviceability) limit state and return period. It is understood that these values correspond to a 50-year return period, yet no damping values are presented for serviceability limit state considerations associated with shorter return periods.

5. With regard to the structural design of tall buildings

- Outrigger and belt structures constitute a very effective and efficient means to decrease lateral displacements and accelerations of, bending-dominated, central core structures.

6. Concerning human comfort criteria

- No consensus exists among the international specialists about which criteria to adopt in tall building design to guarantee the occupant's comfort.

7.2 Recommendations

The recommendations following from the abovementioned conclusions are presented in this section.

It is recommended that:

1. Concerning the evaluation and comparison of the lateral load design of the analysed four tall buildings

- Wind tunnel / specialist studies should be carried out to determine more accurately the force coefficient, assess interference effects, investigate the effects of mass and stiffness discontinuities in case of Torre de Cristal and Torre Caja Madrid, and finally to assess the susceptibility to vortex-shedding of Torre Sacyr Vallehermoso.

2. Regarding the method of comparison

- Further research is desired to determine the influence of the lateral load design of tall buildings on the financial feasibility, in order to make rational design decisions based on accurate quantitative considerations.

3. Concerning the Eurocode 1 recommendations

- The ambiguity in the definition of the equivalent mass in appendix F may be solved by stating explicitly that the fundamental modal mass is calculated otherwise.
- A simple formula may be included to calculate the along-wind fundamental equivalent mass from the equivalent mass, based on the fundamental mode shape parameter $\zeta_{,,}$

$$m_{1,x} = m_e \cdot \frac{\int_0^h \left(\frac{z}{h}\right)^\zeta \cdot dz}{h} \quad (7.2.1)$$

- Values of the logarithmic decrement of structural damping may be included to assess serviceability limit states with short return periods. It should at least be stated to which return periods the proposed damping values correspond.

4. Concerning the structural design of tall buildings

- The possibility of outrigger-optimisation of bending-dominated lateral load resisting systems should always be considered in the structural design of tall buildings.
- Load factors have to be applied to building drifts (corresponding to a structural serviceability limit state), when used to calculate dimensional tolerances for façade elements and fixings (ultimate limit state).

5. With regard to human comfort criteria

- Further research is needed because it seems that no consensus, with regard to which criteria should be adopted, will be reached in the near future.

List of references

- [1] Aerospace Division of the American Society of Civil Engineers, *Wind tunnel studies of buildings and structures. ASCE manuals and reports on engineering practice no. 67*. United States of America: American Society of Civil Engineers, 1999.
- [2] Baker, W.F., *The world's tallest building, Burj Dubai, U.A.E.*, CTBUH Conference in Seoul, 2004, pp.1168-1169
- [3] Boggs, D, *Acceleration indexes for human comfort in tall buildings - peak or rms? July 1995*.
www.cppwind.com/support/papers/papers/structural/PEAKvsRMS.pdf.
- [4] Boggs, D.W. and J.A. Peterka, *Wind speeds for design of temporary structures*, Structures Congress '92 Compact Papers, ASCE, 1992.
- [5] Calavera Ruiz, J., *Proyecto y cálculo de estructuras de hormigón*. Spain: Infoprint, 1999.
- [6] Chen, P.W. and L.E. Robertson, *Human perception thresholds of horizontal motion*. Journal of Structural Division, August 1972, pp.1681-1695.
- [7] Clough, R.W., and J. Penzien, *Dynamics of structures*. United States of America: McGraw-Hill, 1975.
- [8] Council on Tall Buildings and Urban Habitat, *Tall buildings in numbers. Tall buildings in the world: past, present & future. CTBUH Journal*, 2 (2008), pp.40-41.
- [9] Council on Tall Buildings and Urban Habitat, *One hundred and one of the world's tallest buildings*. Australia: The Images Publishing Group, 2006.
- [10] European Committee for Standardization, *EN 1990. Eurocode - Basis of structural design*. Brussels: European Committee for Standardization, 2002.
- [11] European Committee for Standardization, *EN 1991-1-1. Eurocode 1: Actions on structures - Part 1-1: General actions - Densities, self-weight, imposed loads for buildings*. Brussels: European Committee for Standardization, 2002.
- [12] European Committee for Standardization, *EN 1991-1-4. Eurocode 1: Actions on structures - Part 1-4: General actions - Wind Actions*. Brussels: European Committee for Standardization, 2005.
- [13] European Committee for Standardization, *EN 1992-1-1. Eurocode 2: Design of concrete structures - Part 1-1: General rules and rules for buildings*. Brussels: European Committee for Standardization, 2004.
- [14] European Committee for Standardization, *prEN 1998. Eurocode 8: Design of structures for earthquake resistance – Part 1: General rules, seismic actions and rules for*. Brussels: European Committee for Standardization, 2003.
- [15] Hansen, R.J et al., *Human response to wind-induced motion of buildings*. Journal of Structural Division, July 1973, pp.1589-1605.
- [16] Hormigón y acero, *Edificios altos de Cuatro Torres Business Area*, V. 59 nº 249, July – September 2008.
- [17] INTEMAC, *El incendio del edificio Windsor de Madrid. Investigación del comportamiento al fuego y de la capacidad resistente residual de la estructura tras el incendio*, Notas de información técnica NIT 2 – 05, December 2005.
- [18] International Organization for Standardization, *International Standard ISO 6897-1984. Guidelines for the evaluation of fixed structures, especially*

- buildings and off-shore structures, to low-frequency horizontal motion (0,063 to 1 Hz)*. Switzerland: International Organization for Standardization, 1984.
- [19] Irwin, A.W., *Human response to dynamic motion of structure*. The Structural Engineer, V56A, No. 9 (1978), pp.237-244.
- [20] Irwin, P.A. and W.F. Baker, *The wind engineering of the Burj Dubai Tower*, CTBUH 7th World Congress: New York, 2005.
- [21] Isyumov, N., 'Criteria for acceptable wind-induced motions of tall buildings'. *International conference on tall buildings*. Rio de Janeiro: Council on Tall Buildings and Urban Habitat, 1993.
- [22] Joint Committee on Structural Safety, *JCSS probabilistic model code. Part 2: loads*. February 2001. www.jcss.ethz.ch/publications/PMC/PART_II.pdf.
- [23] Kareem, A. et al., *Mitigation of motions of tall buildings with specific examples of recent applications*, Wind and Structures, Vol. 2, No. 3, 1999, p.201-251.
- [24] Liu, H., *Wind engineering: a handbook for structural engineers*. United States of America: Prentice-Hall, Inc., 1991.
- [25] Lungu, D. and P. van Gelder, *Characteristics of wind turbulence with applications to wind codes*. December 2008.
www.citg.tudelft.nl/live/ServeBinary?id=ec906edd-af0e-4ba1-bcd8-18e7e7cd73ab&binary=/doc/paper22.pdf
- [26] Martínez Calzón, J., *Hormigones de alta resistencia en la edificación de gran altura. Aplicación particular al Edificio Torre Espacio en el Paseo de la Castellana Madrid*. Hormigón y acero, 228-229 (2003), pp.5-14.
- [27] Ministerio de Fomento, *Norma básica de la edificación NBE AE-88: Acciones en la edificación*. 6th edition. Madrid: Ministerio de Fomento. Centro de Publicaciones, 1999.
- [28] Ministerio de Fomento, *Norma de construcción sísmorresistente: parte general y edificación (NCSE-02)*. Madrid: Ministerio de Fomento, 2002.
- [29] Münchener Rückversicherungs-Gesellschaft, *Rascacielos*. München: Münchener Rückversicherungs-Gesellschaft, 2000.
- [30] National Fire Protection Association August 2005, *U.S. experience with sprinklers and other fire extinguishing equipment*. July 2007.
www.nfpa.org/assets/files//PDF/OSsprinklers.pdf
- [31] Simiu, E., and R.H. Scanlan, *Wind effects on structures: fundamentals and applications to design*. 3rd edition. United States of America: John Wiley & Sons, 1996.
- [32] Smith, R. F. and S. Killa, *Bahrain World Trade Center (BWTC): the first large scale integration of wind turbines in a building*. The Structural Design of Tall and Special Buildings, 16 (2007), pp.429-439.
- [33] Stafford Smith, B. and A. Coull, *Tall building structures: analysis and design*. United States of America: John Wiley & Sons, 1991.
- [34] Tamura, Y. et al., *Evaluation perception of wind-induced vibration in buildings*, Structures & Buildings, 159 Issue SB5, pp.283-293.
- [35] Taranath, Bungale S., *Structural analysis and design of tall buildings*. United States of America: McGraw-Hill, 1988.
- [36] Taranath, Bungale S., *Wind and earthquake resistant buildings: structural analysis and design*. United States of America: Marcel Dekker, 2005.

Sites on World Wide Web

- [37] www.ctbuh.org
- [38] www.firesprinklerassoc.org
- [39] www.jcss.ethz.ch
- [40] www.wikipedia.org

APPENDICES TO THE REPORT:

LATERAL LOAD DESIGN OF TALL BUILDINGS

EVALUATION AND COMPARISON OF FOUR TALL BUILDINGS IN MADRID, SPAIN



Author: P.P. Hoogendoorn
Date: January 12th 2009

Table of contents

| | |
|---|-----------|
| List of figures | iii |
| List of tables | iv |
| I Parametric study on optimum locations of single-outrigger structures | 1 |
| I.1 Compatibility of rotation | 2 |
| I.1.1 Core rotation | 2 |
| I.1.2 Outrigger rotation | 2 |
| I.2 Results | 5 |
| II Wind loading..... | 10 |
| II.1 Validity of Eurocode mean wind velocity profile | 10 |
| II.2 Mean wind velocity profile | 13 |
| II.2.1 Simplified logarithmic formula | 13 |
| II.2.2 Eurocode expression | 15 |
| II.2.3 Comparison | 15 |
| II.3 Relative turbulence intensity | 16 |
| II.4 Reynolds number | 19 |
| II.5 Structural vibrations..... | 21 |
| II.5.1 Vortex shedding and the lock-in phenomenon..... | 21 |
| II.5.2 Across-wind galloping..... | 23 |
| II.5.3 Wake galloping | 24 |
| II.5.4 Torsional divergence | 25 |
| II.5.5 Flutter | 26 |
| II.5.6 Buffeting | 26 |
| III Structural analysis | 28 |
| III.1 General considerations | 28 |
| III.1.1 Peak wind pressure profile | 28 |
| III.1.2 Determination of the structural factor..... | 30 |
| III.2 Torre Espacio | 36 |
| III.2.1 Equivalent static wind loading..... | 36 |
| III.2.2 Building accelerations..... | 40 |
| III.2.3 Effective axial stiffness of vertical concrete members | 44 |
| III.3 Torre de Cristal..... | 60 |
| III.3.1 Equivalent static wind loading..... | 60 |
| III.3.2 Building accelerations..... | 64 |
| III.3.3 Effective axial stiffness of vertical concrete members | 68 |
| III.4 Torre Sacyr Vallehermoso..... | 71 |
| III.4.1 Equivalent static wind loading..... | 71 |
| III.4.2 Building accelerations..... | 75 |
| III.4.3 Effective axial stiffness of vertical concrete members | 79 |
| III.5 Torre Caja Madrid | 87 |
| III.5.1 Equivalent static wind loading..... | 87 |
| III.5.2 Building accelerations..... | 91 |
| III.5.3 Effective axial stiffness of vertical concrete members | 95 |

| | | |
|------|--------------------------------|-----|
| IV | Comparison | 100 |
| IV.1 | Mean concrete area | 100 |
| IV.2 | LLD-factor | 101 |
| IV.3 | Mean gross floor area | 102 |
| IV.4 | Mean effective lease span..... | 102 |
| | List of references | 105 |

List of figures

| | |
|---|-----|
| Figure I.1-1: Mechanical representation and bending moment diagram | 1 |
| Figure I.1-1: Outrigger rotation | 3 |
| Figure I.2-1: Reduction of top deflection as a function of ω | 7 |
| Figure I.2-2: Optimum location as a function of ω for top deflection reduction..... | 7 |
| Figure I.2-3: Reduction of the overturning base moment as a function of ω | 9 |
| Figure I.2-4: Optimum location as a function of ω for base moment reduction | 9 |
| Figure II.1-1: Wind profile characteristics per terrain category, according to (II.1.1) | 11 |
| Figure II.1-2: Wind profile characteristics per terrain category, according to (II.1.3) | 12 |
| Figure II.1-3: Error of EC mean wind profiles with terrain roughness and height | 12 |
| Figure II.3-1: Relative turbulence intensity according to (II.3.1) | 17 |
| Figure II.3-2: Relative turbulence intensity according to (II.3.2) | 18 |
| Figure II.3-3: Ratio of relative turbulence intensity according to (II.3.1) and (II.3.2) | 19 |
| Figure II.5-1: Typical flow diagrams around a prismatic cylinder in laminar flow [4]..... | 21 |
| Figure II.5-2: Lock-in phenomenon [4]..... | 22 |
| Figure II.5-3: Strouhal numbers for different cross-sections [1]..... | 23 |
| Figure II.5-4: Across-wind galloping [3] | 23 |
| Figure II.5-5: Lift and drag coefficient as a function of angle of attack [3] | 24 |
| Figure II.5-6: Wake galloping [3]..... | 25 |
| Figure II.5-7: Torsional divergence [3]..... | 25 |
| Figure II.5-8: Wake buffeting [3] | 27 |
| Figure III.2-1: Core structures..... | 44 |
| Figure III.2-2: Lateral core sections | 53 |
| Figure III.2-3: Central core sections in plan | 55 |
| Figure III.2-4: Central core sections in elevation | 55 |
| Figure III.2-5: Lateral core sections | 58 |
| Figure III.4-1: Column sections..... | 80 |
| Figure III.4-2: Core sections | 84 |
| Figure III.5-1: Terminology shear walls..... | 95 |
| Figure IV.1-1: LLRS area Torre Espacio | 100 |
| Figure IV.1-2: LLRS area Torre de Cristal | 100 |
| Figure IV.1-3: LLRS area Torre Sacyr Vallehermoso | 100 |
| Figure IV.1-4: LLRS area Torre Caja Madrid..... | 101 |
| Figure IV.4-1: Equivalent lease span Torre Espacio | 103 |
| Figure IV.4-2: Equivalent lease span Torre de Cristal | 103 |
| Figure IV.4-3: Equivalent lease span Torre Sacyr Vallehermoso | 103 |
| Figure IV.4-4: Equivalent lease span Torre Caja Madrid..... | 103 |

List of tables

| | |
|--|-----|
| Table II.1-1: Wind profile characteristics for $v_{m,II}(10\text{ m}) = 26,0\text{ m/s}$ | 11 |
| Table II.1-2: Error for wind velocity, pressure, base shear and bending moment | 13 |
| Table II.3-1: Proponed values for β | 17 |
| Table II.3-2: Error in relative turbulence intensity | 19 |
| Table II.5-1: Distinct ranges of Reynolds numbers..... | 22 |
| Table IV.1-1: LLRS concrete area | 101 |
| Table IV.2-1: Lateral load design factor..... | 102 |
| Table IV.3-1: Mean gross floor area | 102 |
| Table IV.4-1: Equivalent lease span..... | 104 |

I Parametric study on optimum locations of single-outrigger structures

This appendix presents a parametric study on the behaviour of single-outrigger structures in tall buildings. Results are presented in terms of the optimum outrigger location, as a function of a dimensionless factor ω that relates the core, column and outrigger stiffness, for the top deflection and base overturning moment. Furthermore, the effectiveness of the top deflection and base moment reduction is presented as a function of the relative stiffness parameter ω .

After a short description of the structure and its parameters, section I.1 treats the derivation of the formula that results from the rotational compatibility between the core and outrigger structure. Section I.2 presents the obtained results in terms of optimum locations.

Due to the discontinuity represented by the outrigger structure no continuum mechanics approach can be efficiently used. Firstly a qualitative moment distribution, along the height of the building is sketched, after which the compatibility between the core and outrigger rotation is used to solve the problem. A generalised method for solving multiple-outrigger structure problems is presented in reference [5].

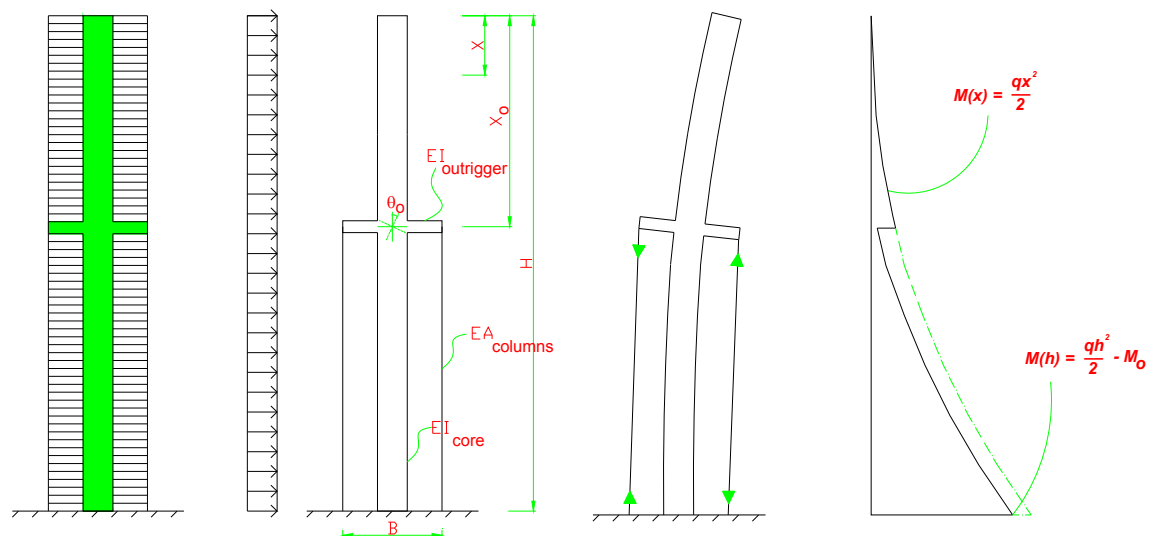


Figure I.1-1: Mechanical representation and bending moment diagram

Let the building structure be represented as shown in figure I.1-1. The structural behaviour is assumed to be linear elastic. The core is rigidly connected to the outrigger structure and the foundation and axial forces only are assumed to be transmitted by the outrigger to the columns. The sectional properties of all structural elements are considered to be constant throughout the height of the building. Furthermore, a constant wind pressure is assumed for reasons of calculation simplicity.

The bending moment diagram as a function of the height is sketched in figure I.1-1 and is expressed by

$$M(x) = \frac{qx^2}{2} \quad \text{for } 0 \leq x < x_o \quad (1.1.1)$$

$$M(x) = \frac{qx^2}{2} - M_o \quad \text{for } x_o < x \leq H$$

M_o is the outrigger-induced bending moment due to the simultaneous compression and tension of the opposite perimeter columns. The distance from the outrigger to the top of the building is denoted x_o .

1.1 Compatibility of rotation

The method presented here is based on the rotation compatibility between the core and outrigger at the interconnection level x_o .

$$\theta_{co}(x_o) = \theta_o \quad (1.1.2)$$

1.1.1 Core rotation

The left-hand side term of (1.1.2), being the core rotation at height x_o , is calculated according to

$$\theta_{co}(x_o) = \frac{1}{EI_{co}} \int_{x_o}^H \left(\frac{q \cdot x^2}{2} - M_o \right) \cdot dx \quad (1.1.3)$$

which after integration yields

$$\theta_{co}(x_o) = \frac{q \cdot (H^3 - x_o^3)}{6 \cdot EI_{co}} - \frac{M_o \cdot (H - x_o)}{EI_{co}} \quad (1.1.4)$$

Note that the constant of integration is equal to 0 following from the boundary condition at base level, i.e. the restrained core rotation at height H.

1.1.2 Outrigger rotation

The rotation of the outrigger θ_o due to the moment M_o is composed of two parts: the rotation $\theta_{o,cl}$ due to the axial deformation of the perimeter columns and the rotation $\theta_{o,o}$ due to the flexibility of the outrigger itself (figure 1.1-1).

Rotation due to the columns

The shortening of the right-hand side perimeter columns, and elongation of the columns on the opposite side, equals

$$\Delta l = \frac{M_o \cdot L}{B \cdot EA_{cl}} \quad (I.1.5)$$

The rotation is then given by

$$\theta_{o.cl} = \frac{2 \cdot \Delta l}{B} = \frac{2 \cdot M_o \cdot (H - x_o)}{B^2 \cdot EA_{cl}} \quad (I.1.6)$$

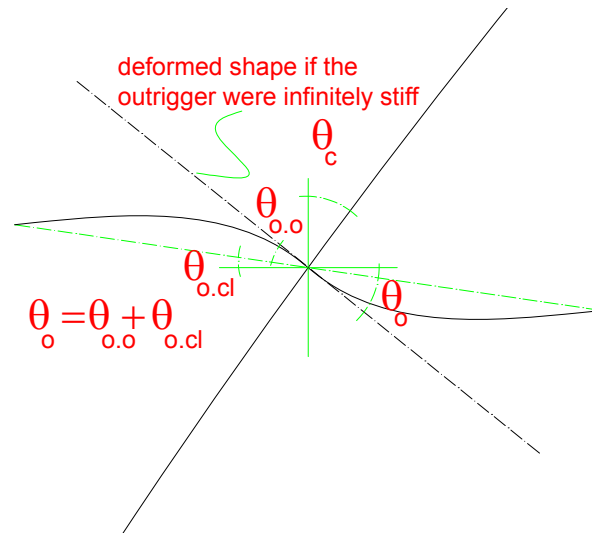


Figure I.1-1: Outrigger rotation

Rotation due to the outrigger's flexibility

Let us calculate the rotation of the outrigger on the left-hand side due to the moment $M_o/2$ acting on that part. The Euler-Bernoulli beam theory shows that the second derivative of the deflection u varies linearly with the bending moment divided by the flexural stiffness EI

$$\frac{M(x)}{EI_o} = \ddot{u}(x) = \frac{M_o \cdot x}{EI_o \cdot B} \quad (I.1.7)$$

where B is the total building width and the moment increases linearly from 0 at the left-hand side perimeter column to $M_o/2$ at the intersection with the core at $B/2$. Integration of (I.7) yields

$$\dot{u}(x) = \frac{M_o \cdot x^2}{2 \cdot EI \cdot B} + C_1 \quad (I.1.8)$$

and after further integration

$$u(x) = \frac{M_o \cdot x^3}{6 \cdot EI \cdot B} + C_1 \cdot x + C_2 \quad (I.1.9)$$

The two constants of integration C_1 and C_2 are solved by considering the following boundary conditions for the outrigger deflection:

$$u(0) = 0 \quad \text{and} \quad u(B/2) = 0 \quad (I.1.10)$$

from which follows

$$C_2 = 0 \quad \text{and} \quad C_1 = -\frac{M_o \cdot B}{24 \cdot EI} \quad (I.1.11)$$

The rotation of the outrigger at the intersection with the core can now be calculated with (I.8)

$$\dot{u}\left(\frac{B}{2}\right) = \frac{M_o \cdot B}{8 \cdot EI} - \frac{M_o \cdot B}{24 \cdot EI} = \frac{M_o \cdot B}{12 \cdot EI} \quad (I.1.12)$$

Note that the effective flexural stiffness of the outrigger should be used, i.e. taking into account the rigid-arm effect at the intersection with the core.

$$EI_{o,eff} = \left(1 + \frac{a}{b}\right)^3 \cdot EI_o \quad (I.1.13)$$

where a represents the distance from the centre of the core to the outrigger and b is the outrigger's free span.

Total outrigger rotation

The total outrigger rotation θ_o at the core intersection is the sum of (I.6) and (I.12)

$$\theta_o = \frac{2 \cdot M_o \cdot (H - x_o)}{B^2 \cdot EA_{column}} + \frac{M_o \cdot B}{12 \cdot EI_o} \quad (I.1.14)$$

Employing (I.4) and (I.14) and rewriting (I.2) yields

$$\frac{q \cdot (H^3 - x_o^3)}{6 \cdot EI_{co}} = \frac{2 \cdot M_o \cdot (H - x_o)}{B^2 \cdot EA_{cl}} + \frac{M_o \cdot B}{12 \cdot EI_o} + \frac{M_o \cdot (H - x_o)}{EI_{co}} \quad (I.1.15)$$

and after rearranging

$$\frac{q \cdot (H^3 - x_o^3)}{6 \cdot EI_{co}} = M_o \left[\frac{2 \cdot (H - x_o)}{B^2 \cdot EA_{cl}} + \frac{B}{12 \cdot EI_o} + \frac{(H - x_o)}{EI_{co}} \right] \quad (I.1.16)$$

finally resulting in

$$M_o = \frac{q}{6} \left[\frac{H^3 - x_o^3}{\frac{2 \cdot EI_{co} \cdot (H - x_o)}{B^2 \cdot EA_{cl}} + \frac{B \cdot EI_{co}}{12 \cdot EI_o} + (H - x_o)} \right] \quad (I.1.17)$$

The following dimensionless structural parameters are defined:

$$\alpha = \frac{EI_{co}}{EA_{cl}} \cdot \frac{2}{B^2} \quad (I.1.18)$$

representing the core-to-column stiffness

$$\beta = \frac{EI_{co}}{EI_o} \cdot \frac{B}{H} \quad (I.1.19)$$

representing the core-to-outrigger stiffness

$$\omega = \frac{\beta}{12 \cdot (1 + \alpha)} \quad (I.1.20)$$

relating the two latter parameters.

Expression (I.17) can then be written in terms of α and β

$$M_o = \frac{q}{6} \left[\frac{H^3 - x_o^3}{(1 + \alpha) \cdot (H - x_o) + \frac{\beta \cdot h}{12}} \right] \quad (I.1.21)$$

and, finally in terms of ω

$$M_o = \frac{q}{6 \cdot (1 + \alpha)} \left[\frac{H^3 - x_o^3}{(H - x_o) + \omega \cdot H} \right] \quad (I.1.22)$$

1.2 Results

An expression has been obtained for the bending moment induced by a single-outrigger structure. Expression (I.22) can now be used to determine the effectiveness and optimum location of single-outrigger structures to reduce the top building deflection and base moment.

Top deflection

The resulting top deflection is calculated by subtracting the drift reduction due to the outrigger restraining moment from the top deflection if the lateral load resisting system were composed only of the core.

$$\delta = \frac{q \cdot H^4}{8 \cdot EI_{co}} - \frac{1}{2 \cdot EI_{co}} \left[M_o \cdot (H^2 - x_o^2) \right] \quad (1.2.1)$$

The second term follows from the application of the moment-area method on the outrigger-induced moment M_o .

$$\delta_{red.o} = - \left(\frac{1}{EI_{co}} \cdot M_o \cdot (H - x_o) \right) \cdot \left(x_o + \frac{H - x_o}{2} \right) \quad (1.2.2)$$

The effectiveness and optimum location of the outrigger structure can now be calculated for all values of ω . The effectiveness is determined by the reduction in relation to the top deflection of the core-only structure, i.e. the second term in (1.2.1) in relation to the first term. Figure 1.2-1 shows the results for ω between 0 and 1. A small value of ω corresponds to a relatively high flexural stiffness of the outrigger, while a high value of ω corresponds to a relatively high axial stiffness of the columns.

Note that service cores in buildings typically contain many openings to provide for access for people and installations, which highly increases the shear deformation of the structure. Besides, the foundation also causes part of the lateral building displacement due to its rotational flexibility. Both aspects increase the total lateral displacement and, therefore, reduce the reduction caused by the outrigger in terms of total lateral displacement. Nevertheless, important reductions of the lateral displacement can be achieved by employing an outrigger structure.

The optimum single-outrigger locations are found by minimising (1.2.1) or simply by connecting the maxima of figure 1.2-1. For different values of ω the dimensionless optimum location x_o/H of the outrigger is shown in figure 1.2-2.

It is shown that for a single-outrigger braced structure the optimum location lies approximately in between $0,40 H$ and $0,30 H$ from the top, for practical values of ω . Furthermore, the optimum moves upwards with increasing values of ω .

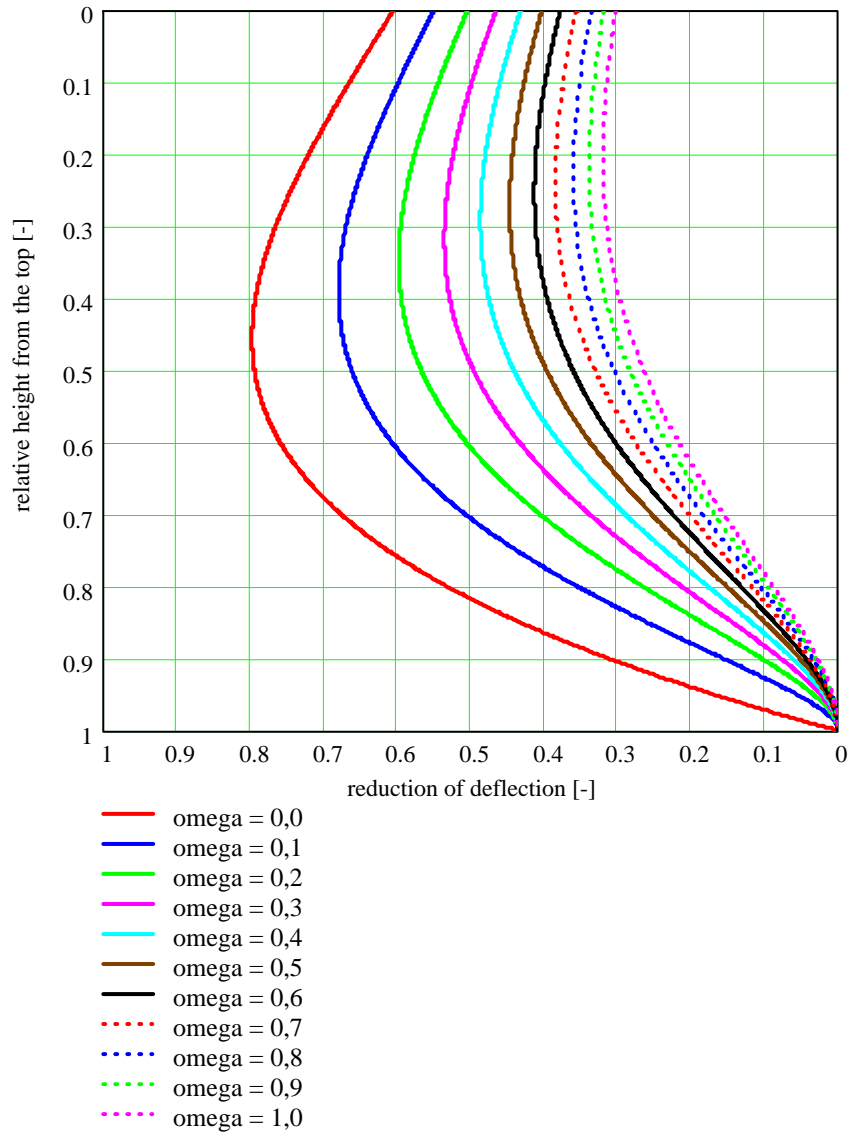


Figure I.2-1: Reduction of top deflection as a function of ω

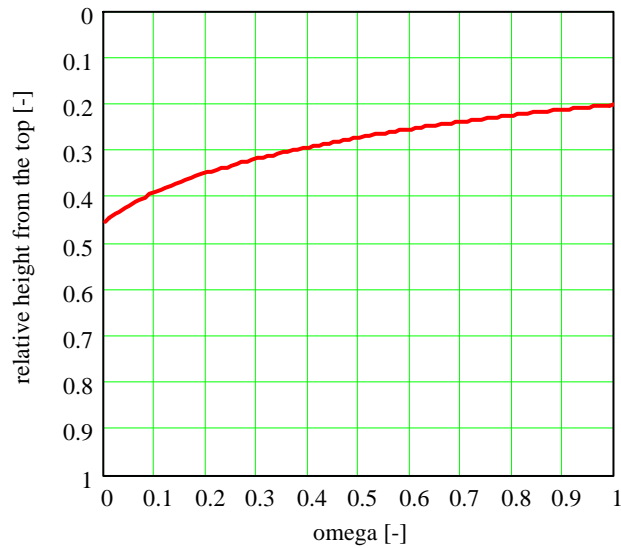


Figure I.2-2: Optimum location as a function of ω for top deflection reduction

Overturning base moment

A similar parametric study has been carried out for the overturning base moment. The reduction of the base moment has been calculated as a function of the dimensionless structural parameter ω . The reduction reflects the resulting base moment of the single-outrigger structure in relation to the core structure without outrigger.

$$\frac{\frac{q \cdot H^2}{2} - M_o}{\frac{q \cdot H^2}{2}} \quad (1.2.3)$$

The corresponding reductions as a function of ω are presented in figure I.2-3.

The optimum locations of the outrigger in order to minimise the base overturning moment, i.e. maximising (1.1.22), are plotted in figure I.2-4. Note that the optimum outrigger location for the base moment does not guarantee that the bending moment along the height of the structure does not exceed the overturning base moment. The latter is especially true for the lower left part of the graph in figure I.2-4, i.e. for levels near the base and for relatively very stiff outrigger structures.

The optimum, in terms of base moment reduction, is located in the lower half of the building height. The optimum moves upwards for increasing values of ω .

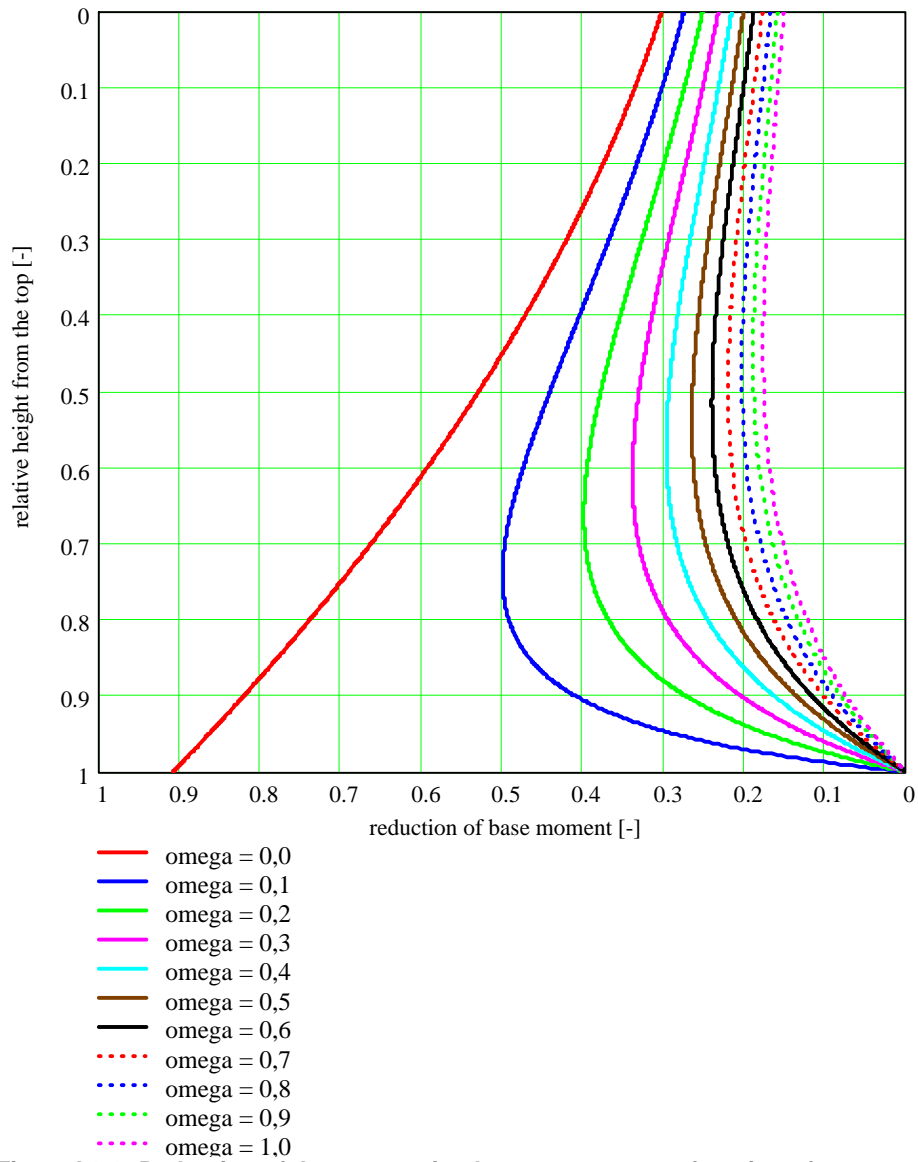


Figure I.2-3: Reduction of the overturning base moment as a function of ω

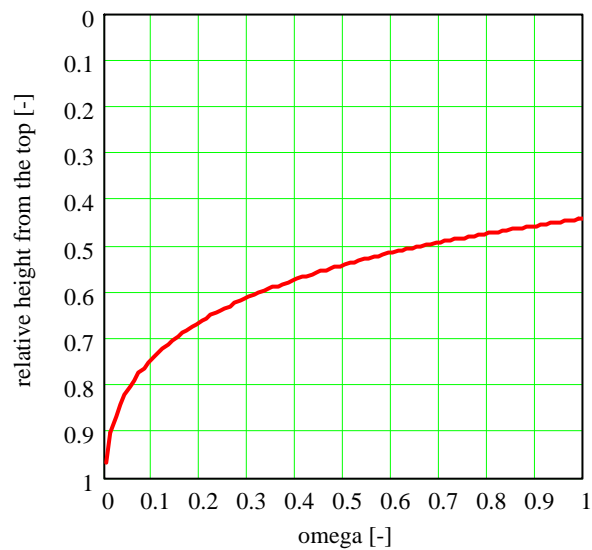


Figure I.2-4: Optimum location as a function of ω for base moment reduction

II Wind loading

II.1 Validity of Eurocode mean wind velocity profile

The variation of the mean wind velocity with height over horizontal terrain of homogenous roughness can be described by a logarithmic law. The logarithmic profile is valid for moderate and strong winds (mean hourly velocity > 10 m/s) when thermal effects are neglected [JCSS].

$$v_m(z) = \frac{1}{k} \cdot v_*(z_0) \cdot \left[\ln\left(\frac{z}{z_0}\right) + 5,75 \frac{z}{\delta} - 1,87 \left(\frac{z}{\delta}\right)^2 - 1,33 \left(\frac{z}{\delta}\right)^3 + 0,25 \left(\frac{z}{\delta}\right)^4 \right] \quad (\text{II.1.1})$$

| | | |
|-------|------------|--|
| where | $v_m(z)$ | mean wind velocity at height z above ground [m/s] |
| | k | von Karman constant, approximately equal to 0,4 [-] |
| | $v_*(z_0)$ | = $\frac{v_m(z) \cdot k}{\ln\left(\frac{z}{z_0}\right)}$ friction velocity [m/s] |
| | z_0 | roughness length [m] |
| | δ | = $\frac{v_*(z_0)}{6 \cdot f_c}$ boundary layer depth [m] |
| | f_c | = $2 \cdot \Omega \cdot \sin(\phi)$ Coriolis parameter [1/s] |
| | Ω | $0.726 \cdot 10^{-4}$ angular rotation velocity [rad/s] |
| | ϕ | latitude of location [deg] |

Let us calculate the mean velocity profiles for the five terrain categories defined by the Eurocode in table 6.1.2. The 10 minute-averaged mean wind velocity with an annual probability of occurrence of 0,02, measured at 10 m above ground with roughness characteristics corresponding to terrain category II ($z_0 = 0,05$ m), for Madrid is 26,0 m/s. With this value we can calculate the friction velocity and the corresponding boundary layer depth according to a latitude of approximately 40° for the mean wind profile over a terrain category II. It is shown in [4] that the friction velocities in two different terrain categories are related according to

$$\frac{v_{*,1}}{v_{*,2}} = \left(\frac{z_{0,1}}{z_{0,2}} \right)^{0,0706} \quad (\text{II.1.2})$$

With (II.1.2) one can calculate the mean wind velocity profiles for all terrain categories. The mean wind profile characteristics are presented in table 1 in terms of the roughness length, the friction velocity and the boundary layer depth.

| terrain category | z_0 [m] | $v_s(z_0)$ [m/s] | δ [m] |
|------------------|-----------|------------------|--------------|
| 0 | 0,003 | 1,61 | 2.879 |
| I | 0,010 | 1,75 | 3.132 |
| II | 0,050 | 1,96 | 3.505 |
| III | 0,300 | 2,23 | 3.974 |
| IV | 1,000 | 2,42 | 4.323 |

Table II.1-1: Wind profile characteristics for $v_{m,II}(10\text{ m}) = 26,0\text{ m/s}$

The mean wind velocity profiles, for all five terrain categories, according to formula (II.1.1) and $v_{m,II}(10\text{ m}) = 26,0\text{ m/s}$ are shown in figure II-1.

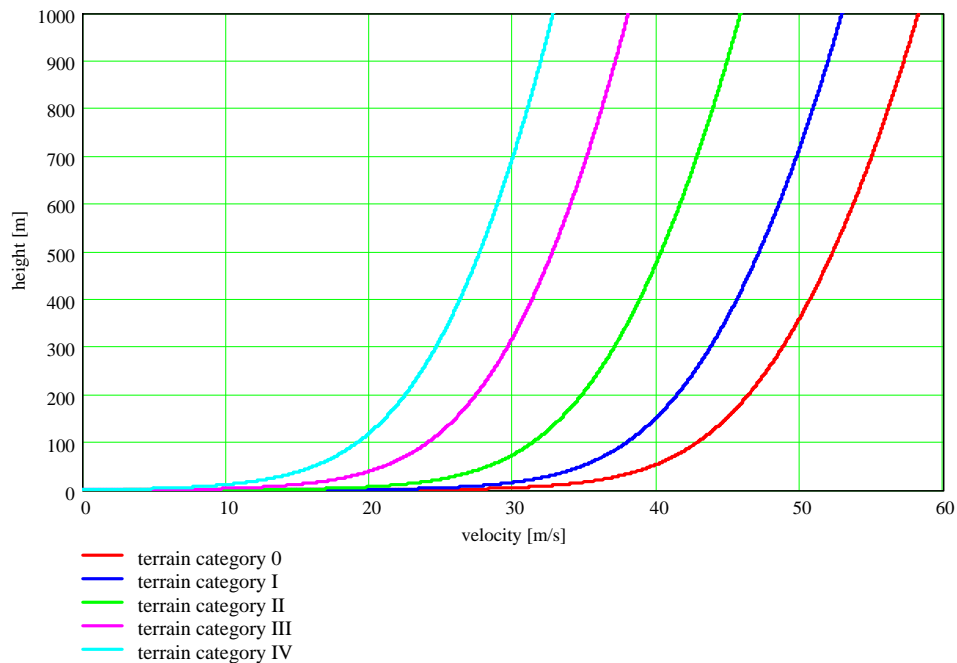


Figure II.1-1: Wind profile characteristics per terrain category, according to (II.1.1)

The Eurocode expression for the mean wind velocity neglects the terms in brackets of (II.1.1) that depend on the boundary layer depth δ , and hence adopts:

$$v_m(z) = \frac{1}{\kappa} \cdot v_s(z_0) \cdot \ln\left(\frac{z}{z_0}\right) \quad (\text{II.1.3})$$

Plots of the Eurocode mean velocity profiles, for all five terrain categories, are obtained and shown in figure II.1-2.

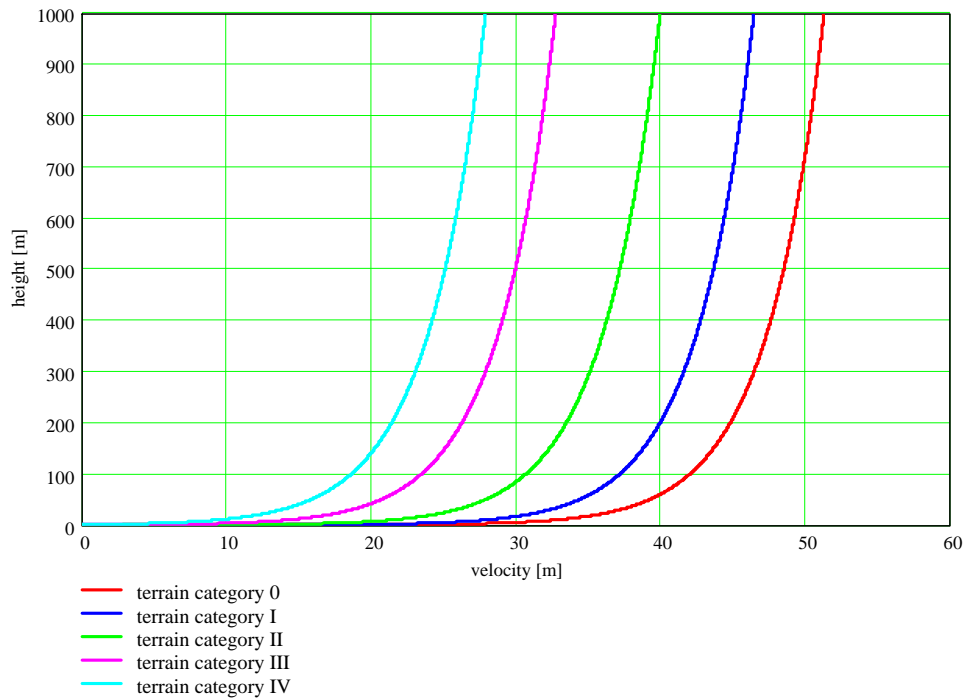


Figure II.1-2: Wind profile characteristics per terrain category, according to (II.1.3)

The simplified mean wind profiles, adopted by the Eurocode, underestimate the mean wind velocities. It is interesting, however, to see exactly what the error is for each terrain category for different heights z .

Figure II.1-3 present the ratio of the Eurocode wind profiles and those following from (II.1.1).

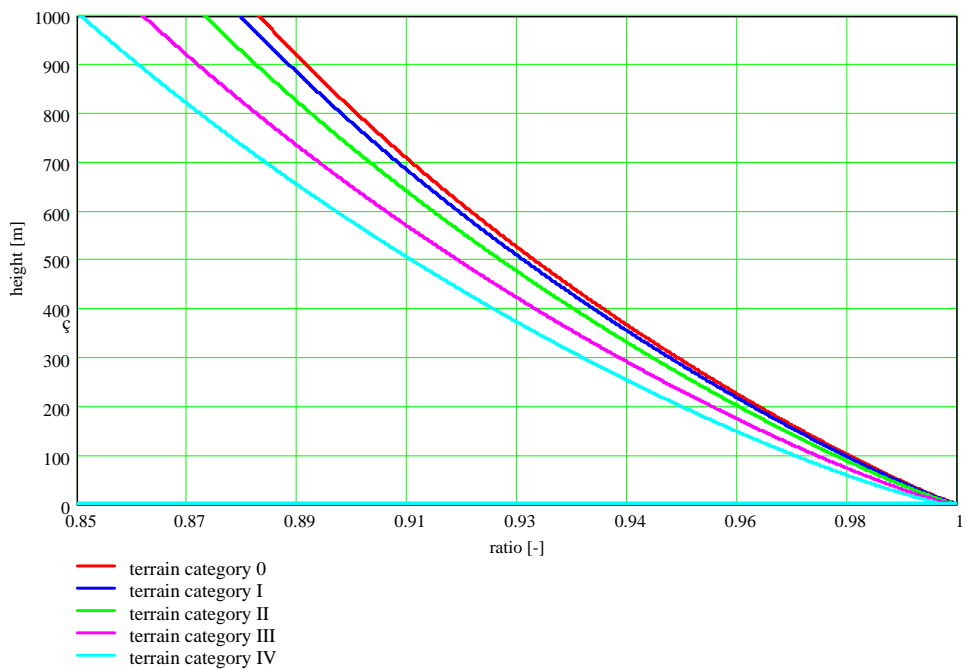


Figure II.1-3: Error of EC mean wind profiles with terrain roughness and height

The Eurocode wind load prescriptions are valid for buildings with a height up to 200 m. Table II.1-2 shows the error of the Eurocode formulation (II.1.3) with respect to formula (II.1.1) in terms of the mean wind velocity and pressure, for all terrain categories at the maximum height of 200 m. The errors in base shear and overturning moment are calculated for prismatic buildings. Above mentioned values have been calculated as well for a height of 250 m in a terrain category III, corresponding to the case under analysis in this thesis.

| terrain category | height [m] | error [-] | | | |
|------------------|------------|--------------|--------------|------------|-------------|
| | | velocity (h) | pressure (h) | base shear | base moment |
| 0 | 200 | 3,4% | 6,7% | 3,9% | 5,3% |
| I | 200 | 3,5% | 6,9% | 4,1% | 5,5% |
| II | 200 | 3,7% | 7,3% | 4,5% | 5,9% |
| III | 200 | 4,2% | 8,2% | 5,3% | 6,7% |
| III | 250 | 5,0% | 9,8% | 6,3% | 7,9% |
| IV | 200 | 4,7% | 9,2% | 6,2% | 7,6% |

Table II.1-2: Error for wind velocity, pressure, base shear and bending moment

Note that maximum wind velocity and pressure errors at the maximum height are 4,7% and 9,2% respectively. In terms of base shear and bending moment the errors range in between 3,9% - 6,2% and 5,3% - 7,6% respectively for all terrain categories. It can be seen that the errors for a height of 250 m in a terrain category III are only slightly greater than the errors implicitly accepted by the Eurocode, i.e. for the maximum height in terrain category IV.

II.2 Mean wind velocity profile

In this appendix it is shown that the Eurocode formulation of the mean wind velocity variation with height is based on the simplified logarithmic expression.

II.2.1 Simplified logarithmic formula

The simplified logarithmic expression for the variation of the mean velocity over horizontal terrain is

$$v_m(z) = \frac{1}{k} \cdot v_*(z_0) \cdot \ln\left(\frac{z}{z_0}\right) \quad (\text{II.2.1})$$

where $v_m(z)$ mean wind velocity at height z [m/s]
 k von Karman constant approximately equal to 0,4 [-]

$$v_*(z_0) = \sqrt{\frac{\tau_0}{\rho}} \text{ friction velocity at height } z_0 \text{ [m/s]}$$

τ_0 shear stress at the surface
 ρ density of air 1,25 [kg/m³]
 z_0 roughness length [m]

The shear stress is defined by

$$\tau_0 = \kappa \cdot \rho \cdot v(z_{ref})^2 \quad (II.2.2)$$

where $\kappa = \left[\frac{k}{\ln(z_{ref} / z_{0,ref})} \right]^2$ surface drag coefficient [-]
 z_{ref} reference height, usually 10 [m]
 $v(z_{ref})$ wind velocity at reference height [m/s]

Substitution of the friction velocity in formula (II.2.1) yields

$$v_m(z) = \frac{1}{k} \cdot \frac{k^2 \cdot v(z_{ref})^2}{\ln\left(\frac{z_{ref}}{z_{0,ref}}\right)^2} \cdot \ln\left(\frac{z}{z_0}\right) \quad (II.2.3)$$

and after rearrangement

$$v_m(z) = \frac{\ln\left(\frac{z}{z_0}\right)}{\ln\left(\frac{z_{ref}}{z_{0,ref}}\right)} \cdot v(z_{ref}) \quad (II.2.4)$$

The friction velocities in two different terrain categories are related by [4]

$$\frac{v_{*,1}}{v_{*,2}} = \left(\frac{z_{0,1}}{z_{0,2}} \right)^{0,0706} \quad (II.2.5)$$

The mean wind velocity is proportional to the friction velocity, because of which, using formula (II.2.5), one is now able to write the expression for the variation of the mean wind velocity with height and terrain roughness (assuming a reference roughness length).

$$v_m(z) = \left(\frac{z_0}{z_{0,ref}} \right)^{0,0706} \cdot \frac{\ln\left(\frac{z}{z_0}\right)}{\ln\left(\frac{z_{ref}}{z_{0,ref}}\right)} \cdot v(z_{ref}) \quad (II.2.6)$$

II.2.2 Eurocode expression

The Eurocode formulation for the variation of the mean wind speed with height and terrain category is

$$v_m(z) = c_r(z) \cdot c_o(z) \cdot v_b \quad (II.2.7)$$

where $v_m(z)$ mean wind velocity at height z [m/s]
 $c_r(z)$ roughness factor at height z [-]
 c_o orography factor [-]
 v_b basic wind velocity [m/s]

The roughness factor at height z is given by

$$c_r(z) = k_r \cdot \ln\left(\frac{z}{z_0}\right) \quad (II.2.8)$$

where $k_r = 0.19 \cdot \left(\frac{z_0}{z_{0,II}}\right)^{0.07}$ terrain factor

z_0 roughness length of terrain category
 $z_{0,II}$ roughness length of terrain category II

The reader is reminded that the basic wind velocity for strength and deflection calculations is the 10 minute-averaged wind velocity with an annual possibility of occurrence of 0,02, measured at 10 m above ground in a terrain category II (open terrain).

For the mean velocity over flat horizontal terrain, hence the orography factor equals 1, expression (II.2.1) can be rewritten to

$$v_m(z) = 0.19 \cdot \left(\frac{z_0}{z_{0,II}}\right)^{0.07} \cdot \ln\left(\frac{z}{z_0}\right) \cdot v_{m,II}(10m) \quad (II.2.9)$$

II.2.3 Comparison

When we equate both expressions for the variation of the mean wind velocity (II.2.6) and (II.2.9), and consider that the reference height is 10 m, we obtain

$$\frac{1}{\ln\left(\frac{10m}{z_{0,ref}}\right)} \cdot \left(\frac{z_0}{z_{0,ref}}\right)^{0.0706} \cdot \ln\left(\frac{z}{z_0}\right) \cdot v(10m) = 0.19 \cdot \left(\frac{z_0}{z_{0,II}}\right)^{0.07} \cdot \ln\left(\frac{z}{z_0}\right) \cdot v_{m,II}(10m) \quad (II.2.10)$$

It is clearly seen that the equation holds for $z_{0,ref} = 0,05$ m and $v = v_{m,II}$, and hence for terrain category II. The Eurocode has taken equation (II.2.1) and fitted it for the 10-minute averaged mean wind velocity with an annual possibility of occurrence of 0,02, measured at 10 m above ground in a terrain category II.

The relation between two mean wind velocities with different terrain roughness and height z is

$$\frac{v_{m,1}(z)}{v_{m,2}(z)} = \frac{\frac{1}{k} \cdot v_{*,1}(z_{0,1}) \cdot \ln\left(\frac{z}{z_{0,1}}\right)}{\frac{1}{k} \cdot v_{*,2}(z_{0,2}) \cdot \ln\left(\frac{z}{z_{0,2}}\right)} = \left(\frac{z_{0,1}}{z_{0,2}}\right)^{0,07} \cdot \frac{\ln\left(\frac{z}{z_{0,1}}\right)}{\ln\left(\frac{z}{z_{0,2}}\right)} \quad (II.3.10)$$

II.3 Relative turbulence intensity

In this appendix the relative turbulence intensity according to the Eurocode (6.1.11) is compared to that proposed by [2].

The simplified expression adopted by the Eurocode is

$$I_v(z) = \frac{1}{c_o(z) \cdot \ln\left(\frac{z}{z_0}\right)} \quad (II.3.1)$$

where $I_v(z)$ longitudinal relative turbulence intensity [-]
 $c_o(z)$ orography factor being 1,0 for flat terrain [-]
 z height [m]
 z_0 roughness length [m]

Figure II.3-1 shows the variation of the relative turbulence intensity with height for the different terrain categories and, thus, terrain roughness.

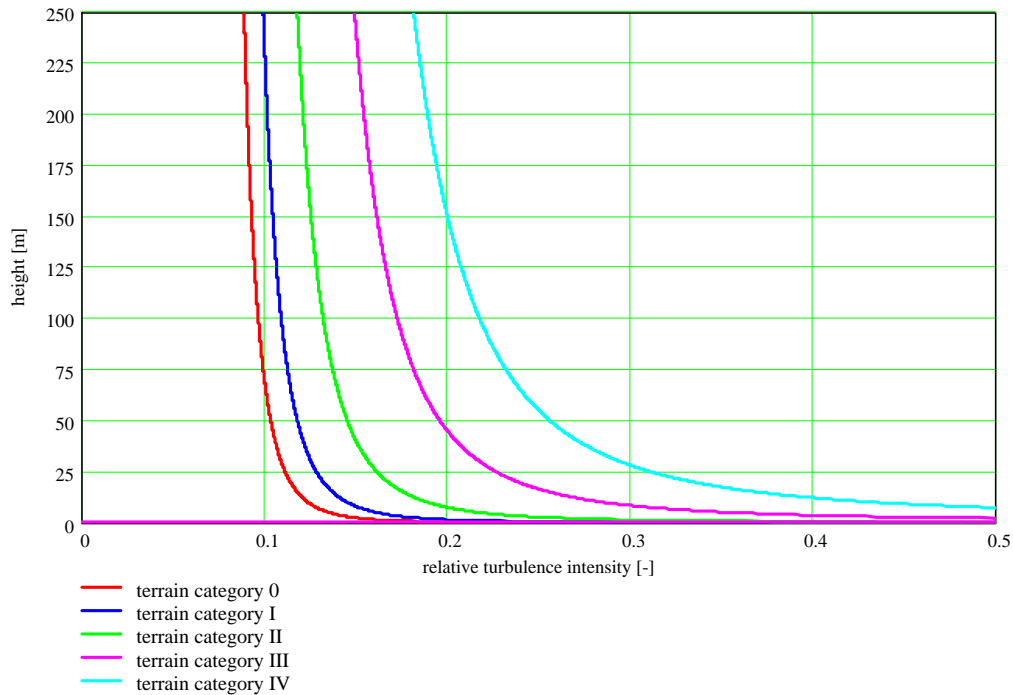


Figure II.3-1: Relative turbulence intensity according to (II.3.1)

Reference [2] recommends calculating the relative turbulence intensity according to

$$I_v(z) = \frac{\beta \cdot \left(1 - \frac{z}{\delta}\right) \cdot v_*}{v_m(z)} \quad (\text{II.3.2})$$

where β values listed in the upper row in table II.3-1 [-]
 δ boundary layer depth [m]
 v_* friction velocity [m/s]
 $v_m(z)$ mean wind velocity according to (6.1.1) [m/s]

| | | | | | | | | |
|-------------|-------|------|------|------|------|------|------|------|
| z_0 [-] | 0,005 | 0,01 | 0,05 | 0,07 | 0,30 | 1,00 | 2,00 | 2,50 |
| β [2] | - | 3,10 | 2,70 | - | 2,30 | 2,10 | 2,00 | - |
| β [4] | 2,55 | - | - | 2,45 | 2,29 | 2,20 | - | 2,00 |

Table II.3-1: Proposed values for β

Reference [4] states that the turbulence intensity does not vary with height and gives the next expression

$$\sigma_v(z)^2 = \beta \cdot v_*^2 \quad (\text{II.3.3})$$

because of which the square root value of β , as presented in [2], is shown in table II.3-1 for reasons of comparison. Note the dispersion of the recommended values in between both references.

Figure II.3-2 presents the relative turbulence intensity variation with height for the terrain categories defined by the Eurocode.

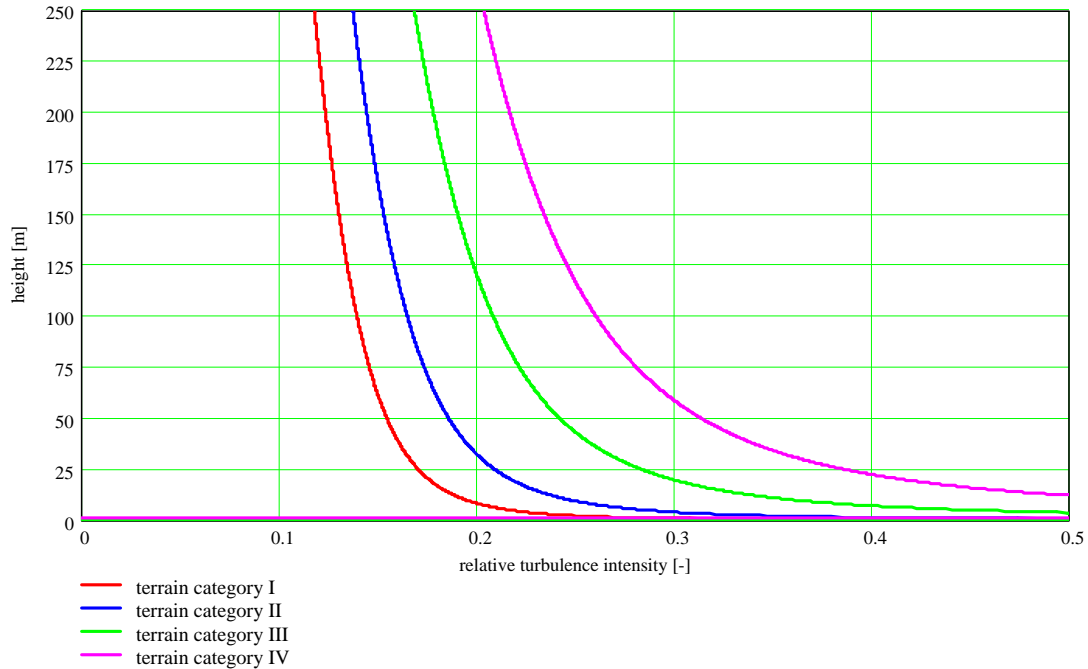


Figure II.3-2: Relative turbulence intensity according to (II.3.2)

The values have not been calculated for terrain category 0 since [2] does not provide values for β for the corresponding roughness length.

Figure II.3-3 shows the ratio of the values calculated with (II.3.1) and formula (II.3.2). Note that the Eurocode considerably underestimates the longitudinal relative turbulence intensity in comparison to [2]. Table II.3-2 lists the relative minimum and maximum errors for the different terrain categories.

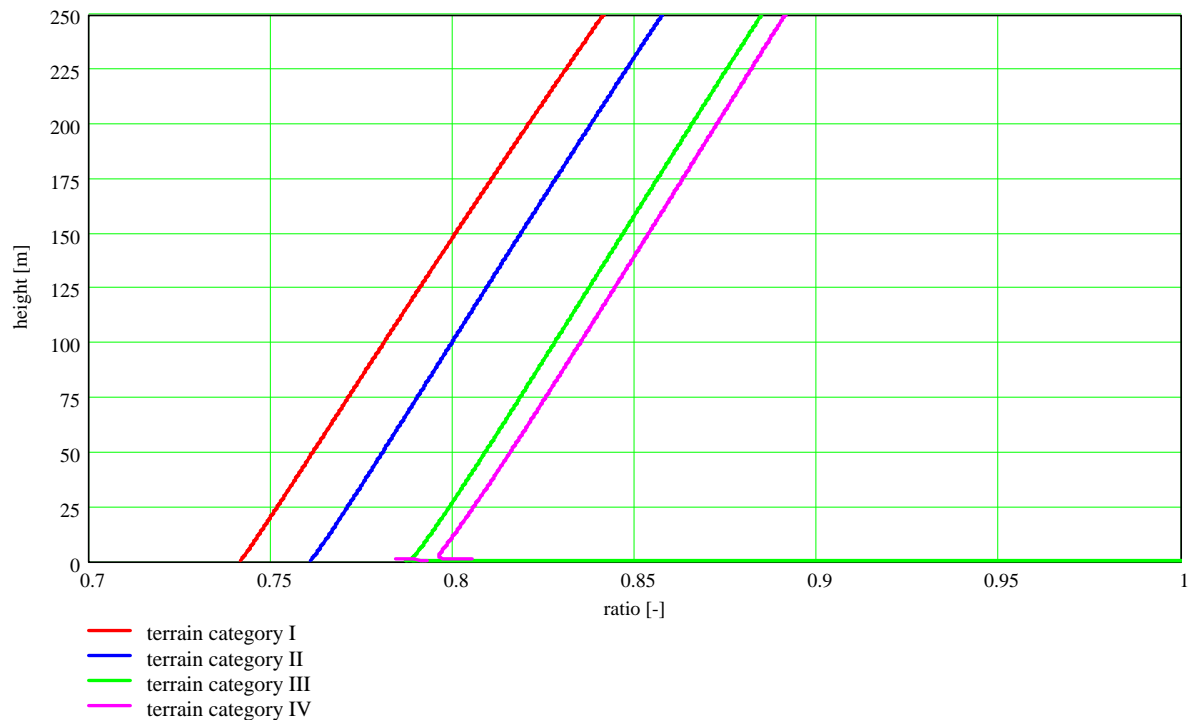


Figure II.3-3: Ratio of relative turbulence intensity according to (II.3.1) and (II.3.2)

The maximum underestimation is for the smallest roughness lengths and greatest heights. The errors found in table II.3.2 are surprisingly high and go up to 25,8 % for a wind over terrain category I at 200 m.

| height [m] | z_{min} | 200 m |
|----------------------|-----------|-------|
| terrain category I | 17,9% | 25,8% |
| terrain category II | 16,2% | 23,8% |
| terrain category III | 13,5% | 21,0% |
| terrain category IV | 12,8% | 20,1% |

Table II.3-2: Error in relative turbulence intensity

It is noted that the values of β proposed by [4] would lead to a reasonable fit for terrain category I and II and would lead to overestimation of the Eurocode values for terrain category III and IV, of up to 13,6 % for the latter.

II.4 Reynolds number

All fluids have a certain viscosity and although the viscosity of air under normal conditions is relatively small it can, in some cases, play an important role.

An air flows along a smooth surface adheres to it, which decelerates the air flow. The layer in which the air flow is decelerated is called the boundary layer. The adherence of the air to the surface is due to its viscosity. On the other hand, since it has a mass, air is subjected to inertial forces. The relation of viscosity to inertial effects determines the air flow characteristics around any given body.

The non-dimensional Reynolds number Re is the ratio of inertial to viscous forces. Let a certain air volume have a typical surface dimension of D . The pressure caused by the air flow with velocity v is, according to Bernoulli's theorem, is of the order of

$$\frac{1}{2} \cdot \rho \cdot v^2 \quad (11.4.1)$$

which results in inertial forces of the order of

$$\rho v^2 D^2 \quad (11.4.2)$$

Imagine two plates at a small vertical distance D separated by a homogeneous substance. Consider an applied horizontal force on the upper plate, when the substance undergoes a shear flow, instead of elastic shear, it is called a Newtonian or viscous fluid. The applied force is proportional to the velocity and area of the plate and inversely proportional to the distance D . Viscous shear stresses are, then, defined by

$$\tau = \frac{F}{A} = \mu \cdot \frac{\delta v}{\delta D} \quad (11.4.3)$$

where μ is a proportionality factor called viscosity. The resulting viscous forces are of the order of

$$\frac{\mu v}{D} D^2 \quad (11.4.4)$$

After rearrangement the expression for the Reynolds number becomes

$$Re = \frac{\rho v^2 D^2}{\mu v D^2 / D} = \frac{\rho v D}{\mu} = \frac{v D}{\nu} \quad (11.4.5)$$

, where $\nu = \frac{\mu}{\rho}$ is called the kinematic viscosity. In normal temperatures ν is approximately equal to $15 \times 10^{-6} \text{ m}^2/\text{s}$.

For small Reynolds numbers the viscous forces predominate and for large Reynolds numbers the inertial forces are the stronger ones.

A flow around a body develops a wide variety of Reynolds number, depending on the location in which the air flow characteristics are studied. When the global air flow around a body is considered the dimension D should be associated with some overall global dimension of that body.

II.5 Structural vibrations

II.5.1 Vortex shedding and the lock-in phenomenon

In figure II.5.1 several 2-dimensional flow diagrams are presented, where the upstream flow is considered to be laminar, constant in time and direction. For $Re \approx 1$ the streamlines are completely attached to the cylinder downstream. It can be clearly seen that no flow separation occurs. In diagram b, for $30 < Re < 5 \times 10^3$, the flow separates of the cylinder surface downstream and two symmetric vortices are created; large eddies in the wake of the cylinder. The regular shedding of vortices creates an unsteady but laminar flow. For increased Reynolds numbers the symmetric vortices are broken and replaced by cyclically alternating vortices, formed alternately near the top and bottom of the cylinder. This vortex trail downstream is named after Von Karman, which first reported the existence of such phenomenon. A more and more turbulent wake, with vortices shed from the separation points, is created downstream of the body after flow separation for $5 \times 10^3 < Re < 2 \times 10^5$. In this stage a high drag is generated on the structure. Before reaching the critical Reynolds number ($Re = 2 \times 10^5$) flow separation occurs at the two sides of the cylinder generating a wide wake with a rather regular vortex shedding pattern.

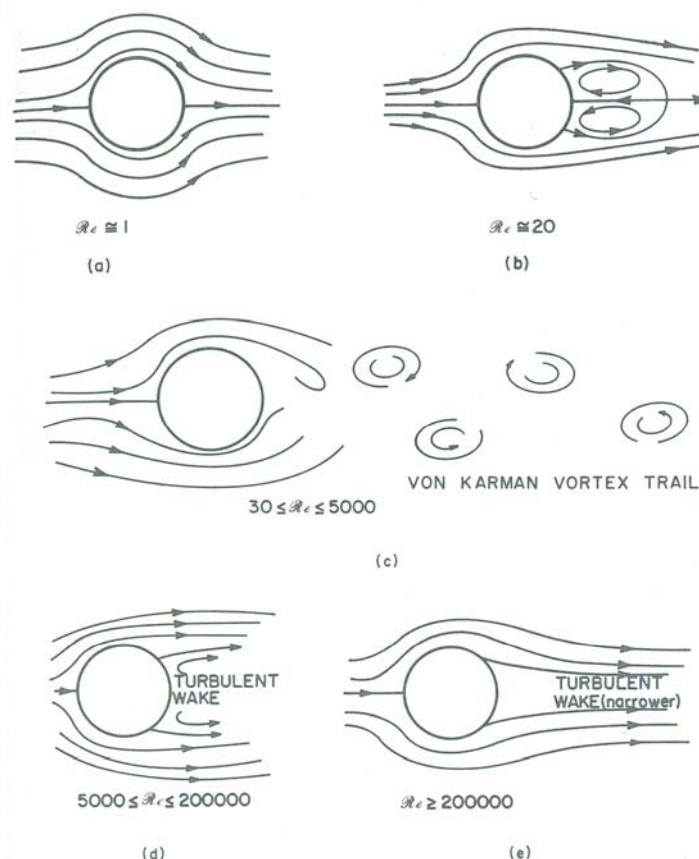


Figure II.5-1: Typical flow diagrams around a prismatic cylinder in laminar flow [4]

For higher Re the flow separation points move downstream causing the wake to narrow down which results in a sudden drop of the drag. For Reynolds numbers 2×10^5

$< Re < 4 \times 10^6$ the vortex shedding in the downstream wake is rather random. The vortex shedding restores some regularity when $Re > 4 \times 10^6$.

Table II.5-1 lists the three ranges of Reynolds numbers and their different characteristics according to [3].

| range | Re | shedding characteristics |
|---------------|---------------------------------|------------------------------|
| subcritical | $30 - 2 \times 10^5$ | regular (constant frequency) |
| supercritical | $2 \times 10^5 - 4 \times 10^6$ | random (variable frequency) |
| hypercritical | $> 4 \times 10^6$ | regular (constant frequency) |

Table II.5-1: Distinct ranges of Reynolds numbers

For prismatic bodies other than cylinders the same distinct vortex-shedding phenomena can be indicated.

The frequency of regular vortex shedding can be calculated by the dimensionless Strouhal number

$$S = \frac{n \cdot D}{v} \tag{II.5.1}$$

- where
- S Strouhal number [-]
 - n full cycle frequency of vortex shedding [Hz]
 - D characteristic body dimension normal to the flow [m]
 - v relative velocity [m/s]

S takes on different values that depend upon the cross-section of the prism considered, and in the case of cylinders also depends on the Reynolds number. Appendix E of Eurocode 1 presents a table with recommended values of S for different cross-sections (see figures II.5-2 and II.5-3).

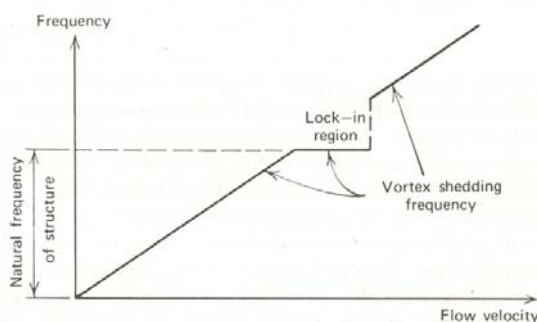

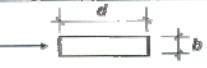






Figure II.5-2: Lock-in phenomenon [4]

Resonance occurs when the wind velocity is such that the vortex shedding frequency becomes close to the natural frequency of the structure. If resonance occurs a further increase of the wind velocity will not change the shedding frequency. At this point it is the natural frequency of the structure that controls the shedding frequency. This phenomenon is called lock-in and is illustrated in figure II.5-2.

Note that a wind velocity above or below the lock-in region will not cause resonance.

The critical wind velocity at which the frequency of vortex shedding equals a natural frequency of the structure is inversely proportional to the Strouhal number. Cross-sections with a high value of S are more susceptible to vortex shedding induced vibration.

| Cross-section | St |
|--|----------------------|
|  for all Re numbers | 0,98 |
|  $0,8 \leq d/b \leq 10$ | See Figure E.1 |
|  linear interpolation $d/b = 1$ $d/b = 1,5$ $d/b = 2$ | 0,11 0,10 0,14 |
|  linear interpolation $d/b = 1$ $d/b = 2$ | 0,13 0,08 |
|  linear interpolation $d/b = 1$ $d/b = 2$ | 0,16 0,12 |
|  linear interpolation $d/b = 1,3$ $d/b = 2,0$ | 0,17 0,07 |

NOTE: Interpolations for diagonal sections are based on d/b and not $d/cos(\theta)$.

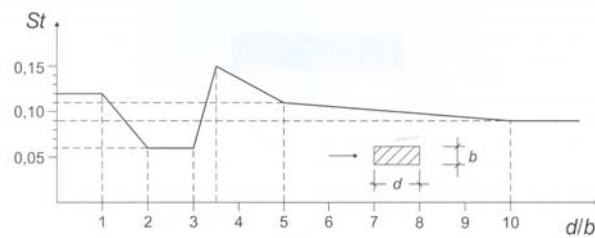


Figure II.5-3: Strouhal numbers for different cross-sections [1]

The Eurocode states that no vortex shedding effects have to be calculated if the critical wind velocity is more than 25 % greater than the 10 minute mean wind velocity at the height of the structure under consideration. With this limit it is considered that the structure remains, with an acceptable level of probability, on the left-hand side of the lock-in region shown in figure II.5-2.

II.5.2 Cross-wind galloping

Across-wind galloping is a low-frequency, large-amplitude vibration in the across-wind direction. For steady wind conditions ice-coated power lines or cable-suspended bridge decks can show this type of aeroelastic instability. Slender structures with a rectangular or D-shaped cross section are specifically susceptible to galloping.

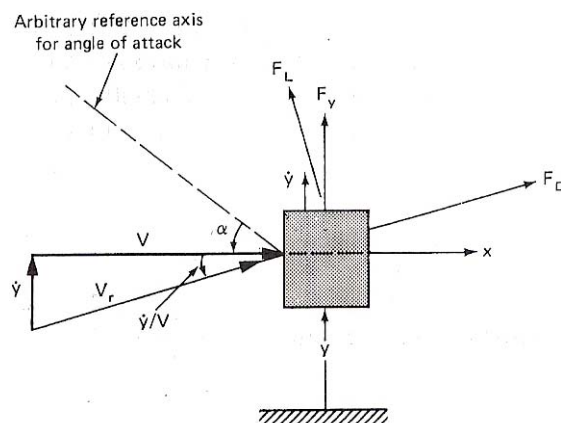


Figure II.5-4: Across-wind galloping [3]

Figure II.5.4 illustrates the galloping problem. A steady wind flow exerts the structure with a certain magnitude and angle of attack. Due to a wind disturbance, for example a cross-wind turbulence component, the structure moves in the direction perpendicular to the wind. This movement changes both the magnitude and angle of attack of the relative velocity. This change in angle of attack can either generate an increase or decrease in the lift on the structure.

If this increase in lift generates a movement in the initial direction galloping instability can occur. When the generated movement is counteracting the initial one, logically, the situation is stable. A necessary condition for across-wind galloping to occur is the Glauert-Den Hartog criterion, derived in [4] and defined

$$\frac{dC_L}{d\alpha} + C_D < 0 \quad (II.5.2)$$

where C_L lift coefficient
 C_D drag coefficient

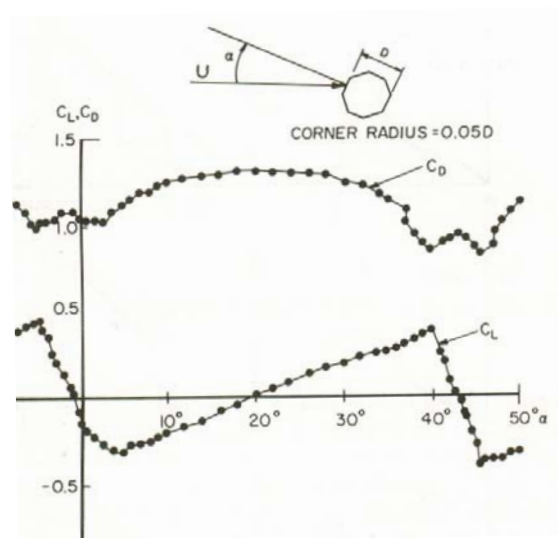


Figure II.5-5: Lift and drag coefficient as a function of angle of attack [3]

The force coefficient for any body as a function of the angle of attack can be determined by wind tunnel studies, see figure II.5-5. It is clear from expression (II.5.2) that across-wind galloping can only occur where the lift coefficient diagram has a negative slope. Furthermore cylinders, due to their symmetry and thus $\frac{dC_L}{d\alpha} = 0$, cannot gallop.

II.5.3 Wake galloping

When two cylinders are located within a few diameters one to the other and one is located within the wake of the other, wake galloping can occur. The downstream cylinder wake will move in an elliptic path as shown in figure II.5-6. Depending on whether the downstream cylinder is located in the lower or upper half of the wake the

elliptic movement will be clockwise or counter clockwise. This instability is often noted with grouped power lines in between mechanical spacers.

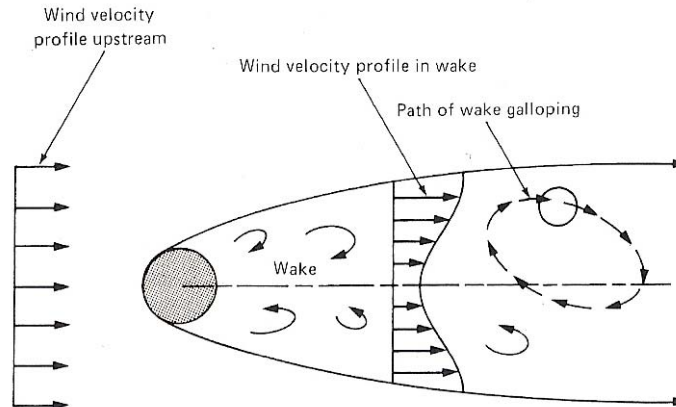


Figure II.5-6: Wake galloping [3]

Just like cross-wind galloping, wake galloping is associated to mean aerodynamic phenomena instead of instantaneous.

II.5.4 Torsional divergence

Torsional divergence is characterised practically by the same behaviour as galloping is; only that instead of a translational vibration a rotational vibration is generated, see figure 6.3.3. Plate-like structures are susceptible to this kind of instability, such as for example the deck of a cable suspended bridge or aircraft wings.

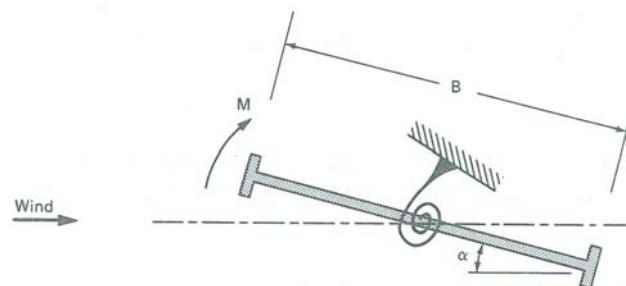


Figure II.5-7: Torsional divergence [3]

For a small angle of attack a drag, lift and bending moment is generated. The latter leads to an increase of α which, in turn, leads to a greater moment etc. Finally a magnitude of the twisting moment is reached which in combination to the torsional stiffness leads to an unstable situation. According to figure II.5-7 the equilibrium condition of the aerodynamic moment and rotation leads to

$$\frac{1}{2} \cdot \rho \cdot v^2 \cdot B^2 \cdot C_M(\alpha) = k_T \cdot \alpha \quad (II.5.3)$$

where v wind velocity [m/s]
 B width [m]
 C_M moment coefficient depending on α [-]
 k_T rotational spring constant [Nm/m]

The following criterion for the initiation of torsional divergence can now be drawn up

$$\frac{dC_M}{d\alpha} > \frac{2 \cdot k_T}{\rho \cdot v^2 \cdot B^2} \quad (11.5-4)$$

In this case the left-hand side term is, as in the case of across-wind galloping, determined by wind tunnel test.

11.5.5 Flutter

The classical case of flutter is an instability associated with the simultaneous existence of across-wind and rotating vibrations. Classical flutter occurs when the structure's natural frequencies of torsional and translational modes have approximately the same magnitude and thus create a coupled vibration response.

Stall flutter is characterised by a sudden drop of lift and increase in drag on an airfoil at large angles of attack. Traffic signs can undergo heavy vibration about their axis due to stall, for wind with an angle of attack close to where flow separation is initiated.

Single-degree-of-freedom flutter can be either torsional or translational. In suspended bridges the flow separation can excite a torsional movement.

Panel flutter is a sustained oscillation of panels caused by the wind passing along the panel. Flag flutter is a phenomenon related to such flutter.

11.5.6 Buffeting

The foregoing types of vibration, except wake galloping, are all self-excited by the structure. Even within a laminar air flow these types of vibrations can occur. Wake buffeting vibration occurs when the wind turbulence, or abrupt disturbances caused by an object upstream of the object considered, causes the object to vibrate. It is noted that buffeting vibration is never generated by the own vibration of the structure itself.

Two types of buffeting occur: buffeting induced by wind turbulence and buffeting vibration caused by upstream buildings or objects. The latter is called wake buffeting or interference and is especially important for tall buildings that are placed nearby. See figure for an illustration of wake buffeting. The four tall buildings under consideration will be subjected to wake buffeting to the other tall buildings in their proximity.

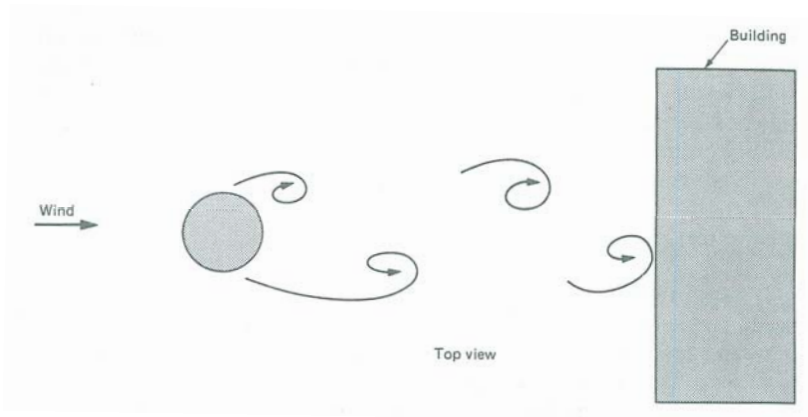


Figure II.5-8: Wake buffeting [3]

III Structural analysis

III.1 General considerations

III.1.1 Peak wind pressure profile

1. Basic wind velocity

$$v_{b,0} := 26.0 \frac{\text{m}}{\text{s}}$$

characteristic 10 minute-averaged wind velocity at 10 m above ground level with an annual probability of occurrence of 0,02

$$v_b := c_{\text{dir}} \cdot c_{\text{season}} \cdot v_{b,0}$$

basic wind velocity with $c_{\text{dir}} = 1.0$ directional factor $v_b = 26.0 \frac{\text{m}}{\text{s}}$
 $c_{\text{season}} = 1.0$ seasonal factor

2. Terrain Category: III

$$z_0 := 0.30 \text{ m}$$

roughness length

$$z_{\text{min}} := 5.0 \text{ m}$$

minimum height

$$z_{0,II} := 0.05 \text{ m}$$

roughness length according to terrain category II

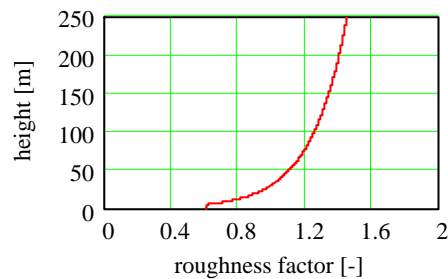
$$k_r := 0.19 \left(\frac{z_0}{z_{0,II}} \right)^{0.07}$$

terrain factor depending on roughness length

$$k_r = 0.22$$

$$c_r(z) := \begin{cases} k_r \cdot \ln\left(\frac{z}{z_0}\right) & \text{if } z_{\text{min}} \leq z \\ k_r \cdot \ln\left(\frac{z_{\text{min}}}{z_0}\right) & \text{if } z_{\text{min}} > z \end{cases}$$

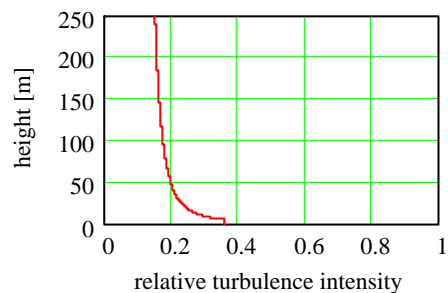
roughness factor at height z



$$I_v(z) := \begin{cases} \frac{k_1}{c_o \cdot \ln\left(\frac{z}{z_0}\right)} & \text{if } z_{\text{min}} \leq z \\ \frac{k_1}{c_o \cdot \ln\left(\frac{z_{\text{min}}}{z_0}\right)} & \text{if } z_{\text{min}} > z \end{cases}$$

relative turbulence intensity at height z with $c_o = 1.0$ orography factor

$k_1 = 1.0$ turbulence factor



3. Wind velocity and pressure profile

$$v_m(z) := c_r(z) \cdot c_o \cdot v_b$$

$$v_p(z) := \sqrt{1 + 7 \cdot I_V(z)} \cdot v_m(z)$$

$$q_m(z) := \frac{1}{2} \cdot \rho \cdot v_m(z)^2$$

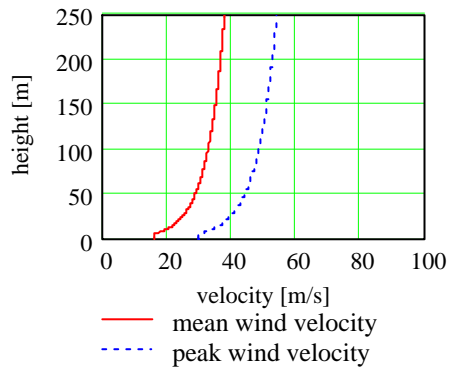
$$q_p(z) := (1 + 7 \cdot I_V(z)) \cdot \frac{1}{2} \cdot \rho \cdot v_m(z)^2$$

the exposure factor $c_e(z)$ is defined by $q_p(z)/q_b$ where q_b is the basic dynamic pressure

$$c_e(z) := (1 + 7 \cdot I_V(z)) \cdot \left(\frac{v_m(z)}{v_b} \right)^2$$

mean wind velocity at height z

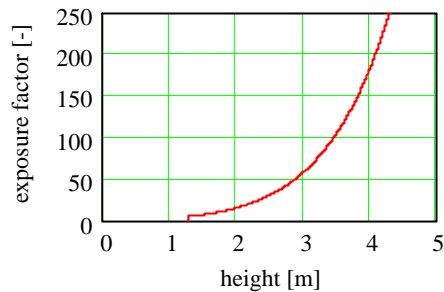
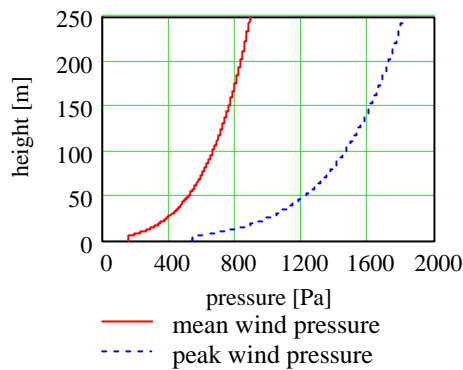
peak wind velocity at height z



mean wind pressure at height z

peak wind pressure at height z

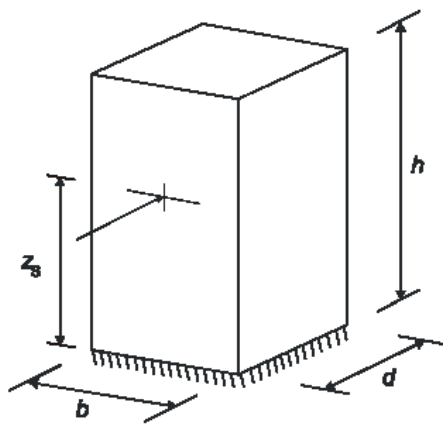
with $\rho = 1.25 \frac{\text{kg}}{\text{m}^3}$ air density



III.1.2 Determination of the structural factor

1. Introduction

In this appendix the process to calculate the structural factor, as defined in Eurocode 1, is presented. Graphs are plotted of all relevant variables using, if necessary, example building and wind characteristics.



The structural factor is an aerodynamic characteristic of the structure, and defined as $c_s \cdot c_d$ where c_s is the size factor and c_d the dynamic factor. The structural factor is calculated at the reference height $z_{ref} = z_s$ of the structure.

The reference height for building structures is prescribed by the Eurocode as $z_{ref} = 0,6 \cdot h$.

$$c_s := \frac{1 + 7 \cdot I_v(z_s) \cdot \sqrt{B^2}}{1 + 7 \cdot I_v(z_s)}$$

The size factor c_s takes into account the lack of full correlation between the pressure peaks over the building surface.

$$c_d := \frac{1 + 2 \cdot k_p \cdot I_v(z_s) \cdot \sqrt{B^2 + R^2}}{1 + 7 \cdot I_v(z_s) \cdot \sqrt{B^2}}$$

The dynamic factor c_d takes into account the resonance of the building structure with the wind turbulence.

| | | |
|-------|------------|---|
| where | $I_v(z_s)$ | relative turbulence intensity at reference height |
| | B | background response factor |
| | R | resonance response factor |
| | k_p | peak factor of the structural response |

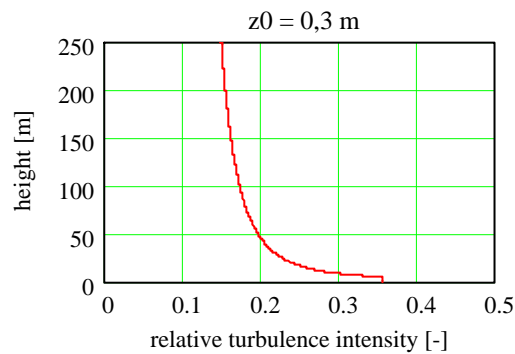
2. Relative turbulence intensity

$$I_V(z) := \begin{cases} \frac{k_1}{c_o \cdot \ln\left(\frac{z}{z_0}\right)} & \text{if } z_{\min} \leq z \\ \frac{k_1}{c_o \cdot \ln\left(\frac{z_{\min}}{z_0}\right)} & \text{if } z_{\min} > z \end{cases}$$

relative turbulence intensity being the ratio of the standard deviation of the wind turbulence and the mean wind velocity at height z

with $c_o = 1.0$ orography factor

$k_1 = 1.0$ turbulence factor



3. Size factor

$$c_s := \frac{1 + 7 \cdot I_V(z_s) \cdot \sqrt{B^2}}{1 + 7 \cdot I_V(z_s)}$$

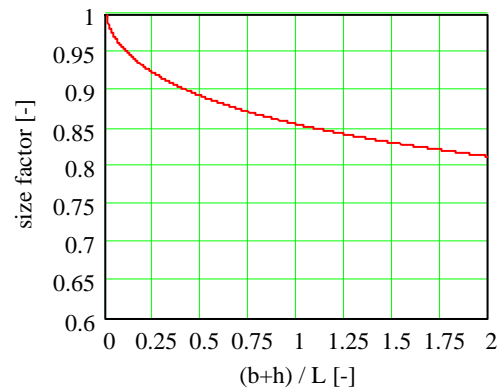
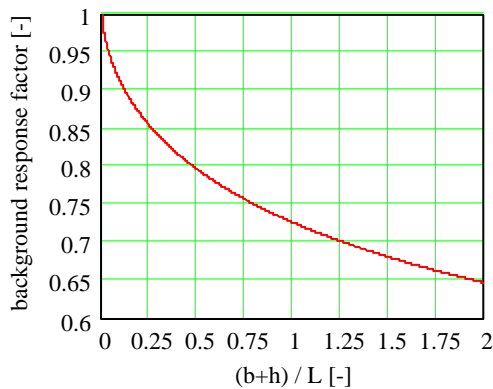
$$B := \sqrt{\frac{1}{1 + 0.9 \cdot \left(\frac{b+h}{L(z_s)}\right)^{0.63}}}$$

background response factor

where b building breadth

h building height

$L(z_s)$ turbulence length scale, representing the mean longitudinal gust size



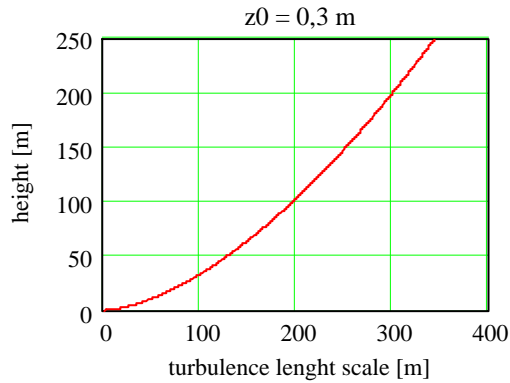
$$L(z) := L_t \cdot \left(\frac{z}{z_t} \right)^\alpha$$

integral length scale of longitudinal turbulence

where $\alpha := 0.67 + 0.05 \ln(z_0)$

$z_t = 200\text{m}$

$L_t = 300\text{m}$



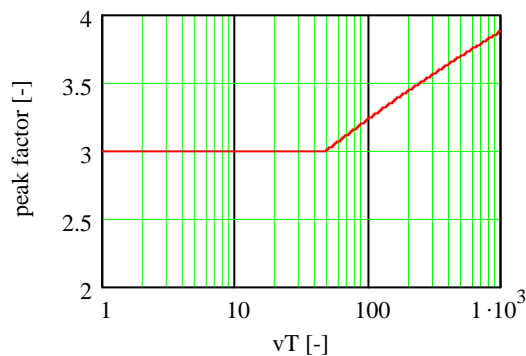
4. Dynamic factor

$$c_d := \frac{1 + 2 \cdot k_p \cdot I_v(z_s) \cdot \sqrt{B^2 + R^2}}{1 + 7 \cdot I_v(z_s) \cdot \sqrt{B^2}}$$

$k_p := \max\left(\sqrt{2 \cdot \ln(v \cdot T)} + \frac{0.6}{\sqrt{2 \cdot \ln(v \cdot T)}}, 3.0\right)$ peak factor of the structural response, being the ratio of the peak value and the root-mean-square value

where v up-crossing frequency

T 10 minutes measurement time



$$v := n_x \cdot \sqrt{\frac{R^2}{B^2 + R^2}}$$

up-crossing frequency

where n_x fundamental building frequency in the considered wind direction

B background response factor

R resonant response factor

$$R := \sqrt{\frac{\pi^2}{2 \cdot \delta_{tot}} \cdot S_L(z_s, n_x) \cdot R_h(\eta_h) \cdot R_b(\eta_b)}$$

resonance response factor

where δ_{tot} logarithmic damping decrement
 S_L spectral density function
 $R_h \cdot R_b$ aerodynamic admittance function

$$\delta_{tot} := \delta_s + \delta_a + \delta_d$$

logarithmic damping decrement

where δ_s structural damping depending of the structural system, according to the table below

δ_a aerodynamic damping

δ_d effective damping dissipative devices

| Structural type | structural damping, δ_s |
|-----------------------------------|--------------------------------|
| reinforced concrete buildings | 0,10 |
| steel buildings | 0,05 |
| mixed structures concrete + steel | 0,08 |

$$\delta_a := \frac{c_f \cdot \rho \cdot v_m(z_s)}{2 \cdot n_x \cdot \mu_e}$$

aerodynamic damping

where c_f force coefficient
 n_x fundamental building frequency in the considered wind direction
 μ_e equivalent mass per unit area
 v_m mean wind velocity
 ρ air density

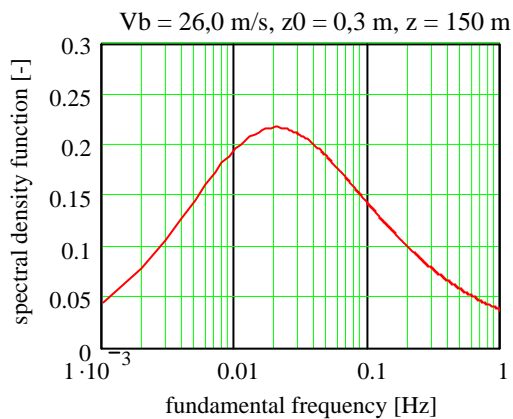
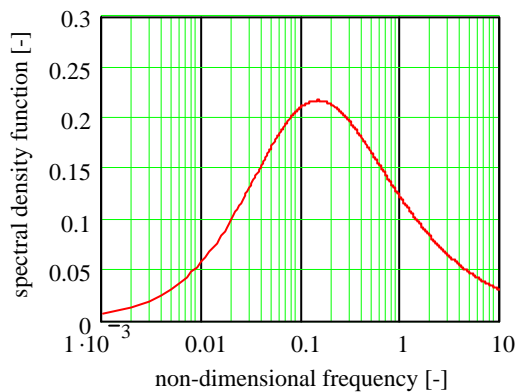
$$S_L(z, n_x) := \frac{6.8 \cdot f_L(z, n_x)}{(1 + 10.2 \cdot f_L(z, n_x))^{\frac{5}{3}}}$$

spectral density function

where f_L non-dimensional frequency

$$f_L(z, n_x) := \frac{n_x \cdot L(z)}{v_m(z)}$$

non-dimensional frequency

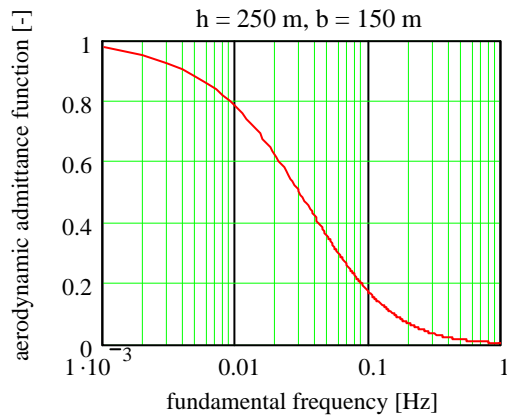


$R_h \cdot R_b$

aerodynamic admittance function

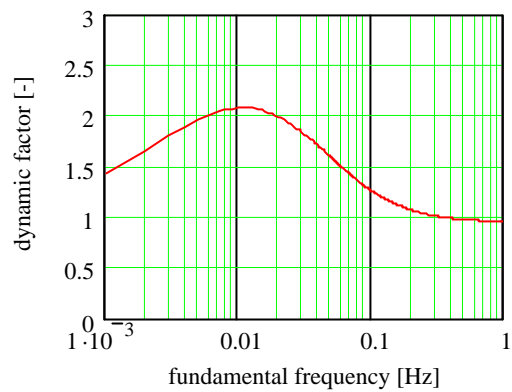
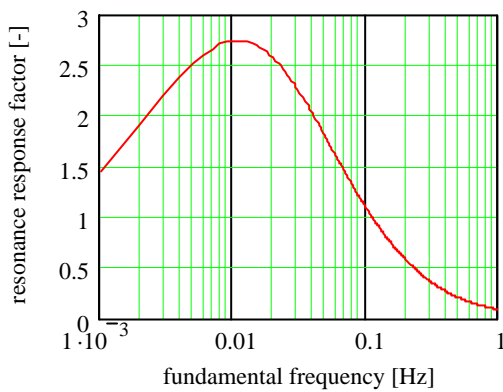
$$R_h(\eta_h) := \frac{1}{\eta_h} - \frac{1}{2 \cdot \eta_h^2} \cdot (1 - e^{-2 \cdot \eta_h}) \quad \text{where} \quad \eta_h := \frac{4.6 \cdot h}{L(z_s)} \cdot f_L(z_s, n_x) \quad F$$

$$R_b(\eta_b) := \frac{1}{\eta_b} - \frac{1}{2 \cdot \eta_b^2} \cdot (1 - e^{-2 \cdot \eta_b}) \quad \text{where} \quad \eta_b := \frac{4.6 \cdot b}{L(z_s)} \cdot f_L(z_s, n_x) \quad F$$



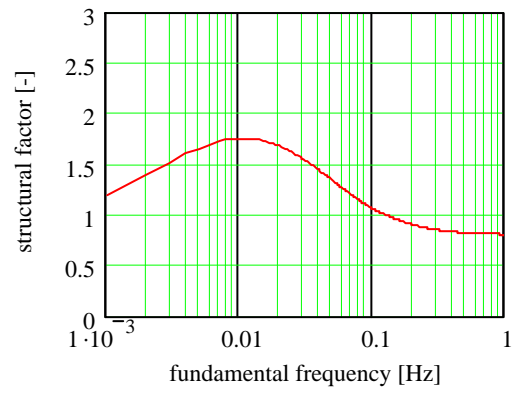
In this graph an example is plotted of the resonance response factor for the following variables

- $v_b = 26,0 \text{ m/s}$
- $z_0 = 0,3 \text{ m Terrain category III}$
- $\delta = 0,10$
- $h = 250 \text{ m}$
- $z_s = 150 \text{ m}$
- $b = 50 \text{ m}$



5. Structural factor

For the above mentioned variables the structural factor, being the product of the size factor and dynamic factor, is now plotted for different fundamental frequencies.



III.2 Torre Espacio

III.2.1 Equivalent static wind loading

Calculation according to Eurocode EN 1991 part 1-4

1. Input variables

| | | | |
|--|---|--------------------|----------------------------------|
| $h := 219.15 \text{ m}$ | height | $c_f := 0.70$ | force coefficient for $v_m(z_s)$ |
| $b := 59.40 \text{ m}$ | breadth | $\delta_s := 0.10$ | structural damping |
| $n_x := 0.135 \text{ Hz}$ | fundamental frequency | $\delta_d := 0.00$ | damping of dissipative devices |
| $m_e := 370.5 \cdot 10^3 \frac{\text{kg}}{\text{m}}$ | equivalent mass per unit length (averaged value over the upper 1/3) | | |

2. Structural factor

Reference height

$$z_s := 0.6h$$

reference height $\Rightarrow z_s = 131.5 \text{ m}$

2.1 Background response

$$B(z) := \sqrt{\frac{1}{1 + 0.9 \left(\frac{b+h}{L(z)} \right)^{0.63}}}$$

Background response factor

$$L(z) := L_t \cdot \left(\frac{z}{z_t} \right)^\alpha$$

turbulence length scale $\Rightarrow L(z_s) = 232.3 \text{ m}$

where $\alpha := 0.67 + 0.05 \ln(z_0)$

$$z_t = 200 \text{ m}$$

$$L_t = 300 \text{ m}$$

2.2 Resonance response

$$R(z, n) := \sqrt{\frac{\pi^2}{2 \cdot \delta_{\text{tot}}} \cdot S_L(z, n) \cdot R_h(z, n) \cdot R_b(z, n)}$$

Background response factor $\Rightarrow B(z_s) = 0.71$

Resonance response factor

$$\delta_{\text{tot}} := \delta_s + \delta_a + \delta_d$$

total damping $\Rightarrow \delta_{\text{tot}} = 0.12$

$$\delta_s = 0.10$$

structural damping

$$\delta_a = 0.02$$

aerodynamic damping

$$\delta_d = 0.00$$

damping of dissipative devices

$$S_L(z, n) := \frac{6.8 f_L^2(z, n)}{\left(1 + 10.2 f_L^2(z, n) \right)^{\frac{5}{3}}}$$

spectral density $\Rightarrow S_L(z_s, n_x) = 0.13$

$$f_L(z, n) := \frac{n \cdot L(z)}{v_m(z)} \quad \text{non-dimensional frequency} \quad \Rightarrow \quad \boxed{f_L(z_s, n_x) = 0.92}$$

$$R_h \cdot R_b \quad \text{aerodynamic admittance function}$$

$$R_h(z, n) := \frac{1}{\eta_h(z, n)} - \frac{1}{2 \cdot \eta_h(z, n)^2} \cdot \left(1 - e^{-2 \cdot \eta_h(z, n)}\right) \quad \text{where } \eta_h(z, n) := \frac{4.6h}{L(z)} \cdot f_L(z, n)$$

$$\Rightarrow \boxed{R_h(z_s, n_x) = 0.22}$$

$$R_b(z, n) := \frac{1}{\eta_b(z, n)} - \frac{1}{2 \cdot \eta_b(z, n)^2} \cdot \left(1 - e^{-2 \cdot \eta_b(z, n)}\right) \quad \text{where } \eta_b(z, n) := \frac{4.6b}{L(z)} \cdot f_L(z, n)$$

$$\Rightarrow \boxed{R_b(z_s, n_x) = 0.55}$$

$$R(z, n) := \sqrt{\frac{\pi^2}{2 \cdot \delta_{tot}} \cdot S_L(z, n) \cdot R_h(z, n) \cdot R_b(z, n)} \quad \text{Resonance response factor} \quad \Rightarrow \quad \boxed{R(z_s, n_x) = 0.80}$$

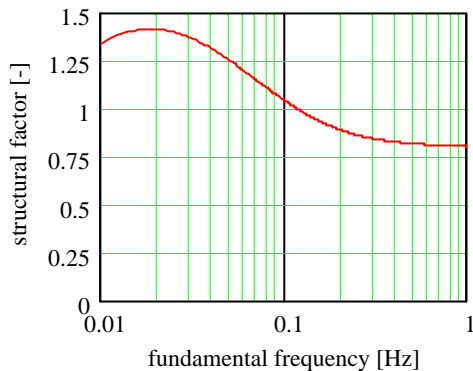
2.3 Results

$$k_p(z, n) := \sqrt{2 \cdot \ln(v(z, n) \cdot T)} + \frac{0.6}{\sqrt{2 \cdot \ln(v(z, n) \cdot T)}} \quad \text{peak factor of the structural response, where}$$

$$v(z, n) := n \cdot \sqrt{\frac{R(z, n)^2}{B(z)^2 + R(z, n)^2}} \quad \text{peak factor} \quad \Rightarrow \quad \boxed{k_p(z_s, n_x) = 3.07}$$

$$c_s(z) := \frac{1 + 7 \cdot I_V(z) \cdot \sqrt{B(z)^2}}{1 + 7 \cdot I_V(z)} \quad \text{Size factor} \quad \Rightarrow \quad \boxed{c_s(z_s) = 0.84}$$

$$c_d(z, n) := \frac{1 + 2 \cdot k_p(z, n) \cdot I_V(z) \cdot \sqrt{B(z)^2 + R(z, n)^2}}{1 + 7 \cdot I_V(z) \cdot \sqrt{B(z)^2}} \quad \text{Dynamic factor} \quad \Rightarrow \quad \boxed{c_d(z_s, n_x) = 1.15}$$



$$\text{Structural factor} \Rightarrow \boxed{c_s(z_s) \cdot c_d(z_s, n_x) = 0.97}$$

| STOREY ₁ = | HEIGHT ₁ = | Z ₁ = | EQ_ST_PEAK_PRESSURE ₁ = |
|-----------------------|-----------------------|------------------|------------------------------------|
| "B" | 4.00 m | -0.10 m | 1.23 kPa |
| "E1" | 4.00 | 3.90 | 1.23 |
| "E2" | 4.00 | 7.90 | 1.23 |
| "E3" | 4.10 | 11.90 | 1.23 |
| "M1" | 4.00 | 16.00 | 1.23 |
| "M1e" | 3.60 | 20.00 | 1.23 |
| 1 | 4.00 | 23.60 | 1.23 |
| 2 | 4.00 | 27.60 | 1.23 |
| 3 | 4.00 | 31.60 | 1.23 |
| 4 | 4.00 | 35.60 | 1.23 |
| 5 | 4.00 | 39.60 | 1.23 |
| 6 | 4.00 | 43.60 | 1.23 |
| 7 | 4.00 | 47.60 | 1.23 |
| 8 | 4.00 | 51.60 | 1.23 |
| 9 | 4.00 | 55.60 | 1.23 |
| 10 | 4.00 | 59.60 | 1.23 |
| 11 | 4.00 | 63.60 | 1.25 |
| 12 | 4.00 | 67.60 | 1.27 |
| 13 | 4.00 | 71.60 | 1.29 |
| 14 | 4.00 | 75.60 | 1.31 |
| 15 | 4.00 | 79.60 | 1.33 |
| 16 | 4.00 | 83.60 | 1.35 |
| 17 | 4.00 | 87.60 | 1.36 |
| 18 | 4.00 | 91.60 | 1.38 |
| 19 | 4.00 | 95.60 | 1.39 |
| 20 | 4.00 | 99.60 | 1.41 |
| 21 | 4.00 | 103.60 | 1.42 |
| 22 | 4.00 | 107.60 | 1.43 |
| 23 | 4.00 | 111.60 | 1.45 |
| 24 | 4.00 | 115.60 | 1.46 |
| 25 | 4.00 | 119.60 | 1.47 |
| 26 | 4.00 | 123.60 | 1.48 |
| 27 | 4.00 | 127.60 | 1.49 |
| 28 | 4.10 | 131.60 | 1.51 |

| STOREY ₁ = | HEIGHT ₁ = | Z ₁ = | EQ_ST_PEAK_PRESSURE ₁ |
|-----------------------|-----------------------|------------------|----------------------------------|
| "M2" | 3.90 m | 135.70 m | 1.52 kPa |
| 29 | 4.00 | 139.60 | 1.53 |
| 30 | 4.00 | 143.60 | 1.54 |
| 31 | 4.00 | 147.60 | 1.55 |
| 32 | 4.00 | 151.60 | 1.56 |
| 33 | 4.00 | 155.60 | 1.57 |
| 34 | 4.00 | 159.60 | 1.58 |
| 35 | 4.00 | 163.60 | 1.70 |
| 36 | 4.00 | 167.60 | 1.70 |
| 37 | 4.00 | 171.60 | 1.70 |
| 38 | 4.00 | 175.60 | 1.70 |
| 39 | 4.00 | 179.60 | 1.70 |
| 40 | 4.00 | 183.60 | 1.70 |
| 41 | 4.00 | 187.60 | 1.70 |
| 42 | 4.00 | 191.60 | 1.70 |
| 43 | 4.00 | 195.60 | 1.70 |
| 44 | 4.00 | 199.60 | 1.70 |
| 45 | 4.40 | 203.60 | 1.70 |
| "M3" | 3.80 | 208.00 | 1.70 |
| "M3e" | 3.30 | 211.80 | 1.70 |
| "CU" | 4.05 | 215.10 | 1.70 |
| "CO" | 0.00 | 219.15 | 1.70 |

III.2.2 Building accelerations

Calculation according to Eurocode EN 1991 part 1-4

1. Input variables

$$h_{\text{foundation}} := 18.4 \text{ m}$$

height between grade and the foundation level

$$z_{\text{occ.floor}} := 203.6 \text{ m}$$

height of the top occupied floor

$$\zeta := 1.3$$

mode exponent best fitting actual mode shape

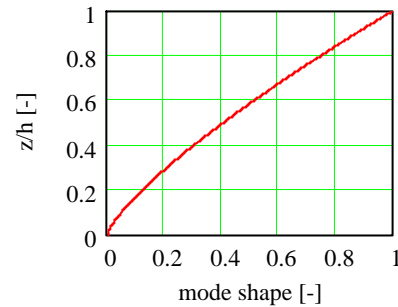
$$A_{1,x} := 0.42$$

area under the actual mode shape function

$$\Phi_{1,x}(z) := \left(\frac{z + h_{\text{foundation}}}{h + h_{\text{foundation}}} \right)^{\zeta}$$

approximated mode shape =>

$$T_{\text{return}} = 10$$



2. Accelerations

2.1 Calculation unknown variables

$$R(z, n) := \sqrt{\frac{\pi^2}{2 \cdot \delta_{\text{tot}}} \cdot S_L(z, n) \cdot R_h(z, n) \cdot R_b(z, n)}$$

Resonance response factor

$$\delta_{\text{tot}} := 0.01 \cdot 2\pi$$

total damping =>

$$\delta_{\text{tot}} = 0.06$$

$$S_L(z, n) := \frac{6.8 \cdot f_L(z, n)}{(1 + 10.2 \cdot f_L(z, n))^{\frac{5}{3}}}$$

spectral density =>

$$S_L(z_s, n_x) = 0.12$$

$$f_L(z, n) := \frac{n \cdot L(z)}{v_m(z)}$$

non-dimensional frequency =>

$$f_L(z_s, n_x) = 1.02$$

$$R_h \cdot R_b$$

aerodynamic admittance function

$$R_h(z, n) := \frac{1}{\eta_h(z, n)} - \frac{1}{2 \cdot \eta_h(z, n)^2} \cdot \left(1 - e^{-2 \cdot \eta_h(z, n)} \right) \quad \text{where } \eta_h(z, n) := \frac{4.6 \cdot h}{L(z)} \cdot f_L(z, n)$$

$$\Rightarrow R_h(z_s, n_x) = 0.20$$

$$R_b(z, n) := \frac{1}{\eta_b(z, n)} - \frac{1}{2 \cdot \eta_b(z, n)^2} \cdot \left(1 - e^{-2 \cdot \eta_b(z, n)} \right) \quad \text{where } \eta_b(z, n) := \frac{4.6 \cdot b}{L(z)} \cdot f_L(z, n)$$

$$\Rightarrow R_b(z_s, n_x) = 0.52$$

$$R(z, n) := \sqrt{\frac{\pi^2}{2 \cdot \delta_{\text{tot}}} \cdot S_L(z, n) \cdot R_h(z, n) \cdot R_b(z, n)}$$

Resonance response factor =>

$$R(z_s, n_x) = 0.99$$

$$K_x := (2 \cdot \zeta + 1) \cdot \frac{\left((\zeta + 1) \cdot \ln\left(\frac{z_s}{z_0}\right) + 0.5 \right) - 1}{(\zeta + 1)^2 \cdot \ln\left(\frac{z_s}{z_0}\right)}$$

adimensional factor =>

$$K_x = 1.58$$

$$m_{1,x} := A_{1,x} m_e$$

equivalent modal
mass per unit
length =>

$$m_{1,x} = 155.6 \times 10^3 \frac{\text{kg}}{\text{m}}$$

$$k_p := \sqrt{2 \cdot \ln(v \cdot T)} + \frac{0.6}{\sqrt{2 \cdot \ln(v \cdot T)}}$$

peak factor of the
structural response =>

$$k_p = 3.17$$

with $v := n_x$

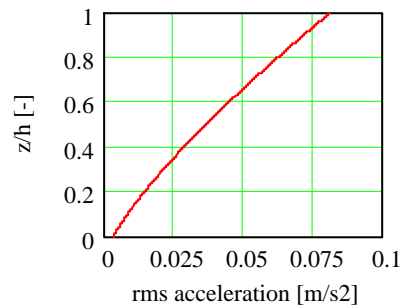
2.2 Results for $T_{\text{return}} = 10$ years

$$\sigma_{a,x}(z, n) := \frac{c_f \cdot \rho \cdot b \cdot I_v(z_s) \cdot v_m(z_s)^2}{m_{1,x}} \cdot R(z_s, n_x) \cdot K_x \cdot \Phi_{1,x}(z)$$

value at top occupied floor:

$$\sigma_{a,x}(z_{\text{occ.floor}}, n_x) = 0.074 \frac{\text{m}}{\text{s}^2}$$

$$\sigma_{a,x}(z_{\text{occ.floor}}, n_x) = 7.6 \times 10^{-3} g$$

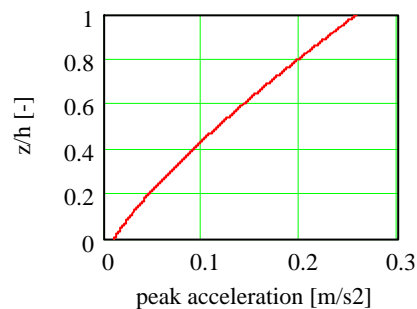


$$a_{\text{peak},x}(z, n) := \frac{c_f \cdot \rho \cdot b \cdot k_p \cdot I_v(z_s) \cdot v_m(z_s)^2}{m_{1,x}} \cdot R(z_s, n_x) \cdot K_x \cdot \Phi_{1,x}(z)$$

value at top occupied floor:

$$a_{\text{peak},x}(z_{\text{occ.floor}}, n_x) = 0.235 \frac{\text{m}}{\text{s}^2}$$

$$a_{\text{peak},x}(z_{\text{occ.floor}}, n_x) = 24.0 \times 10^{-3} g$$

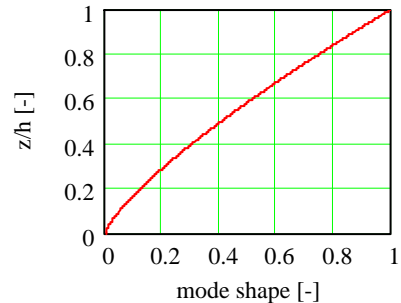


Calculation according to Eurocode EN 1991 part 1-4

1. Input variables

| | |
|---|---|
| $h_{\text{foundation}} := 18.4 \text{ m}$ | height between grade and the foundation level |
| $z_{\text{occ.floor}} := 203.6 \text{ m}$ | height of the top occupied floor |
| $\zeta := 1.3$ | mode exponent best fitting actual mode shape |
| $A_{1,x} := 0.42$ | area under the actual mode shape function |
| $\Phi_{1,x}(z) := \left(\frac{z + h_{\text{foundation}}}{h + h_{\text{foundation}}} \right)^{\zeta}$ | approximated mode shape => |

$$T_{\text{return}} = 5$$



2. Accelerations

2.1 Calculation unknown variables

$$R(z, n) := \sqrt{\frac{2}{\pi} \cdot S_L(z, n) \cdot R_h(z, n) \cdot R_b(z, n)} \cdot 2 \cdot \delta_{\text{tot}}$$

Resonance response factor

$$\delta_{\text{tot}} := 0.01 \cdot 2\pi$$

total damping =>

$$\delta_{\text{tot}} = 0.06$$

$$S_L(z, n) := \frac{6.8 \cdot f_L(z, n)}{(1 + 10.2 \cdot f_L(z, n))^{\frac{5}{3}}}$$

spectral density =>

$$S_L(z_s, n_x) = 0.12$$

$$f_L(z, n) := \frac{n \cdot L(z)}{v_m(z)}$$

non-dimensional frequency =>

$$f_L(z_s, n_x) = 1.08$$

$$R_h \cdot R_b$$

aerodynamic admittance function

$$R_h(z, n) := \frac{1}{\eta_h(z, n)} - \frac{1}{2 \cdot \eta_h(z, n)^2} \cdot \left(1 - e^{-2 \cdot \eta_h(z, n)} \right) \quad \text{where } \eta_h(z, n) := \frac{4.6 \cdot h}{L(z)} \cdot f_L(z, n)$$

$$\Rightarrow R_h(z_s, n_x) = 0.19$$

$$R_b(z, n) := \frac{1}{\eta_b(z, n)} - \frac{1}{2 \cdot \eta_b(z, n)^2} \cdot \left(1 - e^{-2 \cdot \eta_b(z, n)} \right) \quad \text{where } \eta_b(z, n) := \frac{4.6 \cdot b}{L(z)} \cdot f_L(z, n)$$

$$\Rightarrow R_b(z_s, n_x) = 0.50$$

$$R(z, n) := \sqrt{\frac{2}{\pi} \cdot S_L(z, n) \cdot R_h(z, n) \cdot R_b(z, n)} \cdot 2 \cdot \delta_{\text{tot}}$$

Resonance response factor =>

$$R(z_s, n_x) = 0.94$$

$$K_x := (2 \cdot \zeta + 1) \cdot \frac{\left((\zeta + 1) \cdot \ln\left(\frac{z_s}{z_0}\right) + 0.5 \right) - 1}{(\zeta + 1)^2 \cdot \ln\left(\frac{z_s}{z_0}\right)}$$

adimensional factor =>

$$K_x = 1.58$$

$$m_{1,x} := A_{1,x} m_e$$

equivalent modal
mass per unit
length =>

$$m_{1,x} = 155.6 \times 10^3 \frac{\text{kg}}{\text{m}}$$

$$k_p := \sqrt{2 \cdot \ln(v \cdot T)} + \frac{0.6}{\sqrt{2 \cdot \ln(v \cdot T)}}$$

peak factor of the
structural response =>

$$k_p = 3.17$$

with $v := n_x$

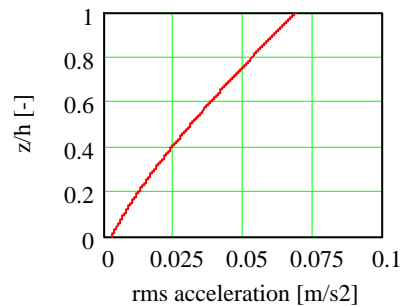
2.2 Results for $T_{\text{return}} = 5$ years

$$\sigma_{a,x}(z, n) := \frac{c_f \cdot \rho \cdot b \cdot I_v(z_s) \cdot v_m(z_s)^2}{m_{1,x}} \cdot R(z_s, n_x) \cdot K_x \cdot \Phi_{1,x}(z)$$

value at top occupied floor:

$$\sigma_{a,x}(z_{\text{occ.floor}}, n_x) = 0.063 \frac{\text{m}}{\text{s}^2}$$

$$\sigma_{a,x}(z_{\text{occ.floor}}, n_x) = 6.4 \times 10^{-3} g$$

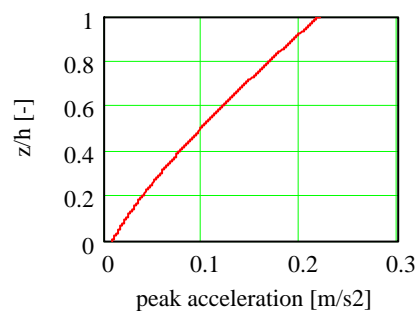


$$a_{\text{peak},x}(z, n) := \frac{c_f \cdot \rho \cdot b \cdot k_p \cdot I_v(z_s) \cdot v_m(z_s)^2}{m_{1,x}} \cdot R(z_s, n_x) \cdot K_x \cdot \Phi_{1,x}(z)$$

value at top occupied floor:

$$a_{\text{peak},x}(z_{\text{occ.floor}}, n_x) = 0.200 \frac{\text{m}}{\text{s}^2}$$

$$a_{\text{peak},x}(z_{\text{occ.floor}}, n_x) = 20.4 \times 10^{-3} g$$



III.2.3 Effective axial stiffness of vertical concrete members

This subsection of appendix III.2 provides the calculation of the effective axial stiffness of the vertical concrete elements. The factor k (see subsection 5.1.2) is determined by which the axial stiffness of the gross concrete section is multiplied in the finite element model.

Firstly, the columns are treated and thereafter the core sections are dealt with. The adopted terminology for the different core sections is illustrated in figure III.2-1.

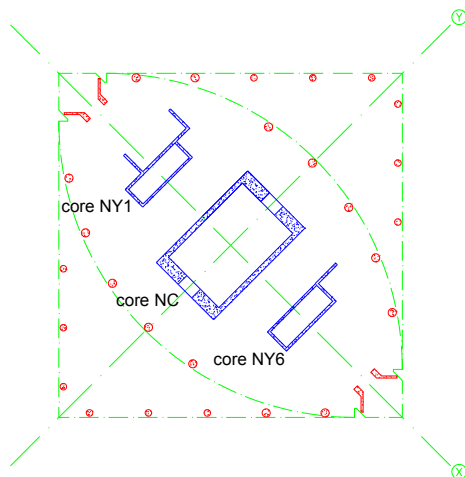


Figure III.2-1: Core structures

Columns

| Section | S12A93 | | | |
|-----------------------------------|--------------------------|----------------------------|--------------------------|--|
| Materials | | fck [MPa] | E [MPa] | |
| rolled steel | S 355 | 355 | 2,10E+05 | |
| mild steel | B 500 | 500 | 2,10E+05 | |
| concrete | C 70/85 | 70 | 4,06E+04 | |
| Geometry | | | | |
| diameter | 1200 mm | longitudinal reinforcement | A93 | |
| rolled section | - | | 60 # of bars | |
| steel plate | - | | 32 ϕ [mm] | |
| Calculation | | Results | | |
| <i>wide flange section</i> | | <i>equivalent column</i> | | |
| A | 0,00E+00 mm ² | A;column | 1,13E+06 mm ² | |
| E | 2,10E+05 MPa | EA;column | 5,41E+10 MPa | |
| <i>steel plate</i> | | | | |
| A | 0,00E+00 mm ² | Δ EA due to steel | 18% | |
| E | 2,10E+05 MPa | | | |
| <i>longitudinal reinforcement</i> | | | | |
| A | 4,83E+04 mm ² | | | |
| E | 2,10E+05 MPa | | | |
| <i>concrete</i> | | | | |
| A | 1,08E+06 mm ² | | | |
| E | 4,06E+04 MPa | | | |

| Section | S12A23 | | | |
|-----------------------------------|--------------------------|----------------------------|----------------------------|--|
| Materials | | fck [MPa] | E [MPa] | |
| rolled steel | S 355 | 355 | 2,10E+05 | |
| mild steel | B 500 | 500 | 2,10E+05 | |
| concrete | C 70/85 | 70 | 4,06E+04 | |
| Geometry | | | | |
| diameter | 1200 mm | longitudinal reinforcement | A23 | |
| rolled section | - | | 18 # of bars | |
| steel plate | - | | 32 ϕ [mm] | |
| Calculation | | Results | | |
| <i>wide flange section</i> | | <i>equivalent column</i> | | |
| A | 0,00E+00 mm ² | A;column | 1,13E+06 mm ² | |
| E | 2,10E+05 MPa | EA;column | 4,84E+10 N/mm ² | |
| <i>steel plate</i> | | | | |
| A | 0,00E+00 mm ² | Δ EA due to steel | 5% | |
| E | 2,10E+05 MPa | | | |
| <i>longitudinal reinforcement</i> | | | | |
| A | 1,45E+04 mm ² | | | |
| E | 2,10E+05 MPa | | | |
| <i>concrete</i> | | | | |
| A | 1,12E+06 mm ² | | | |
| E | 4,06E+04 MPa | | | |

| Section | S10H30A63-C70/85 | | | |
|-----------------------------------|--------------------------|----------------------------|--------------------------|--|
| Materials | | fck [MPa] | E [MPa] | |
| rolled steel | S 355 | 355 | 2,10E+05 | |
| mild steel | B 500 | 500 | 2,10E+05 | |
| concrete | C 70/85 | 70 | 4,06E+04 | |
| Geometry | | | | |
| diameter | 1000 mm | longitudinal reinforcement | A63 | |
| rolled section | HEM-300 | | 40 # of bars | |
| steel plate | - | | 32 ϕ [mm] | |
| Calculation | | Results | | |
| <i>wide flange section</i> | | <i>equivalent column</i> | | |
| A | 3,03E+04 mm ² | A;column | 7,85E+05 mm ² | |
| E | 2,10E+05 MPa | EA;column | 4,25E+10 MPa | |
| <i>steel plate</i> | | | | |
| A | 0,00E+00 mm ² | Δ EA due to steel | 33% | |
| E | 2,10E+05 MPa | | | |
| <i>longitudinal reinforcement</i> | | | | |
| A | 3,22E+04 mm ² | | | |
| E | 2,10E+05 MPa | | | |
| <i>concrete</i> | | | | |
| A | 7,23E+05 mm ² | | | |
| E | 4,06E+04 MPa | | | |

| Section | S10H50C1A63-C70/85 | | | |
|-----------------------------------|--------------------------|----------------------------|----------------------------|--|
| Materials | | fck [MPa] | E [MPa] | |
| rolled steel | S 355 | 355 | 2,10E+05 | |
| mild steel | B 500 | 500 | 2,10E+05 | |
| concrete | C 70/85 | 70 | 4,06E+04 | |
| Geometry | | | | |
| diameter | 1000 mm | longitudinal reinforcement | A63 | |
| rolled section | HEM-500 | | 40 # of bars | |
| steel plate | 2 x 390 x 30 | | 32 ϕ [mm] | |
| Calculation | | Results | | |
| <i>wide flange section</i> | | <i>equivalent column</i> | | |
| A | 3,44E+04 mm ² | A;column | 7,85E+05 mm ² | |
| E | 2,10E+05 MPa | EA;column | 4,71E+10 N/mm ² | |
| <i>steel plate</i> | | | | |
| A | 2,34E+04 mm ² | Δ EA due to steel | 48% | |
| E | 2,10E+05 MPa | | | |
| <i>longitudinal reinforcement</i> | | | | |
| A | 3,22E+04 mm ² | | | |
| E | 2,10E+05 MPa | | | |
| <i>concrete</i> | | | | |
| A | 6,95E+05 mm ² | | | |
| E | 4,06E+04 MPa | | | |

| Section | S10H50C2A63-C70/85 | | | |
|-----------------------------------|--------------------------|----------------------------|----------------------------|--|
| Materials | | fck [MPa] | E [MPa] | |
| rolled steel | S 355 | 355 | 2,10E+05 | |
| mild steel | B 500 | 500 | 2,10E+05 | |
| concrete | C 70/85 | 70 | 4,06E+04 | |
| Geometry | | | | |
| diameter | 1000 mm | longitudinal reinforcement | A63 | |
| rolled section | HEM-500 | | 40 # of bars | |
| steel plate | 2 x 390 x 50 | | 32 ϕ [mm] | |
| Calculation | | Results | | |
| <i>wide flange section</i> | | <i>equivalent column</i> | | |
| A | 3,44E+04 mm ² | A;column | 7,85E+05 mm ² | |
| E | 2,10E+05 MPa | EA;column | 4,98E+10 N/mm ² | |
| <i>steel plate</i> | | | | |
| A | 3,90E+04 mm ² | Δ EA due to steel | 56% | |
| E | 2,10E+05 MPa | | | |
| <i>longitudinal reinforcement</i> | | | | |
| A | 3,22E+04 mm ² | | | |
| E | 2,10E+05 MPa | | | |
| <i>concrete</i> | | | | |
| A | 6,80E+05 mm ² | | | |
| E | 4,06E+04 MPa | | | |

| Section | S10A13-C70/85 | | | |
|-----------------------------------|--------------------------|----------------------------|----------------------------|--|
| Materials | | fck [MPa] | E [MPa] | |
| rolled steel | S 355 | 355 | 2,10E+05 | |
| mild steel | B 500 | 500 | 2,10E+05 | |
| concrete | C 70/85 | 70 | 4,06E+04 | |
| Geometry | | | | |
| diameter | 1000 mm | longitudinal reinforcement | A13 | |
| rolled section | - | | 12 # of bars | |
| steel plate | - | | 32 ϕ [mm] | |
| Calculation | | Results | | |
| <i>wide flange section</i> | | <i>equivalent column</i> | | |
| A | 0,00E+00 mm ² | A;column | 7,85E+05 mm ² | |
| E | 2,10E+05 MPa | EA;column | 3,35E+10 N/mm ² | |
| <i>steel plate</i> | | | | |
| A | 0,00E+00 mm ² | Δ EA due to steel | 5% | |
| E | 2,10E+05 MPa | | | |
| <i>longitudinal reinforcement</i> | | | | |
| A | 9,65E+03 mm ² | | | |
| E | 2,10E+05 MPa | | | |
| <i>concrete</i> | | | | |
| A | 7,76E+05 mm ² | | | |
| E | 4,06E+04 MPa | | | |

| Section S10A93-C40/50 | | | |
|----------------------------|--------------|----------------------------|----------------|
| Materials | | fck [MPa] | E [MPa] |
| rolled steel | S 355 | 355 | 2,10E+05 |
| mild steel | B 500 | 500 | 2,10E+05 |
| concrete | C 40/50 | 40 | 3,45E+04 |
| Geometry | | | |
| diameter | 1000 mm | longitudinal reinforcement | A93 |
| rolled section | - | | 60 # of bars |
| steel plate | - | | 32 ϕ [mm] |
| Calculation | | Results | |
| wide flange section | | equivalent column | |
| A | 0,00E+00 mm2 | A;column | 7,85E+05 mm2 |
| E | 2,10E+05 MPa | EA;column | 3,56E+10 N/mm2 |
| steel plate | | | |
| A | 0,00E+00 mm2 | Δ EA due to steel | 31% |
| E | 2,10E+05 MPa | | |
| longitudinal reinforcement | | | |
| A | 4,83E+04 mm2 | | |
| E | 2,10E+05 MPa | | |
| concrete | | | |
| A | 7,37E+05 mm2 | | |
| E | 3,45E+04 MPa | | |

| Section S10A33-C40/50 | | | |
|----------------------------|--------------|----------------------------|----------------|
| Materials | | fck [MPa] | E [MPa] |
| rolled steel | S 355 | 355 | 2,10E+05 |
| mild steel | B 500 | 500 | 2,10E+05 |
| concrete | C 40/50 | 40 | 3,45E+04 |
| Geometry | | | |
| diameter | 1000 mm | longitudinal reinforcement | A33 |
| rolled section | - | | 24 # of bars |
| steel plate | - | | 32 ϕ [mm] |
| Calculation | | Results | |
| wide flange section | | equivalent column | |
| A | 0,00E+00 mm2 | A;column | 7,85E+05 mm2 |
| E | 2,10E+05 MPa | EA;column | 3,05E+10 N/mm2 |
| steel plate | | | |
| A | 0,00E+00 mm2 | Δ EA due to steel | 12% |
| E | 2,10E+05 MPa | | |
| longitudinal reinforcement | | | |
| A | 1,93E+04 mm2 | | |
| E | 2,10E+05 MPa | | |
| concrete | | | |
| A | 7,66E+05 mm2 | | |
| E | 3,45E+04 MPa | | |

| Section S10A83-C40/50 | | | |
|----------------------------|--------------|----------------------------|----------------|
| Materials | | fck [MPa] | E [MPa] |
| rolled steel | S 355 | 355 | 2,10E+05 |
| mild steel | B 500 | 500 | 2,10E+05 |
| concrete | C 40/50 | 40 | 3,45E+04 |
| Geometry | | | |
| diameter | 1000 mm | longitudinal reinforcement | A83 |
| rolled section | - | | 50 # of bars |
| steel plate | - | | 32 ϕ [mm] |
| Calculation | | Results | |
| wide flange section | | equivalent column | |
| A | 0,00E+00 mm2 | A;column | 7,85E+05 mm2 |
| E | 2,10E+05 MPa | EA;column | 3,42E+10 N/mm2 |
| steel plate | | | |
| A | 0,00E+00 mm2 | Δ EA due to steel | 26% |
| E | 2,10E+05 MPa | | |
| longitudinal reinforcement | | | |
| A | 4,02E+04 mm2 | | |
| E | 2,10E+05 MPa | | |
| concrete | | | |
| A | 7,45E+05 mm2 | | |
| E | 3,45E+04 MPa | | |

| Section S10A63-C70/85 | | | |
|----------------------------|--------------|----------------------------|----------------|
| Materials | | fck [MPa] | E [MPa] |
| rolled steel | S 355 | 355 | 2,10E+05 |
| mild steel | B 500 | 500 | 2,10E+05 |
| concrete | C 70/85 | 70 | 4,06E+04 |
| Geometry | | | |
| diameter | 1000 mm | longitudinal reinforcement | A63 |
| rolled section | - | | 40 # of bars |
| steel plate | - | | 32 ϕ [mm] |
| Calculation | | Results | |
| wide flange section | | equivalent column | |
| A | 0,00E+00 mm2 | A;column | 7,85E+05 mm2 |
| E | 2,10E+05 MPa | EA;column | 3,73E+10 N/mm2 |
| steel plate | | | |
| A | 0,00E+00 mm2 | Δ EA due to steel | 17% |
| E | 2,10E+05 MPa | | |
| longitudinal reinforcement | | | |
| A | 3,22E+04 mm2 | | |
| E | 2,10E+05 MPa | | |
| concrete | | | |
| A | 7,53E+05 mm2 | | |
| E | 4,06E+04 MPa | | |

| Section S10A63-C40/50 | | | |
|----------------------------|--------------|----------------------------|----------------|
| Materials | | fck [MPa] | E [MPa] |
| rolled steel | S 355 | 355 | 2,10E+05 |
| mild steel | B 500 | 500 | 2,10E+05 |
| concrete | C 40/50 | 40 | 3,45E+04 |
| Geometry | | | |
| diameter | 1000 mm | longitudinal reinforcement | A63 |
| rolled section | - | | 40 # of bars |
| steel plate | - | | 32 ϕ [mm] |
| Calculation | | Results | |
| wide flange section | | equivalent column | |
| A | 0,00E+00 mm2 | A;column | 7,85E+05 mm2 |
| E | 2,10E+05 MPa | EA;column | 3,28E+10 N/mm2 |
| steel plate | | | |
| A | 0,00E+00 mm2 | Δ EA due to steel | 21% |
| E | 2,10E+05 MPa | | |
| longitudinal reinforcement | | | |
| A | 3,22E+04 mm2 | | |
| E | 2,10E+05 MPa | | |
| concrete | | | |
| A | 7,53E+05 mm2 | | |
| E | 3,45E+04 MPa | | |

| Section S9A63-C40/50 | | | |
|----------------------------|--------------|----------------------------|----------------|
| Materials | | fck [MPa] | E [MPa] |
| rolled steel | S 355 | 355 | 2,10E+05 |
| mild steel | B 500 | 500 | 2,10E+05 |
| concrete | C 40/50 | 40 | 3,45E+04 |
| Geometry | | | |
| diameter | 900 mm | longitudinal reinforcement | A63 |
| rolled section | - | | 40 # of bars |
| steel plate | - | | 32 ϕ [mm] |
| Calculation | | Results | |
| wide flange section | | equivalent column | |
| A | 0,00E+00 mm2 | A;column | 6,36E+05 mm2 |
| E | 2,10E+05 MPa | EA;column | 2,76E+10 N/mm2 |
| steel plate | | | |
| A | 0,00E+00 mm2 | Δ EA due to steel | 26% |
| E | 2,10E+05 MPa | | |
| longitudinal reinforcement | | | |
| A | 3,22E+04 mm2 | | |
| E | 2,10E+05 MPa | | |
| concrete | | | |
| A | 6,04E+05 mm2 | | |
| E | 3,45E+04 MPa | | |

| Section | | S9A53-C40/50 | |
|----------------------------|--------------|----------------------------|----------------|
| Materials | | fck [MPa] | E [MPa] |
| rolled steel | S 355 | 355 | 2,10E+05 |
| mild steel | B 500 | 500 | 2,10E+05 |
| concrete | C 40/50 | 40 | 3,45E+04 |
| Geometry | | | |
| diameter | 900 mm | longitudinal reinforcement | A53 |
| rolled section | - | | 32 # of bars |
| steel plate | - | | 32 ϕ [mm] |
| Calculation | | Results | |
| wide flange section | | equivalent column | |
| A | 0,00E+00 mm2 | A;column | 6,36E+05 mm2 |
| E | 2,10E+05 MPa | EA;column | 2,65E+10 N/mm2 |
| steel plate | | | |
| A | 0,00E+00 mm2 | Δ EA due to steel | 21% |
| E | 2,10E+05 MPa | | |
| longitudinal reinforcement | | | |
| A | 2,57E+04 mm2 | | |
| E | 2,10E+05 MPa | | |
| concrete | | | |
| A | 6,10E+05 mm2 | | |
| E | 3,45E+04 MPa | | |

| Section | | S8A43-C30/40 | |
|----------------------------|--------------|----------------------------|----------------|
| Materials | | fck [MPa] | E [MPa] |
| rolled steel | S 355 | 355 | 2,10E+05 |
| mild steel | B 500 | 500 | 2,10E+05 |
| concrete | C 30/40 | 30 | 3,19E+04 |
| Geometry | | | |
| diameter | 800 mm | longitudinal reinforcement | A43 |
| rolled section | - | | 30 # of bars |
| steel plate | - | | 32 ϕ [mm] |
| Calculation | | Results | |
| wide flange section | | equivalent column | |
| A | 0,00E+00 mm2 | A;column | 5,03E+05 mm2 |
| E | 2,10E+05 MPa | EA;column | 2,04E+10 N/mm2 |
| steel plate | | | |
| A | 0,00E+00 mm2 | Δ EA due to steel | 27% |
| E | 2,10E+05 MPa | | |
| longitudinal reinforcement | | | |
| A | 2,41E+04 mm2 | | |
| E | 2,10E+05 MPa | | |
| concrete | | | |
| A | 4,79E+05 mm2 | | |
| E | 3,19E+04 MPa | | |

| Section | | S9A33-C40/50 | |
|----------------------------|--------------|----------------------------|----------------|
| Materials | | fck [MPa] | E [MPa] |
| rolled steel | S 355 | 355 | 2,10E+05 |
| mild steel | B 500 | 500 | 2,10E+05 |
| concrete | C 40/50 | 40 | 3,45E+04 |
| Geometry | | | |
| diameter | 900 mm | longitudinal reinforcement | A53 |
| rolled section | - | | 24 # of bars |
| steel plate | - | | 32 ϕ [mm] |
| Calculation | | Results | |
| wide flange section | | equivalent column | |
| A | 0,00E+00 mm2 | A;column | 6,36E+05 mm2 |
| E | 2,10E+05 MPa | EA;column | 2,54E+10 N/mm2 |
| steel plate | | | |
| A | 0,00E+00 mm2 | Δ EA due to steel | 15% |
| E | 2,10E+05 MPa | | |
| longitudinal reinforcement | | | |
| A | 1,93E+04 mm2 | | |
| E | 2,10E+05 MPa | | |
| concrete | | | |
| A | 6,17E+05 mm2 | | |
| E | 3,45E+04 MPa | | |

| Section | | S8A22-C40/50 | |
|----------------------------|--------------|----------------------------|----------------|
| Materials | | fck [MPa] | E [MPa] |
| rolled steel | S 355 | 355 | 2,10E+05 |
| mild steel | B 500 | 500 | 2,10E+05 |
| concrete | C 40/50 | 40 | 3,45E+04 |
| Geometry | | | |
| diameter | 800 mm | longitudinal reinforcement | A22 |
| rolled section | - | | 18 # of bars |
| steel plate | - | | 25 ϕ [mm] |
| Calculation | | Results | |
| wide flange section | | equivalent column | |
| A | 0,00E+00 mm2 | A;column | 5,03E+05 mm2 |
| E | 2,10E+05 MPa | EA;column | 1,89E+10 N/mm2 |
| steel plate | | | |
| A | 0,00E+00 mm2 | Δ EA due to steel | 9% |
| E | 2,10E+05 MPa | | |
| longitudinal reinforcement | | | |
| A | 8,84E+03 mm2 | | |
| E | 2,10E+05 MPa | | |
| concrete | | | |
| A | 4,94E+05 mm2 | | |
| E | 3,45E+04 MPa | | |

| Section | | S8A43-C40/50 | |
|----------------------------|--------------|----------------------------|----------------|
| Materials | | fck [MPa] | E [MPa] |
| rolled steel | S 355 | 355 | 2,10E+05 |
| mild steel | B 500 | 500 | 2,10E+05 |
| concrete | C 40/50 | 40 | 3,45E+04 |
| Geometry | | | |
| diameter | 800 mm | longitudinal reinforcement | A43 |
| rolled section | - | | 30 # of bars |
| steel plate | - | | 32 ϕ [mm] |
| Calculation | | Results | |
| wide flange section | | equivalent column | |
| A | 0,00E+00 mm2 | A;column | 5,03E+05 mm2 |
| E | 2,10E+05 MPa | EA;column | 2,16E+10 N/mm2 |
| steel plate | | | |
| A | 0,00E+00 mm2 | Δ EA due to steel | 24% |
| E | 2,10E+05 MPa | | |
| longitudinal reinforcement | | | |
| A | 2,41E+04 mm2 | | |
| E | 2,10E+05 MPa | | |
| concrete | | | |
| A | 4,79E+05 mm2 | | |
| E | 3,45E+04 MPa | | |

| Section | | S8A22-C30/40 | |
|----------------------------|--------------|----------------------------|----------------|
| Materials | | fck [MPa] | E [MPa] |
| rolled steel | S 355 | 355 | 2,10E+05 |
| mild steel | B 500 | 500 | 2,10E+05 |
| concrete | C 30/40 | 30 | 3,19E+04 |
| Geometry | | | |
| diameter | 800 mm | longitudinal reinforcement | A22 |
| rolled section | - | | 18 # of bars |
| steel plate | - | | 25 ϕ [mm] |
| Calculation | | Results | |
| wide flange section | | equivalent column | |
| A | 0,00E+00 mm2 | A;column | 5,03E+05 mm2 |
| E | 2,10E+05 MPa | EA;column | 1,76E+10 N/mm2 |
| steel plate | | | |
| A | 0,00E+00 mm2 | Δ EA due to steel | 10% |
| E | 2,10E+05 MPa | | |
| longitudinal reinforcement | | | |
| A | 8,84E+03 mm2 | | |
| E | 2,10E+05 MPa | | |
| concrete | | | |
| A | 4,94E+05 mm2 | | |
| E | 3,19E+04 MPa | | |

| Section S8A23-C30/40 | | | |
|----------------------------|--------------|----------------------------|----------------|
| Materials | | fck [MPa] | E [MPa] |
| rolled steel | S 355 | 355 | 2,10E+05 |
| mild steel | B 500 | 500 | 2,10E+05 |
| concrete | C 30/40 | 30 | 3,19E+04 |
| Geometry | | | |
| diameter | 800 mm | longitudinal reinforcement | A23 |
| rolled section | - | | 18 # of bars |
| steel plate | - | | 32 ϕ [mm] |
| Calculation | | Results | |
| wide flange section | | equivalent column | |
| A | 0,00E+00 mm2 | A;column | 5,03E+05 mm2 |
| E | 2,10E+05 MPa | EA;column | 1,86E+10 N/mm2 |
| steel plate | | | |
| A | 0,00E+00 mm2 | Δ EA due to steel | 16% |
| E | 2,10E+05 MPa | | |
| longitudinal reinforcement | | | |
| A | 1,45E+04 mm2 | | |
| E | 2,10E+05 MPa | | |
| concrete | | | |
| A | 4,88E+05 mm2 | | |
| E | 3,19E+04 MPa | | |

| Section S8A73-C70/85 | | | |
|----------------------------|--------------|----------------------------|----------------|
| Materials | | fck [MPa] | E [MPa] |
| rolled steel | S 355 | 355 | 2,10E+05 |
| mild steel | B 500 | 500 | 2,10E+05 |
| concrete | C 70/85 | 70 | 4,06E+04 |
| Geometry | | | |
| diameter | 800 mm | longitudinal reinforcement | A73 |
| rolled section | - | | 45 # of bars |
| steel plate | - | | 32 ϕ [mm] |
| Calculation | | Results | |
| wide flange section | | equivalent column | |
| A | 0,00E+00 mm2 | A;column | 5,03E+05 mm2 |
| E | 2,10E+05 MPa | EA;column | 2,65E+10 N/mm2 |
| steel plate | | | |
| A | 0,00E+00 mm2 | Δ EA due to steel | 30% |
| E | 2,10E+05 MPa | | |
| longitudinal reinforcement | | | |
| A | 3,62E+04 mm2 | | |
| E | 2,10E+05 MPa | | |
| concrete | | | |
| A | 4,66E+05 mm2 | | |
| E | 4,06E+04 MPa | | |

| Section S8A13-C30/40 | | | |
|----------------------------|--------------|----------------------------|----------------|
| Materials | | fck [MPa] | E [MPa] |
| rolled steel | S 355 | 355 | 2,10E+05 |
| mild steel | B 500 | 500 | 2,10E+05 |
| concrete | C 30/40 | 30 | 3,19E+04 |
| Geometry | | | |
| diameter | 800 mm | longitudinal reinforcement | A13 |
| rolled section | - | | 12 # of bars |
| steel plate | - | | 32 ϕ [mm] |
| Calculation | | Results | |
| wide flange section | | equivalent column | |
| A | 0,00E+00 mm2 | A;column | 5,03E+05 mm2 |
| E | 2,10E+05 MPa | EA;column | 1,78E+10 N/mm2 |
| steel plate | | | |
| A | 0,00E+00 mm2 | Δ EA due to steel | 11% |
| E | 2,10E+05 MPa | | |
| longitudinal reinforcement | | | |
| A | 9,65E+03 mm2 | | |
| E | 2,10E+05 MPa | | |
| concrete | | | |
| A | 4,93E+05 mm2 | | |
| E | 3,19E+04 MPa | | |

| Section S8A73-C40/50 | | | |
|----------------------------|--------------|----------------------------|----------------|
| Materials | | fck [MPa] | E [MPa] |
| rolled steel | S 355 | 355 | 2,10E+05 |
| mild steel | B 500 | 500 | 2,10E+05 |
| concrete | C 40/50 | 40 | 3,45E+04 |
| Geometry | | | |
| diameter | 800 mm | longitudinal reinforcement | A73 |
| rolled section | - | | 45 # of bars |
| steel plate | - | | 32 ϕ [mm] |
| Calculation | | Results | |
| wide flange section | | equivalent column | |
| A | 0,00E+00 mm2 | A;column | 5,03E+05 mm2 |
| E | 2,10E+05 MPa | EA;column | 2,37E+10 N/mm2 |
| steel plate | | | |
| A | 0,00E+00 mm2 | Δ EA due to steel | 37% |
| E | 2,10E+05 MPa | | |
| longitudinal reinforcement | | | |
| A | 3,62E+04 mm2 | | |
| E | 2,10E+05 MPa | | |
| concrete | | | |
| A | 4,66E+05 mm2 | | |
| E | 3,45E+04 MPa | | |

| Section S8A12-C30/40 | | | |
|----------------------------|--------------|----------------------------|----------------|
| Materials | | fck [MPa] | E [MPa] |
| rolled steel | S 355 | 355 | 2,10E+05 |
| mild steel | B 500 | 500 | 2,10E+05 |
| concrete | C 30/40 | 30 | 3,19E+04 |
| Geometry | | | |
| diameter | 800 mm | longitudinal reinforcement | A12 |
| rolled section | - | | 12 # of bars |
| steel plate | - | | 25 ϕ [mm] |
| Calculation | | Results | |
| wide flange section | | equivalent column | |
| A | 0,00E+00 mm2 | A;column | 5,03E+05 mm2 |
| E | 2,10E+05 MPa | EA;column | 1,71E+10 N/mm2 |
| steel plate | | | |
| A | 0,00E+00 mm2 | Δ EA due to steel | 7% |
| E | 2,10E+05 MPa | | |
| longitudinal reinforcement | | | |
| A | 5,89E+03 mm2 | | |
| E | 2,10E+05 MPa | | |
| concrete | | | |
| A | 4,97E+05 mm2 | | |
| E | 3,19E+04 MPa | | |

| Section S8A11-C40/50 | | | |
|----------------------------|--------------|----------------------------|----------------|
| Materials | | fck [MPa] | E [MPa] |
| rolled steel | S 355 | 355 | 2,10E+05 |
| mild steel | B 500 | 500 | 2,10E+05 |
| concrete | C 40/50 | 40 | 3,45E+04 |
| Geometry | | | |
| diameter | 800 mm | longitudinal reinforcement | A11 |
| rolled section | - | | 12 # of bars |
| steel plate | - | | 20 ϕ [mm] |
| Calculation | | Results | |
| wide flange section | | equivalent column | |
| A | 0,00E+00 mm2 | A;column | 5,03E+05 mm2 |
| E | 2,10E+05 MPa | EA;column | 1,80E+10 N/mm2 |
| steel plate | | | |
| A | 0,00E+00 mm2 | Δ EA due to steel | 4% |
| E | 2,10E+05 MPa | | |
| longitudinal reinforcement | | | |
| A | 3,77E+03 mm2 | | |
| E | 2,10E+05 MPa | | |
| concrete | | | |
| A | 4,99E+05 mm2 | | |
| E | 3,45E+04 MPa | | |

| Section | | S8A12-C40/50 | |
|-----------------------------------|--------------|----------------------------|----------------|
| Materials | | fck [MPa] | E [MPa] |
| rolled steel | S 355 | 355 | 2,10E+05 |
| mild steel | B 500 | 500 | 2,10E+05 |
| concrete | C 40/50 | 40 | 3,45E+04 |
| Geometry | | | |
| diameter | 800 mm | longitudinal reinforcement | A12 |
| rolled section | - | | 12 # of bars |
| steel plate | - | | 25 ϕ [mm] |
| Calculation | | Results | |
| <i>wide flange section</i> | | <i>equivalent column</i> | |
| A | 0,00E+00 mm2 | A;column | 5,03E+05 mm2 |
| E | 2,10E+05 MPa | EA;column | 1,84E+10 N/mm2 |
| <i>steel plate</i> | | | |
| A | 0,00E+00 mm2 | Δ EA due to steel | 6% |
| E | 2,10E+05 MPa | | |
| <i>longitudinal reinforcement</i> | | | |
| A | 5,89E+03 mm2 | | |
| E | 2,10E+05 MPa | | |
| <i>concrete</i> | | | |
| A | 4,97E+05 mm2 | | |
| E | 3,45E+04 MPa | | |

| Section | | S8A23-C40/50 | |
|-----------------------------------|--------------|----------------------------|----------------|
| Materials | | fck [MPa] | E [MPa] |
| rolled steel | S 355 | 355 | 2,10E+05 |
| mild steel | B 500 | 500 | 2,10E+05 |
| concrete | C 40/50 | 40 | 3,45E+04 |
| Geometry | | | |
| diameter | 800 mm | longitudinal reinforcement | A23 |
| rolled section | - | | 18 # of bars |
| steel plate | - | | 32 ϕ [mm] |
| Calculation | | Results | |
| <i>wide flange section</i> | | <i>equivalent column</i> | |
| A | 0,00E+00 mm2 | A;column | 5,03E+05 mm2 |
| E | 2,10E+05 MPa | EA;column | 1,99E+10 N/mm2 |
| <i>steel plate</i> | | | |
| A | 0,00E+00 mm2 | Δ EA due to steel | 15% |
| E | 2,10E+05 MPa | | |
| <i>longitudinal reinforcement</i> | | | |
| A | 1,45E+04 mm2 | | |
| E | 2,10E+05 MPa | | |
| <i>concrete</i> | | | |
| A | 4,88E+05 mm2 | | |
| E | 3,45E+04 MPa | | |

| Section | | S8A13-C40/50 | |
|-----------------------------------|--------------|----------------------------|----------------|
| Materials | | fck [MPa] | E [MPa] |
| rolled steel | S 355 | 355 | 2,10E+05 |
| mild steel | B 500 | 500 | 2,10E+05 |
| concrete | C 40/50 | 40 | 3,45E+04 |
| Geometry | | | |
| diameter | 800 mm | longitudinal reinforcement | A13 |
| rolled section | - | | 12 # of bars |
| steel plate | - | | 32 ϕ [mm] |
| Calculation | | Results | |
| <i>wide flange section</i> | | <i>equivalent column</i> | |
| A | 0,00E+00 mm2 | A;column | 5,03E+05 mm2 |
| E | 2,10E+05 MPa | EA;column | 1,90E+10 N/mm2 |
| <i>steel plate</i> | | | |
| A | 0,00E+00 mm2 | Δ EA due to steel | 10% |
| E | 2,10E+05 MPa | | |
| <i>longitudinal reinforcement</i> | | | |
| A | 9,65E+03 mm2 | | |
| E | 2,10E+05 MPa | | |
| <i>concrete</i> | | | |
| A | 4,93E+05 mm2 | | |
| E | 3,45E+04 MPa | | |

| Section | | S8A23-C70/85 | |
|-----------------------------------|--------------|----------------------------|----------------|
| Materials | | fck [MPa] | E [MPa] |
| rolled steel | S 355 | 355 | 2,10E+05 |
| mild steel | B 500 | 500 | 2,10E+05 |
| concrete | C 70/85 | 70 | 4,06E+04 |
| Geometry | | | |
| diameter | 800 mm | longitudinal reinforcement | A23 |
| rolled section | - | | 18 # of bars |
| steel plate | - | | 32 ϕ [mm] |
| Calculation | | Results | |
| <i>wide flange section</i> | | <i>equivalent column</i> | |
| A | 0,00E+00 mm2 | A;column | 5,03E+05 mm2 |
| E | 2,10E+05 MPa | EA;column | 2,29E+10 N/mm2 |
| <i>steel plate</i> | | | |
| A | 0,00E+00 mm2 | Δ EA due to steel | 12% |
| E | 2,10E+05 MPa | | |
| <i>longitudinal reinforcement</i> | | | |
| A | 1,45E+04 mm2 | | |
| E | 2,10E+05 MPa | | |
| <i>concrete</i> | | | |
| A | 4,88E+05 mm2 | | |
| E | 4,06E+04 MPa | | |

| Section | | S8A22-C70/85 | |
|-----------------------------------|--------------|----------------------------|----------------|
| Materials | | fck [MPa] | E [MPa] |
| rolled steel | S 355 | 355 | 2,10E+05 |
| mild steel | B 500 | 500 | 2,10E+05 |
| concrete | C 70/85 | 70 | 4,06E+04 |
| Geometry | | | |
| diameter | 800 mm | longitudinal reinforcement | A22 |
| rolled section | - | | 18 # of bars |
| steel plate | - | | 25 ϕ [mm] |
| Calculation | | Results | |
| <i>wide flange section</i> | | <i>equivalent column</i> | |
| A | 0,00E+00 mm2 | A;column | 5,03E+05 mm2 |
| E | 2,10E+05 MPa | EA;column | 2,19E+10 N/mm2 |
| <i>steel plate</i> | | | |
| A | 0,00E+00 mm2 | Δ EA due to steel | 7% |
| E | 2,10E+05 MPa | | |
| <i>longitudinal reinforcement</i> | | | |
| A | 8,84E+03 mm2 | | |
| E | 2,10E+05 MPa | | |
| <i>concrete</i> | | | |
| A | 4,94E+05 mm2 | | |
| E | 4,06E+04 MPa | | |

| Section | | S8A33-C30/40 | |
|-----------------------------------|--------------|----------------------------|----------------|
| Materials | | fck [MPa] | E [MPa] |
| rolled steel | S 355 | 355 | 2,10E+05 |
| mild steel | B 500 | 500 | 2,10E+05 |
| concrete | C 30/40 | 30 | 3,19E+04 |
| Geometry | | | |
| diameter | 800 mm | longitudinal reinforcement | A33 |
| rolled section | - | | 24 # of bars |
| steel plate | - | | 32 ϕ [mm] |
| Calculation | | Results | |
| <i>wide flange section</i> | | <i>equivalent column</i> | |
| A | 0,00E+00 mm2 | A;column | 5,03E+05 mm2 |
| E | 2,10E+05 MPa | EA;column | 1,95E+10 N/mm2 |
| <i>steel plate</i> | | | |
| A | 0,00E+00 mm2 | Δ EA due to steel | 21% |
| E | 2,10E+05 MPa | | |
| <i>longitudinal reinforcement</i> | | | |
| A | 1,93E+04 mm2 | | |
| E | 2,10E+05 MPa | | |
| <i>concrete</i> | | | |
| A | 4,83E+05 mm2 | | |
| E | 3,19E+04 MPa | | |

| Section | | | | S8A33-C40/50 | | | |
|-----------------------------------|--------------|--------------------------|----------------|--------------|--|----------------|--|
| Materials | | | fck [MPa] | | | E [MPa] | |
| rolled steel | S 355 | | 355 | | | 2,10E+05 | |
| mild steel | B 500 | | 500 | | | 2,10E+05 | |
| concrete | C 40/50 | | 40 | | | 3,45E+04 | |
| Geometry | | | | | | | |
| diameter | 800 mm | longitudinal | | | | A33 | |
| rolled section | - | reinforcement | | | | 24 # of bars | |
| steel plate | - | | | | | 32 ϕ [mm] | |
| Calculation | | Results | | | | | |
| <i>wide flange section</i> | | <i>equivalent column</i> | | | | | |
| A | 0,00E+00 mm2 | A;column | 5,03E+05 mm2 | | | | |
| E | 2,10E+05 MPa | EA;column | 2,07E+10 N/mm2 | | | | |
| <i>steel plate</i> | | | | | | | |
| A | 0,00E+00 mm2 | Δ EA due to steel | | | | 20% | |
| E | 2,10E+05 MPa | | | | | | |
| <i>longitudinal reinforcement</i> | | | | | | | |
| A | 1,93E+04 mm2 | | | | | | |
| E | 2,10E+05 MPa | | | | | | |
| <i>concrete</i> | | | | | | | |
| A | 4,83E+05 mm2 | | | | | | |
| E | 3,45E+04 MPa | | | | | | |

| Section | | | | S6A13-C30/40 | | | |
|-----------------------------------|--------------|--------------------------|----------------|--------------|--|----------------|--|
| Materials | | | fck [MPa] | | | E [MPa] | |
| rolled steel | S 355 | | 355 | | | 2,10E+05 | |
| mild steel | B 500 | | 500 | | | 2,10E+05 | |
| concrete | C 30/40 | | 30 | | | 3,19E+04 | |
| Geometry | | | | | | | |
| diameter | 600 mm | longitudinal | | | | A13 | |
| rolled section | - | reinforcement | | | | 12 # of bars | |
| steel plate | - | | | | | 32 ϕ [mm] | |
| Calculation | | Results | | | | | |
| <i>wide flange section</i> | | <i>equivalent column</i> | | | | | |
| A | 0,00E+00 mm2 | A;column | 2,83E+05 mm2 | | | | |
| E | 2,10E+05 MPa | EA;column | 1,07E+10 N/mm2 | | | | |
| <i>steel plate</i> | | | | | | | |
| A | 0,00E+00 mm2 | Δ EA due to steel | | | | 19% | |
| E | 2,10E+05 MPa | | | | | | |
| <i>longitudinal reinforcement</i> | | | | | | | |
| A | 9,65E+03 mm2 | | | | | | |
| E | 2,10E+05 MPa | | | | | | |
| <i>concrete</i> | | | | | | | |
| A | 2,73E+05 mm2 | | | | | | |
| E | 3,19E+04 MPa | | | | | | |

| Section | | | | S8A33-C70/85 | | | |
|-----------------------------------|--------------|--------------------------|----------------|--------------|--|----------------|--|
| Materials | | | fck [MPa] | | | E [MPa] | |
| rolled steel | S 355 | | 355 | | | 2,10E+05 | |
| mild steel | B 500 | | 500 | | | 2,10E+05 | |
| concrete | C 70/85 | | 70 | | | 4,06E+04 | |
| Geometry | | | | | | | |
| diameter | 800 mm | longitudinal | | | | A33 | |
| rolled section | - | reinforcement | | | | 24 # of bars | |
| steel plate | - | | | | | 32 ϕ [mm] | |
| Calculation | | Results | | | | | |
| <i>wide flange section</i> | | <i>equivalent column</i> | | | | | |
| A | 0,00E+00 mm2 | A;column | 5,03E+05 mm2 | | | | |
| E | 2,10E+05 MPa | EA;column | 2,37E+10 N/mm2 | | | | |
| <i>steel plate</i> | | | | | | | |
| A | 0,00E+00 mm2 | Δ EA due to steel | | | | 16% | |
| E | 2,10E+05 MPa | | | | | | |
| <i>longitudinal reinforcement</i> | | | | | | | |
| A | 1,93E+04 mm2 | | | | | | |
| E | 2,10E+05 MPa | | | | | | |
| <i>concrete</i> | | | | | | | |
| A | 4,83E+05 mm2 | | | | | | |
| E | 4,06E+04 MPa | | | | | | |

| Section | | | | S6A12-C30/40 | | | |
|-----------------------------------|--------------|--------------------------|----------------|--------------|--|----------------|--|
| Materials | | | fck [MPa] | | | E [MPa] | |
| rolled steel | S 355 | | 355 | | | 2,10E+05 | |
| mild steel | B 500 | | 500 | | | 2,10E+05 | |
| concrete | C 30/40 | | 30 | | | 3,19E+04 | |
| Geometry | | | | | | | |
| diameter | 600 mm | longitudinal | | | | A12 | |
| rolled section | - | reinforcement | | | | 12 # of bars | |
| steel plate | - | | | | | 25 ϕ [mm] | |
| Calculation | | Results | | | | | |
| <i>wide flange section</i> | | <i>equivalent column</i> | | | | | |
| A | 0,00E+00 mm2 | A;column | 2,83E+05 mm2 | | | | |
| E | 2,10E+05 MPa | EA;column | 1,01E+10 N/mm2 | | | | |
| <i>steel plate</i> | | | | | | | |
| A | 0,00E+00 mm2 | Δ EA due to steel | | | | 12% | |
| E | 2,10E+05 MPa | | | | | | |
| <i>longitudinal reinforcement</i> | | | | | | | |
| A | 5,89E+03 mm2 | | | | | | |
| E | 2,10E+05 MPa | | | | | | |
| <i>concrete</i> | | | | | | | |
| A | 2,77E+05 mm2 | | | | | | |
| E | 3,19E+04 MPa | | | | | | |

| Section | | | | S6A23-C30/40 | | | |
|-----------------------------------|--------------|--------------------------|----------------|--------------|--|----------------|--|
| Materials | | | fck [MPa] | | | E [MPa] | |
| rolled steel | S 355 | | 355 | | | 2,10E+05 | |
| mild steel | B 500 | | 500 | | | 2,10E+05 | |
| concrete | C 30/40 | | 30 | | | 3,19E+04 | |
| Geometry | | | | | | | |
| diameter | 600 mm | longitudinal | | | | A23 | |
| rolled section | - | reinforcement | | | | 18 # of bars | |
| steel plate | - | | | | | 32 ϕ [mm] | |
| Calculation | | Results | | | | | |
| <i>wide flange section</i> | | <i>equivalent column</i> | | | | | |
| A | 0,00E+00 mm2 | A;column | 2,83E+05 mm2 | | | | |
| E | 2,10E+05 MPa | EA;column | 1,16E+10 N/mm2 | | | | |
| <i>steel plate</i> | | | | | | | |
| A | 0,00E+00 mm2 | Δ EA due to steel | | | | 29% | |
| E | 2,10E+05 MPa | | | | | | |
| <i>longitudinal reinforcement</i> | | | | | | | |
| A | 1,45E+04 mm2 | | | | | | |
| E | 2,10E+05 MPa | | | | | | |
| <i>concrete</i> | | | | | | | |
| A | 2,68E+05 mm2 | | | | | | |
| E | 3,19E+04 MPa | | | | | | |

| Section | | | | S6A11-C30/40 | | | |
|-----------------------------------|--------------|--------------------------|----------------|--------------|--|----------------|--|
| Materials | | | fck [MPa] | | | E [MPa] | |
| rolled steel | S 355 | | 355 | | | 2,10E+05 | |
| mild steel | B 500 | | 500 | | | 2,10E+05 | |
| concrete | C 30/40 | | 30 | | | 3,19E+04 | |
| Geometry | | | | | | | |
| diameter | 600 mm | longitudinal | | | | A11 | |
| rolled section | - | reinforcement | | | | 12 # of bars | |
| steel plate | - | | | | | 20 ϕ [mm] | |
| Calculation | | Results | | | | | |
| <i>wide flange section</i> | | <i>equivalent column</i> | | | | | |
| A | 0,00E+00 mm2 | A;column | 2,83E+05 mm2 | | | | |
| E | 2,10E+05 MPa | EA;column | 9,70E+09 N/mm2 | | | | |
| <i>steel plate</i> | | | | | | | |
| A | 0,00E+00 mm2 | Δ EA due to steel | | | | 7% | |
| E | 2,10E+05 MPa | | | | | | |
| <i>longitudinal reinforcement</i> | | | | | | | |
| A | 3,77E+03 mm2 | | | | | | |
| E | 2,10E+05 MPa | | | | | | |
| <i>concrete</i> | | | | | | | |
| A | 2,79E+05 mm2 | | | | | | |
| E | 3,19E+04 MPa | | | | | | |

| Section | | R200-C70/85 | |
|----------------------------|--------------------------|----------------------------|--------------------------|
| Materials | | fck [MPa] | E [MPa] |
| mild steel | B 500 | 500 | 2,10E+05 |
| concrete | C 70/85 | 70 | 4,06E+04 |
| Geometry | | | |
| width | 1200 mm | longitudinal reinforcement | 40 # of bars |
| breadth | 1200 mm | | 32 ϕ [mm] |
| Calculation | | Results | |
| longitudinal reinforcement | | equivalent column | |
| A | 3,22E+04 mm ² | A;column | 1,44E+06 mm ² |
| E | 2,10E+05 MPa | EA;column | 6,39E+10 MPA |
| concrete | | | |
| A | 1,41E+06 mm ² | Δ EA due to steel | 9% |
| E | 4,06E+04 MPa | | |

| Section | | R3-C40/50 | |
|----------------------------|--------------------------|----------------------------|----------------------------|
| Materials | | fck [MPa] | E [MPa] |
| mild steel | B 500 | 500 | 2,10E+05 |
| concrete | C 40/50 | 40 | 3,45E+04 |
| Geometry | | | |
| width | 600 mm | longitudinal reinforcement | 10 # of bars |
| breadth | 400 mm | | 16 ϕ [mm] |
| Calculation | | Results | |
| longitudinal reinforcement | | equivalent column | |
| A | 2,01E+03 mm ² | A;column | 2,40E+05 mm ² |
| E | 2,10E+05 MPa | EA;column | 8,64E+09 N/mm ² |
| concrete | | | |
| A | 2,38E+05 mm ² | Δ EA due to steel | 4% |
| E | 3,45E+04 MPa | | |

| Section | | R800-C30/40 | |
|----------------------------|--------------------------|----------------------------|----------------------------|
| Materials | | fck [MPa] | E [MPa] |
| mild steel | B 500 | 500 | 2,10E+05 |
| concrete | C 30/40 | 30 | 3,19E+04 |
| Geometry | | | |
| width | 800 mm | longitudinal reinforcement | 24 # of bars |
| breadth | 600 mm | | 25 ϕ [mm] |
| Calculation | | Results | |
| longitudinal reinforcement | | equivalent column | |
| A | 1,18E+04 mm ² | A;column | 4,80E+05 mm ² |
| E | 2,10E+05 MPa | EA;column | 1,74E+10 N/mm ² |
| concrete | | | |
| A | 4,68E+05 mm ² | Δ EA due to steel | 14% |
| E | 3,19E+04 MPa | | |

| Section | | R4-C40/50 | |
|----------------------------|--------------------------|----------------------------|----------------------------|
| Materials | | fck [MPa] | E [MPa] |
| mild steel | B 500 | 500 | 2,10E+05 |
| concrete | C 40/50 | 40 | 3,45E+04 |
| Geometry | | | |
| width | 700 mm | longitudinal reinforcement | 12 # of bars |
| breadth | 400 mm | | 16 ϕ [mm] |
| Calculation | | Results | |
| longitudinal reinforcement | | equivalent column | |
| A | 2,41E+03 mm ² | A;column | 2,80E+05 mm ² |
| E | 2,10E+05 MPa | EA;column | 1,01E+10 N/mm ² |
| concrete | | | |
| A | 2,78E+05 mm ² | Δ EA due to steel | 4% |
| E | 3,45E+04 MPa | | |

| Section | | R1-C40/50 | |
|----------------------------|--------------------------|----------------------------|----------------------------|
| Materials | | fck [MPa] | E [MPa] |
| mild steel | B 500 | 500 | 2,10E+05 |
| concrete | C 40/50 | 40 | 3,45E+04 |
| Geometry | | | |
| width | 400 mm | longitudinal reinforcement | 8 # of bars |
| breadth | 400 mm | | 16 ϕ [mm] |
| Calculation | | Results | |
| longitudinal reinforcement | | equivalent column | |
| A | 1,61E+03 mm ² | A;column | 1,60E+05 mm ² |
| E | 2,10E+05 MPa | EA;column | 5,81E+09 N/mm ² |
| concrete | | | |
| A | 1,58E+05 mm ² | Δ EA due to steel | 5% |
| E | 3,45E+04 MPa | | |

| Section | | R5-C40/50 | |
|----------------------------|--------------------------|----------------------------|----------------------------|
| Materials | | fck [MPa] | E [MPa] |
| mild steel | B 500 | 500 | 2,10E+05 |
| concrete | C 40/50 | 40 | 3,45E+04 |
| Geometry | | | |
| width | 800 mm | longitudinal reinforcement | 12 # of bars |
| breadth | 400 mm | | 16 ϕ [mm] |
| Calculation | | Results | |
| longitudinal reinforcement | | equivalent column | |
| A | 2,41E+03 mm ² | A;column | 3,20E+05 mm ² |
| E | 2,10E+05 MPa | EA;column | 1,15E+10 N/mm ² |
| concrete | | | |
| A | 3,18E+05 mm ² | Δ EA due to steel | 4% |
| E | 3,45E+04 MPa | | |

| Section | | R2-C40/50 | |
|----------------------------|--------------------------|----------------------------|----------------------------|
| Materials | | fck [MPa] | E [MPa] |
| mild steel | B 500 | 500 | 2,10E+05 |
| concrete | C 40/50 | 40 | 3,45E+04 |
| Geometry | | | |
| width | 500 mm | longitudinal reinforcement | 10 # of bars |
| breadth | 400 mm | | 16 ϕ [mm] |
| Calculation | | Results | |
| longitudinal reinforcement | | equivalent column | |
| A | 2,01E+03 mm ² | A;column | 2,00E+05 mm ² |
| E | 2,10E+05 MPa | EA;column | 7,26E+09 N/mm ² |
| concrete | | | |
| A | 1,98E+05 mm ² | Δ EA due to steel | 5% |
| E | 3,45E+04 MPa | | |

| Section | | R10-C40/50 | |
|----------------------------|--------------------------|----------------------------|----------------------------|
| Materials | | fck [MPa] | E [MPa] |
| mild steel | B 500 | 500 | 2,10E+05 |
| concrete | C 40/50 | 40 | 3,45E+04 |
| Geometry | | | |
| width | 250 mm | longitudinal reinforcement | 4 # of bars |
| breadth | 250 mm | | 16 ϕ [mm] |
| Calculation | | Results | |
| longitudinal reinforcement | | equivalent column | |
| A | 8,04E+02 mm ² | A;column | 6,25E+04 mm ² |
| E | 2,10E+05 MPa | EA;column | 2,30E+09 N/mm ² |
| concrete | | | |
| A | 6,17E+04 mm ² | Δ EA due to steel | 7% |
| E | 3,45E+04 MPa | | |

| Section R20-C40/50 | | | |
|----------------------------|--------------------------|--------------------------|----------------------------|
| Materials | | fck [MPa] | E [MPa] |
| mild steel | B 500 | 500 | 2,10E+05 |
| concrete | C 40/50 | 40 | 3,45E+04 |
| Geometry | | | |
| width | 900 mm | longitudinal | 14 # of bars |
| breadth | 300 mm | reinforcement | 16 ϕ [mm] |
| Calculation | | Results | |
| longitudinal reinforcement | | equivalent column | |
| A | 2,81E+03 mm ² | A;column | 2,70E+05 mm ² |
| E | 2,10E+05 MPa | EA;column | 9,82E+09 N/mm ² |
| concrete | | | |
| A | 2,67E+05 mm ² | Δ EA due to steel | 5% |
| E | 3,45E+04 MPa | | |
| Section R21-C40/50 | | | |
| Materials | | fck [MPa] | E [MPa] |
| mild steel | B 500 | 500 | 2,10E+05 |
| concrete | C 40/50 | 40 | 3,45E+04 |
| Geometry | | | |
| width | 450 mm | longitudinal | 8 # of bars |
| breadth | 300 mm | reinforcement | 16 ϕ [mm] |
| Calculation | | Results | |
| longitudinal reinforcement | | equivalent column | |
| A | 1,61E+03 mm ² | A;column | 1,35E+05 mm ² |
| E | 2,10E+05 MPa | EA;column | 4,94E+09 N/mm ² |
| concrete | | | |
| A | 1,33E+05 mm ² | Δ EA due to steel | 6% |
| E | 3,45E+04 MPa | | |
| Section R30-C40/50 | | | |
| Materials | | fck [MPa] | E [MPa] |
| mild steel | B 500 | 500 | 2,10E+05 |
| concrete | C 40/50 | 40 | 3,45E+04 |
| Geometry | | | |
| width | 400 mm | longitudinal | 8 # of bars |
| breadth | 400 mm | reinforcement | 16 ϕ [mm] |
| Calculation | | Results | |
| longitudinal reinforcement | | equivalent column | |
| A | 1,61E+03 mm ² | A;column | 1,60E+05 mm ² |
| E | 2,10E+05 MPa | EA;column | 5,81E+09 N/mm ² |
| concrete | | | |
| A | 1,58E+05 mm ² | Δ EA due to steel | 5% |
| E | 3,45E+04 MPa | | |

Lateral core NY1

In what follows the effective axial stiffness is calculated for the shear walls composing the lateral core NY1, according to the sections defined in figure III.2-2.

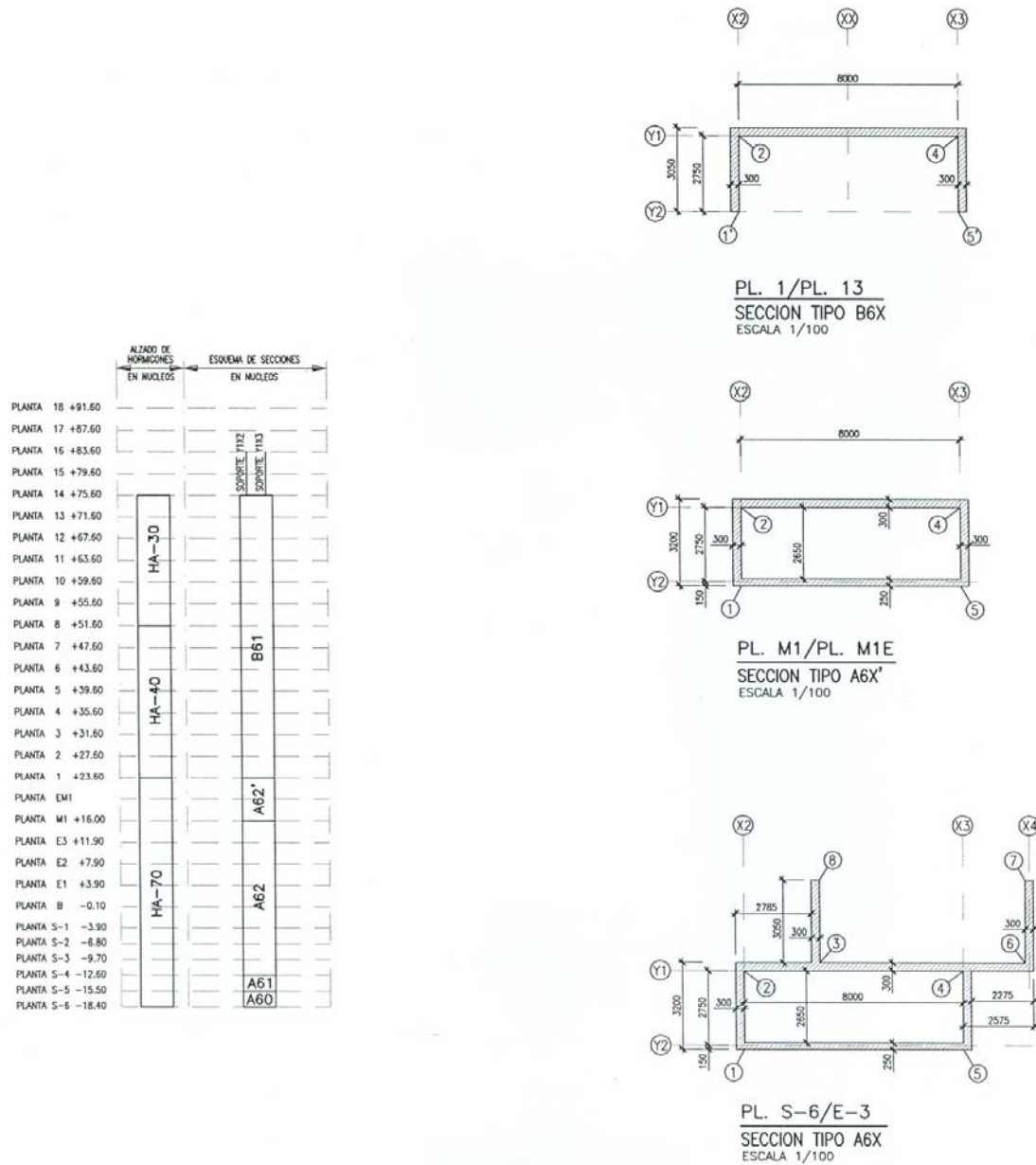


Figure III.2-2: Lateral core sections

| Section | NY1-A60 | Shear wall | 250 mm |
|----------------------------|--------------|----------------------------|--------------------------------|
| Materials | | | |
| mild steel | B 500 | fck [MPa] 500 | E [MPa] 2,10E+05 |
| concrete | C 70/85 | 70 | 4,06E+04 |
| Geometry | | | |
| thickness | 250 mm | longitudinal reinforcement | ϕ [mm] ctc [mm] 25 100 |
| width considered | 1000 mm | | 25 100 |
| | | | 0 100 |
| Calculation | | Results | |
| longitudinal reinforcement | | equivalent wall | |
| A | 9,82E+03 mm2 | A;wall | 2,50E+05 mm2 |
| E | 2,10E+05 MPa | EA;wall | 1,18E+10 MPa |
| concrete | | | |
| A | 2,40E+05 mm2 | Δ EA due to steel | 16% |
| E | 4,06E+04 MPa | | |

| Section | NY1-A60 | Shear wall | 300 mm |
|----------------------------|--------------|----------------------------|--------------------------------|
| Materials | | | |
| mild steel | B 500 | fck [MPa] 500 | E [MPa] 2,10E+05 |
| concrete | C 70/85 | 70 | 4,06E+04 |
| Geometry | | | |
| thickness | 300 mm | longitudinal reinforcement | ϕ [mm] ctc [mm] 25 100 |
| width considered | 1000 mm | | 25 100 |
| | | | 0 100 |
| Calculation | | Results | |
| longitudinal reinforcement | | equivalent wall | |
| A | 9,82E+03 mm2 | A;wall | 3,00E+05 mm2 |
| E | 2,10E+05 MPa | EA;wall | 1,38E+10 MPa |
| concrete | | | |
| A | 2,90E+05 mm2 | Δ EA due to steel | 14% |
| E | 4,06E+04 MPa | | |

| Section | NY1-A61 | Shear wall | 250 mm |
|----------------------------|--------------|----------------------------|--------------------------------|
| Materials | | | |
| mild steel | B 500 | fck [MPa] 500 | E [MPa] 2,10E+05 |
| concrete | C 70/85 | 70 | 4,06E+04 |
| Geometry | | | |
| thickness | 250 mm | longitudinal reinforcement | ϕ [mm] ctc [mm] 25 200 |
| width considered | 1000 mm | | 25 200 |
| | | | 0 100 |
| Calculation | | Results | |
| longitudinal reinforcement | | equivalent wall | |
| A | 4,91E+03 mm2 | A;wall | 2,50E+05 mm2 |
| E | 2,10E+05 MPa | EA;wall | 1,10E+10 MPa |
| concrete | | | |
| A | 2,45E+05 mm2 | Δ EA due to steel | 8% |
| E | 4,06E+04 MPa | | |

| Section | NY1-A61 | Shear wall | 300 mm |
|----------------------------|--------------|----------------------------|--------------------------------|
| Materials | | | |
| mild steel | B 500 | fck [MPa] 500 | E [MPa] 2,10E+05 |
| concrete | C 70/85 | 70 | 4,06E+04 |
| Geometry | | | |
| thickness | 300 mm | longitudinal reinforcement | ϕ [mm] ctc [mm] 25 200 |
| width considered | 1000 mm | | 25 200 |
| | | | 0 100 |
| Calculation | | Results | |
| longitudinal reinforcement | | equivalent wall | |
| A | 4,91E+03 mm2 | A;wall | 3,00E+05 mm2 |
| E | 2,10E+05 MPa | EA;wall | 1,30E+10 MPa |
| concrete | | | |
| A | 2,95E+05 mm2 | Δ EA due to steel | 7% |
| E | 4,06E+04 MPa | | |

| Section | NY1-A62 | Shear wall | 250 mm |
|----------------------------|--------------|----------------------------|--------------------------------|
| Materials | | | |
| mild steel | B 500 | fck [MPa] 500 | E [MPa] 2,10E+05 |
| concrete | C 70/85 | 70 | 4,06E+04 |
| Geometry | | | |
| thickness | 250 mm | longitudinal reinforcement | ϕ [mm] ctc [mm] 20 200 |
| width considered | 1000 mm | | 20 200 |
| | | | 0 100 |
| Calculation | | Results | |
| longitudinal reinforcement | | equivalent wall | |
| A | 3,14E+03 mm2 | A;wall | 2,50E+05 mm2 |
| E | 2,10E+05 MPa | EA;wall | 1,07E+10 MPa |
| concrete | | | |
| A | 2,47E+05 mm2 | Δ EA due to steel | 5% |
| E | 4,06E+04 MPa | | |

| Section | NY1-A62 | Shear wall | 300 mm |
|----------------------------|--------------|----------------------------|--------------------------------|
| Materials | | | |
| mild steel | B 500 | fck [MPa] 500 | E [MPa] 2,10E+05 |
| concrete | C 70/85 | 70 | 4,06E+04 |
| Geometry | | | |
| thickness | 300 mm | longitudinal reinforcement | ϕ [mm] ctc [mm] 20 200 |
| width considered | 1000 mm | | 20 200 |
| | | | 0 100 |
| Calculation | | Results | |
| longitudinal reinforcement | | equivalent wall | |
| A | 3,14E+03 mm2 | A;wall | 3,00E+05 mm2 |
| E | 2,10E+05 MPa | EA;wall | 1,27E+10 MPa |
| concrete | | | |
| A | 2,97E+05 mm2 | Δ EA due to steel | 4% |
| E | 4,06E+04 MPa | | |

| Section | NY1-B61 | Shear wall | 300 mm |
|----------------------------|--------------|----------------------------|--------------------------------|
| Materials | | | |
| mild steel | B 500 | fck [MPa] 500 | E [MPa] 2,10E+05 |
| concrete | C 40/50 | 40 | 3,45E+04 |
| Geometry | | | |
| thickness | 300 mm | longitudinal reinforcement | ϕ [mm] ctc [mm] 16 200 |
| width considered | 1000 mm | | 16 200 |
| | | | 0 100 |
| Calculation | | Results | |
| longitudinal reinforcement | | equivalent wall | |
| A | 2,01E+03 mm2 | A;wall | 3,00E+05 mm2 |
| E | 2,10E+05 MPa | EA;wall | 1,07E+10 MPa |
| concrete | | | |
| A | 2,98E+05 mm2 | Δ EA due to steel | 3% |
| E | 3,45E+04 MPa | | |

Central core NC

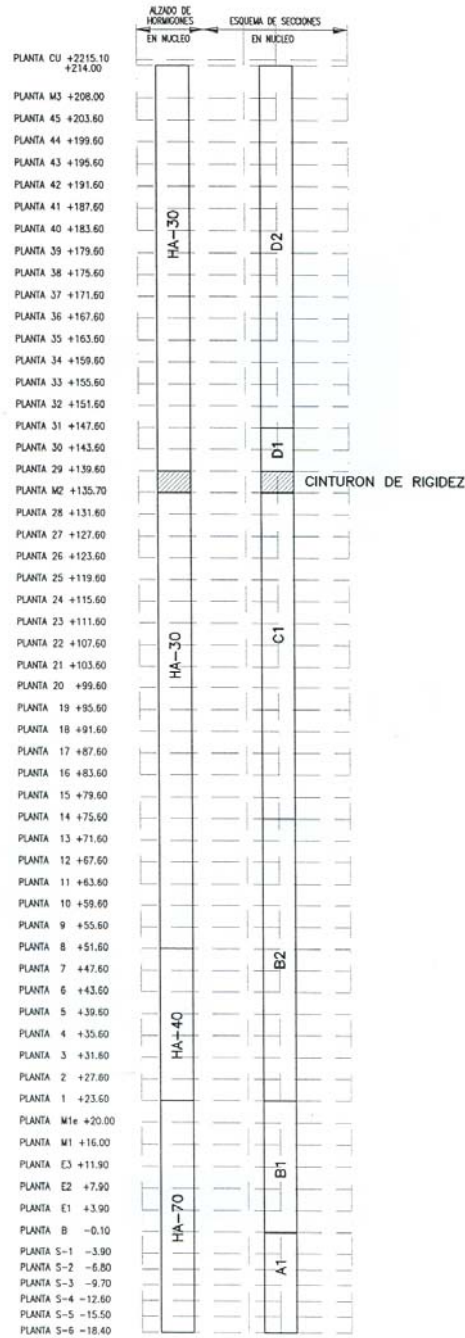


Figure III.2-3 and III.2-4 show the schematically the core sections in elevation and section respectively.

Hereafter, the effective axial stiffness of these core sections is computed.

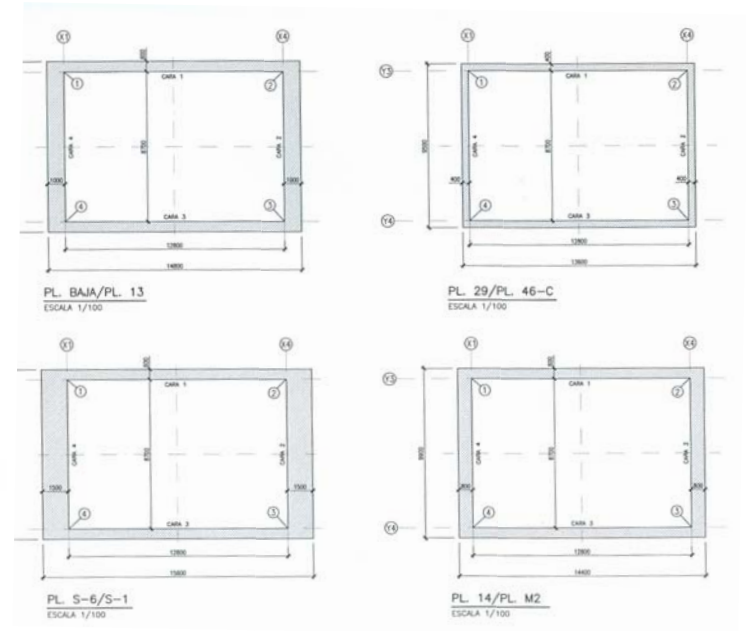


Figure III.2-3: Central core sections in plan

Figure III.2-4: Central core sections in elevation

| Section | NC-A1 | Shear wall | 2 and 4 |
|----------------------------|--------------------------|----------------------------|--------------------------|
| Materials | | fck [MPa] | E [MPa] |
| mild steel | B 500 | 500 | 2,10E+05 |
| concrete | C 70/85 | 70 | 4,06E+04 |
| Geometry | | | φ [mm] ctc [mm] |
| thickness | 1500 mm | longitudinal reinforcement | 32 100 |
| width considered | 1000 mm | | 32 100 |
| | | | 25 100 |
| Calculation | | Results | |
| longitudinal reinforcement | | equivalent wall | |
| A | 2,10E+04 mm ² | A;wall | 1,50E+06 mm ² |
| E | 2,10E+05 MPa | EA;wall | 6,44E+10 MPa |
| concrete | | | |
| A | 1,48E+06 mm ² | Δ EA due to steel | 6% |
| E | 4,06E+04 MPa | | |

| Section | NC-B2-C40/50 | Shear wall | 2 and 4 |
|----------------------------|--------------------------|----------------------------|--------------------------|
| Materials | | fck [MPa] | E [MPa] |
| mild steel | B 500 | 500 | 2,10E+05 |
| concrete | C 40/50 | 40 | 3,45E+04 |
| Geometry | | | φ [mm] ctc [mm] |
| thickness | 1000 mm | longitudinal reinforcement | 32 100 |
| width considered | 1000 mm | | 25 100 |
| | | | |
| Calculation | | Results | |
| longitudinal reinforcement | | equivalent wall | |
| A | 1,30E+04 mm ² | A;wall | 1,00E+06 mm ² |
| E | 2,10E+05 MPa | EA;wall | 3,68E+10 MPa |
| concrete | | | |
| A | 9,87E+05 mm ² | Δ EA due to steel | 7% |
| E | 3,45E+04 MPa | | |

| Section | NC-A1 | Shear wall | 1 and 3 |
|----------------------------|--------------------------|----------------------------|--------------------------|
| Materials | | fck [MPa] | E [MPa] |
| mild steel | B 500 | 500 | 2,10E+05 |
| concrete | C 70/85 | 70 | 4,06E+04 |
| Geometry | | | φ [mm] ctc [mm] |
| thickness | 600 mm | longitudinal reinforcement | 20 200 |
| width considered | 1000 mm | | 20 200 |
| | | | |
| Calculation | | Results | |
| longitudinal reinforcement | | equivalent wall | |
| A | 3,14E+03 mm ² | A;wall | 6,00E+05 mm ² |
| E | 2,10E+05 MPa | EA;wall | 2,49E+10 MPa |
| concrete | | | |
| A | 5,97E+05 mm ² | Δ EA due to steel | 2% |
| E | 4,06E+04 MPa | | |

| Section | NC-B2-C40/50 | Shear wall | 1 and 3 |
|----------------------------|--------------------------|----------------------------|--------------------------|
| Materials | | fck [MPa] | E [MPa] |
| mild steel | B 500 | 500 | 2,10E+05 |
| concrete | C 40/50 | 40 | 3,45E+04 |
| Geometry | | | φ [mm] ctc [mm] |
| thickness | 600 mm | longitudinal reinforcement | 20 200 |
| width considered | 1000 mm | | 20 200 |
| | | | |
| Calculation | | Results | |
| longitudinal reinforcement | | equivalent wall | |
| A | 3,14E+03 mm ² | A;wall | 6,00E+05 mm ² |
| E | 2,10E+05 MPa | EA;wall | 2,13E+10 MPa |
| concrete | | | |
| A | 5,97E+05 mm ² | Δ EA due to steel | 3% |
| E | 3,45E+04 MPa | | |

| Section | NC-B1 | Shear wall | 2 and 4 |
|----------------------------|--------------------------|----------------------------|--------------------------|
| Materials | | fck [MPa] | E [MPa] |
| mild steel | B 500 | 500 | 2,10E+05 |
| concrete | C 70/85 | 70 | 4,06E+04 |
| Geometry | | | φ [mm] ctc [mm] |
| thickness | 1000 mm | longitudinal reinforcement | 32 100 |
| width considered | 1000 mm | | 25 100 |
| | | | 25 100 |
| Calculation | | Results | |
| longitudinal reinforcement | | equivalent wall | |
| A | 1,79E+04 mm ² | A;wall | 1,00E+06 mm ² |
| E | 2,10E+05 MPa | EA;wall | 4,36E+10 MPa |
| concrete | | | |
| A | 9,82E+05 mm ² | Δ EA due to steel | 7% |
| E | 4,06E+04 MPa | | |

| Section | NC-B2-C30/40 | Shear wall | 2 and 4 |
|----------------------------|--------------------------|----------------------------|--------------------------|
| Materials | | fck [MPa] | E [MPa] |
| mild steel | B 500 | 500 | 2,10E+05 |
| concrete | C 30/40 | 30 | 3,19E+04 |
| Geometry | | | φ [mm] ctc [mm] |
| thickness | 1000 mm | longitudinal reinforcement | 32 100 |
| width considered | 1000 mm | | 25 100 |
| | | | |
| Calculation | | Results | |
| longitudinal reinforcement | | equivalent wall | |
| A | 1,30E+04 mm ² | A;wall | 1,00E+06 mm ² |
| E | 2,10E+05 MPa | EA;wall | 3,42E+10 MPa |
| concrete | | | |
| A | 9,87E+05 mm ² | Δ EA due to steel | 7% |
| E | 3,19E+04 MPa | | |

| Section | NC-B1 | Shear wall | 1 and 3 |
|----------------------------|--------------------------|----------------------------|--------------------------|
| Materials | | fck [MPa] | E [MPa] |
| mild steel | B 500 | 500 | 2,10E+05 |
| concrete | C 70/85 | 70 | 4,06E+04 |
| Geometry | | | φ [mm] ctc [mm] |
| thickness | 600 mm | longitudinal reinforcement | 20 200 |
| width considered | 1000 mm | | 20 200 |
| | | | |
| Calculation | | Results | |
| longitudinal reinforcement | | equivalent wall | |
| A | 3,14E+03 mm ² | A;wall | 6,00E+05 mm ² |
| E | 2,10E+05 MPa | EA;wall | 2,49E+10 MPa |
| concrete | | | |
| A | 5,97E+05 mm ² | Δ EA due to steel | 2% |
| E | 4,06E+04 MPa | | |

| Section | NC-B2-C30/40 | Shear wall | 1 and 3 |
|----------------------------|--------------------------|----------------------------|--------------------------|
| Materials | | fck [MPa] | E [MPa] |
| mild steel | B 500 | 500 | 2,10E+05 |
| concrete | C 30/40 | 30 | 3,19E+04 |
| Geometry | | | φ [mm] ctc [mm] |
| thickness | 600 mm | longitudinal reinforcement | 20 200 |
| width considered | 1000 mm | | 20 200 |
| | | | |
| Calculation | | Results | |
| longitudinal reinforcement | | equivalent wall | |
| A | 3,14E+03 mm ² | A;wall | 6,00E+05 mm ² |
| E | 2,10E+05 MPa | EA;wall | 1,97E+10 MPa |
| concrete | | | |
| A | 5,97E+05 mm ² | Δ EA due to steel | 3% |
| E | 3,19E+04 MPa | | |

| Section | NC-C1 | Shear wall | 2 and 4 | |
|----------------------------|--------------------------|----------------------------|----------|-----------------|
| Materials | | fck [MPa] | E [MPa] | |
| mild steel | B 500 | 500 | 2,10E+05 | |
| concrete | C 30/40 | 30 | 3,19E+04 | |
| Geometry | | | φ [mm] | ctc [mm] |
| thickness | 800 mm | longitudinal reinforcement | 25 | 100 |
| width | | | 16 | 100 |
| considered | 1000 mm | | | |
| Calculation | | Results | | |
| longitudinal reinforcement | | equivalent wall | | |
| A | 6,92E+03 mm ² | A;wall | 8,00E+05 | mm ² |
| E | 2,10E+05 MPa | EA;wall | 2,68E+10 | MPa |
| concrete | | | | |
| A | 7,93E+05 mm ² | Δ EA due to steel | 5% | |
| E | 3,19E+04 MPa | | | |

| Core | NC-D2 | Shear wall | 2 and 4 | |
|----------------------------|--------------------------|----------------------------|----------|-----------------|
| Materials | | fck [MPa] | E [MPa] | |
| mild steel | B 500 | 500 | 2,10E+05 | |
| concrete | C 30/40 | 30 | 3,19E+04 | |
| Geometry | | | φ [mm] | ctc [mm] |
| thickness | 400 mm | longitudinal reinforcement | 20 | 200 |
| width | | | 16 | 200 |
| considered | 1000 mm | | | |
| Calculation | | Results | | |
| longitudinal reinforcement | | equivalent wall | | |
| A | 2,58E+03 mm ² | A;wall | 4,00E+05 | mm ² |
| E | 2,10E+05 MPa | EA;wall | 1,32E+10 | MPa |
| concrete | | | | |
| A | 3,97E+05 mm ² | Δ EA due to steel | 4% | |
| E | 3,19E+04 MPa | | | |

| Section | NC-C1 | Shear wall | 1 and 3 | |
|----------------------------|--------------------------|----------------------------|----------|-----------------|
| Materials | | fck [MPa] | E [MPa] | |
| mild steel | B 500 | 500 | 2,10E+05 | |
| concrete | C 30/40 | 30 | 3,19E+04 | |
| Geometry | | | φ [mm] | ctc [mm] |
| thickness | 600 mm | longitudinal reinforcement | 20 | 200 |
| width | | | 20 | 200 |
| considered | 1000 mm | | | |
| Calculation | | Results | | |
| longitudinal reinforcement | | equivalent wall | | |
| A | 3,14E+03 mm ² | A;wall | 6,00E+05 | mm ² |
| E | 2,10E+05 MPa | EA;wall | 1,97E+10 | MPa |
| concrete | | | | |
| A | 5,97E+05 mm ² | Δ EA due to steel | 3% | |
| E | 3,19E+04 MPa | | | |

| Core | NC-D2 | Shear wall | 1 and 3 | |
|----------------------------|--------------------------|----------------------------|----------|-----------------|
| Materials | | fck [MPa] | E [MPa] | |
| mild steel | B 500 | 500 | 2,10E+05 | |
| concrete | C 30/40 | 30 | 3,19E+04 | |
| Geometry | | | φ [mm] | ctc [mm] |
| thickness | 400 mm | longitudinal reinforcement | 16 | 200 |
| width | | | 16 | 200 |
| considered | 1000 mm | | | |
| Calculation | | Results | | |
| longitudinal reinforcement | | equivalent wall | | |
| A | 2,01E+03 mm ² | A;wall | 4,00E+05 | mm ² |
| E | 2,10E+05 MPa | EA;wall | 1,31E+10 | MPa |
| concrete | | | | |
| A | 3,98E+05 mm ² | Δ EA due to steel | 3% | |
| E | 3,19E+04 MPa | | | |

| Core | NC-D1 | Shear wall | 2 and 4 | |
|----------------------------|--------------------------|----------------------------|----------|-----------------|
| Materials | | fck [MPa] | E [MPa] | |
| mild steel | B 500 | 500 | 2,10E+05 | |
| concrete | C 30/40 | 30 | 3,19E+04 | |
| Geometry | | | φ [mm] | ctc [mm] |
| thickness | 400 mm | longitudinal reinforcement | 20 | 200 |
| width | | | 20 | 200 |
| considered | 1000 mm | | | |
| Calculation | | Results | | |
| longitudinal reinforcement | | equivalent wall | | |
| A | 3,14E+03 mm ² | A;wall | 4,00E+05 | mm ² |
| E | 2,10E+05 MPa | EA;wall | 1,33E+10 | MPa |
| concrete | | | | |
| A | 3,97E+05 mm ² | Δ EA due to steel | 4% | |
| E | 3,19E+04 MPa | | | |

| Core | NC-D1 | Shear wall | 1 and 3 | |
|----------------------------|--------------------------|----------------------------|----------|-----------------|
| Materials | | fck [MPa] | E [MPa] | |
| mild steel | B 500 | 500 | 2,10E+05 | |
| concrete | C 30/40 | 30 | 3,19E+04 | |
| Geometry | | | φ [mm] | ctc [mm] |
| thickness | 400 mm | longitudinal reinforcement | 20 | 200 |
| width | | | 20 | 200 |
| considered | 1000 mm | | | |
| Calculation | | Results | | |
| longitudinal reinforcement | | equivalent wall | | |
| A | 3,14E+03 mm ² | A;wall | 4,00E+05 | mm ² |
| E | 2,10E+05 MPa | EA;wall | 1,33E+10 | MPa |
| concrete | | | | |
| A | 3,97E+05 mm ² | Δ EA due to steel | 4% | |
| E | 3,19E+04 MPa | | | |

Lateral core NY6

Hereafter, the effective axial stiffness is calculated for the shear walls composing the lateral core NY6, according to the sections defined in figure III.2-5.

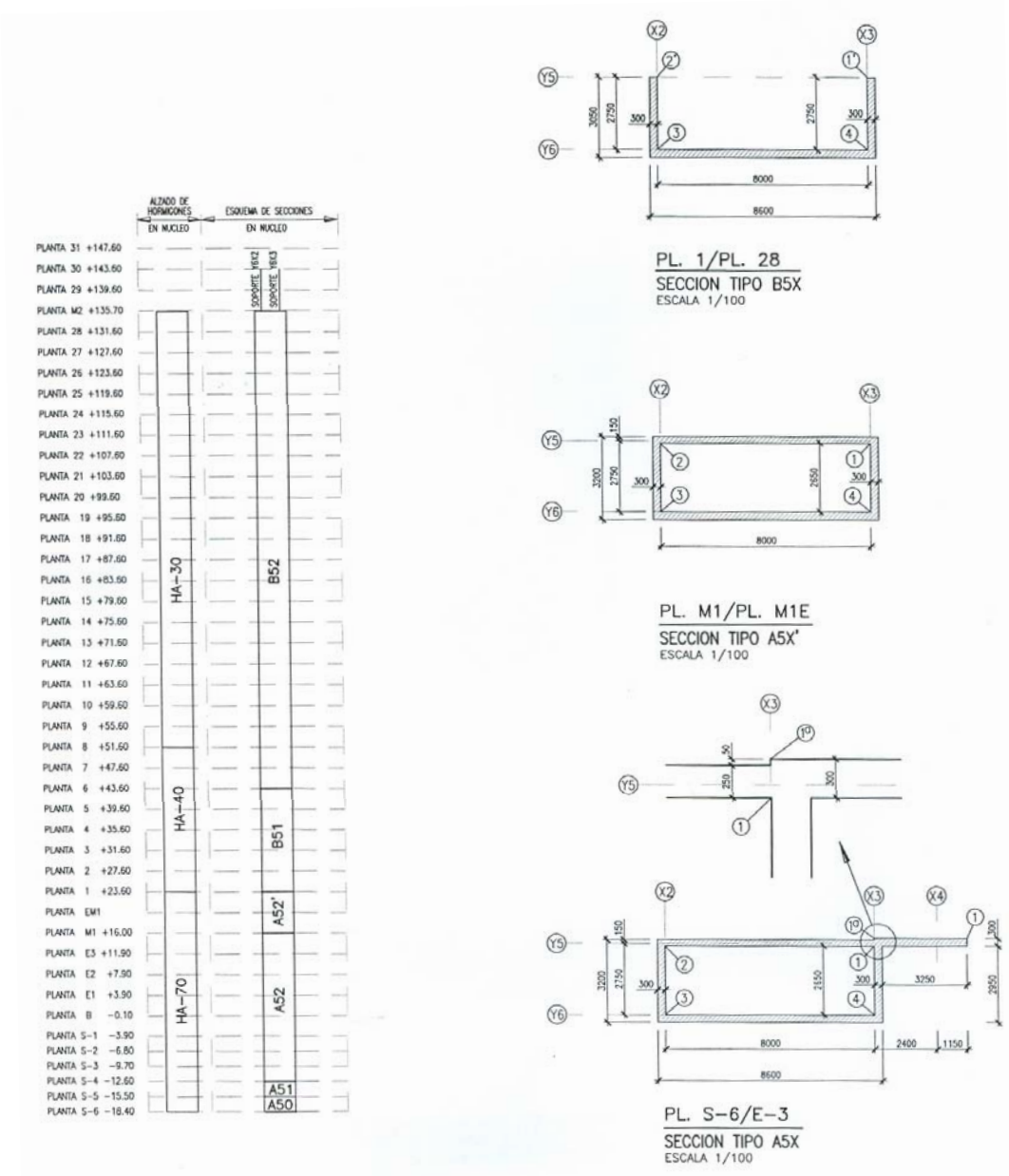


Figure III.2-5: Lateral core sections

| Section | NY6-A50 | Shear wall | all | |
|----------------------------|--------------|----------------------------|----------------|------------------|
| Materials | | | | |
| mild steel | B 500 | fck [MPa] | 500 | E [MPa] 2,10E+05 |
| concrete | C 70/85 | | 70 | 4,06E+04 |
| Geometry | | | | |
| thickness | 300 mm | longitudinal reinforcement | φ [mm] | ctc [mm] |
| width considered | 1000 mm | | 25 | 100 |
| | | | 25 | 100 |
| | | | 0 | 100 |
| Calculation | | | Results | |
| longitudinal reinforcement | | equivalent wall | | |
| A | 9,82E+03 mm2 | A;wall | 3,00E+05 mm2 | |
| E | 2,10E+05 MPa | EA;wall | 1,38E+10 MPa | |
| concrete | | | | |
| A | 2,90E+05 mm2 | Δ EA due to steel | 14% | |
| E | 4,06E+04 MPa | | | |

| Section | NY6-B52-C40/50 | Shear wall | all | |
|----------------------------|----------------|----------------------------|----------------|------------------|
| Materials | | | | |
| mild steel | B 500 | fck [MPa] | 500 | E [MPa] 2,10E+05 |
| concrete | C 40/50 | | 40 | 3,45E+04 |
| Geometry | | | | |
| thickness | 300 mm | longitudinal reinforcement | φ [mm] | ctc [mm] |
| width considered | 1000 mm | | 16 | 200 |
| | | | 16 | 200 |
| | | | 0 | 100 |
| Calculation | | | Results | |
| longitudinal reinforcement | | equivalent wall | | |
| A | 2,01E+03 mm2 | A;wall | 3,00E+05 mm2 | |
| E | 2,10E+05 MPa | EA;wall | 1,07E+10 MPa | |
| concrete | | | | |
| A | 2,98E+05 mm2 | Δ EA due to steel | 3% | |
| E | 3,45E+04 MPa | | | |

| Section | NY6-A51 | Shear wall | all | |
|----------------------------|--------------|----------------------------|----------------|------------------|
| Materials | | | | |
| mild steel | B 500 | fck [MPa] | 500 | E [MPa] 2,10E+05 |
| concrete | C 70/85 | | 70 | 4,06E+04 |
| Geometry | | | | |
| thickness | 300 mm | longitudinal reinforcement | φ [mm] | ctc [mm] |
| width considered | 1000 mm | | 25 | 200 |
| | | | 25 | 200 |
| | | | 0 | 100 |
| Calculation | | | Results | |
| longitudinal reinforcement | | equivalent wall | | |
| A | 4,91E+03 mm2 | A;wall | 3,00E+05 mm2 | |
| E | 2,10E+05 MPa | EA;wall | 1,30E+10 MPa | |
| concrete | | | | |
| A | 2,95E+05 mm2 | Δ EA due to steel | 7% | |
| E | 4,06E+04 MPa | | | |

| Section | NY6-B52-C30/37 | Shear wall | all | |
|----------------------------|----------------|----------------------------|----------------|------------------|
| Materials | | | | |
| mild steel | B 500 | fck [MPa] | 500 | E [MPa] 2,10E+05 |
| concrete | C 30/37 | | 0 | 1,90E+04 |
| Geometry | | | | |
| thickness | 300 mm | longitudinal reinforcement | φ [mm] | ctc [mm] |
| width considered | 1000 mm | | 16 | 200 |
| | | | 16 | 200 |
| | | | 0 | 100 |
| Calculation | | | Results | |
| longitudinal reinforcement | | equivalent wall | | |
| A | 2,01E+03 mm2 | A;wall | 3,00E+05 mm2 | |
| E | 2,10E+05 MPa | EA;wall | 6,08E+09 MPa | |
| concrete | | | | |
| A | 2,98E+05 mm2 | Δ EA due to steel | 7% | |
| E | 1,90E+04 MPa | | | |

| Section | NY6-A52 | Shear wall | all | |
|----------------------------|--------------|----------------------------|----------------|------------------|
| Materials | | | | |
| mild steel | B 500 | fck [MPa] | 500 | E [MPa] 2,10E+05 |
| concrete | C 70/85 | | 70 | 4,06E+04 |
| Geometry | | | | |
| thickness | 300 mm | longitudinal reinforcement | φ [mm] | ctc [mm] |
| width considered | 1000 mm | | 20 | 200 |
| | | | 20 | 200 |
| | | | 0 | 100 |
| Calculation | | | Results | |
| longitudinal reinforcement | | equivalent wall | | |
| A | 3,14E+03 mm2 | A;wall | 3,00E+05 mm2 | |
| E | 2,10E+05 MPa | EA;wall | 1,27E+10 MPa | |
| concrete | | | | |
| A | 2,97E+05 mm2 | Δ EA due to steel | 4% | |
| E | 4,06E+04 MPa | | | |

| Section | NY6-B51 | Shear wall | all | |
|----------------------------|--------------|----------------------------|----------------|------------------|
| Materials | | | | |
| mild steel | B 500 | fck [MPa] | 500 | E [MPa] 2,10E+05 |
| concrete | C 40/50 | | 40 | 3,45E+04 |
| Geometry | | | | |
| thickness | 300 mm | longitudinal reinforcement | φ [mm] | ctc [mm] |
| width considered | 1000 mm | | 20 | 200 |
| | | | 20 | 200 |
| | | | 0 | 100 |
| Calculation | | | Results | |
| longitudinal reinforcement | | equivalent wall | | |
| A | 3,14E+03 mm2 | A;wall | 3,00E+05 mm2 | |
| E | 2,10E+05 MPa | EA;wall | 1,09E+10 MPa | |
| concrete | | | | |
| A | 2,97E+05 mm2 | Δ EA due to steel | 5% | |
| E | 3,45E+04 MPa | | | |

III.3 Torre de Cristal

III.3.1 Equivalent static wind loading

Calculation according to Eurocode EN 1991 part 1-4

1. Input variables

| | | | |
|--|---|-------------------------------------|---|
| $h := 249.20\text{ m}$ | height | $h_{\text{eff}} := 235.46\text{ m}$ | effective height of the building measured along the vertical axis |
| $b := 48.85\text{ m}$ | breadth | | |
| $n_x := 0.156\text{ Hz}$ | fundamental frequency | $c_f := 0.88$ | force coefficient for $v_m(z_s)$ |
| | | $\delta_s := 0.10$ | structural damping |
| $m_e := 313.9 \cdot 10^3 \cdot \frac{\text{kg}}{\text{m}}$ | equivalent mass per unit length (averaged value over the upper 1/3) | $\delta_d := 0.00$ | damping of dissipative devices |

2. Structural factor

Reference height

$$z_s := 0.6 h_{\text{eff}}$$

reference height $\Rightarrow z_s = 141.3\text{ m}$

2.1 Background response

$$B(z) := \sqrt{\frac{1}{1 + 0.9 \left(\frac{b + h_{\text{eff}}}{L(z)} \right)^{0.63}}}$$

$$L(z) := L_t \cdot \left(\frac{z}{z_t} \right)^\alpha$$

Background response factor

turbulence length scale $\Rightarrow L(z_s) = 242.7\text{ m}$

where $\alpha := 0.67 + 0.05 \ln(z_0)$

$$z_t = 200\text{ m}$$

$$L_t = 300\text{ m}$$

Background response factor $\Rightarrow B(z_s) = 0.71$

2.2 Resonance response

$$R(z, n) := \sqrt{\frac{\pi^2}{2 \cdot \delta_{\text{tot}}} \cdot S_L(z, n) \cdot R_h(z, n) \cdot R_b(z, n)}$$

Resonance response factor

$$\delta_{\text{tot}} := \delta_s + \delta_a + \delta_d$$

total damping $\Rightarrow \delta_{\text{tot}} = 0.12$

$$\delta_s = 0.10$$

structural damping

$$\delta_a = 0.02$$

aerodynamic damping

$$\delta_d = 0.00$$

damping of dissipative devices

$$S_L(z, n) := \frac{6.8 f_L(z, n)}{(1 + 10.2 f_L(z, n))^{\frac{5}{3}}}$$

spectral density $\Rightarrow S_L(z_s, n_x) = 0.12$

$$f_L(z, n) := \frac{n \cdot L(z)}{v_m(z)} \quad \text{non-dimensional frequency} \quad \Rightarrow \quad \boxed{f_L(z_s, n_x) = 1.10}$$

$$R_h \cdot R_b \quad \text{aerodynamic admittance function}$$

$$R_h(z, n) := \frac{1}{\eta_h(z, n)} - \frac{1}{2 \cdot \eta_h(z, n)^2} \cdot \left(1 - e^{-2 \cdot \eta_h(z, n)}\right) \quad \text{where } \eta_h(z, n) := \frac{4.6 \cdot h_{\text{eff}}}{L(z)} \cdot f_L(z, n)$$

$$\Rightarrow \boxed{R_h(z_s, n_x) = 0.17}$$

$$R_b(z, n) := \frac{1}{\eta_b(z, n)} - \frac{1}{2 \cdot \eta_b(z, n)^2} \cdot \left(1 - e^{-2 \cdot \eta_b(z, n)}\right) \quad \text{where } \eta_b(z, n) := \frac{4.6 \cdot b}{L(z)} \cdot f_L(z, n)$$

$$\Rightarrow \boxed{R_b(z_s, n_x) = 0.56}$$

$$R(z, n) := \sqrt{\frac{\pi^2}{2 \cdot \delta_{\text{tot}}} \cdot S_L(z, n) \cdot R_h(z, n) \cdot R_b(z, n)} \quad \text{Resonance response factor} \quad \Rightarrow \quad \boxed{R(z_s, n_x) = 0.69}$$

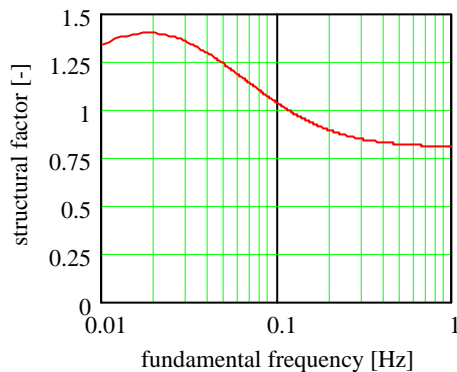
2.3 Results

$$k_p(z, n) := \sqrt{2 \cdot \ln(v(z, n) \cdot T)} + \frac{0.6}{\sqrt{2 \cdot \ln(v(z, n) \cdot T)}} \quad \text{peak factor of the structural response, where}$$

$$v(z, n) := n \cdot \sqrt{\frac{R(z, n)^2}{B(z)^2 + R(z, n)^2}} \quad \text{peak factor} \quad \Rightarrow \quad \boxed{k_p(z_s, n_x) = 3.10}$$

$$c_s(z) := \frac{1 + 7 \cdot I_V(z) \cdot \sqrt{B(z)^2}}{1 + 7 \cdot I_V(z)} \quad \text{Size factor} \quad \Rightarrow \quad \boxed{c_s(z_s) = 0.84}$$

$$c_d(z, n) := \frac{1 + 2 \cdot k_p(z, n) \cdot I_V(z) \cdot \sqrt{B(z)^2 + R(z, n)^2}}{1 + 7 \cdot I_V(z) \cdot \sqrt{B(z)^2}} \quad \text{Dynamic factor} \quad \Rightarrow \quad \boxed{c_d(z_s, n_x) = 1.10}$$



$$\text{Structural factor} \Rightarrow \boxed{c_s(z_s) \cdot c_d(z_s, n_x) = 0.93}$$

| STOREY ₁ = | HEIGHT ₁ = | Z ₁ = | EQ_ST_PEAK_PRESSURE ₁ |
|-----------------------|-----------------------|------------------|----------------------------------|
| "NB" | 5.62 m | 0.00 m | 1.13 kPa |
| 1 | 7.60 | 5.62 | 1.13 |
| "M1" | 3.99 | 13.22 | 1.13 |
| "M1" | 3.61 | 17.21 | 1.13 |
| 2 | 4.20 | 20.82 | 1.13 |
| 3 | 4.20 | 25.02 | 1.13 |
| 4 | 4.20 | 29.22 | 1.13 |
| 5 | 4.20 | 33.42 | 1.13 |
| 6 | 4.20 | 37.62 | 1.13 |
| 7 | 4.20 | 41.82 | 1.13 |
| 8 | 4.20 | 46.02 | 1.13 |
| 9 | 4.20 | 50.22 | 1.13 |
| 10 | 4.20 | 54.42 | 1.16 |
| 11 | 4.20 | 58.62 | 1.18 |
| 12 | 4.20 | 62.82 | 1.21 |
| 13 | 4.20 | 67.02 | 1.23 |
| 14 | 4.20 | 71.22 | 1.25 |
| 15 | 4.20 | 75.42 | 1.26 |
| 16 | 4.20 | 79.62 | 1.28 |
| 17 | 4.20 | 83.82 | 1.30 |
| 18 | 4.20 | 88.02 | 1.32 |
| 19 | 4.20 | 92.22 | 1.33 |
| 20 | 4.20 | 96.42 | 1.35 |
| 21 | 4.20 | 100.62 | 1.36 |
| 22 | 4.20 | 104.82 | 1.38 |
| 23 | 4.20 | 109.02 | 1.39 |
| 24 | 4.20 | 113.22 | 1.40 |
| 25 | 4.20 | 117.42 | 1.41 |
| 26 | 4.20 | 121.62 | 1.43 |
| 27 | 4.20 | 125.82 | 1.44 |
| 28 | 4.20 | 130.02 | 1.45 |
| 29 | 4.20 | 134.22 | 1.46 |
| 30 | 4.20 | 138.42 | 1.47 |
| 31 | 4.40 | 142.62 | 1.48 |

| STOREY _i = | HEIGHT _i = | Z _i = | EQ_ST_PEAK_PRESSUR |
|-----------------------|-----------------------|------------------|--------------------|
| "M3" | 4.50 m | 147.02 m | 1.49 kPa |
| 32 | 4.20 | 151.52 | 1.50 |
| 33 | 4.20 | 155.72 | 1.51 |
| 34 | 4.20 | 159.92 | 1.52 |
| 35 | 4.20 | 164.12 | 1.53 |
| 36 | 4.20 | 168.32 | 1.54 |
| 37 | 4.20 | 172.52 | 1.55 |
| 38 | 4.20 | 176.72 | 1.56 |
| 39 | 4.20 | 180.92 | 1.57 |
| 40 | 4.20 | 185.12 | 1.58 |
| 41 | 4.20 | 189.32 | 1.58 |
| 42 | 4.20 | 193.52 | 1.59 |
| 43 | 4.20 | 197.72 | 1.60 |
| 44 | 4.20 | 201.92 | 1.69 |
| 45 | 4.20 | 206.12 | 1.69 |
| 46 | 4.48 | 210.32 | 1.69 |
| "R1" | 4.62 | 214.80 | 1.69 |
| "R2" | 4.20 | 219.42 | 1.69 |
| "R3" | 4.20 | 223.62 | 1.69 |
| "R4" | 4.20 | 227.82 | 1.69 |
| "R5" | 4.20 | 232.02 | 1.69 |
| "R6" | 4.20 | 236.22 | 1.69 |
| "R7" | 4.20 | 240.42 | 1.69 |
| "R8" | 4.52 | 244.62 | 1.69 |
| "CO" | 0.00 | 249.14 | 1.69 |

III.3.2 Building accelerations

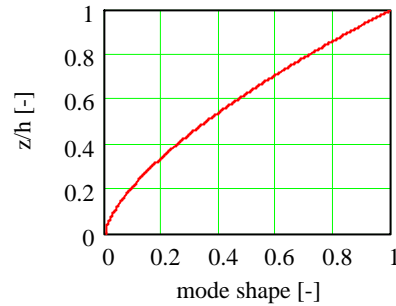
Calculation according to Eurocode EN 1991 part 1-4

1. Input variables

| | |
|--|---|
| $h_{\text{foundation}} := 19.08 \text{ m}$ | height between grade and the foundation level |
| $z_{\text{occ.floor}} := 210.0 \text{ m}$ | height of the top occupied floor |
| $\zeta := 1.5$ | mode exponent best fitting actual mode shape |
| $A_{1,x} := 0.39$ | area under the actual mode shape function |

$$\Phi_{1,x}(z) := \left(\frac{z + h_{\text{foundation}}}{h_{\text{eff}} + h_{\text{foundation}}} \right)^{\zeta}$$

$$T_{\text{return}} = 10$$



2. Accelerations

2.1 Calculation unknown variables

$$R(z, n) := \sqrt{\frac{\pi^2}{2 \cdot \delta_{\text{tot}}} \cdot S_L(z, n) \cdot R_h(z, n) \cdot R_b(z, n)}$$

Resonance response factor

$$\delta_{\text{tot}} := 0.01 \cdot 2\pi$$

total damping

=>

$$\delta_{\text{tot}} = 0.06$$

$$S_L(z, n) := \frac{6.8 \cdot f_L(z, n)}{(1 + 10.2 \cdot f_L(z, n))^{\frac{5}{3}}}$$

spectral density

=>

$$S_L(z_s, n_x) = 0.11$$

$$f_L(z, n) := \frac{n \cdot L(z)}{v_m(z)}$$

non-dimensional frequency

=>

$$f_L(z_s, n_x) = 1.22$$

$R_h \cdot R_b$

aerodynamic admittance function

$$R_h(z, n) := \frac{1}{\eta_h(z, n)} - \frac{1}{2 \cdot \eta_h(z, n)^2} \cdot \left(1 - e^{-2 \cdot \eta_h(z, n)} \right) \quad \text{where } \eta_h(z, n) := \frac{4.6h}{L(z)} \cdot f_L(z, n)$$

=>

$$R_h(z_s, n_x) = 0.16$$

$$R_b(z, n) := \frac{1}{\eta_b(z, n)} - \frac{1}{2 \cdot \eta_b(z, n)^2} \cdot \left(1 - e^{-2 \cdot \eta_b(z, n)} \right) \quad \text{where } \eta_b(z, n) := \frac{4.6b}{L(z)} \cdot f_L(z, n)$$

=>

$$R_b(z_s, n_x) = 0.53$$

$$R(z, n) := \sqrt{\frac{\pi^2}{2 \cdot \delta_{\text{tot}}} \cdot S_L(z, n) \cdot R_h(z, n) \cdot R_b(z, n)}$$

Resonance response factor

=>

$$R(z_s, n_x) = 0.85$$

$$K_x := (2 \cdot \zeta + 1) \cdot \frac{\left((\zeta + 1) \cdot \ln\left(\frac{z_s}{z_0}\right) + 0.5 \right) - 1}{(\zeta + 1)^2 \cdot \ln\left(\frac{z_s}{z_0}\right)}$$

adimensional factor =>

$$K_x = 1.63$$

$$m_{1,x} := A_{1,x} m_e$$

equivalent modal
mass per unit
length =>

$$m_{1,x} = 122.4 \times 10^3 \frac{\text{kg}}{\text{m}}$$

$$k_p := \sqrt{2 \cdot \ln(v \cdot T)} + \frac{0.6}{\sqrt{2 \cdot \ln(v \cdot T)}}$$

peak factor of the
structural response =>

$$k_p = 3.21$$

with $v := n_x$

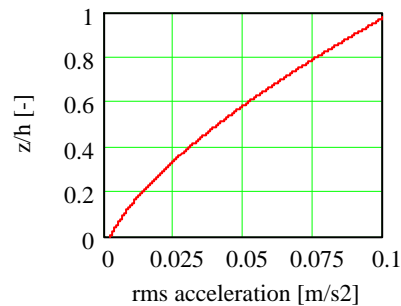
2.2 Results for $T_{\text{return}} = 10$ years

$$\sigma_{a,x}(z, n) := \frac{c_f \cdot \rho \cdot b \cdot I_v(z_s) \cdot v_m(z_s)^2}{m_{1,x}} \cdot R(z_s, n_x) \cdot K_x \cdot \Phi_{1,x}(z)$$

value at top occupied floor:

$$\sigma_{a,x}(z_{\text{occ.floor}}, n_x) = 0.082 \frac{\text{m}}{\text{s}^2}$$

$$\sigma_{a,x}(z_{\text{occ.floor}}, n_x) = 8.3 \times 10^{-3} \text{ g}$$

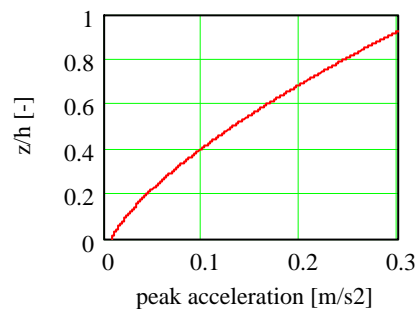


$$a_{\text{peak},x}(z, n) := \frac{c_f \cdot \rho \cdot b \cdot k_p \cdot I_v(z_s) \cdot v_m(z_s)^2}{m_{1,x}} \cdot R(z_s, n_x) \cdot K_x \cdot \Phi_{1,x}(z)$$

value at top occupied floor:

$$a_{\text{peak},x}(z_{\text{occ.floor}}, n_x) = 0.263 \frac{\text{m}}{\text{s}^2}$$

$$a_{\text{peak},x}(z_{\text{occ.floor}}, n_x) = 26.8 \times 10^{-3} \text{ g}$$

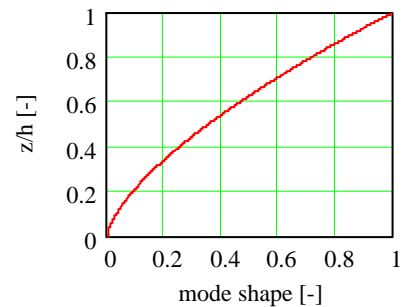


Calculation according to Eurocode EN 1991 part 1-4

1. Input variables

| | |
|--|---|
| $h_{\text{foundation}} := 19.08 \text{ m}$ | height between grade and the foundation level |
| $z_{\text{occ.floor}} := 210.0 \text{ m}$ | height of the top occupied floor |
| $\zeta := 1.5$ | mode exponent best fitting actual mode shape |
| $A_{1,x} := 0.39$ | area under the actual mode shape function |
| $\Phi_{1,x}(z) := \left(\frac{z + h_{\text{foundation}}}{h_{\text{eff}} + h_{\text{foundation}}} \right)^{\zeta}$ | |

$$T_{\text{return}} = 5$$



2. Accelerations

2.1 Calculation unknown variables

$$R(z, n) := \sqrt{\frac{2}{\pi} \cdot S_L(z, n) \cdot R_h(z, n) \cdot R_b(z, n)} \cdot 2 \cdot \delta_{\text{tot}}$$

Resonance response factor

$$\delta_{\text{tot}} := 0.01 \cdot 2\pi$$

total damping

=>

$$\delta_{\text{tot}} = 0.06$$

$$S_L(z, n) := \frac{6.8 \cdot f_L(z, n)}{(1 + 10.2 \cdot f_L(z, n))^{\frac{5}{3}}}$$

spectral density

=>

$$S_L(z_s, n_x) = 0.11$$

$$f_L(z, n) := \frac{n \cdot L(z)}{v_m(z)}$$

non-dimensional frequency

=>

$$f_L(z_s, n_x) = 1.29$$

$R_h \cdot R_b$

aerodynamic admittance function

$$R_h(z, n) := \frac{1}{\eta_h(z, n)} - \frac{1}{2 \cdot \eta_h(z, n)^2} \cdot \left(1 - e^{-2 \cdot \eta_h(z, n)} \right) \quad \text{where } \eta_h(z, n) := \frac{4.6 \cdot h}{L(z)} \cdot f_L(z, n)$$

=>

$$R_h(z_s, n_x) = 0.15$$

$$R_b(z, n) := \frac{1}{\eta_b(z, n)} - \frac{1}{2 \cdot \eta_b(z, n)^2} \cdot \left(1 - e^{-2 \cdot \eta_b(z, n)} \right) \quad \text{where } \eta_b(z, n) := \frac{4.6 \cdot b}{L(z)} \cdot f_L(z, n)$$

=>

$$R_b(z_s, n_x) = 0.52$$

$$R(z, n) := \sqrt{\frac{2}{\pi} \cdot S_L(z, n) \cdot R_h(z, n) \cdot R_b(z, n)} \cdot 2 \cdot \delta_{\text{tot}}$$

Resonance response factor

=>

$$R(z_s, n_x) = 0.81$$

$$K_x := (2 \cdot \zeta + 1) \cdot \frac{\left((\zeta + 1) \cdot \ln\left(\frac{z_s}{z_0}\right) + 0.5 \right) - 1}{(\zeta + 1)^2 \cdot \ln\left(\frac{z_s}{z_0}\right)}$$

adimensional factor =>

$$K_x = 1.63$$

$$m_{1,x} := A_{1,x} m_e$$

equivalent modal
mass per unit
length =>

$$m_{1,x} = 122.4 \times 10^3 \frac{\text{kg}}{\text{m}}$$

$$k_p := \sqrt{2 \cdot \ln(v \cdot T)} + \frac{0.6}{\sqrt{2 \cdot \ln(v \cdot T)}}$$

peak factor of the
structural response =>

$$k_p = 3.21$$

with $v := n_x$

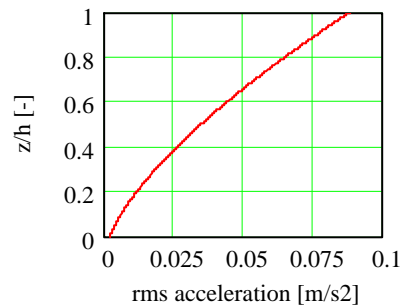
2.2 Results for $T_{\text{return}} = 5$ years

$$\sigma_{a,x}(z, n) := \frac{c_f \cdot \rho \cdot b \cdot I_v(z_s) \cdot v_m(z_s)^2}{m_{1,x}} \cdot R(z_s, n_x) \cdot K_x \cdot \Phi_{1,x}(z)$$

value at top occupied floor:

$$\sigma_{a,x}(z_{\text{occ.floor}}, n_x) = 0.069 \frac{\text{m}}{\text{s}^2}$$

$$\sigma_{a,x}(z_{\text{occ.floor}}, n_x) = 7.1 \times 10^{-3} \text{ g}$$

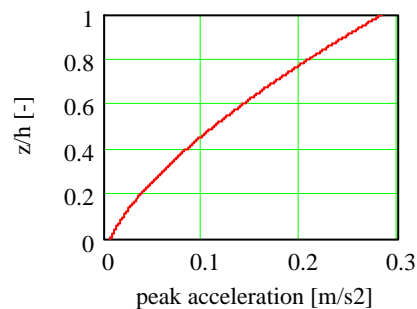


$$a_{\text{peak},x}(z, n) := \frac{c_f \cdot \rho \cdot b \cdot k_p \cdot I_v(z_s) \cdot v_m(z_s)^2}{m_{1,x}} \cdot R(z_s, n_x) \cdot K_x \cdot \Phi_{1,x}(z)$$

value at top occupied floor:

$$a_{\text{peak},x}(z_{\text{occ.floor}}, n_x) = 0.223 \frac{\text{m}}{\text{s}^2}$$

$$a_{\text{peak},x}(z_{\text{occ.floor}}, n_x) = 22.8 \times 10^{-3} \text{ g}$$



III.3.3 Effective axial stiffness of vertical concrete members

This subsection provides the calculation of the effective axial stiffness of the vertical concrete elements. The factor k (see subsection 5.1.2) is determined by which the axial stiffness of the gross concrete section is multiplied in the finite element model.

Firstly the columns are treated and afterwards the core sections are dealt with.

As far as the composite columns are concerned, a number of approximately 200 different columns are defined in the project drawings. A mean value of the factor k has been calculated for every different column diameter. A mean steel section and mild steel reinforcement area is computed for every diameter. The following column diameters have been adopted with the corresponding height range:

- 950 mm from basement level -6 up to mechanical level M1
- 900 mm from mechanical level M1 to the 2nd storey
- 850 mm from the 2nd to the 11th storey
- 800 mm from the 11th to the 26th storey
- 750 mm from the 26th to the 34th storey
- 700 mm from the 34th to the upper mechanical level M4

The calculation of the effective axial stiffness of the shear walls has been carried out only for the section at basement level -6. Values of factor k are been obtained that are smaller than 5% due to the relative small amount of reinforcement. Because of the latter, the calculation for the other shear wall sections is omitted, considering in every shear wall the gross concrete section only.

Columns

| Section | | D950 S6-M1 | |
|-----------------------------------|--------------|--------------------------|--------------|
| Materials | | fck [MPa] | E [MPa] |
| rolled steel | S 355 | 355 | 2,10E+05 |
| mild steel | B 500 | 500 | 2,10E+05 |
| concrete | C 45/55 | 45 | 3,57E+04 |
| Geometry | | | |
| diameter | 950 mm | | |
| Calculation | | Results | |
| <i>wide flange section</i> | | <i>equivalent column</i> | |
| A;mean | 7,95E+04 mm2 | A;column | 7,09E+05 mm2 |
| E | 2,10E+05 MPa | EA;column | 4,18E+10 MPa |
| <i>longitudinal reinforcement</i> | | Δ EA due to steel | 65% |
| A;mean | 1,50E+04 mm2 | | |
| E | 2,10E+05 MPa | | |
| <i>concrete</i> | | | |
| A | 6,14E+05 mm2 | | |
| E | 3,57E+04 MPa | | |

| Section | | D800 11-26 | |
|-----------------------------------|--------------|--------------------------|--------------|
| Materials | | fck [MPa] | E [MPa] |
| rolled steel | S 355 | 355 | 2,10E+05 |
| mild steel | B 500 | 500 | 2,10E+05 |
| concrete | C 45/55 | 45 | 3,57E+04 |
| Geometry | | | |
| diameter | 800 mm | | |
| Calculation | | Results | |
| <i>wide flange section</i> | | <i>equivalent column</i> | |
| A;mean | 3,59E+04 mm2 | A;column | 5,03E+05 mm2 |
| E | 2,10E+05 MPa | EA;column | 2,50E+10 MPa |
| <i>longitudinal reinforcement</i> | | Δ EA due to steel | 39% |
| A;mean | 4,40E+03 mm2 | | |
| E | 2,10E+05 MPa | | |
| <i>concrete</i> | | | |
| A | 4,62E+05 mm2 | | |
| E | 3,57E+04 MPa | | |

| Section | | D900 M1-2 | |
|-----------------------------------|--------------|--------------------------|--------------|
| Materials | | fck [MPa] | E [MPa] |
| rolled steel | S 355 | 355 | 2,10E+05 |
| mild steel | B 500 | 500 | 2,10E+05 |
| concrete | C 45/55 | 45 | 3,57E+04 |
| Geometry | | | |
| diameter | 900 mm | | |
| Calculation | | Results | |
| <i>wide flange section</i> | | <i>equivalent column</i> | |
| A;mean | 6,33E+04 mm2 | A;column | 6,36E+05 mm2 |
| E | 2,10E+05 MPa | EA;column | 3,53E+10 MPa |
| <i>longitudinal reinforcement</i> | | Δ EA due to steel | 55% |
| A;mean | 8,84E+03 mm2 | | |
| E | 2,10E+05 MPa | | |
| <i>concrete</i> | | | |
| A | 5,64E+05 mm2 | | |
| E | 3,57E+04 MPa | | |

| Section | | D750 26-34 | |
|-----------------------------------|--------------|--------------------------|--------------|
| Materials | | fck [MPa] | E [MPa] |
| rolled steel | S 355 | 355 | 2,10E+05 |
| mild steel | B 500 | 500 | 2,10E+05 |
| concrete | C 45/55 | 45 | 3,57E+04 |
| Geometry | | | |
| diameter | 750 mm | | |
| Calculation | | Results | |
| <i>wide flange section</i> | | <i>equivalent column</i> | |
| A;mean | 2,38E+04 mm2 | A;column | 4,42E+05 mm2 |
| E | 2,10E+05 MPa | EA;column | 2,07E+10 MPa |
| <i>longitudinal reinforcement</i> | | Δ EA due to steel | 31% |
| A;mean | 4,40E+03 mm2 | | |
| E | 2,10E+05 MPa | | |
| <i>concrete</i> | | | |
| A | 4,14E+05 mm2 | | |
| E | 3,57E+04 MPa | | |

| Section | | D850 2-11 | |
|-----------------------------------|--------------|--------------------------|--------------|
| Materials | | fck [MPa] | E [MPa] |
| rolled steel | S 355 | 355 | 2,10E+05 |
| mild steel | B 500 | 500 | 2,10E+05 |
| concrete | C 45/55 | 45 | 3,57E+04 |
| Geometry | | | |
| diameter | 850 mm | | |
| Calculation | | Results | |
| <i>wide flange section</i> | | <i>equivalent column</i> | |
| A;mean | 5,03E+04 mm2 | A;column | 5,67E+05 mm2 |
| E | 2,10E+05 MPa | EA;column | 2,99E+10 MPa |
| <i>longitudinal reinforcement</i> | | Δ EA due to steel | 48% |
| A;mean | 5,03E+03 mm2 | | |
| E | 2,10E+05 MPa | | |
| <i>concrete</i> | | | |
| A | 5,12E+05 mm2 | | |
| E | 3,57E+04 MPa | | |

| Section | | D700 34-M4 | |
|-----------------------------------|--------------|--------------------------|--------------|
| Materials | | fck [MPa] | E [MPa] |
| rolled steel | S 355 | 355 | 2,10E+05 |
| mild steel | B 500 | 500 | 2,10E+05 |
| concrete | C 45/55 | 45 | 3,57E+04 |
| Geometry | | | |
| diameter | 700 mm | | |
| Calculation | | Results | |
| <i>wide flange section</i> | | <i>equivalent column</i> | |
| A;mean | 1,79E+04 mm2 | A;column | 3,85E+05 mm2 |
| E | 2,10E+05 MPa | EA;column | 1,75E+10 MPa |
| <i>longitudinal reinforcement</i> | | Δ EA due to steel | 28% |
| A;mean | 3,77E+03 mm2 | | |
| E | 2,10E+05 MPa | | |
| <i>concrete</i> | | | |
| A | 3,63E+05 mm2 | | |
| E | 3,57E+04 MPa | | |

Core

| Section | Basement S6 | Shear wall | longitudinal | |
|-----------------------------------|--------------------------|----------------------------|--------------------------|----------|
| <i>Materials</i> | | fck [MPa] | E [MPa] | |
| mild steel | B 500 | 500 | 2,10E+05 | |
| concrete | C 45/55 | 45 | 3,57E+04 | |
| <i>Geometry</i> | | | φ [mm] | ctc [mm] |
| thickness | 1200 mm | longitudinal reinforcement | 25 | 300 |
| width | | | 25 | 300 |
| considered | 1000 mm | | 0 | 100 |
| Calculation | | Results | | |
| <i>longitudinal reinforcement</i> | | <i>equivalent wall</i> | | |
| A | 3,27E+03 mm ² | A;wall | 1,20E+06 mm ² | |
| E | 2,10E+05 MPa | EA;wall | 4,34E+10 MPa | |
| <i>concrete</i> | | | | |
| A | 1,20E+06 mm ² | Δ EA due to steel | 1% | |
| E | 3,57E+04 MPa | | | |

| Section | Basement S6 | Shear wall | transversal | |
|-----------------------------------|--------------------------|----------------------------|--------------------------|----------|
| <i>Materials</i> | | fck [MPa] | E [MPa] | |
| mild steel | B 500 | 500 | 2,10E+05 | |
| concrete | C 45/55 | 45 | 3,57E+04 | |
| <i>Geometry</i> | | | φ [mm] | ctc [mm] |
| thickness | 500 mm | longitudinal reinforcement | 25 | 300 |
| width | | | 25 | 300 |
| considered | 1000 mm | | 0 | 100 |
| Calculation | | Results | | |
| <i>longitudinal reinforcement</i> | | <i>equivalent wall</i> | | |
| A | 3,27E+03 mm ² | A;wall | 5,00E+05 mm ² | |
| E | 2,10E+05 MPa | EA;wall | 1,84E+10 MPa | |
| <i>concrete</i> | | | | |
| A | 4,97E+05 mm ² | Δ EA due to steel | 3% | |
| E | 3,57E+04 MPa | | | |

III.4 Torre Sacyr Vallehermoso

III.4.1 Equivalent static wind loading

Calculation according to Eurocode EN 1991 part 1-4

1. Input variables

| | | | |
|--|---|--------------------|----------------------------------|
| $h := 231.80\text{m}$ | height | $c_f := 0.62$ | force coefficient for $v_m(z_s)$ |
| $b := 47.00\text{m}$ | breadth | $\delta_s := 0.10$ | structural damping |
| $n_x := 0.131\text{Hz}$ | fundamental frequency | $\delta_d := 0.00$ | damping of dissipative devices |
| $m_e := 439.6 \cdot 10^3 \cdot \frac{\text{kg}}{\text{m}}$ | equivalent mass per unit length (averaged value over the upper 1/3) | | |

2. Structural factor

Reference height

$$z_s := 0.6h$$

reference height $\Rightarrow z_s = 139.1\text{m}$

2.1 Background response

$$B(z) := \frac{1}{\sqrt{1 + 0.9 \left(\frac{b+h}{L(z)} \right)^{0.63}}}$$

Background response factor

$$L(z) := L_t \cdot \left(\frac{z}{z_t} \right)^\alpha$$

turbulence length scale $\Rightarrow L(z_s) = 240.4\text{m}$

where $\alpha := 0.67 + 0.05 \ln(z_0)$

$$z_t = 200\text{m}$$

$$L_t = 300\text{m}$$

2.2 Resonance response

Background response factor $\Rightarrow B(z_s) = 0.71$

$$R(z, n) := \sqrt{\frac{\pi^2}{2 \cdot \delta_{\text{tot}}} \cdot S_L(z, n) \cdot R_h(z, n) \cdot R_b(z, n)}$$

Resonance response factor

$$\delta_{\text{tot}} := \delta_s + \delta_a + \delta_d$$

total damping $\Rightarrow \delta_{\text{tot}} = 0.11$

$$\delta_s = 0.10$$

structural damping

$$\delta_a = 0.01$$

aerodynamic damping

$$\delta_d = 0.00$$

damping of dissipative devices

$$S_L(z, n) := \frac{6.8 f_L(z, n)}{\left(1 + 10.2 f_L(z, n) \right)^{\frac{5}{3}}}$$

spectral density $\Rightarrow S_L(z_s, n_x) = 0.13$

$$f_L(z, n) := \frac{n \cdot L(z)}{v_m(z)} \quad \text{non-dimensional frequency} \quad \Rightarrow \quad \boxed{f_L(z_s, n_x) = 0.92}$$

$$R_h \cdot R_b \quad \text{aerodynamic admittance function}$$

$$R_h(z, n) := \frac{1}{\eta_h(z, n)} - \frac{1}{2 \cdot \eta_h(z, n)^2} \cdot \left(1 - e^{-2 \cdot \eta_h(z, n)}\right) \quad \text{where } \eta_h(z, n) := \frac{4.6h}{L(z)} \cdot f_L(z, n)$$

$$\Rightarrow \boxed{R_h(z_s, n_x) = 0.22}$$

$$R_b(z, n) := \frac{1}{\eta_b(z, n)} - \frac{1}{2 \cdot \eta_b(z, n)^2} \cdot \left(1 - e^{-2 \cdot \eta_b(z, n)}\right) \quad \text{where } \eta_b(z, n) := \frac{4.6b}{L(z)} \cdot f_L(z, n)$$

$$\Rightarrow \boxed{R_b(z_s, n_x) = 0.62}$$

$$R(z, n) := \sqrt{\frac{\pi^2}{2 \cdot \delta_{tot}} \cdot S_L(z, n) \cdot R_h(z, n) \cdot R_b(z, n)} \quad \text{Resonance response factor} \quad \Rightarrow \quad \boxed{R(z_s, n_x) = 0.87}$$

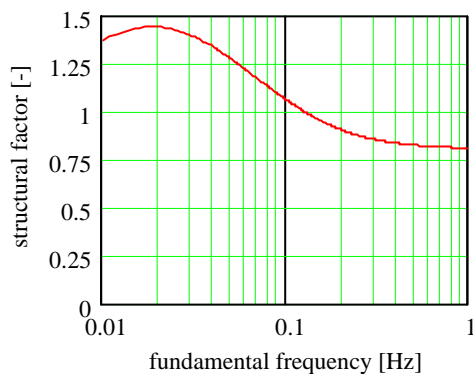
2.3 Results

$$k_p(z, n) := \sqrt{2 \cdot \ln(v(z, n) \cdot T)} + \frac{0.6}{\sqrt{2 \cdot \ln(v(z, n) \cdot T)}} \quad \text{peak factor of the structural response, where}$$

$$v(z, n) := n \cdot \sqrt{\frac{R(z, n)^2}{B(z)^2 + R(z, n)^2}} \quad \text{peak factor} \quad \Rightarrow \quad \boxed{k_p(z_s, n_x) = 3.08}$$

$$c_s(z) := \frac{1 + 7 \cdot I_V(z) \cdot \sqrt{B(z)^2}}{1 + 7 \cdot I_V(z)} \quad \text{Size factor} \quad \Rightarrow \quad \boxed{c_s(z_s) = 0.85}$$

$$c_d(z, n) := \frac{1 + 2 \cdot k_p(z, n) \cdot I_V(z) \cdot \sqrt{B(z)^2 + R(z, n)^2}}{1 + 7 \cdot I_V(z) \cdot \sqrt{B(z)^2}} \quad \text{Dynamic factor} \quad \Rightarrow \quad \boxed{c_d(z_s, n_x) = 1.17}$$



$$\text{Structural factor} \Rightarrow \boxed{c_s(z_s) \cdot c_d(z_s, n_x) = 0.99}$$

| STOREY ₁ = | HEIGHT ₁ = | Z ₁ = | EQ_ST_PEAK_PRESSURE ₁ = |
|-----------------------|-----------------------|------------------|------------------------------------|
| 0 | 4.00 m | -0.20 m | 1.18 kPa |
| 1 | 4.00 | 3.80 | 1.18 |
| 2 | 4.00 | 7.80 | 1.18 |
| 3 | 4.00 | 11.80 | 1.18 |
| 4 | 4.00 | 15.80 | 1.18 |
| 5 | 4.00 | 19.80 | 1.18 |
| 6 | 4.00 | 23.80 | 1.18 |
| 7 | 4.00 | 27.80 | 1.18 |
| 8 | 4.00 | 31.80 | 1.18 |
| 9 | 4.00 | 35.80 | 1.18 |
| 10 | 4.00 | 39.80 | 1.18 |
| 11 | 4.00 | 43.80 | 1.18 |
| 12 | 4.00 | 47.80 | 1.19 |
| 13 | 4.00 | 51.80 | 1.22 |
| 14 | 4.00 | 55.80 | 1.24 |
| 15 | 4.00 | 59.80 | 1.27 |
| 16 | 4.00 | 63.80 | 1.29 |
| 17 | 4.00 | 67.80 | 1.31 |
| 18 | 4.00 | 71.80 | 1.33 |
| 19 | 4.00 | 75.80 | 1.35 |
| 20 | 4.00 | 79.80 | 1.37 |
| 21 | 4.00 | 83.80 | 1.38 |
| 22 | 4.00 | 87.80 | 1.40 |
| 23 | 4.00 | 91.80 | 1.42 |
| 24 | 4.00 | 95.80 | 1.43 |
| 25 | 4.00 | 99.80 | 1.45 |
| 26 | 4.00 | 103.80 | 1.46 |
| 27 | 4.00 | 107.80 | 1.47 |
| 28 | 4.00 | 111.80 | 1.49 |
| 29 | 4.00 | 115.80 | 1.50 |
| 30 | 4.00 | 119.80 | 1.51 |
| 31 | 4.00 | 123.80 | 1.53 |
| 32 | 4.00 | 127.80 | 1.54 |
| 33 | 4.00 | 131.80 | 1.55 |

| STOREY ₁ | HEIGHT ₁ = | Z ₁ = | EQ_ST_PEAK_PRESSURE ₁ |
|---------------------|-----------------------|------------------|----------------------------------|
| 34 | 4.00 m | 135.80 m | 1.56 kPa |
| 35 | 4.00 | 139.80 | 1.57 |
| 36 | 4.00 | 143.80 | 1.58 |
| 37 | 4.00 | 147.80 | 1.59 |
| 38 | 4.00 | 151.80 | 1.60 |
| 39 | 4.00 | 155.80 | 1.61 |
| 40 | 4.00 | 159.80 | 1.62 |
| 41 | 4.00 | 163.80 | 1.63 |
| 42 | 4.00 | 167.80 | 1.64 |
| 43 | 4.00 | 171.80 | 1.65 |
| 44 | 4.00 | 175.80 | 1.66 |
| 45 | 4.00 | 179.80 | 1.67 |
| 46 | 4.00 | 183.80 | 1.67 |
| 47 | 4.00 | 187.80 | 1.77 |
| 48 | 4.00 | 191.80 | 1.77 |
| 49 | 4.00 | 195.80 | 1.77 |
| 50 | 4.00 | 199.80 | 1.77 |
| 51 | 4.00 | 203.80 | 1.77 |
| 52 | 4.00 | 207.80 | 1.77 |
| 53 | 4.00 | 211.80 | 1.77 |
| 54 | 4.00 | 215.80 | 1.77 |
| 55 | 4.00 | 219.80 | 1.77 |
| 56 | 4.00 | 223.80 | 1.77 |
| 57 | 4.00 | 227.80 | 1.77 |
| 58 | 4.00 | 231.80 | 1.77 |

III.4.2 Building accelerations

Calculation according to Eurocode EN 1991 part 1-4

1. Input variables

$$h_{\text{foundation}} := 20.6 \text{ m}$$

height between grade and the foundation level

$$z_{\text{occ.floor}} := 195.80 \text{ m}$$

height of the top occupied floor

$$\zeta := 1.4$$

mode exponent best fitting actual mode shape

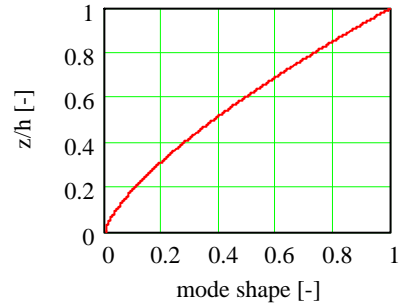
$$A_{1,x} := 0.4$$

area under the actual mode shape function

$$\Phi_{1,x}(z) := \left(\frac{z + h_{\text{foundation}}}{h + h_{\text{foundation}}} \right)^{\zeta}$$

approximated mode shape =>

$$T_{\text{return}} = 10$$



2. Accelerations

2.1 Calculation unknown variables

$$R(z, n) := \sqrt{\frac{\pi^2}{2 \cdot \delta_{\text{tot}}} \cdot S_L(z, n) \cdot R_h(z, n) \cdot R_b(z, n)}$$

Resonance response factor

$$\delta_{\text{tot}} := 0.01 \cdot 2\pi$$

total damping =>

$$\delta_{\text{tot}} = 0.06$$

$$S_L(z, n) := \frac{6.8 \cdot f_L(z, n)}{(1 + 10.2 \cdot f_L(z, n))^{\frac{5}{3}}}$$

spectral density =>

$$S_L(z_s, n_x) = 0.12$$

$$f_L(z, n) := \frac{n \cdot L(z)}{v_m(z)}$$

non-dimensional frequency =>

$$f_L(z_s, n_x) = 1.01$$

$$R_h \cdot R_b$$

aerodynamic admittance function

$$R_h(z, n) := \frac{1}{\eta_h(z, n)} - \frac{1}{2 \cdot \eta_h(z, n)^2} \cdot \left(1 - e^{-2 \cdot \eta_h(z, n)} \right) \quad \text{where } \eta_h(z, n) := \frac{4.6h}{L(z)} \cdot f_L(z, n)$$

$$\Rightarrow R_h(z_s, n_x) = 0.20$$

$$R_b(z, n) := \frac{1}{\eta_b(z, n)} - \frac{1}{2 \cdot \eta_b(z, n)^2} \cdot \left(1 - e^{-2 \cdot \eta_b(z, n)} \right) \quad \text{where } \eta_b(z, n) := \frac{4.6b}{L(z)} \cdot f_L(z, n)$$

$$\Rightarrow R_b(z_s, n_x) = 0.59$$

$$R(z, n) := \sqrt{\frac{\pi^2}{2 \cdot \delta_{\text{tot}}} \cdot S_L(z, n) \cdot R_h(z, n) \cdot R_b(z, n)}$$

Resonance response factor =>

$$R(z_s, n_x) = 1.05$$

$$K_x := (2 \cdot \zeta + 1) \cdot \frac{(\zeta + 1) \cdot \left(\ln \left(\frac{z_s}{z_0} \right) + 0.5 \right) - 1}{(\zeta + 1)^2 \cdot \ln \left(\frac{z_s}{z_0} \right)}$$

adimensional factor =>

$$K_x = 1.6$$

$$m_{1,x} := A_{1,x} m_e$$

equivalent modal
mass per unit
length =>

$$m_{1,x} = 180.2 \times 10^3 \frac{\text{kg}}{\text{m}}$$

$$k_p := \sqrt{2 \cdot \ln(v \cdot T)} + \frac{0.6}{\sqrt{2 \cdot \ln(v \cdot T)}}$$

peak factor of the
structural response =>

$$k_p = 3.16$$

with $v := n_x$

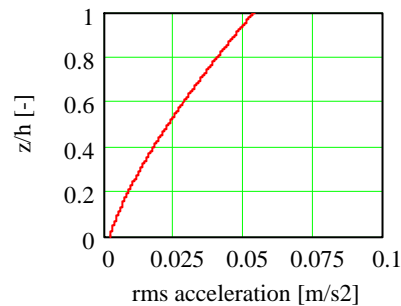
2.2 Results for $T_{\text{return}} = 10$ years

$$\sigma_{a,x}(z, n) := \frac{c_f \cdot \rho \cdot b \cdot I_v(z_s) \cdot v_m(z_s)^2}{m_{1,x}} \cdot R(z_s, n_x) \cdot K_x \cdot \Phi_{1,x}(z)$$

value at top occupied floor:

$$\sigma_{a,x}(z_{\text{occ.floor}}, n_x) = 0.043 \frac{\text{m}}{\text{s}^2}$$

$$\sigma_{a,x}(z_{\text{occ.floor}}, n_x) = 4.4 \times 10^{-3} \text{ g}$$

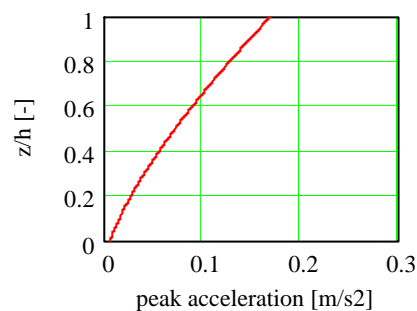


$$a_{\text{peak},x}(z, n) := \frac{c_f \cdot \rho \cdot b \cdot k_p \cdot I_v(z_s) \cdot v_m(z_s)^2}{m_{1,x}} \cdot R(z_s, n_x) \cdot K_x \cdot \Phi_{1,x}(z)$$

value at top occupied floor:

$$a_{\text{peak},x}(z_{\text{occ.floor}}, n_x) = 0.136 \frac{\text{m}}{\text{s}^2}$$

$$a_{\text{peak},x}(z_{\text{occ.floor}}, n_x) = 13.9 \times 10^{-3} \text{ g}$$



Calculation according to Eurocode EN 1991 part 1-4

1. Input variables

$$h_{\text{foundation}} := 20.6 \text{ m}$$

height between grade and the foundation level

$$z_{\text{occ.floor}} := 195.80 \text{ m}$$

height of the top occupied floor

$$\zeta := 1.4$$

mode exponent best fitting actual mode shape

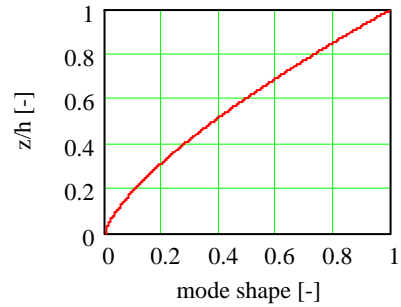
$$A_{1,x} := 0.4$$

area under the actual mode shape function

$$\Phi_{1,x}(z) := \left(\frac{z + h_{\text{foundation}}}{h + h_{\text{foundation}}} \right)^{\zeta}$$

approximated mode shape =>

$$T_{\text{return}} = 5$$



2. Accelerations

2.1 Calculation unknown variables

$$R(z, n) := \sqrt{\frac{\pi^2}{2 \cdot \delta_{\text{tot}}} \cdot S_L(z, n) \cdot R_h(z, n) \cdot R_b(z, n)}$$

Resonance response factor

$$\delta_{\text{tot}} := 0.01 \cdot 2\pi$$

total damping =>

$$\delta_{\text{tot}} = 0.06$$

$$S_L(z, n) := \frac{6.8 \cdot f_L(z, n)}{(1 + 10.2 \cdot f_L(z, n))^{\frac{5}{3}}}$$

spectral density =>

$$S_L(z_s, n_x) = 0.12$$

$$f_L(z, n) := \frac{n \cdot L(z)}{v_m(z)}$$

non-dimensional frequency =>

$$f_L(z_s, n_x) = 1.07$$

$$R_h \cdot R_b$$

aerodynamic admittance function

$$R_h(z, n) := \frac{1}{\eta_h(z, n)} - \frac{1}{2 \cdot \eta_h(z, n)^2} \cdot \left(1 - e^{-2 \cdot \eta_h(z, n)} \right) \quad \text{where } \eta_h(z, n) := \frac{4.6 \cdot h}{L(z)} \cdot f_L(z, n)$$

$$\Rightarrow R_h(z_s, n_x) = 0.19$$

$$R_b(z, n) := \frac{1}{\eta_b(z, n)} - \frac{1}{2 \cdot \eta_b(z, n)^2} \cdot \left(1 - e^{-2 \cdot \eta_b(z, n)} \right) \quad \text{where } \eta_b(z, n) := \frac{4.6 \cdot b}{L(z)} \cdot f_L(z, n)$$

$$\Rightarrow R_b(z_s, n_x) = 0.58$$

$$R(z, n) := \sqrt{\frac{\pi^2}{2 \cdot \delta_{\text{tot}}} \cdot S_L(z, n) \cdot R_h(z, n) \cdot R_b(z, n)}$$

Resonance response factor =>

$$R(z_s, n_x) = 1.00$$

$$K_x := (2 \cdot \zeta + 1) \cdot \frac{(\zeta + 1) \cdot \left(\ln \left(\frac{z_s}{z_0} \right) + 0.5 \right) - 1}{(\zeta + 1)^2 \cdot \ln \left(\frac{z_s}{z_0} \right)}$$

dimensional factor =>

$$K_x = 1.6$$

$$m_{1,x} := A_{1,x} \cdot m_e$$

equivalent modal
mass per unit
length =>

$$m_{1,x} = 180.2 \times 10^3 \frac{\text{kg}}{\text{m}}$$

$$k_p := \sqrt{2 \cdot \ln(v \cdot T)} + \frac{0.6}{\sqrt{2 \cdot \ln(v \cdot T)}}$$

peak factor of the
structural response =>

$$k_p = 3.16$$

with $v := n_x$

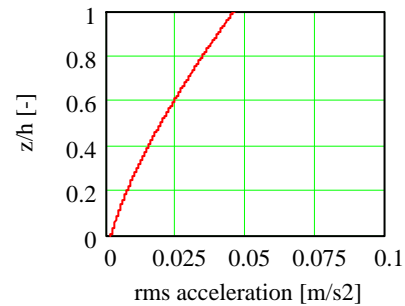
2.2 Results for $T_{\text{return}} = 5$ years

$$\sigma_{a,x}(z, n) := \frac{c_f \cdot \rho \cdot b \cdot I_v(z_s) \cdot v_m(z_s)^2}{m_{1,x}} \cdot R(z_s, n_x) \cdot K_x \cdot \Phi_{1,x}(z)$$

value at top occupied floor:

$$\sigma_{a,x}(z_{\text{occ.floor}}, n_x) = 0.037 \frac{\text{m}}{\text{s}^2}$$

$$\sigma_{a,x}(z_{\text{occ.floor}}, n_x) = 3.7 \times 10^{-3} g$$

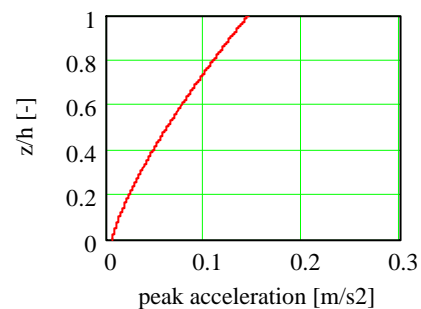


$$a_{\text{peak},x}(z, n) := \frac{c_f \cdot \rho \cdot b \cdot k_p \cdot I_v(z_s) \cdot v_m(z_s)^2}{m_{1,x}} \cdot R(z_s, n_x) \cdot K_x \cdot \Phi_{1,x}(z)$$

value at top occupied floor:

$$a_{\text{peak},x}(z_{\text{occ.floor}}, n_x) = 0.116 \frac{\text{m}}{\text{s}^2}$$

$$a_{\text{peak},x}(z_{\text{occ.floor}}, n_x) = 11.8 \times 10^{-3} g$$



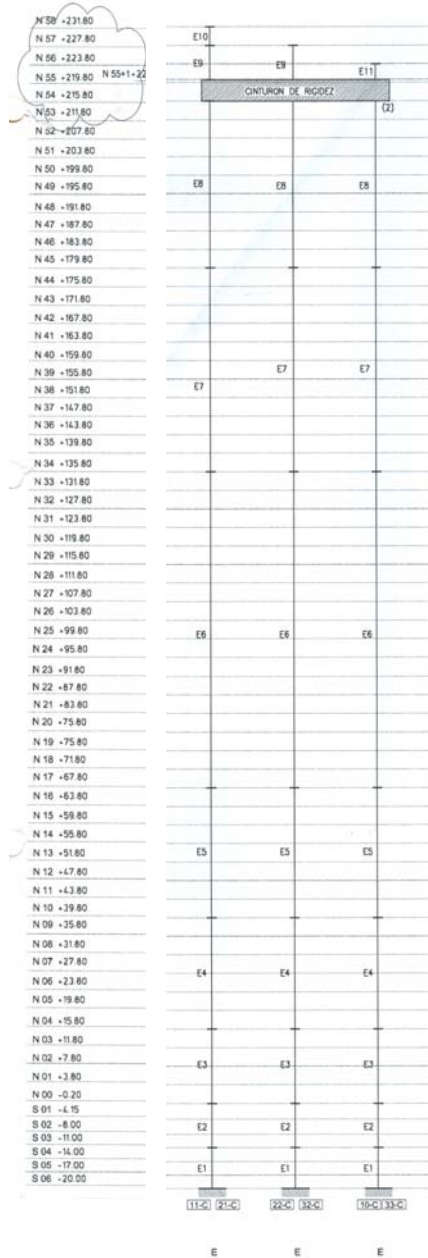
III.4.3 Effective axial stiffness of vertical concrete members

The calculation of the effective axial stiffness of the vertical concrete elements is presented in this subsection. The factor k (see subsection 5.1.2) is determined by which the axial stiffness of the gross concrete section is multiplied in the finite element model.

Firstly, the columns are dealt with and thereafter the core structure.

Columns

The connection of the floor beams with both the columns and the core allow rotation and therefore do not transmit (considerable) bending moments. The interaction between the columns and the core is therefore, as far as the lateral load resisting system is concerned, limited to the six inner radial columns connected by the outrigger structure.



The calculations of the effective axial stiffness are performed only for sections of those columns. The results are presented in ascending order of the corresponding sections. Figure III.4-1 shows the terminology adopted for the different sections of the columns 10C, 11C, 21C, 22C, 32C and 33C.

Figure III.4-1: Column sections

| Section | | E1-C70/85 | |
|----------------------------|--------------------------|----------------------------|--------------------------|
| Materials | | | |
| rolled steel | S 355 | fck [MPa] | E [MPa] |
| | | 355 | 2,10E+05 |
| mild steel | B 500 | 500 | 2,10E+05 |
| concrete | C 70/85 | 70 | 4,06E+04 |
| Geometry | | | |
| cross-sectional dimensions | 1450 mm | longitudinal reinforcement | 58 # of bars |
| | 600 mm | | 32 ϕ [mm] |
| rolled section | - | | |
| Calculation | | Results | |
| wide flange section | | equivalent column | |
| A | 0,00E+00 mm ² | A;column | 8,70E+05 mm ² |
| E | 2,10E+05 MPa | EA;column | 4,32E+10 MPa |
| longitudinal reinforcement | | | |
| A | 4,66E+04 mm ² | Δ EA due to steel | 23% |
| E | 2,10E+05 MPa | | |
| concrete | | | |
| A | 8,23E+05 mm ² | | |
| E | 4,06E+04 MPa | | |

| Section | | E4-C70/85 | |
|----------------------------|--------------------------|----------------------------|--------------------------|
| Materials | | | |
| rolled steel | S 355 | fck [MPa] | E [MPa] |
| | | 355 | 2,10E+05 |
| mild steel | B 500 | 500 | 2,10E+05 |
| concrete | C 70/85 | 70 | 4,06E+04 |
| Geometry | | | |
| cross-sectional dimensions | 900 mm | longitudinal reinforcement | 25 # of bars |
| | 760 mm | | 32 ϕ [mm] |
| rolled section | HEM-300 | | |
| Calculation | | Results | |
| wide flange section | | equivalent column | |
| A | 3,03E+04 mm ² | A;column | 6,84E+05 mm ² |
| E | 2,10E+05 MPa | EA;column | 3,63E+10 MPa |
| longitudinal reinforcement | | | |
| A | 2,01E+04 mm ² | Δ EA due to steel | 29% |
| E | 2,10E+05 MPa | | |
| concrete | | | |
| A | 6,34E+05 mm ² | | |
| E | 4,06E+04 MPa | | |

| Section | | E2-C70/85 | |
|----------------------------|--------------------------|----------------------------|--------------------------|
| Materials | | | |
| rolled steel | S 355 | fck [MPa] | E [MPa] |
| | | 355 | 2,10E+05 |
| mild steel | B 500 | 500 | 2,10E+05 |
| concrete | C 70/85 | 70 | 4,06E+04 |
| Geometry | | | |
| cross-sectional dimensions | 1450 mm | longitudinal reinforcement | 54 # of bars |
| | 600 mm | | 32 ϕ [mm] |
| rolled section | - | | |
| Calculation | | Results | |
| wide flange section | | equivalent column | |
| A | 0,00E+00 mm ² | A;column | 8,70E+05 mm ² |
| E | 2,10E+05 MPa | EA;column | 4,27E+10 MPa |
| longitudinal reinforcement | | | |
| A | 4,34E+04 mm ² | Δ EA due to steel | 21% |
| E | 2,10E+05 MPa | | |
| concrete | | | |
| A | 8,27E+05 mm ² | | |
| E | 4,06E+04 MPa | | |

| Section | | E5-C70/85 | |
|----------------------------|--------------------------|----------------------------|--------------------------|
| Materials | | | |
| rolled steel | S 355 | fck [MPa] | E [MPa] |
| | | 355 | 2,10E+05 |
| mild steel | B 500 | 500 | 2,10E+05 |
| concrete | C 70/85 | 70 | 4,06E+04 |
| Geometry | | | |
| cross-sectional dimensions | 900 mm | longitudinal reinforcement | 25 # of bars |
| | 760 mm | | 32 ϕ [mm] |
| rolled section | HEM-240 | | |
| Calculation | | Results | |
| wide flange section | | equivalent column | |
| A | 2,00E+04 mm ² | A;column | 6,84E+05 mm ² |
| E | 2,10E+05 MPa | EA;column | 3,46E+10 MPa |
| longitudinal reinforcement | | | |
| A | 2,01E+04 mm ² | Δ EA due to steel | 24% |
| E | 2,10E+05 MPa | | |
| concrete | | | |
| A | 6,44E+05 mm ² | | |
| E | 4,06E+04 MPa | | |

| Section | | E3-C70/85 | |
|----------------------------|--------------------------|----------------------------|----------------------------|
| Materials | | | |
| rolled steel | S 355 | fck [MPa] | E [MPa] |
| | | 355 | 2,10E+05 |
| mild steel | B 500 | 500 | 2,10E+05 |
| concrete | C 70/85 | 70 | 4,06E+04 |
| Geometry | | | |
| cross-sectional dimensions | 1450 mm | longitudinal reinforcement | 46 # of bars |
| | 600 mm | | 32 ϕ [mm] |
| rolled section | - | | |
| Calculation | | Results | |
| wide flange section | | equivalent column | |
| A | 0,00E+00 mm ² | A;column | 8,70E+05 mm ² |
| E | 2,10E+05 MPa | EA;column | 4,16E+10 N/mm ² |
| longitudinal reinforcement | | | |
| A | 3,70E+04 mm ² | Δ EA due to steel | 19% |
| E | 2,10E+05 MPa | | |
| concrete | | | |
| A | 8,33E+05 mm ² | | |
| E | 4,06E+04 MPa | | |

| Section | | E6-C70/85 | |
|----------------------------|--------------------------|----------------------------|--------------------------|
| Materials | | | |
| rolled steel | S 355 | fck [MPa] | E [MPa] |
| | | 355 | 2,10E+05 |
| mild steel | B 500 | 500 | 2,10E+05 |
| concrete | C 70/85 | 70 | 4,06E+04 |
| Geometry | | | |
| cross-sectional dimensions | 900 mm | longitudinal reinforcement | 23 # of bars |
| | 721 mm | | 32 ϕ [mm] |
| rolled section | HEM-240 | | |
| Calculation | | Results | |
| wide flange section | | equivalent column | |
| A | 2,00E+04 mm ² | A;column | 6,49E+05 mm ² |
| E | 2,10E+05 MPa | EA;column | 3,29E+10 MPa |
| longitudinal reinforcement | | | |
| A | 1,85E+04 mm ² | Δ EA due to steel | 25% |
| E | 2,10E+05 MPa | | |
| concrete | | | |
| A | 6,10E+05 mm ² | | |
| E | 4,06E+04 MPa | | |

| Section | | E6-C45/55 | |
|----------------------------|--------------------------|----------------------------|--------------------------|
| Materials | | | |
| rolled steel | S 355 | fck [MPa] | E [MPa] |
| | | 355 | 2,10E+05 |
| mild steel | B 500 | | 500 2,10E+05 |
| concrete | C 45/55 | | 45 3,57E+04 |
| Geometry | | | |
| cross-sectional dimensions | 900 mm | longitudinal reinforcement | 23 # of bars |
| | 721 mm | | 32 ϕ [mm] |
| rolled section | HEM-240 | | |
| Calculation | | Results | |
| wide flange section | | equivalent column | |
| A | 2,00E+04 mm ² | A;column | 6,49E+05 mm ² |
| E | 2,10E+05 MPa | EA;column | 2,99E+10 MPa |
| longitudinal reinforcement | | | |
| A | 1,85E+04 mm ² | Δ EA due to steel | 27% |
| E | 2,10E+05 MPa | | |
| concrete | | | |
| A | 6,10E+05 mm ² | | |
| E | 3,57E+04 MPa | | |

| Section | | E8-C30/37 | |
|----------------------------|--------------------------|----------------------------|--------------------------|
| Materials | | | |
| rolled steel | S 355 | fck [MPa] | E [MPa] |
| | | 355 | 2,10E+05 |
| mild steel | B 500 | | 500 2,10E+05 |
| concrete | C 30/37 | | 30 3,19E+04 |
| Geometry | | | |
| cross-sectional dimensions | 700 mm | longitudinal reinforcement | 20 # of bars |
| | 500 mm | | 32 ϕ [mm] |
| rolled section | HEM-240 | | |
| Calculation | | Results | |
| wide flange section | | equivalent column | |
| A | 2,00E+04 mm ² | A;column | 3,50E+05 mm ² |
| E | 2,10E+05 MPa | EA;column | 1,76E+10 MPa |
| longitudinal reinforcement | | | |
| A | 1,61E+04 mm ² | Δ EA due to steel | 43% |
| E | 2,10E+05 MPa | | |
| concrete | | | |
| A | 3,14E+05 mm ² | | |
| E | 3,19E+04 MPa | | |

| Section | | E7-C45/55 | |
|----------------------------|--------------------------|----------------------------|--------------------------|
| Materials | | | |
| rolled steel | S 355 | fck [MPa] | E [MPa] |
| | | 355 | 2,10E+05 |
| mild steel | B 500 | | 500 2,10E+05 |
| concrete | C 45/55 | | 45 3,57E+04 |
| Geometry | | | |
| cross-sectional dimensions | 700 mm | longitudinal reinforcement | 20 # of bars |
| | 500 mm | | 25 ϕ [mm] |
| rolled section | HEM-240 | | |
| Calculation | | Results | |
| wide flange section | | equivalent column | |
| A | 2,00E+04 mm ² | A;column | 3,50E+05 mm ² |
| E | 2,10E+05 MPa | EA;column | 1,77E+10 MPa |
| longitudinal reinforcement | | | |
| A | 9,82E+03 mm ² | Δ EA due to steel | 35% |
| E | 2,10E+05 MPa | | |
| concrete | | | |
| A | 3,20E+05 mm ² | | |
| E | 3,57E+04 MPa | | |

| Section | | E9-C30/37 | |
|----------------------------|--------------------------|----------------------------|--------------------------|
| Materials | | | |
| rolled steel | S 355 | fck [MPa] | E [MPa] |
| | | 355 | 2,10E+05 |
| mild steel | B 500 | | 500 2,10E+05 |
| concrete | C 30/37 | | 30 3,19E+04 |
| Geometry | | | |
| cross-sectional dimensions | 900 mm | longitudinal reinforcement | 26 # of bars |
| | 800 mm | | 32 ϕ [mm] |
| rolled section | - | | |
| Calculation | | Results | |
| wide flange section | | equivalent column | |
| A | 0,00E+00 mm ² | A;column | 7,20E+05 mm ² |
| E | 2,10E+05 MPa | EA;column | 2,67E+10 MPa |
| longitudinal reinforcement | | | |
| A | 2,09E+04 mm ² | Δ EA due to steel | 16% |
| E | 2,10E+05 MPa | | |
| concrete | | | |
| A | 6,99E+05 mm ² | | |
| E | 3,19E+04 MPa | | |

| Section | | E7-C30/37 | |
|----------------------------|--------------------------|----------------------------|--------------------------|
| Materials | | | |
| rolled steel | S 355 | fck [MPa] | E [MPa] |
| | | 355 | 2,10E+05 |
| mild steel | B 500 | | 500 2,10E+05 |
| concrete | C 30/37 | | 30 3,19E+04 |
| Geometry | | | |
| cross-sectional dimensions | 700 mm | longitudinal reinforcement | 20 # of bars |
| | 500 mm | | 25 ϕ [mm] |
| rolled section | HEM-240 | | |
| Calculation | | Results | |
| wide flange section | | equivalent column | |
| A | 2,00E+04 mm ² | A;column | 3,50E+05 mm ² |
| E | 2,10E+05 MPa | EA;column | 1,65E+10 MPa |
| longitudinal reinforcement | | | |
| A | 9,82E+03 mm ² | Δ EA due to steel | 38% |
| E | 2,10E+05 MPa | | |
| concrete | | | |
| A | 3,20E+05 mm ² | | |
| E | 3,19E+04 MPa | | |

| Section | | E10-C30/37 | |
|----------------------------|--------------------------|----------------------------|--------------------------|
| Materials | | | |
| rolled steel | S 355 | fck [MPa] | E [MPa] |
| | | 355 | 2,10E+05 |
| mild steel | B 500 | | 500 2,10E+05 |
| concrete | C 30/37 | | 30 3,19E+04 |
| Geometry | | | |
| cross-sectional dimensions | 700 mm | longitudinal reinforcement | 20 # of bars |
| | 500 mm | | 20 ϕ [mm] |
| rolled section | - | | |
| Calculation | | Results | |
| wide flange section | | equivalent column | |
| A | 0,00E+00 mm ² | A;column | 3,50E+05 mm ² |
| E | 2,10E+05 MPa | EA;column | 1,23E+10 MPa |
| longitudinal reinforcement | | | |
| A | 6,28E+03 mm ² | Δ EA due to steel | 11% |
| E | 2,10E+05 MPa | | |
| concrete | | | |
| A | 3,44E+05 mm ² | | |
| E | 3,19E+04 MPa | | |

| Section | | E11-C30/37 | |
|-----------------------------------|--------------------------|----------------------------|--------------------------|
| Materials | | fck [MPa] | E [MPa] |
| rolled steel | S 355 | 355 | 2,10E+05 |
| mild steel | B 500 | 500 | 2,10E+05 |
| concrete | C 30/37 | 30 | 3,19E+04 |
| Geometry | | | |
| cross-sectional dimensions | 700 mm | longitudinal reinforcement | 26 # of bars |
| | 500 mm | | 25 ϕ [mm] |
| rolled section | - | | |
| Calculation | | Results | |
| <i>wide flange section</i> | | <i>equivalent column</i> | |
| A | 0,00E+00 mm ² | A:column | 3,50E+05 mm ² |
| E | 2,10E+05 MPa | EA:column | 1,35E+10 MPa |
| <i>longitudinal reinforcement</i> | | | |
| A | 1,28E+04 mm ² | Δ EA due to steel | 20% |
| E | 2,10E+05 MPa | | |
| <i>concrete</i> | | | |
| A | 3,37E+05 mm ² | | |
| E | 3,19E+04 MPa | | |

Core

As far as the core structure is concerned, the terminology of the considered sections is provided in figure III.4-2. The effective axial stiffness is calculated of all shear wall thicknesses at every section.

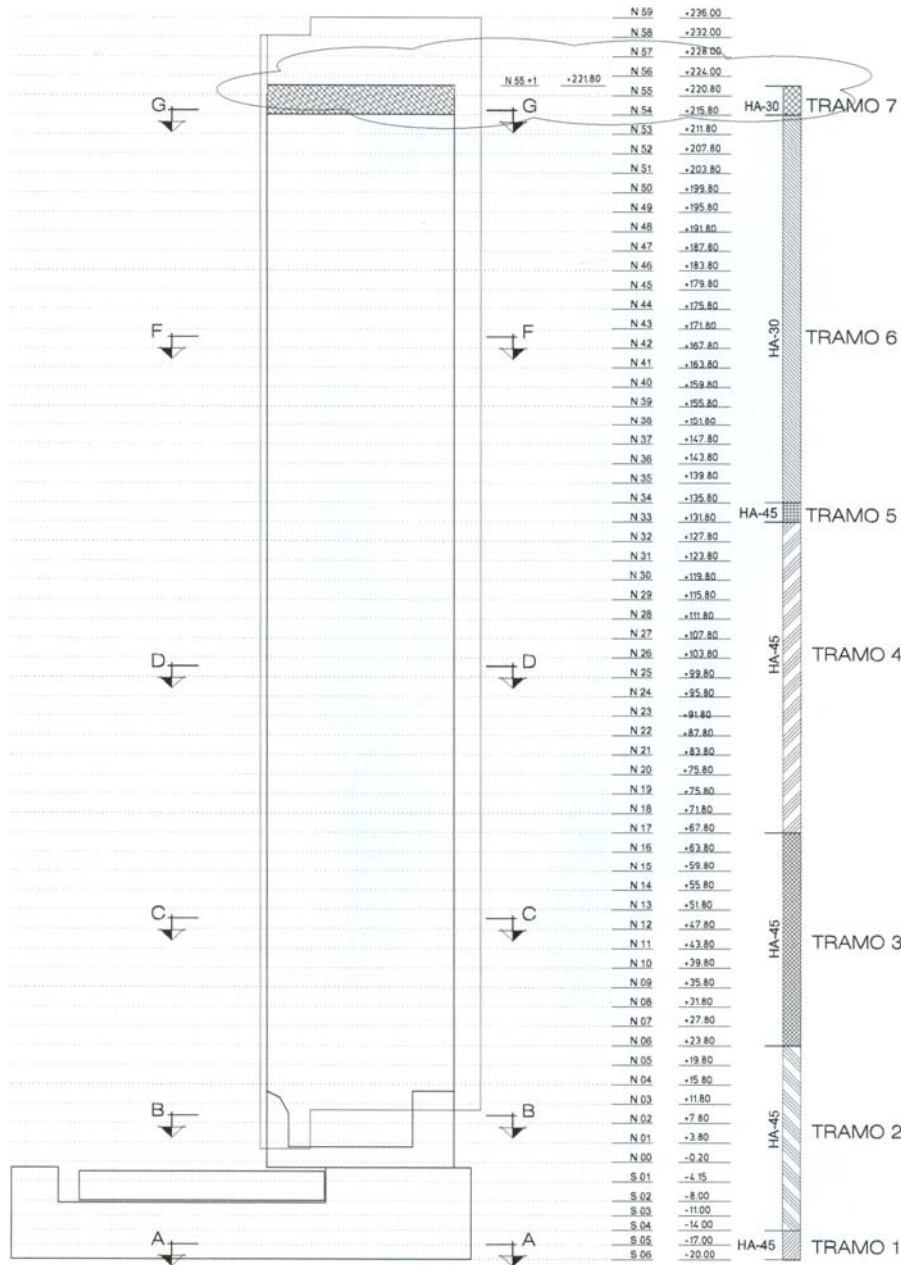


Figure III.4-2: Core sections

| Section | 1 and 2 | Shear wall | 1550 mm |
|----------------------------|--------------|----------------------------|-----------------|
| Materials | | | |
| mild steel | B 500 | fck [MPa] | E [MPa] |
| | | 500 | 2,10E+05 |
| concrete | C 45/55 | 45 | 3,57E+04 |
| Geometry | | | |
| thickness | 1550 mm | longitudinal reinforcement | φ [mm] ctc [mm] |
| width | | | 32 62,5 |
| considered | 1000 mm | | 32 62,5 |
| | | | 0 100 |
| Calculation | | Results | |
| longitudinal reinforcement | | equivalent wall | |
| A | 2,57E+04 mm2 | A;wall | 1,55E+06 mm2 |
| E | 2,10E+05 MPa | EA;wall | 5,98E+10 MPa |
| concrete | | Δ EA due to steel | |
| A | 1,52E+06 mm2 | | 8% |
| E | 3,57E+04 MPa | | |

| Section | 3 | Shear wall | 500 |
|----------------------------|--------------|----------------------------|-----------------|
| Materials | | | |
| mild steel | B 500 | fck [N/mm2] | E [N/mm2] |
| | | 500 | 2,10E+05 |
| concrete | C 45/55 | 45 | 3,57E+04 |
| Geometry | | | |
| thickness | 500 mm | longitudinal reinforcement | φ [mm] ctc [mm] |
| width | | | 25 125 |
| considered | 1000 mm | | 25 125 |
| | | | 0 125 |
| Calculation | | Results | |
| longitudinal reinforcement | | equivalent wall | |
| A | 7,85E+03 mm2 | A;wall | 5,00E+05 mm2 |
| E | 2,10E+05 MPa | EA;wall | 1,92E+10 MPa |
| concrete | | Δ EA due to steel | |
| A | 4,92E+05 mm2 | | 8% |
| E | 3,57E+04 MPa | | |

| Section | 1 and 2 | Shear wall | 500 |
|----------------------------|--------------|----------------------------|-----------------|
| Materials | | | |
| mild steel | B 500 | fck [N/mm2] | E [N/mm2] |
| | | 500 | 2,10E+05 |
| concrete | C 45/55 | 45 | 3,57E+04 |
| Geometry | | | |
| thickness | 500 mm | longitudinal reinforcement | φ [mm] ctc [mm] |
| width | | | 25 125 |
| considered | 1000 mm | | 25 125 |
| | | | 0 125 |
| Calculation | | Results | |
| longitudinal reinforcement | | equivalent wall | |
| A | 7,85E+03 mm2 | A;wall | 5,00E+05 mm2 |
| E | 2,10E+05 MPa | EA;wall | 1,92E+10 MPa |
| concrete | | Δ EA due to steel | |
| A | 4,92E+05 mm2 | | 8% |
| E | 3,57E+04 MPa | | |

| Section | 3 | Shear wall | 300 |
|----------------------------|--------------|----------------------------|-----------------|
| Materials | | | |
| mild steel | B 500 | fck [N/mm2] | E [N/mm2] |
| | | 500 | 2,10E+05 |
| concrete | C 45/55 | 45 | 3,57E+04 |
| Geometry | | | |
| thickness | 300 mm | longitudinal reinforcement | φ [mm] ctc [mm] |
| width | | | 25 250 |
| considered | 1000 mm | | 25 250 |
| | | | 0 125 |
| Calculation | | Results | |
| longitudinal reinforcement | | equivalent wall | |
| A | 3,93E+03 mm2 | A;wall | 3,00E+05 mm2 |
| E | 2,10E+05 MPa | EA;wall | 1,14E+10 MPa |
| concrete | | Δ EA due to steel | |
| A | 2,96E+05 mm2 | | 6% |
| E | 3,57E+04 MPa | | |

| Section | 1 and 2 | Shear wall | 300 |
|----------------------------|--------------|----------------------------|-----------------|
| Materials | | | |
| mild steel | B 500 | fck [N/mm2] | E [N/mm2] |
| | | 500 | 2,10E+05 |
| concrete | C 45/55 | 45 | 3,57E+04 |
| Geometry | | | |
| thickness | 300 mm | longitudinal reinforcement | φ [mm] ctc [mm] |
| width | | | 25 250 |
| considered | 1000 mm | | 25 250 |
| | | | 0 125 |
| Calculation | | Results | |
| longitudinal reinforcement | | equivalent wall | |
| A | 3,93E+03 mm2 | A;wall | 3,00E+05 mm2 |
| E | 2,10E+05 MPa | EA;wall | 1,14E+10 MPa |
| concrete | | Δ EA due to steel | |
| A | 2,96E+05 mm2 | | 6% |
| E | 3,57E+04 MPa | | |

| Section | 4 and 5 | Shear wall | 1550 |
|----------------------------|--------------|----------------------------|-----------------|
| Materials | | | |
| mild steel | B 500 | fck [N/mm2] | E [N/mm2] |
| | | 500 | 2,10E+05 |
| concrete | C 45/55 | 45 | 3,57E+04 |
| Geometry | | | |
| thickness | 1550 mm | longitudinal reinforcement | φ [mm] ctc [mm] |
| width | | | 32 62,5 |
| considered | 1000 mm | | 32 62,5 |
| | | | 0 125 |
| Calculation | | Results | |
| longitudinal reinforcement | | equivalent wall | |
| A | 2,57E+04 mm2 | A;wall | 1,55E+06 mm2 |
| E | 2,10E+05 MPa | EA;wall | 5,98E+10 MPa |
| concrete | | Δ EA due to steel | |
| A | 1,52E+06 mm2 | | 8% |
| E | 3,57E+04 MPa | | |

| Section | 3 | Shear wall | 1550 |
|----------------------------|--------------|----------------------------|-----------------|
| Materials | | | |
| mild steel | B 500 | fck [N/mm2] | E [N/mm2] |
| | | 500 | 2,10E+05 |
| concrete | C 45/55 | 45 | 3,57E+04 |
| Geometry | | | |
| thickness | 1550 mm | longitudinal reinforcement | φ [mm] ctc [mm] |
| width | | | 32 62,5 |
| considered | 1000 mm | | 32 62,5 |
| | | | 0 125 |
| Calculation | | Results | |
| longitudinal reinforcement | | equivalent wall | |
| A | 2,57E+04 mm2 | A;wall | 1,55E+06 mm2 |
| E | 2,10E+05 MPa | EA;wall | 5,98E+10 MPa |
| concrete | | Δ EA due to steel | |
| A | 1,52E+06 mm2 | | 8% |
| E | 3,57E+04 MPa | | |

| Section | 4 and 5 | Shear wall | 350 |
|----------------------------|--------------|----------------------------|-----------------|
| Materials | | | |
| mild steel | B 500 | fck [N/mm2] | E [N/mm2] |
| | | 500 | 2,10E+05 |
| concrete | C 45/55 | 45 | 3,57E+04 |
| Geometry | | | |
| thickness | 350 mm | longitudinal reinforcement | φ [mm] ctc [mm] |
| width | | | 25 125 |
| considered | 1000 mm | | 25 125 |
| | | | 0 125 |
| Calculation | | Results | |
| longitudinal reinforcement | | equivalent wall | |
| A | 7,85E+03 mm2 | A;wall | 3,50E+05 mm2 |
| E | 2,10E+05 MPa | EA;wall | 1,39E+10 MPa |
| concrete | | Δ EA due to steel | |
| A | 3,42E+05 mm2 | | 11% |
| E | 3,57E+04 MPa | | |

| Section | 4 and 5 | | Shear wall | | 300 | |
|----------------------------|----------|-----------------|----------------------------|----------|------------------------|----------|
| Materials | | | | | | |
| mild steel | B 500 | | fck [N/mm ²] | 500 | E [N/mm ²] | 2,10E+05 |
| concrete | C 45/55 | | | 45 | | 3,57E+04 |
| Geometry | | | | | | |
| thickness | 300 | mm | longitudinal reinforcement | φ [mm] | ctc [mm] | 25 |
| width | | | | 25 | 250 | |
| considered | 1000 | mm | | 0 | 125 | |
| | | | | | | |
| Calculation | | | Results | | | |
| longitudinal reinforcement | | | equivalent wall | | | |
| A | 3,93E+03 | mm ² | A;wall | 3,00E+05 | mm ² | |
| E | 2,10E+05 | MPa | EA;wall | 1,14E+10 | MPa | |
| concrete | | | | | | |
| A | 2,96E+05 | mm ² | Δ EA due to steel | | 6% | |
| E | 3,57E+04 | MPa | | | | |

| Section | 7 | | Shear wall | | 1060 | |
|----------------------------|----------|-----------------|----------------------------|----------|------------------------|----------|
| Materials | | | | | | |
| mild steel | B 500 | | fck [N/mm ²] | 500 | E [N/mm ²] | 2,10E+05 |
| concrete | C 30/37 | | | 30 | | 3,19E+04 |
| Geometry | | | | | | |
| thickness | 1060 | mm | longitudinal reinforcement | φ [mm] | ctc [mm] | 25 |
| width | | | | 25 | 110 | |
| considered | 1000 | mm | | 0 | 110 | |
| | | | | | | |
| Calculation | | | Results | | | |
| longitudinal reinforcement | | | equivalent wall | | | |
| A | 8,92E+03 | mm ² | A;wall | 1,06E+06 | mm ² | |
| E | 2,10E+05 | MPa | EA;wall | 3,54E+10 | MPa | |
| concrete | | | | | | |
| A | 1,05E+06 | mm ² | Δ EA due to steel | | 5% | |
| E | 3,19E+04 | MPa | | | | |

| Section | 6 | | Shear wall | | 1060 | |
|----------------------------|----------|-----------------|----------------------------|----------|------------------------|----------|
| Materials | | | | | | |
| mild steel | B 500 | | fck [N/mm ²] | 500 | E [N/mm ²] | 2,10E+05 |
| concrete | C 30/37 | | | 30 | | 3,19E+04 |
| Geometry | | | | | | |
| thickness | 1060 | mm | longitudinal reinforcement | φ [mm] | ctc [mm] | 25 |
| width | | | | 25 | 85 | |
| considered | 1000 | mm | | 0 | 90 | |
| | | | | | | |
| Calculation | | | Results | | | |
| longitudinal reinforcement | | | equivalent wall | | | |
| A | 1,15E+04 | mm ² | A;wall | 1,06E+06 | mm ² | |
| E | 2,10E+05 | MPa | EA;wall | 3,59E+10 | MPa | |
| concrete | | | | | | |
| A | 1,05E+06 | mm ² | Δ EA due to steel | | 6% | |
| E | 3,19E+04 | MPa | | | | |

| Section | 7 | | Shear wall | | 500 | |
|----------------------------|----------|-----------------|----------------------------|----------|------------------------|----------|
| Materials | | | | | | |
| mild steel | B 500 | | fck [N/mm ²] | 500 | E [N/mm ²] | 2,10E+05 |
| concrete | C 30/37 | | | 30 | | 3,19E+04 |
| Geometry | | | | | | |
| thickness | 500 | mm | longitudinal reinforcement | φ [mm] | ctc [mm] | 16 |
| width | | | | 16 | 125 | |
| considered | 1000 | mm | | 0 | 250 | |
| | | | | | | |
| Calculation | | | Results | | | |
| longitudinal reinforcement | | | equivalent wall | | | |
| A | 3,22E+03 | mm ² | A;wall | 5,00E+05 | mm ² | |
| E | 2,10E+05 | MPa | EA;wall | 1,65E+10 | MPa | |
| concrete | | | | | | |
| A | 4,97E+05 | mm ² | Δ EA due to steel | | 4% | |
| E | 3,19E+04 | MPa | | | | |

| Section | 6 | | Shear wall | | 300 | |
|----------------------------|----------|-----------------|----------------------------|----------|------------------------|----------|
| Materials | | | | | | |
| mild steel | B 500 | | fck [N/mm ²] | 500 | E [N/mm ²] | 2,10E+05 |
| concrete | C 30/37 | | | 30 | | 3,19E+04 |
| Geometry | | | | | | |
| thickness | 300 | mm | longitudinal reinforcement | φ [mm] | ctc [mm] | 25 |
| width | | | | 25 | 250 | |
| considered | 1000 | mm | | 0 | 250 | |
| | | | | | | |
| Calculation | | | Results | | | |
| longitudinal reinforcement | | | equivalent wall | | | |
| A | 3,93E+03 | mm ² | A;wall | 3,00E+05 | mm ² | |
| E | 2,10E+05 | MPa | EA;wall | 1,03E+10 | MPa | |
| concrete | | | | | | |
| A | 2,96E+05 | mm ² | Δ EA due to steel | | 7% | |
| E | 3,19E+04 | MPa | | | | |

| Section | 7 | | Shear wall | | 300 | |
|----------------------------|----------|-----------------|----------------------------|----------|------------------------|----------|
| Materials | | | | | | |
| mild steel | B 500 | | fck [N/mm ²] | 500 | E [N/mm ²] | 2,10E+05 |
| concrete | C 30/37 | | | 30 | | 3,19E+04 |
| Geometry | | | | | | |
| thickness | 300 | mm | longitudinal reinforcement | φ [mm] | ctc [mm] | 25 |
| width | | | | 25 | 250 | |
| considered | 1000 | mm | | 0 | 125 | |
| | | | | | | |
| Calculation | | | Results | | | |
| longitudinal reinforcement | | | equivalent wall | | | |
| A | 3,93E+03 | mm ² | A;wall | 3,00E+05 | mm ² | |
| E | 2,10E+05 | MPa | EA;wall | 1,03E+10 | MPa | |
| concrete | | | | | | |
| A | 2,96E+05 | mm ² | Δ EA due to steel | | 7% | |
| E | 3,19E+04 | MPa | | | | |

| Section | 6 | | Shear wall | | 300 | |
|----------------------------|----------|-----------------|----------------------------|----------|------------------------|----------|
| Materials | | | | | | |
| mild steel | B 500 | | fck [N/mm ²] | 500 | E [N/mm ²] | 2,10E+05 |
| concrete | C 30/37 | | | 30 | | 3,19E+04 |
| Geometry | | | | | | |
| thickness | 300 | mm | longitudinal reinforcement | φ [mm] | ctc [mm] | 25 |
| width | | | | 25 | 250 | |
| considered | 1000 | mm | | 0 | 125 | |
| | | | | | | |
| Calculation | | | Results | | | |
| longitudinal reinforcement | | | equivalent wall | | | |
| A | 3,93E+03 | mm ² | A;wall | 3,00E+05 | mm ² | |
| E | 2,10E+05 | MPa | EA;wall | 1,03E+10 | MPa | |
| concrete | | | | | | |
| A | 2,96E+05 | mm ² | Δ EA due to steel | | 7% | |
| E | 3,19E+04 | MPa | | | | |

III.5 Torre Caja Madrid

III.5.1 Equivalent static wind loading

Calculation according to Eurocode EN 1991 part 1-4

1. Input variables

| | | | |
|--|---|--------------------|----------------------------------|
| $h := 249.59 \text{ m}$ | height | $c_f := 1.05$ | force coefficient for $v_m(z_s)$ |
| $b := 53.10 \text{ m}$ | breadth | $\delta_s := 0.10$ | structural damping |
| $n_x := 0.185 \text{ Hz}$ | fundamental frequency | $\delta_d := 0.00$ | damping of dissipative devices |
| $m_e := 398.2 \cdot 10^3 \frac{\text{kg}}{\text{m}}$ | equivalent mass per unit length (averaged value over the upper 1/3) | | |

2. Structural factor

Reference height

$$z_s := 0.6 \cdot h$$

reference height $\Rightarrow z_s = 149.8 \text{ m}$

2.1 Background response

$$B(z) := \sqrt{\frac{1}{1 + 0.9 \left(\frac{b+h}{L(z)} \right)^{0.63}}}$$

Background response factor

$$L(z) := L_t \cdot \left(\frac{z}{z_t} \right)^\alpha$$

turbulence length scale $\Rightarrow L(z_s) = 251.5 \text{ m}$

where $\alpha := 0.67 + 0.05 \ln(z_0)$

$$z_t = 200 \text{ m}$$

$$L_t = 300 \text{ m}$$

2.2 Resonance response

$$R(z, n) := \sqrt{\frac{\pi^2}{2 \cdot \delta_{\text{tot}}} \cdot S_L(z, n) \cdot R_H(z, n) \cdot R_b(z, n)}$$

Background response factor $\Rightarrow B(z_s) = 0.71$

Resonance response factor

$$\delta_{\text{tot}} := \delta_s + \delta_a + \delta_d$$

total damping $\Rightarrow \delta_{\text{tot}} = 0.12$

$$\delta_s = 0.10$$

structural damping

$$\delta_a = 0.02$$

aerodynamic damping

$$\delta_d = 0.00$$

damping of dissipative devices

$$S_L(z, n) := \frac{6.8 f_L(z, n)}{(1 + 10.2 f_L(z, n))^{\frac{5}{3}}}$$

spectral density $\Rightarrow S_L(z_s, n_x) = 0.10$

$$f_L(z, n) := \frac{n \cdot L(z)}{v_m(z)} \quad \text{non-dimensional frequency} \quad \Rightarrow \quad \boxed{f_L(z_s, n_x) = 1.34}$$

$$R_h \cdot R_b \quad \text{aerodynamic admittance function}$$

$$R_h(z, n) := \frac{1}{\eta_h(z, n)} - \frac{1}{2 \cdot \eta_h(z, n)^2} \cdot \left(1 - e^{-2 \cdot \eta_h(z, n)}\right) \quad \text{where } \eta_h(z, n) := \frac{4.6h}{L(z)} \cdot f_L(z, n)$$

$$\Rightarrow \boxed{R_h(z_s, n_x) = 0.15}$$

$$R_b(z, n) := \frac{1}{\eta_b(z, n)} - \frac{1}{2 \cdot \eta_b(z, n)^2} \cdot \left(1 - e^{-2 \cdot \eta_b(z, n)}\right) \quad \text{where } \eta_b(z, n) := \frac{4.6b}{L(z)} \cdot f_L(z, n)$$

$$\Rightarrow \boxed{R_b(z_s, n_x) = 0.50}$$

$$R(z, n) := \frac{\pi^2}{2 \cdot \delta_{tot}} \cdot S_L(z, n) \cdot R_h(z, n) \cdot R_b(z, n) \quad \text{Resonance response factor} \quad \Rightarrow \quad \boxed{R(z_s, n_x) = 0.57}$$

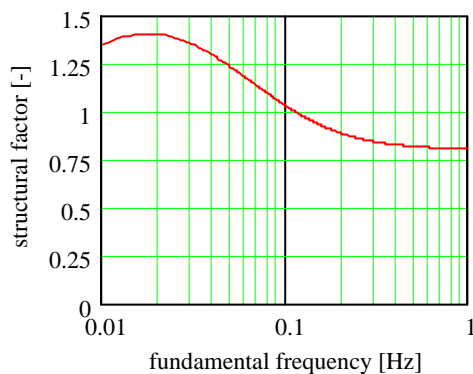
2.3 Results

$$k_p(z, n) := \sqrt{2 \cdot \ln(v(z, n) \cdot T)} + \frac{0.6}{\sqrt{2 \cdot \ln(v(z, n) \cdot T)}} \quad \text{peak factor of the structural response, where}$$

$$v(z, n) := n \cdot \frac{R(z, n)^2}{B(z)^2 + R(z, n)^2} \quad \text{peak factor} \quad \Rightarrow \quad \boxed{k_p(z_s, n_x) = 3.12}$$

$$c_s(z) := \frac{1 + 7 \cdot I_V(z) \cdot \sqrt{B(z)^2}}{1 + 7 \cdot I_V(z)} \quad \text{Size factor} \quad \Rightarrow \quad \boxed{c_s(z_s) = 0.84}$$

$$c_d(z, n) := \frac{1 + 2 \cdot k_p(z, n) \cdot I_V(z) \cdot \sqrt{B(z)^2 + R(z, n)^2}}{1 + 7 \cdot I_V(z) \cdot \sqrt{B(z)^2}} \quad \text{Dynamic factor} \quad \Rightarrow \quad \boxed{c_d(z_s, n_x) = 1.07}$$



$$\text{Structural factor} \Rightarrow \boxed{c_s(z_s) \cdot c_d(z_s, n_x) = 0.90}$$

| STOREY ₁ = | HEIGHT ₁ = | Z ₁ = | EQ_ST_PEAK_PRESSURE ₁ = |
|-----------------------|-----------------------|------------------|------------------------------------|
| "REC" | 5.24 m | -0.05 m | 1.11 kPa |
| "IM1" | 5.05 | 5.19 | 1.11 |
| "IM2" | 5.42 | 10.24 | 1.11 |
| "NIA" | 3.52 | 15.66 | 1.11 |
| "NSA" | 5.43 | 19.18 | 1.11 |
| "IN1" | 4.17 | 24.61 | 1.11 |
| "EIN1" | 5.45 | 28.78 | 1.11 |
| 1 | 4.75 | 34.23 | 1.11 |
| 2 | 4.70 | 38.98 | 1.11 |
| 3 | 4.70 | 43.68 | 1.11 |
| 4 | 4.70 | 48.38 | 1.11 |
| 5 | 4.70 | 53.08 | 1.11 |
| 6 | 4.70 | 57.78 | 1.14 |
| 7 | 4.70 | 62.48 | 1.16 |
| 8 | 4.70 | 67.18 | 1.18 |
| 9 | 4.70 | 71.88 | 1.21 |
| 10 | 4.70 | 76.58 | 1.23 |
| 11 | 5.38 | 81.28 | 1.24 |
| "IN2" | 4.17 | 86.66 | 1.26 |
| "EIN2" | 5.45 | 90.83 | 1.28 |
| 12 | 4.75 | 96.28 | 1.30 |
| 13 | 4.70 | 101.03 | 1.31 |
| 14 | 4.70 | 105.73 | 1.33 |
| 15 | 4.70 | 110.43 | 1.34 |
| 16 | 4.70 | 115.13 | 1.36 |
| 17 | 4.70 | 119.83 | 1.37 |
| 18 | 4.70 | 124.53 | 1.38 |
| 19 | 4.70 | 129.23 | 1.40 |
| 20 | 4.70 | 133.93 | 1.41 |
| 21 | 4.70 | 138.63 | 1.42 |
| 22 | 4.70 | 143.33 | 1.43 |
| 23 | 5.38 | 148.03 | 1.44 |
| "IN3" | 4.17 | 153.41 | 1.46 |
| "EIN3" | 5.45 | 157.58 | 1.46 |

| STOREY ₁ = | HEIGHT ₁ = | Z ₁ = | EQ_ST_PEAK_PRESSURE ₁ |
|-----------------------|-----------------------|------------------|----------------------------------|
| 24 | 4.75 m | 163.03 m | 1.48 kPa |
| 25 | 4.70 | 167.78 | 1.49 |
| 26 | 4.70 | 172.48 | 1.50 |
| 27 | 4.70 | 177.18 | 1.51 |
| 28 | 4.70 | 181.88 | 1.51 |
| 29 | 4.70 | 186.58 | 1.52 |
| 30 | 4.70 | 191.28 | 1.53 |
| 31 | 4.70 | 195.98 | 1.54 |
| 32 | 4.70 | 200.68 | 1.63 |
| 33 | 4.70 | 205.38 | 1.63 |
| 34 | 5.07 | 210.08 | 1.63 |
| "BC" | 4.52 | 215.15 | 1.63 |
| "C BO" | 4.53 | 219.67 | 1.63 |
| "INF A" | 3.95 | 224.20 | 1.63 |
| "INT A" | 5.25 | 228.15 | 1.63 |
| SUP A" | 4.93 | 233.40 | 1.63 |
| T SUP" | 4.17 | 238.33 | 1.63 |
| "EP" | 3.03 | 242.50 | 1.63 |
| "C AR" | 4.06 | 245.53 | 1.63 |
| "C NU" | 0.00 | 249.59 | 1.63 |

III.5.2 Building accelerations

Calculation according to Eurocode EN 1991 part 1-4

1. Input variables

$$h_{\text{foundation}} := 18.15 \text{ m}$$

height between grade and the foundation level

$$T_{\text{return}} = 10$$

$$k_{\text{adj}} := 0.92$$

factor to account for hole in the upper part

$$z_{\text{occ.floor}} := 215.15 \text{ m}$$

height of the top occupied floor

$$\zeta := 1.4$$

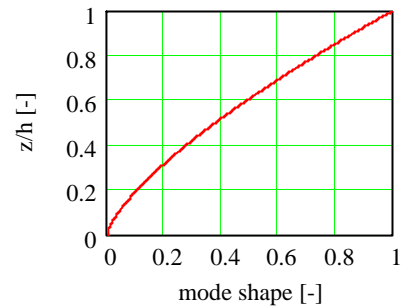
mode exponent best fitting actual mode shape

$$A_{1,x} := 0.4$$

area under the actual mode shape function

$$\Phi_{1,x}(z) := \left(\frac{z + h_{\text{foundation}}}{h + h_{\text{foundation}}} \right)^\zeta$$

approximated mode shape =>



2. Accelerations

2.1 Calculation unknown variables

$$R(z, n) := \sqrt{\frac{\pi^2}{2 \cdot \delta_{\text{tot}}} \cdot S_L(z, n) \cdot R_h(z, n) \cdot R_b(z, n)}$$

Resonance response factor

$$\delta_{\text{tot}} := 0.01 \cdot 2\pi$$

total damping =>

$$\delta_{\text{tot}} = 0.06$$

$$S_L(z, n) := \frac{6.8 f_L(z, n)}{\frac{5}{(1 + 10.2 f_L(z, n))^3}}$$

spectral density =>

$$S_L(z_s, n_x) = 0.10$$

$$f_L(z, n) := \frac{n \cdot L(z)}{v_m(z)}$$

non-dimensional frequency =>

$$f_L(z_s, n_x) = 1.48$$

$$R_h \cdot R_b$$

aerodynamic admittance function

$$R_h(z, n) := \frac{1}{\eta_h(z, n)} - \frac{1}{2 \cdot \eta_h(z, n)^2} \cdot \left(1 - e^{-2 \cdot \eta_h(z, n)} \right) \quad \text{where } \eta_h(z, n) := \frac{4.6 \cdot h}{L(z)} \cdot f_L(z, n)$$

$$\Rightarrow R_h(z_s, n_x) = 0.14$$

$$R_b(z, n) := \frac{1}{\eta_b(z, n)} - \frac{1}{2 \cdot \eta_b(z, n)^2} \cdot \left(1 - e^{-2 \cdot \eta_b(z, n)} \right) \quad \text{where } \eta_b(z, n) := \frac{4.6 \cdot b}{L(z)} \cdot f_L(z, n)$$

$$\Rightarrow R_b(z_s, n_x) = 0.47$$

$$R(z, n) := \sqrt{\frac{\pi^2}{2 \cdot \delta_{\text{tot}}} \cdot S_L(z, n) \cdot R_h(z, n) \cdot R_b(z, n)}$$

Resonance response factor =>

$$R(z_s, n_x) = 0.70$$

$$K_x := (2 \cdot \zeta + 1) \cdot \frac{(\zeta + 1) \cdot \ln\left(\frac{z_s}{z_0}\right) + 0.5 - 1}{(\zeta + 1)^2 \cdot \ln\left(\frac{z_s}{z_0}\right)}$$

adimensional factor =>

$$K_x = 1.6$$

$$m_{1,x} := A_{1,x} \cdot m_e$$

equivalent modal
mass per unit
length =>

$$m_{1,x} = 163.3 \times 10^3 \frac{\text{kg}}{\text{m}}$$

$$k_p := \sqrt{2 \cdot \ln(v \cdot T)} + \frac{0.6}{\sqrt{2 \cdot \ln(v \cdot T)}}$$

peak factor of the
structural response =>

$$k_p = 3.26$$

with $v := n_x$

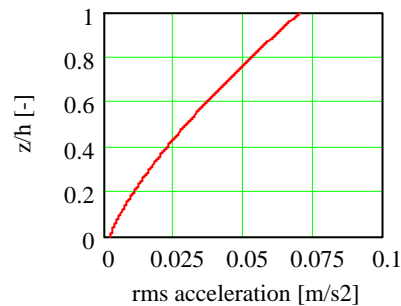
2.2 Results for $T_{\text{return}} = 10$ years

$$\sigma_{a,x}(z, n) := \frac{c_f \cdot \rho \cdot k_{\text{adj}} \cdot b \cdot I_V(z_s) \cdot v_m(z_s)^2}{m_{1,x}} \cdot R(z_s, n_x) \cdot K_x \cdot \Phi_{1,x}(z)$$

value at top occupied floor:

$$\sigma_{a,x}(z_{\text{occ.floor}}, n_x) = 0.058 \frac{\text{m}}{\text{s}^2}$$

$$\sigma_{a,x}(z_{\text{occ.floor}}, n_x) = 5.9 \times 10^{-3} \text{ g}$$

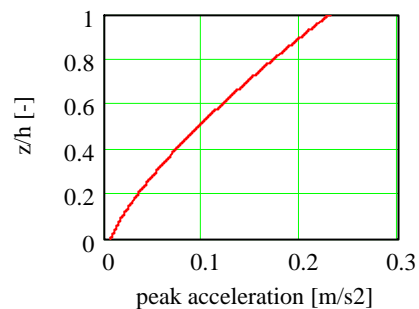


$$a_{\text{peak},x}(z, n) := \frac{c_f \cdot \rho \cdot k_{\text{adj}} \cdot b \cdot k_p \cdot I_V(z_s) \cdot v_m(z_s)^2}{m_{1,x}} \cdot R(z_s, n_x) \cdot K_x \cdot \Phi_{1,x}(z)$$

value at top occupied floor:

$$a_{\text{peak},x}(z_{\text{occ.floor}}, n_x) = 0.189 \frac{\text{m}}{\text{s}^2}$$

$$a_{\text{peak},x}(z_{\text{occ.floor}}, n_x) = 19.3 \times 10^{-3} \text{ g}$$



Calculation according to Eurocode EN 1991 part 1-4

1. Input variables

$$T_{\text{return}} = 5$$

$$h_{\text{foundation}} := 18.15 \text{ m}$$

height between grade and the foundation level

$$k_{\text{adj}} := 0.92$$

factor to account for hole in the upper part

$$z_{\text{occ.floor}} := 215.15 \text{ m}$$

height of the top occupied floor

$$\zeta := 1.4$$

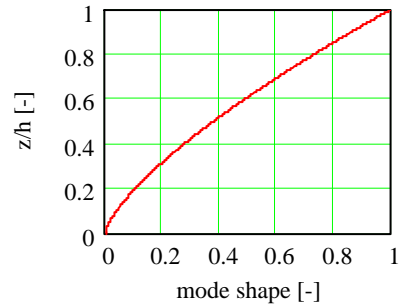
mode exponent best fitting actual mode shape

$$A_{1,x} := 0.4$$

area under the actual mode shape function

$$\Phi_{1,x}(z) := \left(\frac{z + h_{\text{foundation}}}{h + h_{\text{foundation}}} \right)^{\zeta}$$

approximated mode shape =>



2. Accelerations

2.1 Calculation unknown variables

$$R(z, n) := \sqrt{\frac{2}{\pi} \cdot S_L(z, n) \cdot R_h(z, n) \cdot R_b(z, n)} \cdot 2 \cdot \delta_{\text{tot}}$$

Resonance response factor

$$\delta_{\text{tot}} := 0.01 \cdot 2\pi$$

total damping =>

$$\delta_{\text{tot}} = 0.06$$

$$S_L(z, n) := \frac{6.8 \cdot f_L(z, n)}{(1 + 10.2 \cdot f_L(z, n))^{\frac{5}{3}}}$$

spectral density =>

$$S_L(z_s, n_x) = 0.10$$

$$f_L(z, n) := \frac{n \cdot L(z)}{v_m(z)}$$

non-dimensional frequency =>

$$f_L(z_s, n_x) = 1.56$$

$$R_h \cdot R_b$$

aerodynamic admittance function

$$R_h(z, n) := \frac{1}{\eta_h(z, n)} - \frac{1}{2 \cdot \eta_h(z, n)^2} \cdot \left(1 - e^{-2 \cdot \eta_h(z, n)} \right) \quad \text{where } \eta_h(z, n) := \frac{4.6 \cdot h}{L(z)} \cdot f_L(z, n)$$

$$\Rightarrow R_h(z_s, n_x) = 0.13$$

$$R_b(z, n) := \frac{1}{\eta_b(z, n)} - \frac{1}{2 \cdot \eta_b(z, n)^2} \cdot \left(1 - e^{-2 \cdot \eta_b(z, n)} \right) \quad \text{where } \eta_b(z, n) := \frac{4.6 \cdot b}{L(z)} \cdot f_L(z, n)$$

$$\Rightarrow R_b(z_s, n_x) = 0.45$$

$$R(z, n) := \sqrt{\frac{2}{\pi} \cdot S_L(z, n) \cdot R_h(z, n) \cdot R_b(z, n)} \cdot 2 \cdot \delta_{\text{tot}}$$

Resonance response factor =>

$$R(z_s, n_x) = 0.66$$

$$K_x := (2 \cdot \zeta + 1) \cdot \frac{(\zeta + 1) \cdot \ln\left(\frac{z_s}{z_0}\right) + 0.5 - 1}{(\zeta + 1)^2 \cdot \ln\left(\frac{z_s}{z_0}\right)}$$

adimensional factor =>

$$K_x = 1.6$$

$$m_{1,x} := A_{1,x} \cdot m_e$$

equivalent modal
mass per unit
length =>

$$m_{1,x} = 163.3 \times 10^3 \frac{\text{kg}}{\text{m}}$$

$$k_p := \sqrt{2 \cdot \ln(v \cdot T)} + \frac{0.6}{\sqrt{2 \cdot \ln(v \cdot T)}}$$

peak factor of the
structural response =>

$$k_p = 3.26$$

with $v := n_x$

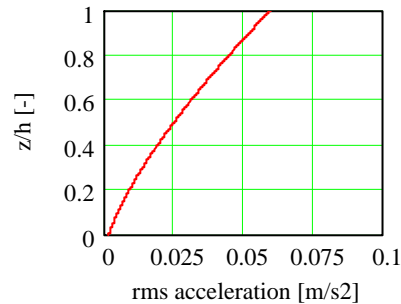
2.2 Results for $T_{\text{return}} = 5$ years

$$\sigma_{a,x}(z, n) := \frac{c_f \cdot \rho \cdot k_{\text{adj}} \cdot b \cdot I_V(z_s) \cdot v_m(z_s)^2}{m_{1,x}} \cdot R(z_s, n_x) \cdot K_x \cdot \Phi_{1,x}(z)$$

value at top occupied floor:

$$\sigma_{a,x}(z_{\text{occ.floor}}, n_x) = 0.049 \frac{\text{m}}{\text{s}^2}$$

$$\sigma_{a,x}(z_{\text{occ.floor}}, n_x) = 5.0 \times 10^{-3} \text{ g}$$

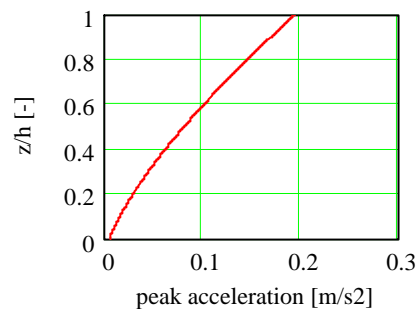


$$a_{\text{peak},x}(z, n) := \frac{c_f \cdot \rho \cdot k_{\text{adj}} \cdot b \cdot k_p \cdot I_V(z_s) \cdot v_m(z_s)^2}{m_{1,x}} \cdot R(z_s, n_x) \cdot K_x \cdot \Phi_{1,x}(z)$$

value at top occupied floor:

$$a_{\text{peak},x}(z_{\text{occ.floor}}, n_x) = 0.160 \frac{\text{m}}{\text{s}^2}$$

$$a_{\text{peak},x}(z_{\text{occ.floor}}, n_x) = 16.3 \times 10^{-3} \text{ g}$$



III.5.3 Effective axial stiffness of vertical concrete members

The effective axial stiffness of the vertical concrete elements is determined in this subsection. The factor k (see subsection 5.1.2) is computed by which the axial stiffness of the gross concrete section is multiplied in the finite element model.

The only vertical concrete elements that constitute the lateral load resisting system in the considered wind direction are the two lateral cores, because of which no calculations are performed for the inner composite columns. Figure III.5-1 demonstrates the terminology adopted in the calculations for the different shear walls.

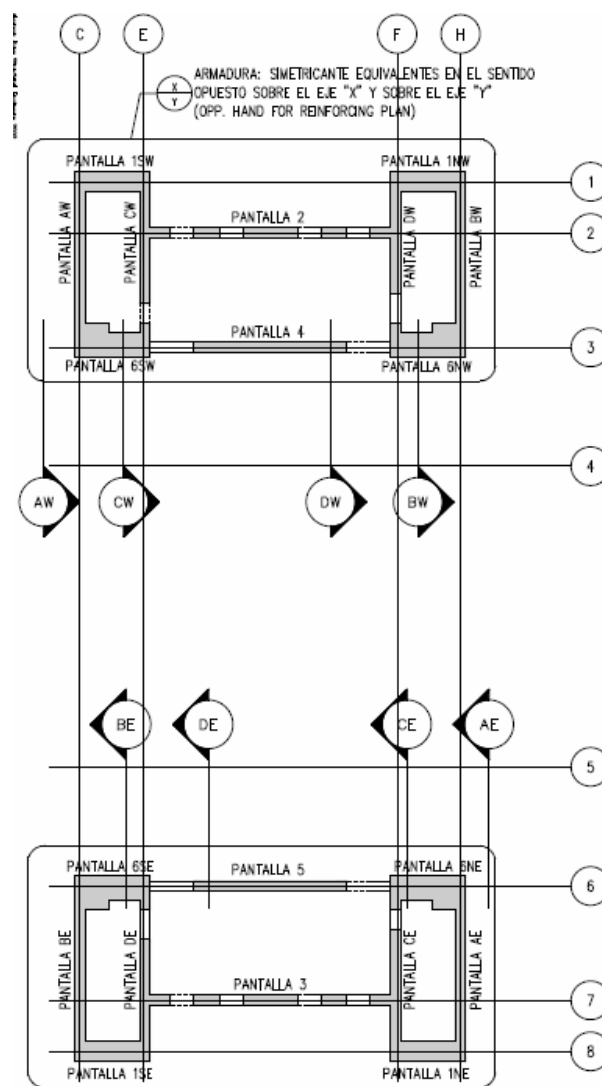


Figure III.5-1: Terminology shear walls

| Section | AE, AW, BE, BW / B5-2 | | Shear wall | | - |
|----------------------------|-----------------------|-----|----------------------------|----------|----------|
| Materials | | | | | |
| mild steel | B 500 | | fck [MPa] | 500 | E [MPa] |
| concrete | C 55/65 | | | 55 | 3,78E+04 |
| Geometry | | | | | |
| thickness | 600 | mm | longitudinal reinforcement | φ [mm] | ctc [mm] |
| width | | | | 20 | 300 |
| considered | 1000 | mm | | 20 | 300 |
| | | | | 0 | 100 |
| Calculation | | | Results | | |
| longitudinal reinforcement | | | equivalent wall | | |
| A | 2,09E+03 | mm2 | A;wall | 6,00E+05 | mm2 |
| E | 2,10E+05 | MPa | EA;wall | 2,30E+10 | MPa |
| concrete | | | | | |
| A | 5,98E+05 | mm2 | Δ EA due to steel | 2% | |
| E | 3,78E+04 | MPa | | | |

| Section | AE,AW,BE,BW / 33-TOP | | Shear wall | | - |
|----------------------------|----------------------|-----|----------------------------|----------|----------|
| Materials | | | | | |
| mild steel | B 500 | | fck [MPa] | 500 | E [MPa] |
| concrete | C 40/50 | | | 40 | 3,45E+04 |
| Geometry | | | | | |
| thickness | 400 | mm | longitudinal reinforcement | φ [mm] | ctc [mm] |
| width | | | | 12 | 300 |
| considered | 1000 | mm | | 12 | 300 |
| | | | | 0 | 100 |
| Calculation | | | Results | | |
| longitudinal reinforcement | | | equivalent wall | | |
| A | 7,54E+02 | mm2 | A;wall | 4,00E+05 | mm2 |
| E | 2,10E+05 | MPa | EA;wall | 1,39E+10 | MPa |
| concrete | | | | | |
| A | 3,99E+05 | mm2 | Δ EA due to steel | 1% | |
| E | 3,45E+04 | MPa | | | |

| Section | AE, AW, BE, BW / 2-13 | | Shear wall | | - |
|----------------------------|-----------------------|-----|----------------------------|----------|----------|
| Materials | | | | | |
| mild steel | B 500 | | fck [MPa] | 500 | E [MPa] |
| concrete | C 50/60 | | | 50 | 3,68E+04 |
| Geometry | | | | | |
| thickness | 600 | mm | longitudinal reinforcement | φ [mm] | ctc [mm] |
| width | | | | 16 | 300 |
| considered | 1000 | mm | | 16 | 300 |
| | | | | 0 | 100 |
| Calculation | | | Results | | |
| longitudinal reinforcement | | | equivalent wall | | |
| A | 1,34E+03 | mm2 | A;wall | 6,00E+05 | mm2 |
| E | 2,10E+05 | MPa | EA;wall | 2,23E+10 | MPa |
| concrete | | | | | |
| A | 5,99E+05 | mm2 | Δ EA due to steel | 1% | |
| E | 3,68E+04 | MPa | | | |

| Section | CE,CW,DE,DW / B5-2 | | Shear wall | | - |
|----------------------------|--------------------|-----|----------------------------|----------|----------|
| Materials | | | | | |
| mild steel | B 500 | | fck [MPa] | 500 | E [MPa] |
| concrete | C 55/65 | | | 55 | 3,78E+04 |
| Geometry | | | | | |
| thickness | 600 | mm | longitudinal reinforcement | φ [mm] | ctc [mm] |
| width | | | | 20 | 300 |
| considered | 1000 | mm | | 20 | 300 |
| | | | | 0 | 100 |
| Calculation | | | Results | | |
| longitudinal reinforcement | | | equivalent wall | | |
| A | 2,09E+03 | mm2 | A;wall | 6,00E+05 | mm2 |
| E | 2,10E+05 | MPa | EA;wall | 2,30E+10 | MPa |
| concrete | | | | | |
| A | 5,98E+05 | mm2 | Δ EA due to steel | 2% | |
| E | 3,78E+04 | MPa | | | |

| Section | AE, AW, BE, BW / 13-25 | | Shear wall | | - |
|----------------------------|------------------------|-----|----------------------------|----------|----------|
| Materials | | | | | |
| mild steel | B 500 | | fck [MPa] | 500 | E [MPa] |
| concrete | C 40/50 | | | 40 | 3,45E+04 |
| Geometry | | | | | |
| thickness | 600 | mm | longitudinal reinforcement | φ [mm] | ctc [mm] |
| width | | | | 16 | 300 |
| considered | 1000 | mm | | 16 | 300 |
| | | | | 0 | 100 |
| Calculation | | | Results | | |
| longitudinal reinforcement | | | equivalent wall | | |
| A | 1,34E+03 | mm2 | A;wall | 6,00E+05 | mm2 |
| E | 2,10E+05 | MPa | EA;wall | 2,10E+10 | MPa |
| concrete | | | | | |
| A | 5,99E+05 | mm2 | Δ EA due to steel | 1% | |
| E | 3,45E+04 | MPa | | | |

| Section | CE,CW,DE,DW / 2-13 | | Shear wall | | - |
|----------------------------|--------------------|-----|----------------------------|----------|----------|
| Materials | | | | | |
| mild steel | B 500 | | fck [MPa] | 500 | E [MPa] |
| concrete | C 50/60 | | | 50 | 3,68E+04 |
| Geometry | | | | | |
| thickness | 600 | mm | longitudinal reinforcement | φ [mm] | ctc [mm] |
| width | | | | 16 | 300 |
| considered | 1000 | mm | | 16 | 300 |
| | | | | 0 | 100 |
| Calculation | | | Results | | |
| longitudinal reinforcement | | | equivalent wall | | |
| A | 1,34E+03 | mm2 | A;wall | 6,00E+05 | mm2 |
| E | 2,10E+05 | MPa | EA;wall | 2,23E+10 | MPa |
| concrete | | | | | |
| A | 5,99E+05 | mm2 | Δ EA due to steel | 1% | |
| E | 3,68E+04 | MPa | | | |

| Section | AE,AW,BE,BW / 25-33 | | Shear wall | | - |
|----------------------------|---------------------|-----|----------------------------|----------|----------|
| Materials | | | | | |
| mild steel | B 500 | | fck [MPa] | 500 | E [MPa] |
| concrete | C 40/50 | | | 40 | 3,45E+04 |
| Geometry | | | | | |
| thickness | 400 | mm | longitudinal reinforcement | φ [mm] | ctc [mm] |
| width | | | | 16 | 300 |
| considered | 1000 | mm | | 16 | 300 |
| | | | | 0 | 100 |
| Calculation | | | Results | | |
| longitudinal reinforcement | | | equivalent wall | | |
| A | 1,34E+03 | mm2 | A;wall | 4,00E+05 | mm2 |
| E | 2,10E+05 | MPa | EA;wall | 1,40E+10 | MPa |
| concrete | | | | | |
| A | 3,99E+05 | mm2 | Δ EA due to steel | 2% | |
| E | 3,45E+04 | MPa | | | |

| Section | CE,CW,DE,DW / 13-25 | | Shear wall | | - |
|----------------------------|---------------------|-----|----------------------------|----------|----------|
| Materials | | | | | |
| mild steel | B 500 | | fck [MPa] | 500 | E [MPa] |
| concrete | C 40/50 | | | 40 | 3,45E+04 |
| Geometry | | | | | |
| thickness | 600 | mm | longitudinal reinforcement | φ [mm] | ctc [mm] |
| width | | | | 16 | 300 |
| considered | 1000 | mm | | 16 | 300 |
| | | | | 0 | 100 |
| Calculation | | | Results | | |
| longitudinal reinforcement | | | equivalent wall | | |
| A | 1,34E+03 | mm2 | A;wall | 6,00E+05 | mm2 |
| E | 2,10E+05 | MPa | EA;wall | 2,10E+10 | MPa |
| concrete | | | | | |
| A | 5,99E+05 | mm2 | Δ EA due to steel | 1% | |
| E | 3,45E+04 | MPa | | | |

| Section | CE,CW,DE,DW / 25-33 | Shear wall | - |
|----------------------------|---------------------|----------------------------|--------------|
| Materials | | | |
| mild steel | B 500 | fck [MPa] | E [MPa] |
| concrete | C 40/50 | 500 | 2,10E+05 |
| | | 40 | 3,45E+04 |
| Geometry | | | |
| thickness | 400 mm | φ [mm] | ctc [mm] |
| width considered | 1000 mm | longitudinal reinforcement | 16 300 |
| | | | 16 300 |
| | | | 0 100 |
| Calculation | | Results | |
| longitudinal reinforcement | | equivalent wall | |
| A | 1,34E+03 mm2 | A;wall | 4,00E+05 mm2 |
| E | 2,10E+05 MPa | EA;wall | 1,40E+10 MPa |
| concrete | | | |
| A | 3,99E+05 mm2 | Δ EA due to steel | 2% |
| E | 3,45E+04 MPa | | |

| Section | 1SE,1NE,1SW,1NW / 13-25 | Shear wall | - |
|----------------------------|-------------------------|----------------------------|--------------|
| Materials | | | |
| mild steel | B 500 | fck [MPa] | E [MPa] |
| concrete | C 40/50 | 500 | 2,10E+05 |
| | | 40 | 3,45E+04 |
| Geometry | | | |
| thickness | 600 mm | φ [mm] | ctc [mm] |
| width considered | 1000 mm | longitudinal reinforcement | 16 300 |
| | | | 16 300 |
| | | | 0 100 |
| Calculation | | Results | |
| longitudinal reinforcement | | equivalent wall | |
| A | 1,34E+03 mm2 | A;wall | 6,00E+05 mm2 |
| E | 2,10E+05 MPa | EA;wall | 2,10E+10 MPa |
| concrete | | | |
| A | 5,99E+05 mm2 | Δ EA due to steel | 1% |
| E | 3,45E+04 MPa | | |

| Section | CE,CW,DE,DW / 33-TOP | Shear wall | - |
|----------------------------|----------------------|----------------------------|--------------|
| Materials | | | |
| mild steel | B 500 | fck [MPa] | E [MPa] |
| concrete | C 40/50 | 500 | 2,10E+05 |
| | | 40 | 3,45E+04 |
| Geometry | | | |
| thickness | 400 mm | φ [mm] | ctc [mm] |
| width considered | 1000 mm | longitudinal reinforcement | 12 300 |
| | | | 12 300 |
| | | | 0 100 |
| Calculation | | Results | |
| longitudinal reinforcement | | equivalent wall | |
| A | 7,54E+02 mm2 | A;wall | 4,00E+05 mm2 |
| E | 2,10E+05 MPa | EA;wall | 1,39E+10 MPa |
| concrete | | | |
| A | 3,99E+05 mm2 | Δ EA due to steel | 1% |
| E | 3,45E+04 MPa | | |

| Section | 1SE,1NE,1SW,1NW / 25-TOP | Shear wall | - |
|----------------------------|--------------------------|----------------------------|--------------|
| Materials | | | |
| mild steel | B 500 | fck [MPa] | E [MPa] |
| concrete | C 40/50 | 500 | 2,10E+05 |
| | | 40 | 3,45E+04 |
| Geometry | | | |
| thickness | 400 mm | φ [mm] | ctc [mm] |
| width considered | 1000 mm | longitudinal reinforcement | 12 300 |
| | | | 12 300 |
| | | | 0 100 |
| Calculation | | Results | |
| longitudinal reinforcement | | equivalent wall | |
| A | 7,54E+02 mm2 | A;wall | 4,00E+05 mm2 |
| E | 2,10E+05 MPa | EA;wall | 1,39E+10 MPa |
| concrete | | | |
| A | 3,99E+05 mm2 | Δ EA due to steel | 1% |
| E | 3,45E+04 MPa | | |

| Section | 1SE,1NE,1SW,1NW / B5-2 | Shear wall | - |
|----------------------------|------------------------|----------------------------|--------------|
| Materials | | | |
| mild steel | B 500 | fck [MPa] | E [MPa] |
| concrete | C 55/67 | 500 | 2,10E+05 |
| | | 55 | 3,78E+04 |
| Geometry | | | |
| thickness | 1200 mm | φ [mm] | ctc [mm] |
| width considered | 1000 mm | longitudinal reinforcement | 25 150 |
| | | | 25 150 |
| | | | 0 100 |
| Calculation | | Results | |
| longitudinal reinforcement | | equivalent wall | |
| A | 6,54E+03 mm2 | A;wall | 1,20E+06 mm2 |
| E | 2,10E+05 MPa | EA;wall | 4,65E+10 MPa |
| concrete | | | |
| A | 1,19E+06 mm2 | Δ EA due to steel | 2% |
| E | 3,78E+04 MPa | | |

| Section | 2, 3 / B5-2 | Shear wall | - |
|----------------------------|--------------|----------------------------|--------------|
| Materials | | | |
| mild steel | B 500 | fck [MPa] | E [MPa] |
| concrete | C 55/67 | 500 | 2,10E+05 |
| | | 55 | 3,78E+04 |
| Geometry | | | |
| thickness | 600 mm | φ [mm] | ctc [mm] |
| width considered | 1000 mm | longitudinal reinforcement | 20 150 |
| | | | 20 150 |
| | | | 0 100 |
| Calculation | | Results | |
| longitudinal reinforcement | | equivalent wall | |
| A | 4,19E+03 mm2 | A;wall | 6,00E+05 mm2 |
| E | 2,10E+05 MPa | EA;wall | 2,34E+10 MPa |
| concrete | | | |
| A | 5,96E+05 mm2 | Δ EA due to steel | 3% |
| E | 3,78E+04 MPa | | |

| Section | 1SE,1NE,1SW,1NW / 2-13 | Shear wall | - |
|----------------------------|------------------------|----------------------------|--------------|
| Materials | | | |
| mild steel | B 500 | fck [MPa] | E [MPa] |
| concrete | C 50/60 | 500 | 2,10E+05 |
| | | 50 | 3,68E+04 |
| Geometry | | | |
| thickness | 1200 mm | φ [mm] | ctc [mm] |
| width considered | 1000 mm | longitudinal reinforcement | 25 300 |
| | | | 25 300 |
| | | | 0 100 |
| Calculation | | Results | |
| longitudinal reinforcement | | equivalent wall | |
| A | 3,27E+03 mm2 | A;wall | 1,20E+06 mm2 |
| E | 2,10E+05 MPa | EA;wall | 4,47E+10 MPa |
| concrete | | | |
| A | 1,20E+06 mm2 | Δ EA due to steel | 1% |
| E | 3,68E+04 MPa | | |

| Section | 2, 3 / 2-13 | Shear wall | - |
|----------------------------|--------------|----------------------------|--------------|
| Materials | | | |
| mild steel | B 500 | fck [MPa] | E [MPa] |
| concrete | C 50/60 | 500 | 2,10E+05 |
| | | 50 | 3,68E+04 |
| Geometry | | | |
| thickness | 600 mm | φ [mm] | ctc [mm] |
| width considered | 1000 mm | longitudinal reinforcement | 16 300 |
| | | | 16 300 |
| | | | 0 100 |
| Calculation | | Results | |
| longitudinal reinforcement | | equivalent wall | |
| A | 1,34E+03 mm2 | A;wall | 6,00E+05 mm2 |
| E | 2,10E+05 MPa | EA;wall | 2,23E+10 MPa |
| concrete | | | |
| A | 5,99E+05 mm2 | Δ EA due to steel | 1% |
| E | 3,68E+04 MPa | | |

| Section 2, 3 / 13-25 | | Shear wall | | - | |
|----------------------------|--------------------------|----------------------------|--------------------------|----------|--|
| Materials | | fck [MPa] | E [MPa] | | |
| mild steel | B 500 | 500 | 2,10E+05 | | |
| concrete | C 40/50 | 40 | 3,45E+04 | | |
| Geometry | | | φ [mm] | ctc [mm] | |
| thickness | 400 mm | longitudinal reinforcement | 16 | 300 | |
| width | | | 16 | 300 | |
| considered | 1000 mm | | 0 | 100 | |
| Calculation | | Results | | | |
| longitudinal reinforcement | | equivalent wall | | | |
| A | 1,34E+03 mm ² | A;wall | 4,00E+05 mm ² | | |
| E | 2,10E+05 MPa | EA;wall | 1,40E+10 MPa | | |
| concrete | | | | | |
| A | 3,99E+05 mm ² | Δ EA due to steel | 2% | | |
| E | 3,45E+04 MPa | | | | |

| Section 4, 5 / 13-25 | | Shear wall | | - | |
|----------------------------|--------------------------|----------------------------|--------------------------|----------|--|
| Materials | | fck [MPa] | E [MPa] | | |
| mild steel | B 500 | 500 | 2,10E+05 | | |
| concrete | C 40/50 | 40 | 3,45E+04 | | |
| Geometry | | | φ [mm] | ctc [mm] | |
| thickness | 600 mm | longitudinal reinforcement | 16 | 300 | |
| width | | | 16 | 300 | |
| considered | 1000 mm | | 0 | 100 | |
| Calculation | | Results | | | |
| longitudinal reinforcement | | equivalent wall | | | |
| A | 1,34E+03 mm ² | A;wall | 6,00E+05 mm ² | | |
| E | 2,10E+05 MPa | EA;wall | 2,10E+10 MPa | | |
| concrete | | | | | |
| A | 5,99E+05 mm ² | Δ EA due to steel | 1% | | |
| E | 3,45E+04 MPa | | | | |

| Section 2, 3 / 25-TOP | | Shear wall | | - | |
|----------------------------|--------------------------|----------------------------|--------------------------|----------|--|
| Materials | | fck [MPa] | E [MPa] | | |
| mild steel | B 500 | 500 | 2,10E+05 | | |
| concrete | C 40/50 | 40 | 3,45E+04 | | |
| Geometry | | | φ [mm] | ctc [mm] | |
| thickness | 400 mm | longitudinal reinforcement | 12 | 300 | |
| width | | | 12 | 300 | |
| considered | 1000 mm | | 0 | 100 | |
| Calculation | | Results | | | |
| longitudinal reinforcement | | equivalent wall | | | |
| A | 7,54E+02 mm ² | A;wall | 4,00E+05 mm ² | | |
| E | 2,10E+05 MPa | EA;wall | 1,39E+10 MPa | | |
| concrete | | | | | |
| A | 3,99E+05 mm ² | Δ EA due to steel | 1% | | |
| E | 3,45E+04 MPa | | | | |

| Section 4, 5 / 25-TOP | | Shear wall | | - | |
|----------------------------|--------------------------|----------------------------|--------------------------|----------|--|
| Materials | | fck [MPa] | E [MPa] | | |
| mild steel | B 500 | 500 | 2,10E+05 | | |
| concrete | C 40/50 | 40 | 3,45E+04 | | |
| Geometry | | | φ [mm] | ctc [mm] | |
| thickness | 400 mm | longitudinal reinforcement | 12 | 300 | |
| width | | | 12 | 300 | |
| considered | 1000 mm | | 0 | 100 | |
| Calculation | | Results | | | |
| longitudinal reinforcement | | equivalent wall | | | |
| A | 7,54E+02 mm ² | A;wall | 4,00E+05 mm ² | | |
| E | 2,10E+05 MPa | EA;wall | 1,39E+10 MPa | | |
| concrete | | | | | |
| A | 3,99E+05 mm ² | Δ EA due to steel | 1% | | |
| E | 3,45E+04 MPa | | | | |

| Section 4, 5 / B5-2 | | Shear wall | | - | |
|----------------------------|--------------------------|----------------------------|--------------------------|----------|--|
| Materials | | fck [MPa] | E [MPa] | | |
| mild steel | B 500 | 500 | 2,10E+05 | | |
| concrete | C 55/67 | 55 | 3,78E+04 | | |
| Geometry | | | φ [mm] | ctc [mm] | |
| thickness | 600 mm | longitudinal reinforcement | 20 | 300 | |
| width | | | 20 | 300 | |
| considered | 1000 mm | | 0 | 100 | |
| Calculation | | Results | | | |
| longitudinal reinforcement | | equivalent wall | | | |
| A | 2,09E+03 mm ² | A;wall | 6,00E+05 mm ² | | |
| E | 2,10E+05 MPa | EA;wall | 2,30E+10 MPa | | |
| concrete | | | | | |
| A | 5,98E+05 mm ² | Δ EA due to steel | 2% | | |
| E | 3,78E+04 MPa | | | | |

| Section 4, 5 / B5-2 | | Shear wall | | Thick walls | |
|----------------------------|--------------------------|----------------------------|--------------------------|-------------|--|
| Materials | | fck [MPa] | E [MPa] | | |
| mild steel | B 500 | 500 | 2,10E+05 | | |
| concrete | C 55/67 | 55 | 3,78E+04 | | |
| Geometry | | | φ [mm] | ctc [mm] | |
| thickness | 1740 mm | longitudinal reinforcement | 32 | 156 | |
| width | | | 25 | 170 | |
| considered | 1000 mm | | 0 | 100 | |
| Calculation | | Results | | | |
| longitudinal reinforcement | | equivalent wall | | | |
| A | 1,32E+04 mm ² | A;wall | 1,74E+06 mm ² | | |
| E | 2,10E+05 MPa | EA;wall | 6,80E+10 MPa | | |
| concrete | | | | | |
| A | 1,73E+06 mm ² | Δ EA due to steel | 3% | | |
| E | 3,78E+04 MPa | | | | |

| Section 4, 5 / 2-13 | | Shear wall | | - | |
|----------------------------|--------------------------|----------------------------|--------------------------|----------|--|
| Materials | | fck [MPa] | E [MPa] | | |
| mild steel | B 500 | 500 | 2,10E+05 | | |
| concrete | C 50/60 | 50 | 3,68E+04 | | |
| Geometry | | | φ [mm] | ctc [mm] | |
| thickness | 600 mm | longitudinal reinforcement | 16 | 300 | |
| width | | | 16 | 300 | |
| considered | 1000 mm | | 0 | 100 | |
| Calculation | | Results | | | |
| longitudinal reinforcement | | equivalent wall | | | |
| A | 1,34E+03 mm ² | A;wall | 6,00E+05 mm ² | | |
| E | 2,10E+05 MPa | EA;wall | 2,23E+10 MPa | | |
| concrete | | | | | |
| A | 5,99E+05 mm ² | Δ EA due to steel | 1% | | |
| E | 3,68E+04 MPa | | | | |

| Section 4, 5 THICK WALLS / 2-13 | | Shear wall | | Thick walls | |
|---------------------------------|--------------------------|----------------------------|--------------------------|-------------|--|
| Materials | | fck [MPa] | E [MPa] | | |
| mild steel | B 500 | 500 | 2,10E+05 | | |
| concrete | C 50/60 | 50 | 3,68E+04 | | |
| Geometry | | | φ [mm] | ctc [mm] | |
| thickness | 1740 mm | longitudinal reinforcement | 32 | 156 | |
| width | | | 25 | 170 | |
| considered | 1000 mm | | 0 | 100 | |
| Calculation | | Results | | | |
| longitudinal reinforcement | | equivalent wall | | | |
| A | 1,32E+04 mm ² | A;wall | 1,74E+06 mm ² | | |
| E | 2,10E+05 MPa | EA;wall | 6,63E+10 MPa | | |
| concrete | | | | | |
| A | 1,73E+06 mm ² | Δ EA due to steel | 4% | | |
| E | 3,68E+04 MPa | | | | |

| Section | 4, 5 / 13-TOP | | Shear wall | Thick walls | |
|----------------------------|---------------|-----------------|-------------------------------|-------------|-----------------|
| Materials | | | fck [MPa] | E [MPa] | |
| mild steel | B 500 | | 500 | 2,10E+05 | |
| concrete | C 40/50 | | 40 | 3,45E+04 | |
| Geometry | | | | φ [mm] | ctc [mm] |
| thickness | 1740 | mm | longitudinal reinforcement | 32 | 156 |
| width considered | 1000 | mm | | 25 | 170 |
| | | | | 0 | 100 |
| Calculation | | | Results | | |
| longitudinal reinforcement | | | equivalent wall | | |
| A | 1,32E+04 | mm ² | A;wall | 1,74E+06 | mm ² |
| E | 2,10E+05 | MPa | EA;wall | 6,24E+10 | MPa |
| concrete | | | | | |
| A | 1,73E+06 | mm ² | Δ EA due to steel | 4% | |
| E | 3,45E+04 | MPa | | | |

IV Comparison

This appendix presents the calculations made for the financial feasibility comparison presented in chapter 6.

IV.1 Mean concrete area

As explained in chapter 6, the construction cost is measured by the mean lateral load design (LLD)-concrete area employed in the lateral load resisting system (LLRS). The concrete area is calculated for a typical basement, low rise, mid rise and high rise section on the buildings.

Figure IV.1-1 to IV.1-4 show four typical sections of all four buildings at basement, low-, mid- and high-rise level.

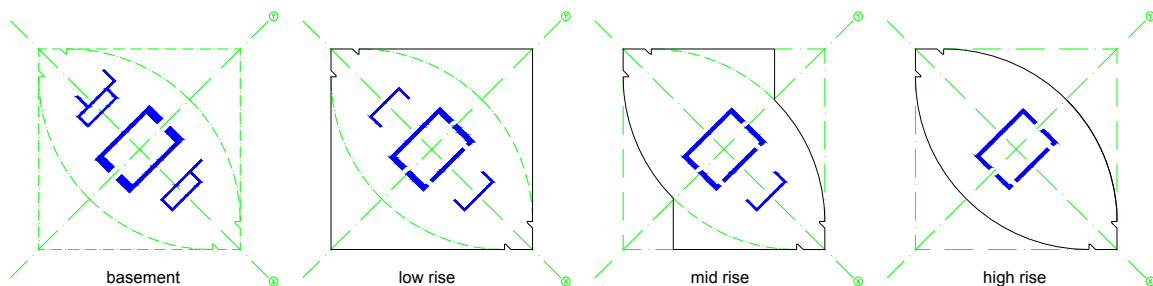


Figure IV.1-1: LLRS area Torre Espacio

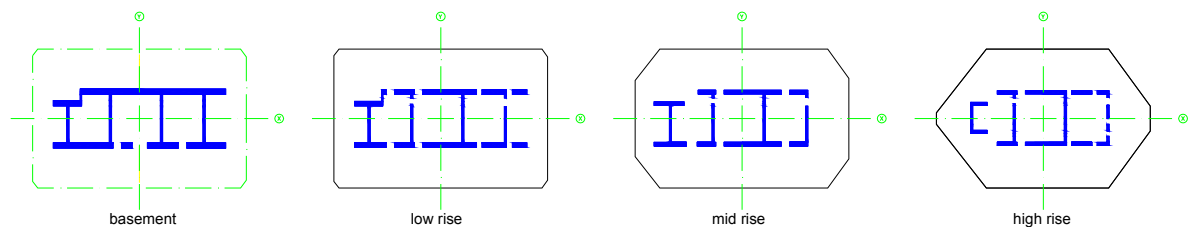


Figure IV.1-2: LLRS area Torre de Cristal

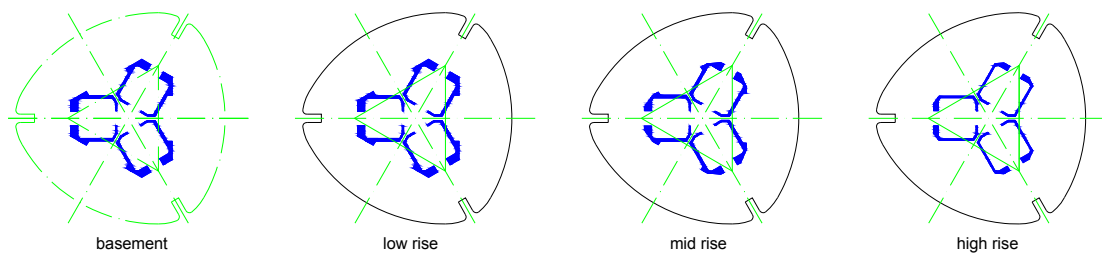


Figure IV.1-3: LLRS area Torre Sacyr Vallehermoso

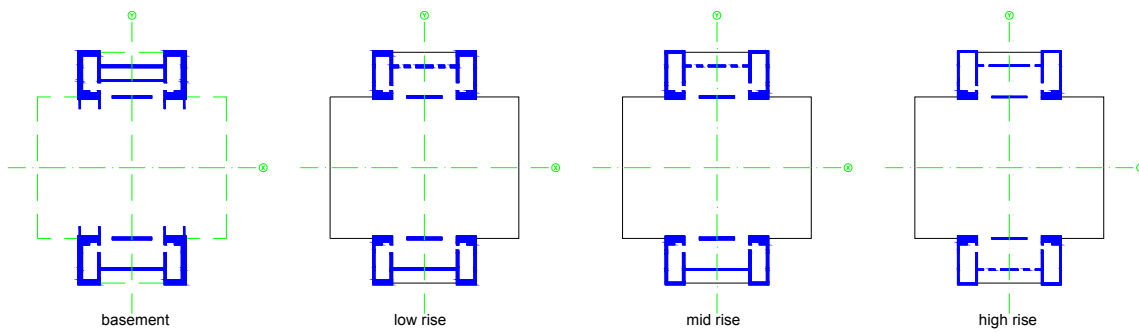


Figure IV.1-4: LLRS area Torre Caja Madrid

The area per section, as well as the mean value, of the blue hatched areas is shown in table IV-1-1.

| | basement [m ²] | low-rise [m ²] | mid-rise [m ²] | high-rise [m ²] | mean [m ²] |
|--------------------------|----------------------------|----------------------------|----------------------------|-----------------------------|------------------------|
| Torre Espacio | 54,1 | 39,6 | 31,8 | 23,2 | 37,2 |
| Torre de Cristal | 106,5 | 86,1 | 64,9 | 51,9 | 77,4 |
| Torre Sacyr Vallehermoso | 59,2 | 59,2 | 49,4 | 33,8 | 50,4 |
| Torre Caja Madrid | 151,3 | 113,0 | 100,2 | 78,1 | 110,6 |

Table IV.1-1: LLRS concrete area

IV.2 LLD-factor

The lateral load design-factor (LLD-factor) reflects which part of the material is used for lateral load design only.

The fundamental load combination used for the calculation of the design stresses under gravity loading has been applied according to Eurocode 0 and Eurocode 1

$$1,35 \cdot G + 1,50 \cdot \alpha_n Q \quad (\text{IV.2-1})$$

where

- G permanent load
- α_n reduction factor for variable loads in design of columns or walls
- Q variable load

The reduction factor for the live load is a function of the number of storeys above the considered structural element of the same category. This factor takes into account the improbability of the simultaneous occurrence of maximum live loads over more than two floors.

$$\alpha_n = \frac{2 + (n - 2) \cdot \psi_0}{n} \quad (\text{IV.2-2})$$

Where

- ψ_0 combination value of variable load, being 0,7 for residential and office area
- n number of storeys

For all buildings α_n equals 0,71 meaning a reduction of the live load of almost 30 %.

Table IV.2-1 shows the Gravity Load Design-factor (GLD-factor) and LLD-factor of the LLRS of the four tall buildings on the right-hand side. The first column represents the axial force in the core structures due to the aforementioned load combination (expression (IV.2-2)). The core area, gravity load mean design stress and the design concrete strength at basement level are presented in the other columns.

| | $N_{d,gr}$ [MN] | A_b [m ²] | $\sigma_{d,gr}$ [MPa] | $f'_{c,d}$ [MPa] | GLD [-] | LLD [-] |
|--------------------------|-----------------|-------------------------|-----------------------|------------------|---------|---------|
| Torre Espacio | 884,8 | 54,1 | 16,4 | 46,7 | 35,1% | 64,9% |
| Torre de Cristal | 1.187,9 | 106,5 | 11,1 | 30,0 | 37,2% | 62,8% |
| Torre Sacyr Vallehermoso | 851,8 | 59,2 | 14,4 | 30,0 | 48,0% | 52,0% |
| Torre Caja Madrid | 2.010,7 | 151,3 | 13,3 | 36,7 | 36,3% | 63,7% |

Table IV.2-1: Lateral load design factor

IV.3 Mean gross floor area

The mean gross floor area (GFA) is taken as the mean value over a typical low, mid and high rise section of the buildings. The results are presented in table IV-3.1. The averaged value over all four buildings is 1566,9 m².

| | low-rise [m ²] | mid-rise [m ²] | high-rise [m ²] | mean [m ²] |
|--------------------------|----------------------------|----------------------------|-----------------------------|------------------------|
| Torre Espacio | 1.760,5 | 1.371,1 | 1.199,6 | 1.443,7 |
| Torre de Cristal | 1.551,8 | 1.482,9 | 1.265,2 | 1.433,3 |
| Torre Sacyr Vallehermoso | 1.526,3 | 1.526,3 | 1.526,3 | 1.526,3 |
| Torre Caja Madrid | 1.864,2 | 1.864,2 | 1.864,2 | 1.864,2 |

Table IV.3-1: Mean gross floor area

IV.4 Mean effective lease span

It is stated in chapter 8 that the smallest dimension of the lettable floor area determines the flexibility of the floor plan. As far as Torre Caja Madrid is concerned, this refers to the distance between the two lateral cores, being the smallest in-plan dimension of the lettable floor area. In the case of interior-core structures the smallest dimension is taken as the effective lease span

The effective lease span is calculated as the distance between two concentric circles: one circle representing the total core-enclosed area and another one representing the total façade-enclosed area.

Figure IV.4-1 to IV.4-4 show four typical sections of all buildings at basement, low, mid and high rise level. The yellow hatched area corresponds to the façade-enclosed area and the pink hatched area corresponds to the core-enclosed area. The effective lease span for every section is calculated by subtracting R_c from R_f .

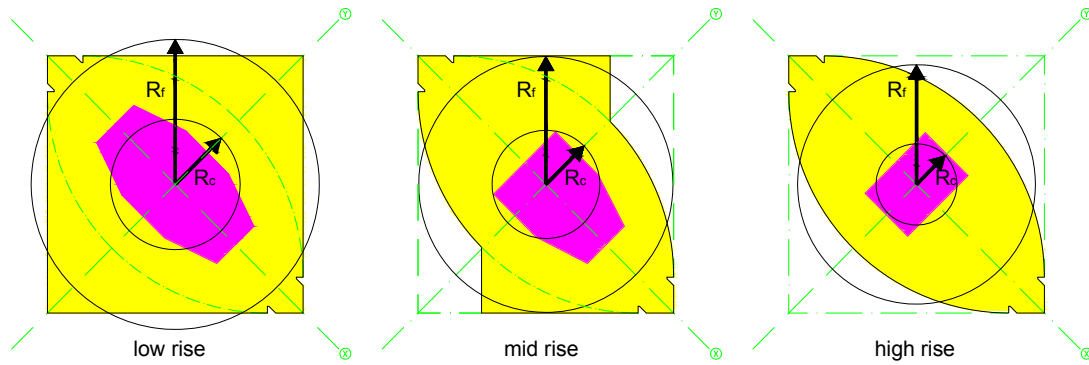


Figure IV.4-1: Equivalent lease span Torre Espacio

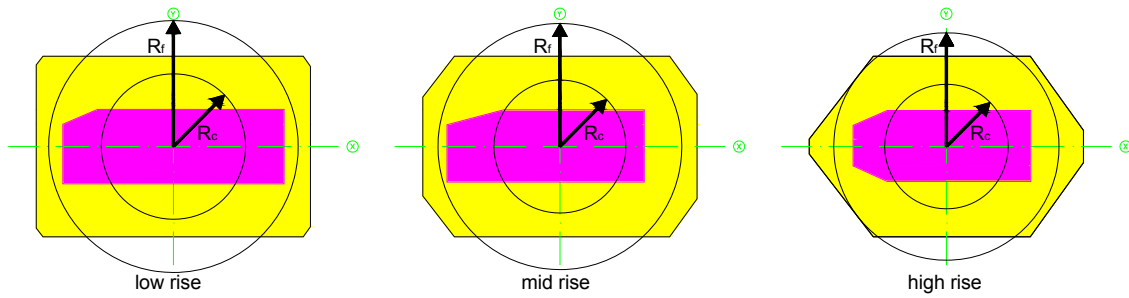


Figure IV.4-2: Equivalent lease span Torre de Cristal

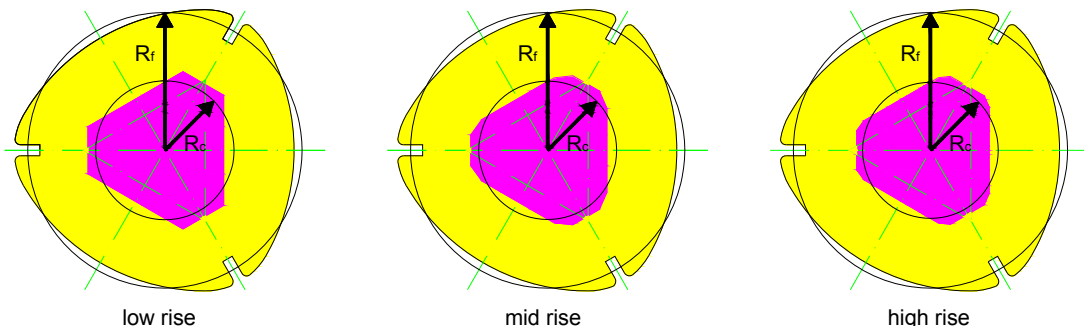


Figure IV.4-3: Equivalent lease span Torre Sacyr Vallehermoso

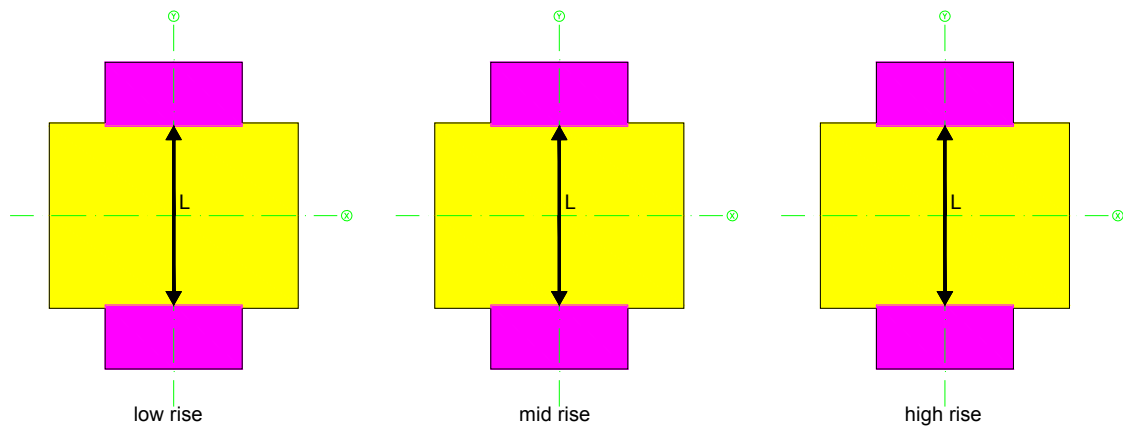


Figure IV.4-4: Equivalent lease span Torre Caja Madrid

Table IV.4-1 presents, from the left to the right-hand side respectively, the façade-enclose area and its equivalent radius, the core-enclosed area and its equivalent radius and the equivalent lease span for a low rise, mid rise and high rise section. The last column shows the mean equivalent lease span.

| | | A_f [m ²] | $R_{f,eq}$ [m] | A_c [m ²] | $R_{c,eq}$ [m] | L_{eq} [m] | $L_{eq,m}$ [m] |
|--------------------------|-----------|-------------------------|----------------|-------------------------|----------------|--------------|----------------|
| Torre Espacio | low rise | 1.760,5 | 23,7 | 357,1 | 10,7 | 13,0 | 12,6 |
| | mid rise | 1.371,1 | 20,9 | 246,1 | 8,9 | 12,0 | |
| | high rise | 1.199,6 | 19,5 | 138,6 | 6,6 | 12,9 | |
| Torre de Cristal | low rise | 1.551,8 | 22,2 | 519,2 | 12,9 | 9,4 | 9,5 |
| | mid rise | 1.482,9 | 21,7 | 434,1 | 11,8 | 10,0 | |
| | high rise | 1.265,2 | 20,1 | 380,1 | 11,0 | 9,1 | |
| Torre Sacyr Vallehermoso | low rise | 1.526,3 | 22,0 | 388,7 | 11,1 | 10,9 | 11,0 |
| | mid rise | 1.526,3 | 22,0 | 386,1 | 11,1 | 11,0 | |
| | high rise | 1.526,3 | 22,0 | 373,7 | 10,9 | 11,1 | |
| Torre Caja Madrid | low rise | 1.864,2 | NA | 520,8 | NA | 31,5 | 31,5 |
| | mid rise | 1.864,2 | NA | 520,8 | NA | 31,5 | |
| | high rise | 1.864,2 | NA | 520,8 | NA | 31,5 | |

Table IV.4-1: Equivalent lease span

List of references

- [1] European Committee for Standardization, *EN 1991-1-4. Eurocode 1: Actions on structures - Part 1-4: General actions - Wind Actions*. Brussels: European Committee for Standardization, 2005.
- [2] Joint Committee on Structural Safety, *JCSS probabilistic model code. Part 2: loads*. August 2008. http://www.jcss.ethz.ch/publications/PMC/PART_II.pdf
- [3] Liu, H., *Wind engineering: a handbook for structural engineers*. United States of America: Prentice-Hall, Inc., 1991.
- [4] Simiu, E., and R.H. Scanlan, *Wind effects on structures: fundamentals and applications to design*. 3rd edition. United States of America: John Wiley & Sons, 1996.
- [5] Stafford Smith, B. and A. Coull, *Tall building structures: analysis and design*. United States of America: John Wiley & Sons, 1991.